FACULTAD DE CIENCIAS

DEPARTAMENTO DE QUÍMICA ORGÁNICA

SYNTHESIS AND PROPERTIES OF SUBPHTHALOCYANINE-BASED SYSTEMS FOR SOLAR ENERGY CONVERSION

GIULIA LAVARDA

Doctoral Thesis

Madrid, 2021

The present work has been developed at the Organic Chemistry Department of the Universidad Autónoma de Madrid under the supervision of Prof. Tomás Torres Cebada, to whom I would like to express my most sincere gratitude.

This work has been funded by the FPU Program of the Ministry of Science, Innovation and Universities (Ref. FPU16/06441).

To date, the results reported in this Thesis have led to the following publications:

1. K. A. Winterfeld, G. Lavarda, J. Guilleme, M. Sekita, D. M. Guldi, T. Torres, G. Bottari, Subphthalocyanines axially substituted with a tetracyanobuta-1,3-diene-aniline moiety: synthesis, structure, and physicochemical properties, *J. Am. Chem. Soc.* **2017**, *139*, 5520-5529.

2. G. Lavarda,† J. Zirzlmeier,† M. Gruber, P. R. Rami, R. R. Tykwinski, T. Torres, D. M. Guldi, Tuning intramolecular Förster resonance energy transfer and activating intramolecular singlet fission, *Angew. Chem. Int. Ed.* **2018**, *57*, 16291-16295.

3. K. A. Winterfeld,† G. Lavarda,† J. Guilleme,† D. M. Guldi, T. Torres, G. Bottari, Subphthalocyanine-tetracyanobuta-1,3-diene-aniline conjugates: stereoisomerism and photophysical properties, *Chem. Sci.* **2019**, *10*, 10997-11005.

4. K. A. Winterfeld,† G. Lavarda,† K. Yoshida,† M. J. Bayerlein, K. Kise, T. Tanaka, A. Osuka, D. M. Guldi, T. Torres, G. Bottari, Synthesis and optical features of axially and peripherally substituted subporphyrins. A paradigmatic example of charge transfer versus exciplex states, *J. Am. Chem. Soc.* **2020**, *142*, 7920-7929.

5. G. Lavarda, N. Bhattacharjee, G. Brancato, T. Torres, G. Bottari, Enabling racemization of axially chiral subphthalocyanine-tetracyanobutadiene-aniline enantiomers by triplet state photogeneration, *Angew. Chem. Int. Ed.* **2020**, *59*, 21224-21229.

6. J. Zirzlmeier,† G. Lavarda,† H. Gotfredsen,† I. Papadopoulos,† L. Chen, T. Clark, R. R. Tykwinski, T. Torres, D. M. Guldi, Modulating the dynamics of Förster resonance energy transfer and singlet fission by variable molecular spacers, *Nanoscale* **2020**, *12*, 23061-23068.

† Shared first authorship.

Other contributions related to this Thesis:

1. D.-P. Medina, I. Papadopoulos, G. Lavarda, H. Gotfredsen, P. R. Rami, R. R. Tykwinski, M. S. Rodríguez-Morgade, D. M. Guldi, T. Torres, Light-harvesting porphyrazines to enable intramolecular singlet fission, *Nanoscale* **2019**, *11*, 22286-22292.

2. G. Lavarda, D. Shimizu, T. Torres, A. Osuka, *meso*-(2-Pyridyl)-boron(III)-subporphyrin: perimeter iridium(III) coordination, *Angew. Chem. Int. Ed.* **2020**, *59*, 3127-3130.

3. B. Berionni Berna, B. Platzer, M. Wolf, G. Lavarda, S. Nardis, P. Galloni, T. Torres, D. M. Guldi, R. Paolesse, Panchromatic light harvesting and stabilizing charge-separated states in corrole-phthalocyanine conjugates through coordinating a subphthalocyanine, *Chem. Eur. J.* **2020**, *26*, 13451-13461.

4. D. Guzmán, I. Papadopoulos, G. Lavarda, P. R. Rami, R. R. Tykwinski, M. S. Rodríguez-Morgade, D. M. Guldi, T. Torres, Controlling intramolecular Förster resonance energy transfer and singlet fission in a subporphyrazine-pentacene conjugate by solvent polarity, *Angew. Chem. Int. Ed.* **2021**, *60*, 1474-1481.

Abbreviations and acronyms

A	Acceptor
BHJ	Bulk Heterojunction
BINOL	1,1'-Bi(2-naphthol)
BODIPY	Boron dipyrromethene
BzSubP	Benzosubporphyrin
CA-RE	Cycloaddition-retroelectrocyclization
CD	Circular Dichroism
CIP	Cahn-Ingold-Prelog
CISS	Chiral-induced Spin Selectivity
COSY	Correlation Spectroscopy
CR	Charge recombination
CS	Charge separation
CSS	Charge-separated State
CT	Charge Transfer
CV	Cyclic Voltammetry
D	Donor
D-A	Donor-Acceptor
DBU	1,8-Diazabicycloundec-7-ene
DCB	Dichlorobenzene
DCM	Dichloromethane
DCTB	trans-2-[3-(4-*tert*-Butylphenyl)-2-methyl-2-propenylidene] malononitrile
DCV	Dicyanovinyl
DFT	Density Functional Theory
DIPEA	*N*,*N*-Diisopropylethylamine
DMF	*N*,*N*-Dimethylformamide
DSSC	Dye-Sensitized Solar Cell
EDG	Electron-donating Group
Fc	Ferrocene

FRET	Förster Resonance Energy Transfer
fsTA	Femtosecond Transient Absorption
FT-IR	Fourier-transform Infrared Spectroscopy
HOMO	Highest Occupied Molecular Orbital
HPLC	High Performance Liquid Chromatography
HRMS	High-resolution Mass Spectrometry
IC	Internal Conversion
i-FRET	Intramolecular Förster Resonance Energy Transfer
IR	Infrared
ISC	Intersystem Crossing
i-SF	Intramolecular Singlet Fission
LOMO	Lowest Occupied Molecular Orbital
MALDI	Matrix-Assisted Laser Desorption/Ionization
MP	Melting Point
MS	Mass Spectrometry
NIR	Near Infrared
NLO	Non-Linear Optics
NMR	Nuclear Magnetic Resonance
NOESY	Nuclear Overhauser Effect Spectroscopy
nsTA	Nanosecond Transient Absorption
Nu	Nucleophile
OD	Optical Density
OFET	Organic Field-Effect Transistor
OLED	Organic Light Emitting Diode
OSC	Organic Solar Cell
P	Porphyrin
Pc	Phthalocyanine
PCE	Power Conversion Efficiency
PDI	Perylene Diimide
PDT	Photodynamic Therapy
PHJ	Planar Heterojunction

Pnc_2	Pentacene dimer
PPG	Polypropylene Glycol
QM	Quantum Mechanics
Rt	Room Temperature
SubNc	Subnaphthalocyanine
SubP	Subporphyrin
SubPc	Subphthalocyanine
SubPz	Subporphyrazine
SF	Singlet Fission
STM	Scanning Tunneling Microscope
SWV	Square-Wave Voltammetry
TCBD	1,1,4,4-Tetracyanobuta-1,3-diene
TCNE	Tetracyanoethylene
TCSPC	Time-correlated Single Photon Counting
TD-DFT	Time-dependent Density Functional Theory
TEA	Triethylamine
THF	Tetrahydrofuran
TIPS	Triisopropylsilyl
TLC	Thin Layer Chromatography
TMS	Trimethylsilyl
TOF	Time of Flight
TTA	Triplet-triplet Annihilation
TTF	Tetrathiafulvalene
UV-vis	Ultraviolet-visible
vr	Vibrational Relaxation
VT	Variable Temperature
XRD	X-ray Diffraction

Table of Contents

Introduction

Subphthalocyanines as molecular materials

Subphthalocyanines: contracted porphyrin analogues

Porphyrins (Ps)[1,2] and their best-known analogues, phthalocyanines (Pcs),[3-6] are among the most investigated macrocyclic systems. Whereas the preparation and study of Ps and Pcs have been object of continuous interest for decades, much less effort has been dedicated to the synthesis and investigation of other synthetic congeners, such as contracted porphyrinoids (Figure 1).[7,8] Thus, the study of contracted porphyrin analogues, namely subporphyrins (SubPs),[8-12] subporphyrazines (SubPzs),[8,13] benzosubporphyrins (BzSubPs),[8,11,12,14] and subphthalocyanines (SubPcs),[8,15,16] is still an expanding research area.

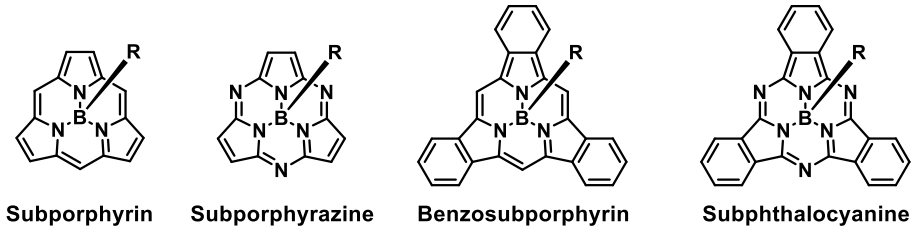

Figure 1. Chemical structure of contracted porphyrinoids.

---

[1] *The Porphyrin Handbook*; *Vols. 1–10* (Eds.: K. M. Kadish, K. M. Smith, R. Guilard), Academic Press, San Diego, CA, **2000**.
[2] *The Porphyrin Handbook*; *Vols. 11–14* (Eds.: K. M. Kadish, K. M. Smith, R. Guilard), Academic Press, San Diego, CA, **2003**.
[3] *The Porphyrin Handbook*; *Vols. 15–20* (Eds.: K. M. Kadish, K. M. Smith, R. Guilard), Academic Press, San Diego, CA, **2003**.
[4] G. de la Torre, C. G. Claessens, T. Torres, *Chem. Commun.* **2007**, 2000-2015.
[5] C. G. Claessens, U. Hahn, T. Torres, *Chem. Rec.* **2008**, *8*, 75-97.
[6] G. de la Torre, G. Bottari, U. Hahn, T. Torres, in *Functional Phthalocyanine Molecular Materials*, J. Jiang Ed., Springer, Berlin, Heidelberg, **2010**, pp. 1-44.
[7] T. Torres, *Angew. Chem. Int. Ed.* **2006**, *45*, 2834-2837.
[8] C. G. Claessens, D. González-Rodríguez, M. S. Rodríguez-Morgade, A. Medina, T. Torres, *Chem. Rev.* **2014**, *114*, 2192-2277.
[9] N. Kobayashi, Y. Takeuchi, A. Matsuda, *Angew. Chem. Int. Ed.* **2007**, *46*, 758-760.
[10] Y. Inokuma, Z. S. Yoon, D. Kim, A. Osuka, *J. Am. Chem. Soc.* **2007**, *129*, 4747-4761.
[11] A. Osuka, E. Tsurumaki, T. Tanaka, *Bull. Chem. Soc. Jpn.* **2011**, *84*, 679-697.
[12] S. Shimizu, *Chem. Rev.* **2017**, *117*, 2730-2784.
[13] M. S. Rodríguez-Morgade, S. Esperanza, T. Torres, J. Barberá, *Chem. Eur. J.* **2005**, *11*, 354-360.
[14] Y. Inokuma, J. H. Kwon, T. K. Ahn, M. C. Yoo, D. Kim, A. Osuka, *Angew. Chem. Int. Ed.* **2006**, *45*, 961-964.
[15] C. G. Claessens, D. González-Rodríguez, T. Torres, *Chem. Rev.* **2002**, *102*, 835-854.
[16] A. Medina, C. G. Claessens, *J. Porphyrins Phthalocyanines* **2009**, *13*, 446-454.

These species, also referred to as subporphyrinoids, are only known as boron derivatives and differ from other porphyrin analogues in the size of the macrocycle, which is composed of three pyrrole or isoindole units. Despite possessing a 14 π-electron aromatic core, subporphyrinoids feature a characteristic cone-shaped geometry conferred by the tetrahedral coordination of the central boron atom, thus representing one of the few known examples of non-planar aromatic molecules. As such, contracted porphyrinoids exhibit peculiar optical and electronic properties which render them extremely attractive compounds. Among contracted porphyrin analogues, SubPcs are undoubtedly the most investigated derivatives.

SubPcs[8,15,16] are aromatic macrocycles composed of three *N*-fused 1,3-diiminoisoindole units arranged around a boron atom, which also bears an axial substituent (Figure 2). The 14 π-electron conjugated system of these derivatives is mainly located in the inner ring, whereas the isoindolic benzenes virtually preserve their electronic structure. In this Thesis, the X_nSubPc-Y notation will be employed to refer to SubPc species, where X and n indicate the nature and the number of the substituents linked to the isoindolic benzene rings, respectively, and Y stands for the apical ligand. In the presence of peripheral substituents different from hydrogen atoms, the latter will not be indicated.

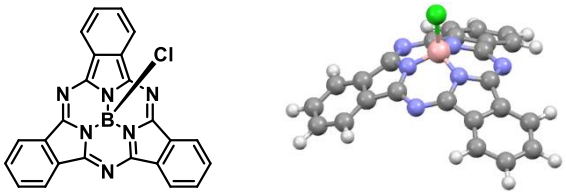

Figure 2. Chemical structure and ball-and-stick model of H_{12}SubPc-Cl.

SubPcs were serendipitously discovered in 1972 by Meller and Ossko in the attempt to synthesize a boron Pc.[17] The condensation reaction of phthalonitrile in the presence of boron trichloride in chloronaphthalene at 200 °C afforded a purple compound which characterization was consistent with the formation of a SubPc bearing an axial chlorine. Two years later, single-crystal X-ray diffraction measurements confirmed the proposed structure.[18]

[17] A. Meller, A. Ossko, *Monatsh. Chem.* **1972**, *103*, 150-155.
[18] H. Kietaibl, *Monatsh. Chem.* **1974**, *105*, 405-418.

Synthesis of SubPcs

SubPcs are synthesized by cyclotrimerization reaction of a phthalonitrile precursor in the presence of a boron-based Lewis acid at high temperatures (140-200 °C) in high-boiling aromatic solvents.[8,15] To date, no publications have been reported on the synthesis of boron-free SubPcs, which preparation constitutes one of the foremost challenges in SubPc chemistry. However, the possibility to incorporate central atoms different from boron within the SubPc core has been widely investigated through theoretical calculations, as will be described later on.

Boron trichloride (BCl_3) and, to a lesser extent, boron tribromide (BBr_3), constitute the most employed boron reagents in SubPc synthesis.[8,15] The reaction of these Lewis acids with a starting phthalonitrile affords the corresponding SubPc-Cl and SubPc-Br species, respectively. Other boron species, such as BF_3,[19] BPh_3,[20,21] $PhBF_2$,[17] $PhBCl_2$,[17,20] or $BuBBr_2$,[21] have also been employed in specific cases. The reactivity of these boron derivatives towards phthalonitriles is closely related to their Lewis acidity, being BBr_3 the most reactive species.[15]

Since the serendipitous discovery of SubPcs in 1972,[17] some significant improvements have been introduced in the synthetic methodology for their preparation. Nowadays, the most employed protocol for the synthesis of SubPc-Cl derivatives consists in the addition of 1 equivalent of BCl_3 from a 1 M solution in *p*-xylene to the corresponding phthalonitrile under argon atmosphere (Scheme 1).[22] The reaction mixture is then refluxed for a time depending on the nature of the starting phthalonitrile. The use of a solution of BCl_3 in *p*-xylene presents several advantages over the use of condensed BCl_3. First, it allows to control the stoichiometry of the reagents, thus minimizing side reactions related to the use of large excesses of a strong Lewis acid. In addition, *p*-xylene can efficiently reduce the two equivalents of chlorine released during the cyclotrimerization reaction, preventing the formation of peripherally chlorinated SubPc by-products.[23] Finally, the reaction is easy to set-up. Slight variations can be introduced in this methodology, such as the use of a 1 M solution of BCl_3 in *p*-xylene in the presence of a co-solvent

[19] R. Potz, M. Göldner, H. Hückstädt, U. Cornelissen, A. Tutaß, H. Homborg, *Z. Anorg. Allg. Chem.* **2000**, *626*, 588-596.
[20] J. Rauschnabel, M. Hanack, *Tetrahedron Lett.* **1995**, *36*, 1629-1632.
[21] M. Geyer, F. Plenzig, J. Rauschnabel, M. Hanack, B. Del Rey, A. Sastre, T. Torres, *Synthesis* **1996**, *1996*, 1139-1151.
[22] C. G. Claessens, D. González-Rodríguez, B. del Rey, T. Torres, G. Mark, H. P. Schuchmann, C. von Sonntag, J. G. MacDonald, R. S. Nohr, *Eur. J. Org. Chem.* **2003**, *2003*, 2547-2551.
[23] C. G. Claessens, D. González-Rodríguez, C. M. McCallum, R. S. Nohr, H.-P. Schuchmann, T. Torres, *J. Porphyrins Phthalocyanines* **2007**, *11*, 181-188.

(*e.g.* chlorobenzene,[24] *o*-dichlorobenzene[25] or 1-chloronaphthalene[26]) or the addition of a 1 M solution of BCl_3 in heptanes[27,28] or dichloromethane[29,30] to the precursor phthalonitrile dissolved in a high-boiling solvent (*e.g. p*-xylene,[30] 1-chloronaphthalene,[28] *o*-dichlorobenzene,[27] or 1,2,4-trichlorobenzene[29]).[31] Microwave irradiation has also been employed for the preparation of SubPcs.[32]

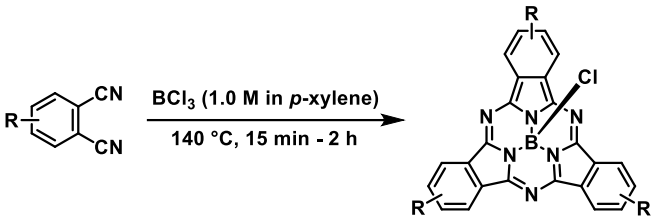

Scheme 1. General synthesis of SubPc-Cl derivatives.

The use of BBr_3 in SubPc synthesis is less common than that of BCl_3 due to the lower stability of SubPc-Br derivatives with respect to their chlorinated analogues, which may lead to the hydrolysis of the initially formed halogenated SubPc to the corresponding SubPc-OH species.[33] For the preparation of SubPc-Br derivatives, BBr_3 is commonly added as a neat liquid to a solution or suspension of the precursor phthalonitrile in a high-boiling solvent as, for example, chlorobenzene,[34] 1-chloronaphthalene,[33] bromobenzene,[19] or toluene/bromobenzene mixtures.[35]

[24] C. Zhang, K. Nakano, M. Nakamura, F. Araoka, K. Tajima, D. Miyajima, *J. Am. Chem. Soc.* **2020**, *142*, 3326-3330.
[25] A. J. Beneto, J. Y. Jeong, J. S. Park, *Dalton Trans.* **2018**, *47*, 16036-16039.
[26] K. Sakamoto, S. Yoshino, M. Takemoto, K. Sugaya, H. Kubo, T. Komoriya, S. Kamei, S. Furukawa, *J. Porphyrins Phthalocyanines* **2015**, *19*, 688-694.
[27] B. A. Kamino, T. P. Bender, *Dalton Trans.* **2013**, *42*, 13145-13150.
[28] I. Roy, D. Shetty, R. Hota, K. Baek, J. Kim, C. Kim, S. Kappert, K. Kim, *Angew. Chem. Int. Ed.* **2015**, *54*, 15152-15155.
[29] L. Zhao, K. Wang, T. Furuyama, J. Jiang, N. Kobayashi, *Chem. Commun.* **2014**, *50*, 7663-7665.
[30] M. Shi, J. Mack, L. Yin, X. Wang, Z. Shen, *J. Mater. Chem. C* **2016**, *4*, 7783-7789.
[31] See ref. 8 for older examples.
[32] M. Obłoza, Ł. Łapok, J. Solarski, T. Pędziński, M. Nowakowska, *Chem. Eur. J.* **2018**, *24*, 17080-17090.
[33] N. Kobayashi, T. Nonomura, *Tetrahedron Lett.* **2002**, *43*, 4253-4255.
[34] G. E. Morse, M. G. Helander, J. F. Maka, Z.-H. Lu, T. P. Bender, *ACS Appl. Mater. Interfaces* **2010**, *2*, 1934-1944.
[35] M. V. Fulford, D. Jaidka, A. S. Paton, G. E. Morse, E. R. Brisson, A. J. Lough, T. P. Bender, *J. Chem. Eng. Data* **2012**, *57*, 2756-2765.

The harsh reaction conditions required for SubPc synthesis considerably limit the variety of functional groups that can be introduced in the starting 1,2-dicyanobenzene, which is typically restricted to halogen atoms, nitro groups, alkyl groups, thioethers, and sulphones.[8]

When the phthalonitrile precursor lacks C_{2v} symmetry, cyclotrimerization leads to a mixture of C_3-symmetric and C_1-symmetric SubPc regioisomers, which are typically separated by column chromatography on silica gel.[36,37] For *meta*-substituted SubPcs, the C_3 and C_1 isomers are obtained in a statistical 1:3 ratio. On the contrary, in the case of *ortho*-substituted SubPc derivatives, steric and electronic factors play a significant role in the regioselectivity of the cyclotrimerization reaction, due to the proximity of the peripheral substituents to the SubPc core.[33,36,38] In turn, each of these C_3- and C_1-symmetric constitutional isomers is intrinsically chiral and is obtained as a racemic mixture of two enantiomers. A detailed discussion on the optical resolution of inherently chiral SubPcs is given in the third Chapter of this Thesis.

Low-symmetry SubPcs can be prepared through reaction of two different phthalonitrile precursors.[27,39-44] Normally, a mixture of SubPc derivatives differing in the nature, number and position of the ring substituents is obtained, which separation is usually achieved through common chromatographic techniques. Both steric factors and relative reactivities affect the selectivity of the reaction, although a clear tendency cannot be defined due to the scarceness of reports on this topic. In general, a partial control can be achieved by tuning the stoichiometry of the reaction in terms of molar ratio between the starting phthalonitrile species.

A two-phase mechanism for SubPc-Cl formation was postulated by Torres and co-workers in 2007 on the basis of computational studies (Scheme 2).[23] In the first stage, Lewis acid activation of the starting phthalonitrile by BCl_3 triggers the formation of intermediate **I**, from which an open trimer is formed *via* successive additions. Subsequently, a ring-closing step completes the formation of the macrocyclic framework. In this stage, the central boron atom acts as template,

---

[36] C. G. Claessens, T. Torres, *Eur. J. Org. Chem.* **2000**, *2000*, 1603-1607.
[37] C. G. Claessens, T. Torres, *Tetrahedron Lett.* **2000**, *41*, 6361-6365.
[38] N. Iida, E. Tokunaga, N. Saito, N. Shibata, *J. Fluorine Chem.* **2015**, *171*, 120-123.
[39] C. G. Claessens, T. Torres, *Chem. Eur. J.* **2000**, *6*, 2168-2172.
[40] D. González-Rodríguez, C. G. Claessens, T. Torres, *J. Porphyrins Phthalocyanines* **2009**, *13*, 203-214.
[41] G. Zango, J. Zirzlmeier, C. G. Claessens, T. Clark, M. V. Martínez-Díaz, D. M. Guldi, T. Torres, *Chem. Sci.* **2015**, *6*, 5571-5577.
[42] L. Sejdarasi, K. J. McAuliffe, B. A. Corbin, E. R. Trivedi, *ChemistrySelect* **2017**, *2*, 7417-7420.
[43] H. Lissau, C. L. Andersen, F. E. Storm, M. Santella, O. Hammerich, T. Hansen, K. V. Mikkelsen, M. B. Nielsen, *Chem. Commun.* **2018**, *54*, 2763-2766.
[44] G. Zango, T. Sakurai, B. Urones, H. Saeki, W. Matsuda, M. V. Martínez-Díaz, S. Seki, T. Torres, *Chem. Eur. J.* **2018**, *24*, 8331-8342.

ensuring the spatial arrangement required for cyclization. In the second phase, a BCl_3-catalyzed concerted elimination of Cl_2 affords the final SubPc valence system.[45] More recently, the crucial catalytic role of BCl_3 was clearly unveiled through an in-depth DFT study of the mechanism of SubPc formation, in which a twenty-three-step reaction pathway was disclosed.[46] In particular, BCl_3 was argued to act as chloride-transfer shuttle in several elementary reactions, thus reducing the activation barrier of the process. Moreover, the importance of the boron halide as activating and templating agent was confirmed.

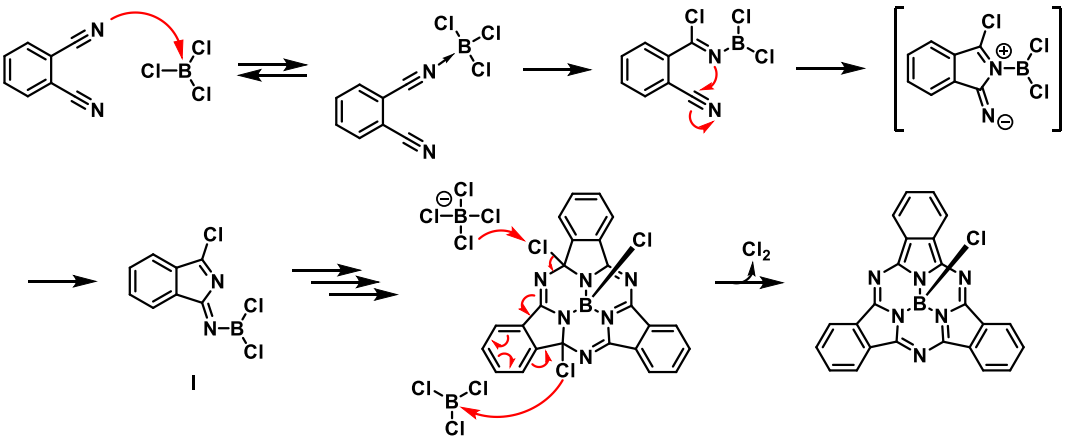

Scheme 2. Key steps of the formation mechanism of SubPc-Cl proposed by Torres and co-workers.[23]

[45] R. S. Nohr, C. M. McCallum, H.-P. Schuchmann, *J. Porphyrins Phthalocyanines* **2010**, *14*, 271-277.
[46] C. Wang, X. Chen, D. Qi, S. Bi, J. Jiang, *Inorg. Chem. Commun.* **2017**, *85*, 9-15.

Reactivity of SubPcs

SubPcs constitute versatile starting materials for a large variety of reactions involving different sites of the preformed macrocycle. In particular, SubPc reactivity can be classified in three main groups: (1) axial reactivity, (2) peripheral reactivity, and (3) ring-expansion reactions (Figure 3).[8,15] These reactivity modes differ in the reactive center: (1) the axial B-X bond, (2) the functional groups linked to the isoindolic benzene rings, or (3) the imine-type SubPc core. Both axial and peripheral reactivity maintain the structure of the macrocycle and produce functionalized SubPcs. In contrast, ring-expansion reaction results in the opening of the SubPc constrained ring and the incorporation on an additional isoindole unit, thus leading to the formation of low-symmetry Pcs.

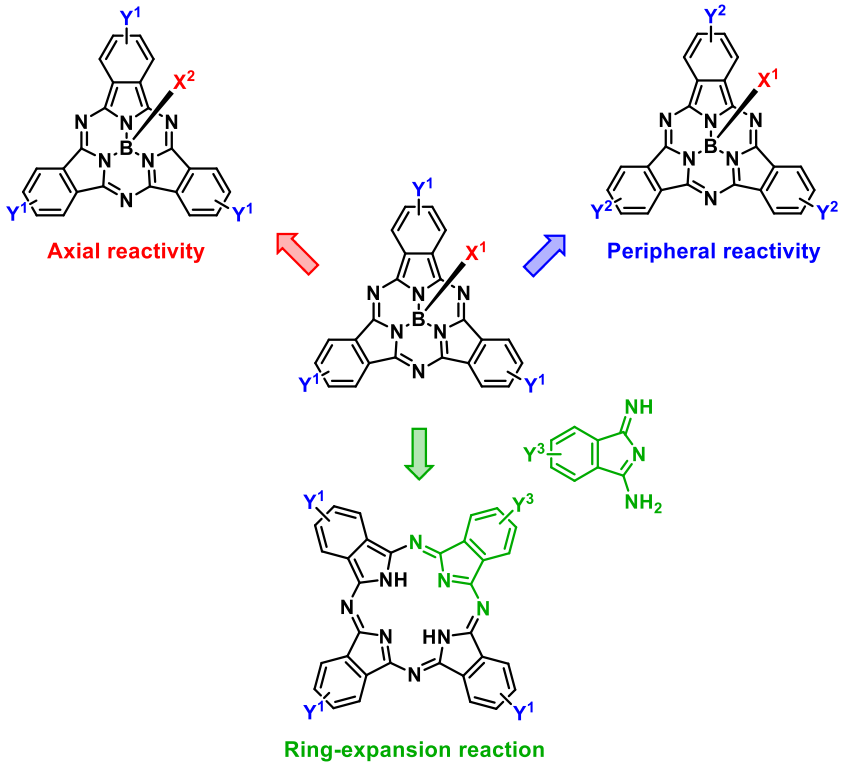

Figure 3. The three main modes of SubPc reactivity.

An additional type of reactivity consists in the formation of ruthenoarene π-complexes of SubPc by reaction with $[Cp^*Ru(MeCN)_3]PF_6$ (Cp^* = pentamethylcyclopentadienyl), in which the SubPc

acts as π-ligand towards the arenophilic Ru(II).[47] When axially phenoxy-substituted SubPcs are employed, direct functionalization of either the apical phenol moiety or one of the isoindolic benzene rings can take place. In particular, metal π-coordination to either the SubPc concave or the SubPc convex side has been observed, being the convex π-surface the most reactive.

Due to the restrictions imposed by the use of boron reagents in SubPc synthesis in terms of variety of both axial and peripheral substituents, the development of strategies for the chemical modification of preformed SubPcs is of paramount importance. As a matter of fact, the introduction of proper functionalities in the SubPc framework permits to tune the photophysical and electrochemical properties of the macrocycle. Moreover, derivatization of the axial and peripheral positions allows to control the organization features of these derivatives, besides enabling the preparation of dimeric, oligomeric or polymeric SubPc-based structures and the integration of SubPcs in multicomponent systems. Here, an overview of the axial and peripheral reactivity of SubPcs is reported, as well as a short description of ring-expansion reactions.

Axial reactivity

Substitution at the boron atom represents a common method for the functionalization of SubPcs and their incorporation into systems of increasing complexity. Generally, the modification of the axial ligand preserves the electronic characteristics of the π-conjugated macrocycle, which are mainly determined by the ring substituents.

Due to the low reactivity of the tetracoordinated boron atom, axial substitution reactions generally require harsh conditions, which may lead to the decomposition of the macrocyclic system.[8] Nevertheless, efficient axial substitution methodologies have been developed during the last decade which are based on the generation of activated SubPc species and allow for the use of milder conditions.

A one-pot, two-step procedure for the replacement of the axial ligand in axially chlorinated SubPcs was presented by Guilleme, González-Rodríguez and Torres in 2011.[48] In this protocol, a highly electrophilic SubPc species with a weakly coordinating axial triflate (OTf) anion is prepared *in situ* by reaction of a SubPc-Cl derivative with silver triflate (AgOTf) or trimethylsilyl triflate (Me_3SiOTf). Subsequent reaction of the SubPc-OTf intermediate with a nucleophile (NuH) in the presence of a hindered tertiary amine (*i.e. N*,*N*-diisopropylethylamine (DIPEA)) affords the corresponding SubPc-Nu species (Scheme 3). The scope of this reaction includes

[47] E. Caballero, J. Fernández-Ariza, V. M. Lynch, C. Romero-Nieto, M. S. Rodríguez-Morgade, J. L. Sessler, D. M. Guldi, T. Torres, *Angew. Chem. Int. Ed.* **2012**, *51*, 11337-11342.
[48] J. Guilleme, D. González-Rodríguez, T. Torres, *Angew. Chem. Int. Ed.* **2011**, *50*, 3506-3509.

oxygen nucleophiles such as alkyl alcohols, aryl alcohols and carboxylic acids, as well as aromatic and aliphatic nitrogen and sulfur nucleophiles, and carbon nucleophiles in the form of alkyl and aryl magnesium bromides. More recently, a couple of SubPc-OTf derivatives were isolated, and their X-ray crystal structures reported.[49,50]

Another strategy for the activation of the axial position was presented by Morse and Bender in 2012.[51] In this procedure, treatment of the SubPc-Cl or SubPc-Br precursor with aluminum chloride ($AlCl_3$) leads to the formation of a complex in which the aluminum interacts with the axial halogen and one of the *meso* nitrogen atoms of the macrocycle. Addition of the nucleophile and subsequent quenching of the resulting complex with a Lewis base yield the corresponding axially substituted SubPc (Scheme 3). Following this protocol, oxygen, sulfur, and nitrogen aromatic nucleophiles could be introduced at the apical position of the SubPc macrocycle. A few years later, activation of SubPcs by $AlCl_3$ was exploited by Nielsen and co-workers for the axial substitution reaction of SubPc-Cl with trimethylsilyl (TMS)-protected alkynes.[52]

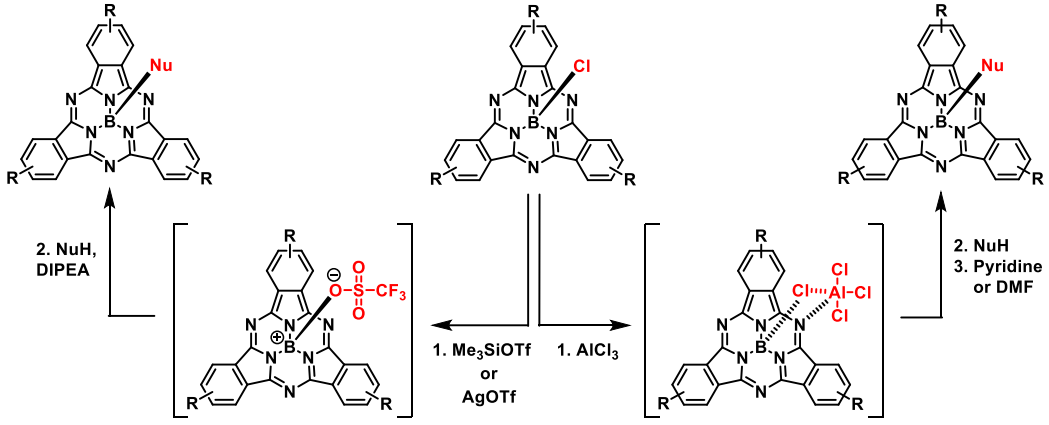

Scheme 3. Axial substitution reaction in SubPcs *via* an activated SubPc-OTf intermediate (left)[48] and *via* activation in the presence of $AlCl_3$ (right).[51]

Besides these approaches, several works have been published in which axial ligand exchange in SubPcs is performed by direct reaction with nucleophiles. Here, the most common procedures employed for these axial substitution reactions are described, along with some recent examples.

---

[49] J. Guilleme, L. Martínez-Fernández, I. Corral, M. Yanez, D. González-Rodríguez, T. Torres, *Org. Lett.* **2015**, *17*, 4722-4725.
[50] Z. Wang, X. Fu, *Organometallics* **2017**, *36*, 285-290.
[51] G. E. Morse, T. P. Bender, *Inorg. Chem.* **2012**, *51*, 6460-6467.
[52] H. Gotfredsen, M. Jevric, S. L. Broman, A. U. Petersen, M. B. Nielsen, *J. Org. Chem.* **2016**, *81*, 1-5.

Formation of B-O bonds. The replacement of the B-Y (Y = Cl, Br) bond with a B-O bond represents by far the most common approach for the axial functionalization of SubPcs.[8]

Substitution of the apical chlorine ligand with phenols is commonly carried out by refluxing the starting SubPc with the corresponding alcohol in a high-boiling point aromatic solvent such as toluene,[41,43,44,53-61] chlorobenzene,[27] *o*-dichlorobenzene[62] or *o*-xylene.[63,31] The reaction can be performed without purification of the SubPc-Cl precursor, by adding the aryl alcohol and the solvent to the crude cyclotrimerization product.[27,41,43,44,54,57,59,63] In some cases, a base such as 1,8-Diazabicycloundec-7-ene (DBU),[54,58] triethylamine,[43,57] pyridine,[60] or DIPEA[61] is added in order to neutralize the generated HCl.[31] Axial substitution with phenols from SubPc-Br precursors has also been exploited, despite being less common.[31,59,64-67]

An in-depth investigation on the mechanism of the axial ligand exchange reaction between SubPc-Cl derivatives and phenols was reported in 2014 by Torres, Corral, González-Rodríguez and co-workers.[68] On the basis of both experimental and theoretical results, a bimolecular σ-bond metathesis mechanism was postulated, in which the phenolic proton assists in weakening the B-Cl bond concomitantly with the formation of the B-O bond (Figure 4). In light of the proposed mechanism, the influence of different parameters on the kinetics of the reaction could

[53] A. S. Paton, A. J. Lough, T. P. Bender, *Ind. Eng. Chem. Res.* **2012**, *51*, 6290-6296.
[54] I. Sanchez-Molina, B. Grimm, R. M. Krick Calderon, C. G. Claessens, D. M. Guldi, T. Torres, *J. Am. Chem. Soc.* **2013**, *135*, 10503-10511.
[55] L. C. K. Viswanath, L. D. Shirtcliff, K. D. Berlin, *J. Porphyrins Phthalocyanines* **2013**, *17*, 1167-1172.
[56] B. Çoşut, S. Yeşilot, M. Durmuş, A. Kılıç, *Dyes and Pigments* **2013**, *98*, 442-449.
[57] M. Ince, A. Medina, J. H. Yum, A. Yella, C. G. Claessens, M. V. Martínez-Díaz, M. Grätzel, M. K. Nazeeruddin, T. Torres, *Chem. Eur. J.* **2014**, *20*, 2016-2021.
[58] C. Duan, G. Zango, M. García Iglesias, F. J. M. Colberts, M. M. Wienk, M. V. Martínez-Díaz, R. A. J. Janssen, T. Torres, *Angew. Chem. Int. Ed.* **2017**, *56*, 148-152.
[59] J. Fernández-Ariza, R. M. K. Calderón, J. Perles, M. S. Rodríguez-Morgade, D. M. Guldi, T. Torres, *Chem. Commun.* **2017**, *53*, 8525-8528.
[60] T. Kawata, Y. Chino, N. Kobayashi, M. Kimura, *Langmuir* **2018**, *34*, 7294-7300.
[61] E. Fazio, K. A. Winterfeld, A. López-Pérez, T. Torres, D. M. Guldi, G. De La Torre, *Nanoscale* **2018**, *10*, 22400-22408.
[62] G. E. Morse, I. Gong, Y. Kawar, A. J. Lough, T. P. Bender, *Cryst. Growth Des.* **2014**, *14*, 2138-2147.
[63] G. M. Eder, B. R. Walker, P. L. McGrier, *RSC advances* **2017**, *7*, 29271-29274.
[64] J. D. Virdo, L. Crandall, J. D. Dang, M. V. Fulford, A. J. Lough, W. S. Durfee, T. P. Bender, *CrystEngComm* **2013**, *15*, 8578-8586.
[65] A. S. Paton, T. P. Bender, *J. Porphyrins Phthalocyanines* **2014**, *18*, 1051-1056.
[66] K. L. Sampson, X. Jiang, E. Bukuroshi, A. Dovijarski, H. Raboui, T. P. Bender, K. M. Kadish, *J. Phys. Chem. A* **2018**, *122*, 4414-4424.
[67] K. L. Sampson, D. S. Josey, Y. Li, J. D. Virdo, Z.-H. Lu, T. P. Bender, *J. Phys. Chem. C* **2018**, *122*, 1091-1102.
[68] J. Guilleme, L. Martínez-Fernández, D. González-Rodríguez, I. Corral, M. Yanez, T. Torres, *J. Am. Chem. Soc.* **2014**, *136*, 14289-14298.

be rationalized. In particular: (a) SubPc-Br derivatives react faster than chloro- and fluoro-substituted species, since the boron-halogen bond becomes weaker by descending along the halogen series; (b) the reaction is faster in the presence of peripheral electron-donating groups as a result of the stabilization of the positive charge developed at the B atom in the transition state; (c) more acidic phenols accelerate the reaction, since they bind more efficiently to the leaving halogen *via* proton coordination; (d) polar solvents induce a faster reaction, as they can stabilize the partial charges generated in the transition state; (e) coordinating solvents able to compete with the phenol in the formation of H-bonds reduce the reaction rate.

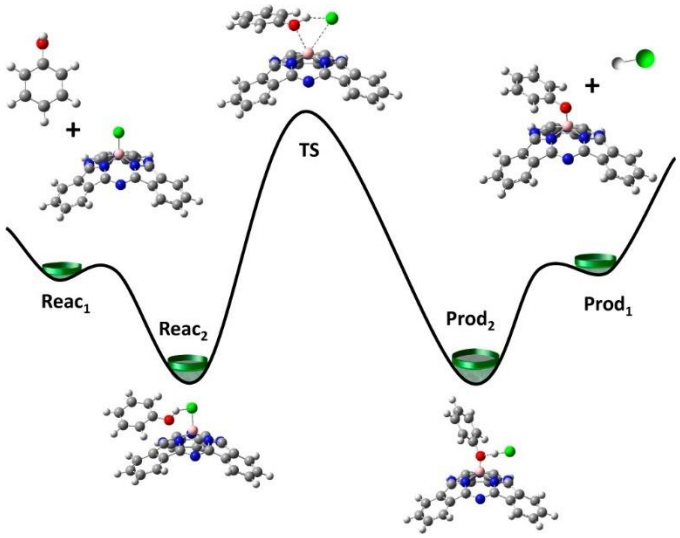

Figure 4. Double-well reaction profile postulated from DFT calculations for the substitution reaction between phenol and SubPc-Cl. Reproduced from ref. 68.

Based on these results, a novel methodology for axial substitution in SubPc-Cl derivatives involving the use of TMS-protected nucleophiles was reported in 2015, which allows for the efficient introduction of aryloxy substituents at the apical position of the macrocycle.[49] In this reaction, the electrophilic TMS functionality plays the role of the phenolic proton, assisting B-Cl bond dissociation through coordination of the halophilic Si center to the leaving chlorine concomitantly with the formation of the new B-O bond.

Axial ligand exchange with alkyl alcohols proceeds in general less efficiently than with phenols due to the lower acidity of the hydroxylic proton.[25,31,69-74] SubPc-Cl and SubPc-Br derivatives can also react with carboxylic acids upon refluxing the SubPc precursor and the acid in high boiling solvents.[31,75,76] SubPc-OH species have been synthesized upon heating under reflux a suspension of the starting axially halogenated SubPc in water,[77] pyridine/water,[78] DMSO/pyridine/water,[79] acetonitrile/water[80] or acetone/water[65] mixtures, whereas μ-oxo SubPc homodimers and heterodimers have been prepared by self-condensation of SubPc-OH derivatives or through reaction of SubPc-OH derivatives with axially halogenated SubPcs.[81-83]

Formation of B-N bonds. The formation of B-N bonds was first made accessible by procedures involving the generation of activated SubPc species (*vide supra*).[48,51] As an exception, the direct reaction of phthalimides with SubPc-Cl in refluxing dichlorobenzene for prolonged reaction times (*i.e.* 90-100 hours) was reported in 2011 by Bender and co-workers.[84] The formation of B-N bonds between encapsulated H_{12}SubPcs and the amino functionalities of the host metal-organic framework upon refluxing the suspension in toluene during 48 hours has also been reported.[85] Interestingly, a stable SubPc-azido derivative was obtained by reaction of a SubPc-Cl precursor with trimethylsilyl azide (Me_3SiN_3) in refluxing toluene.[49]

Formation of B-C bonds. A common protocol for the efficient introduction of ethynyl functionalities at the SubPc axial position consists in the reaction of a SubPc-Cl precursor with a Grignard reagent which is generated *in situ* upon treatment of a terminal alkyne with

[69] Z. Biyiklioglu, *Inorg. Chem. Commun.* **2015**, *55*, 60-64.
[70] Z. Biyiklioglu, H. Alp, *Dalton Trans.* **2016**, *45*, 3838-3843.
[71] E. T. Eçik, E. Özcan, H. Kandemir, I. F. Sengul, B. Çoşut, *Dyes and Pigments* **2017**, *136*, 441-449.
[72] H. Baş, Z. Biyiklioglu, *Inorg. Chim. Acta* **2017**, *467*, 56-61.
[73] Ö. Göktuğ, C. Göl, M. Durmuş, *J. Porphyrins Phthalocyanines* **2017**, *21*, 539-546.
[74] E. Özcan, G. Keşan, B. Topaloğlu, E. T. Eçik, A. Dere, F. Yakuphanoglu, B. Çoşut, *New J. Chem.* **2018**, *42*, 4972-4980.
[75] P. V. Solntsev, K. L. Spurgin, J. R. Sabin, A. A. Heikal, V. N. Nemykin, *Inorg. Chem.* **2012**, *51*, 6537-6547.
[76] K. L. Sampson, B. H. Lessard, E. Cho, T. P. Bender, *Macromol. Chem. Phys.* **2017**, *218*, 1600592.
[77] M. V. Martínez-Díaz, B. del Rey, T. Torres, B. Agricole, C. Mingotaud, N. Cuvillier, G. Rojo, F. Agulló-López, *J. Mater. Chem.* **1999**, *9*, 1521-1526.
[78] S. V. Kudrevich, S. Gilbert, J. E. Van Lier, *J. Org. Chem.* **1996**, *61*, 5706-5707.
[79] M. V. Fulford, A. J. Lough, T. P. Bender, *Acta Cryst. B* **2012**, *68*, 636-645.
[80] B. del Rey, M. V. Martínez-Díaz, J. Barberá, T. Torres, *J. Porphyrins Phthalocyanines* **2000**, *4*, 569-573.
[81] N. Kobayashi, T. Ishizaki, K. Ishii, H. Konami, *J. Am. Chem. Soc.* **1999**, *121*, 9096-9110.
[82] Y. Yamasaki, T. Mori, *Bull. Chem. Soc. Jpn.* **2011**, *84*, 1208-1214.
[83] J. D. Dang, M. V. Fulford, B. A. Kamino, A. S. Paton, T. P. Bender, *Dalton Trans.* **2015**, *44*, 4280-4288.
[84] G. E. Morse, J. S. Castrucci, M. G. Helander, Z.-H. Lu, T. P. Bender, *ACS Appl. Mater. Interfaces* **2011**, *3*, 3538-3544.
[85] A. Santiago-Portillo, S. Remiro-Buenamañana, S. Navalón, H. García, *Dalton Trans.* **2019**, *48*, 17735-17740.

ethylmagnesium bromide (EtMgBr), as reported in the pivotal work of Ziessel and co-workers.[86] Similar procedures have been employed for the reaction of SubPc-Br derivatives with alkyl or aryl Grignard reagents.[87,88] Remarkably, novel SubPc-CN species could be prepared by reaction of SubPc-Cl precursors with trimethylsilyl cyanide (Me_3SiCN), whereas reaction with the TMS derivatives of other carbon nucleophiles was found to lead to the decomposition of the macrocycle.[49]

Formation of B-F, B-Cl and B-Br bonds. Axially fluorinated SubPcs have been prepared by refluxing the corresponding SubPc-Cl, SubPc-Br or SubPc-OAr precursors in toluene in the presence of a large excess of $BF_3{\cdot}OEt_2$.[35,89-92] Recently, the use of $AgBF_4$ for the replacement of the apical chlorine ligand with a fluorine atom has also been reported.[24] Treatment of SubPc-Cl derivatives with an excess of BBr_3 affords the corresponding brominated species,[93] whereas chloro-substituted SubPcs have been obtained from SubPc-OH, SubPc-OPh or SubPc-Br derivatives in the presence of BCl_3,[93] $AlCl_3$[51] or *p*-toluenesulfonyl chloride (TsCl).[94]

Formation of B-B bonds. The only example of B-B bond formation in SubPcs was reported by Torres and co-workers in 2007 and consists in the preparation of a SubPc dimer *via* reductive Wurtz coupling of SubPc-Cl.[95]

[86] F. Camerel, G. Ulrich, P. Retailleau, R. Ziessel, *Angew. Chem. Int. Ed.* **2008**, *47*, 8876-8880.
[87] Y. Yamasaki, T. Mori, *Chem. Lett.* **2010**, *39*, 1108-1109.
[88] C. Bonnier, D. S. Josey, T. P. Bender, *Aust. J. Chem.* **2015**, *68*, 1750-1758.
[89] M. S. Rodríguez-Morgade, C. G. Claessens, A. Medina, D. González-Rodríguez, E. Gutiérrez-Puebla, A. Monge, I. Alkorta, J. Elguero, T. Torres, *Chem. Eur. J.* **2008**, *14*, 1342-1350.
[90] H. Gommans, T. Aernouts, B. Verreet, P. Heremans, A. Medina, C. G. Claessens, T. Torres, *Adv. Funct. Mater.* **2009**, *19*, 3435-3439.
[91] J. Guilleme, J. Aragó, E. Ortí, E. Cavero, T. Sierra, J. Ortega, C. Folcia, J. Etxebarria, D. González-Rodríguez, T. Torres, *J. Mater. Chem. C* **2015**, *3*, 985-989.
[92] K. Cnops, G. Zango, J. Genoe, P. Heremans, M. V. Martínez-Díaz, T. Torres, D. Cheyns, *J. Am. Chem. Soc.* **2015**, *137*, 8991-8997.
[93] D. González-Rodríguez, Ph.D. Thesis, Universidad Autónoma de Madrid, Madrid, Spain, 2003.
[94] A. S. Paton, G. E. Morse, D. Castelino, T. P. Bender, *J. Org. Chem.* **2012**, *77*, 2531-2536.
[95] A. K. Eckert, M. S. Rodríguez-Morgade, T. Torres, *Chem. Commun.* **2007**, 4104-4106.

Peripheral reactivity

The expression "peripheral reactivity" refers to any reaction that produces a chemical modification of the substituents placed at the isoindolic benzene rings of the SubPc framework. Unlike axial ligands, peripheral substituents can produce strong electronic perturbations on the macrocyclic system. Whereas axial substitution reactions are characteristic of SubPc chemistry, peripheral reactivity involves common organic reactions. However, due to the relative chemical instability of these constrained macrocycles, the experimental conditions must be selected in order to prevent the decomposition of the SubPc framework.

The use of metal-catalyzed cross-coupling reactions represent the most frequently employed strategy for functionalization of SubPcs at the periphery.[8,96] As a matter of fact, SubPcs have been employed as precursors in palladium-catalyzed Sonogashira,[43,54,57,91,97-101] Suzuki,[25,59,102,103] Stille,[60] Heck,[104] Hartwig-Buchwald[105] and Miyaura borylation[25] reactions.[31]

Other methodologies have been successfully employed for the chemical modification of peripheral substituents. Alkynylation of peripheral pyridine[104,106,107] and sulfide[28] groups have been employed for the preparation of cationic SubPcs. Acylation of hydroxyl groups has been exploited for the introduction of ester functionalities,[108-110] whereas deprotection of silyl

[96] M. V. Martínez-Díaz, M. Quintiliani, T. Torres, *Synlett* **2008**, *2008*, 1-20.
[97] H. Chan, H.-L. Wong, M. Ng, C.-T. Poon, V. W.-W. Yam, *J. Am. Chem. Soc.* **2017**, *139*, 7256-7263.
[98] H. Gotfredsen, L. Broløs, T. Holmstrøm, J. Sørensen, A. V. Muñoz, M. D. Kilde, A. B. Skov, M. Santella, O. Hammerich, M. B. Nielsen, *Org. Biomol. Chem.* **2017**, *15*, 9809-9823.
[99] H. Gotfredsen, T. Holmstrøm, A. V. a. Muñoz, F. E. Storm, C. G. Tortzen, A. Kadziola, K. V. Mikkelsen, O. Hammerich, M. B. Nielsen, *Org. Lett.* **2018**, *20*, 5821-5825.
[100] Q. Xu, Y. Gao, X. Wu, H. Hang, H. Li, Y. Chen, W. Wang, H. Tong, *New J. Chem.* **2019**, *43*, 16385-16390.
[101] G. Zango, M. Krug, S. Krishna, V. Mariñas, T. Clark, M. V. Martínez-Díaz, D. M. Guldi, T. Torres, *Chem. Sci.* **2020**, *11*, 3448-3459.
[102] M. Á. Revuelta-Maza, E. Fazio, G. de la Torre, T. Torres, *J. Porphyrins Phthalocyanines* **2017**, *21*, 782-789.
[103] H. Hang, X. Wu, Q. Xu, Y. Chen, H. Li, W. Wang, H. Tong, L. Wang, *Dyes and Pigments* **2019**, *160*, 243-251.
[104] I. Sánchez-Molina, A. Soriano, C. G. Claessens, T. Torres, H. J. Bolink, *J. Porphyrins Phthalocyanines* **2013**, *17*, 1016-1021.
[105] J. Guilleme, M. J. Mayoral, J. Calbo, J. Aragó, P. M. Viruela, E. Ortí, T. Torres, D. González-Rodríguez, *Angew. Chem. Int. Ed.* **2015**, *54*, 2543-2547.
[106] M. B. Spesia, E. N. Durantini, *Dyes and Pigments* **2008**, *77*, 229-237.
[107] Ł. Łapok, C. G. Claessens, D. Wöhrle, T. Torres, *Tetrahedron Lett.* **2009**, *50*, 2041-2044.
[108] D. González-Rodríguez, E. Carbonell, D. M. Guldi, T. Torres, *Angew. Chem. Int. Ed.* **2009**, *48*, 8032-8036.
[109] D. González-Rodríguez, M. V. Martínez-Díaz, J. Abel, A. Perl, J. Huskens, L. Echegoyen, T. Torres, *Org. Lett.* **2010**, *12*, 2970-2973.
[110] D. González-Rodríguez, E. Carbonell, G. d. M. Rojas, C. A. Castellanos, D. M. Guldi, T. Torres, *J. Am. Chem. Soc.* **2010**, *132*, 16488-16500.

ether[63,111] groups has been performed to prepare the corresponding hydroxy-substituted SubPcs. Oxidation with *m*-chloroperbenzoic acid (*m*-CPBA) has been used to convert sulfides into sulfoxides or sulfones,[112] while reduction of triple bonds with molecular hydrogen afforded the corresponding alkyl-derivatives[107]. Fullerene moieties have been successfully linked to the SubPc periphery through cyclopropanation (Bingel) reactions.[108,110] Knoevenagel condensation reaction from thiophene-carbaldehyde substituted SubPc has also been reported.[103] Despite the sensitiveness of SubPcs to the cyanide anion, an efficient method for the preparation of peripherally cyano-substituted SubPcs from the corresponding iodo-precursors based on a mild, microwave-assisted palladium-mediated coupling reaction in the presence of zinc cyanide in DMF has been presented by our group.[41,44,92]

Ring-expansion reaction

The preparation of unsymmetrical A_3B Pcs *via* ring-expansion reaction of a SubPc precursor (A_3) in the presence of a diiminoisoindoline derivative (B), which constituted one of the first applications of SubPcs, was first reported by Kobayashi *et al.* in 1990.[113] Since then, many efforts have been dedicated to the study of this type of reactivity.[8,114,115] Different reaction conditions have been explored, and the factors affecting the efficiency of this reaction (*e.g.* the peripheral substituents of the SubPc, the nature of the diiminoisoindoline precursor, solvent and reaction temperature) have been identified. Phthalonitrile derivatives have also been employed as starting material instead of diiminoisoindolines.[116-118]

[111] D. González-Rodríguez, T. Torres, *Eur. J. Org. Chem.* **2009**, *2009*, 1871-1879.
[112] D. González-Rodríguez, T. Torres, *Tetrahedron Lett.* **2009**, *50*, 860-862.
[113] N. Kobayashi, R. Kondo, S. Nakajima, T. Osa, *J. Am. Chem. Soc.* **1990**, *112*, 9640-9641.
[114] A. Wang, L. Long, C. Zhang, *Tetrahedron* **2012**, *68*, 2433-2451.
[115] V. N. Nemykin, S. V. Dudkin, F. Dumoulin, C. Hirel, A. G. Gurek, V. Ahsen, *Arkivoc* **2014**, *1*, 142-204.
[116] S. Chauhan, P. Kumari, *Tetrahedron* **2009**, *65*, 2518-2524.
[117] A. L. Ochoa, T. C. Tempesti, M. B. Spesia, M. E. Milanesio, E. N. Durantini, *Eur. J. Med. Chem.* **2012**, *50*, 280-287.
[118] T. C. Tempesti, M. T. Baumgartner, *J. Porphyrins Phthalocyanines* **2015**, *19*, 1088-1094.

Characterization of SubPcs

Single crystal X-ray diffraction

SubPcs are characterized by a cone-shaped geometry, as confirmed by X-ray diffraction analysis. The nature of the axial and peripheral substituents do not practically affect the position of the N and C atoms of the ring, with the exception of small variations in terms of bond lengths and bond angles at the level of the $Y(N_i)_3$ tetrahedron, where Y indicates the apical ligand and N_i refers to the isoindolic nitrogen atoms.[8] As a matter of fact, the B-Y bond length increases descending along the halogen series, while it is almost independent on the nature of the peripheral substituents of the macrocycle. The N_i-B-N_i and Y-B-N_i bond angles are slightly deformed with respect to that of an ideal tetrahedron. As a general trend, the former decrease and the latter increase as the electronegativity of the atom of the apical substituent directly linked to the central boron increases.

Remarkably, the X-ray crystal structure of a SubPc cation having a weakly coordinating carborane anion has also been reported, showing the tendency of the central boron to adopt a planar geometry, as expected for a tricoordinated B atom.[119]

Mass spectrometry

SubPcs usually present very clean mass spectra in which the major peak corresponds to the molecular ion. In addition, a peak corresponding to the loss of the axial ligand is quite commonly detected.

NMR Spectroscopy

As a consequence of the low tendency of SubPcs to form aggregates in solution, their ^{1}H-NMR spectra are usually characterized by sharp peaks which chemical shifts do not depend on the concentration of the sample. Due to the diatropic ring current generated by the 14 π-electron aromatic core, the signals of the protons of the isoindolic benzene rings appear at low field, whereas the signals of the protons of the axial substituent are shifted upfield with respect to that of the corresponding free ligand.[8] As an example, the axial phenyl group in H_{12}SubPc-Ph gives rise to three signals at 6.63, 6.51 and 5.37 ppm, being the latter the one corresponding to the closest proton to the SubPc core, whereas the signals of the *ortho* and *meta* protons of the macrocyclic framework appear at 8.78-8.76 and 7.81-7.79 ppm, respectively.[48] Peripheral groups influence the chemical shifts of the isoindolic protons in a predictable way, according to

[119] T. Kato, F. S. Tham, P. D. Boyd, C. A. Reed, *Heteroat. Chem.* **2006**, *17*, 209-216.

their electronic nature. On the contrary, the effect of the axial substituent is not as clear. However, variations in the chemical shifts of the isoindolic protons of SubPcs substituted with different axial ligands suggest the existence of a communication between the aromatic macrocycle and the apical substituent.[8]

Infrared spectroscopy

Infrared (IR) spectra of SubPcs are dominated by the bands arising from the bending and stretching of the C-C and C-N bonds of the macrocycle. For SubPcs bearing an axial halogen, a decrease of the wavenumber corresponding to the B-Y stretching (where Y stands for the axial substituent) is observed descending along the halogen series, in accordance with the decreasing electronegativity of the ligand. Values of 2016, 960 and 622 cm^{-1} have been reported, respectively, for the B-F, B-Cl and B-Br stretching in H_{12}SubPc derivatives.[19] Concerning SubPcs axially substituted with alkyloxy or aryloxy ligands, wavenumbers of 1119 cm^{-1} and 1052 cm^{-1} have been found for the B-O stretching in *t*-butoxy- and phenoxy-substituted derivatives, respectively.[19] In the presence of a thiophenoxy axial substituent, a B-S stretching band at 962 cm^{-1} has been observed, whereas axial amino ligands give rise to B-N stretching bands located between 1060 and 1107 cm^{-1}.[48] The decrease of the B-Y stretching wavenumber observed upon replacing an oxygen with a sulfur is in line with the trend observed within the halogen series. On the other hand, the difference between the ν(C=O) and the ν(C-O) wavenumber detected for SubPcs axially substituted with acetate and trifluoroacetate groups confirmed the monodentate ligand character of the apical substituents.[19]

UV-vis absorption spectroscopy

Absorption spectra of SubPcs feature two main bands in the 260-370 region and in the 460-580 region, respectively (Figure 5). The high-energy absorption (*i.e.* Soret band or B band) originates from the $S_0 \rightarrow S_2$ transition, whereas the absorption at higher wavelengths (namely, the Q band) is attributable to the $S_0 \rightarrow S_1$ transition. Moreover, the vibrational structure of the Q band is commonly observed. Although the overall shape of the UV-vis spectra of SubPcs is similar to that of Pcs, both the B and the Q bands are blue-shifted with respect to the corresponding Pc transitions as a consequence of the lower number of π-electron in the aromatic circuit (*i.e.*, 14 in SubPcs *versus* 18 in Pcs). Moreover, the molar extinction coefficients (ε) of the main absorptions decrease when moving from Pcs to SubPcs, being the ε values of the Q band of SubPcs of the order of $5\text{-}6 \cdot 10^4$ M^{-1} cm^{-1}.[8] This could be attributed to the non-planar geometry of the SubPc macrocycle.[81] Concentration effects are generally absent, confirming the low tendency of SubPcs towards aggregation.

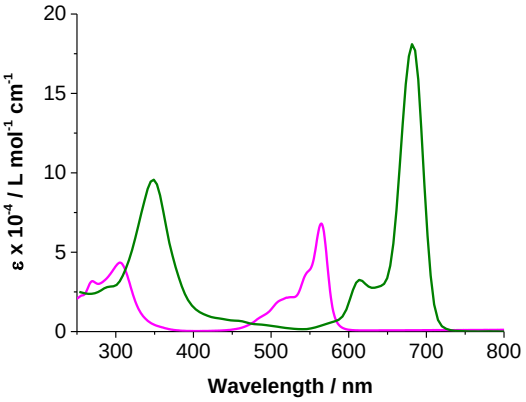

Figure 5. Typical UV-vis spectrum of a SubPc (pink) compared to that of a ZnPc (green).

In general, axial ligands have none or very little influence on the position of the absorption bands.[8,58,66,67,88,120] On the other hand, both electron-donor and electron-withdrawing peripheral substituents able to slightly extend the π-conjugation of the macrocycle produce a bathochromic shift of the Q band with respect to the unsubstituted SubPc derivative.[8,120] When the SubPc is substituted with π-donor atoms (*e.g.* oxygen, nitrogen or sulfur), this effect is generally stronger and increases with the π-donating ability of the heteroatom linked to the macrocycle as well as with the number of π-donor peripheral substituents.[42,111,121,122] Moreover, additional bands in the 400-500 region attributable to $n \rightarrow \pi^*$ transition due to π-donation from the heteroatom lone pair to the macrocycle are observed for these derivatives.

In SubPc-based multicomponent systems, ligand-centered transitions or other photophysical events (*e.g.* ground state charge-transfer processes) can take place, leading to additional features in the absorption spectra of these conjugates.

Emission spectroscopy

Emission spectra of SubPcs are commonly the mirror image of the absorption Q band. Fluorescence emission maxima are usually located between 575 and 670 nm, and are shifted accordingly to the Q-band maxima as a function of the substitution pattern of the macrocycle.[8] In general, very small Stokes shifts (around 10-15 nm) are observed, along with unusually narrow

[120] M. Dowds, M. B. Nielsen, *Mol. Syst. Des. Eng.* **2021**.
[121] D. González-Rodríguez, T. Torres, D. M. Guldi, J. Rivera, M. Á. Herranz, L. Echegoyen, *J. Am. Chem. Soc.* **2004**, *126*, 6301-6313.
[122] D. González-Rodríguez, C. G. Claessens, T. Torres, S. Liu, L. Echegoyen, N. Vila, S. Nonell, *Chem. Eur. J.* **2005**, *11*, 3881-3893.

widths at half of the maximum intensity (*i.e.*, 60-80 nm). Such spectral features suggest a very small geometric distortion between the ground state and the singlet excited state as well as a narrow density of states of the HOMO and LUMO levels.[123] Normally, modulation of solvent polarity does not lead to systematic changes in the absorption and emission maxima, suggesting a negligible variation of the dipole moment between the ground state and the singlet excited state. Singlet excited state energies of approximately 2.1-2.0 eV are commonly calculated from the absorption and emission spectra of SubPcs.[8] These values are significantly higher than those observed for Pcs (around 1.7 eV) and are consistent with the HOMO-LUMO gaps calculated from cyclic voltammetry measurements. Fluorescence quantum yields (ϕ_F) of SubPcs are generally around 0.2-0.5, although higher values can be observed in some cases.[8] In general, low ϕ_F values can be rationalized on the basis of aggregation issues or fast intersystem crossing (ISC) processes in heavy-atom-containing SubPc derivatives. In addition, photoinduced energy transfer and electron transfer events in SubPc-based multicomponent systems may result in the quenching of the SubPc emission.[8,120]

On the other hand, triplet excited state energies of approximately 1.45 eV are commonly calculated from phosphorescence emission maxima, which are located in the near-infrared region.[122] Thus, singlet-triplet energy gaps of around 0.65 eV are normally found for SubPc derivatives, somewhat bigger than those calculated for Pcs (0.5-0.6 eV).[8]

Voltammetry

Both the first oxidation and the first reduction of SubPcs are one-electron processes. Reduction is often reversible, whereas oxidation gives rise to less stable species. Upon scanning at more positive or negative potentials, several redox events are typically observed. These events, which in some cases are multi-electronic, are usually irreversible or quasi-reversible.[8]

The peripheral substitution of the macrocycle influences the first oxidative or reductive half-wave potentials in a predictable way. Generally, the first reductive event is observed between -1.58 and -0.82 V, while the first oxidative event is detected between +1.15 and 0.37 V employing Fc/Fc^+ as internal reference.[8] On the other hand, the nature of the axial ligand influences to a much lesser extent the position of the redox peaks, although it may affect considerably the reversibility of the redox processes.[124]

---

[123] D. D. Díaz, H. J. Bolink, L. Cappelli, C. G. Claessens, E. Coronado, T. Torres, *Tetrahedron Lett.* **2007**, *48*, 4657-4660.

[124] D. González-Rodríguez, T. Torres, M. M. Olmstead, J. Rivera, M. Á. Herranz, L. Echegoyen, C. A. Castellanos, D. M. Guldi, *J. Am. Chem. Soc.* **2006**, *128*, 10680-10681.

Theoretical calculations

Geometry, electronic structure, electrochemical and spectroscopic features of SubPcs have been thoroughly investigated by theoretical calculations.[125-131] Theoretical studies on redox processes in SubPcs evidenced that the cone-shaped geometry and the electronic density distribution of the macrocycle are maintained upon electron exchanges.[127] The effect of the ring substituents,[128] the axial ligand[129] and solvent[130] on the absorption profile of SubPcs have also been explored. The 0-0 energies have been calculated and the origin of the shapes of the absorption and emission bands in terms of vibrational contributions have been unraveled.[131]

The possibility to incorporate central atoms different from boron within the SubPc framework has also been investigated through theoretical calculations.[132-141] The stability of derivatives bearing Al, Ga, Si, Ge, Fe, Co, Ni, Cu or Zn as central atom was found to be lower than that of B-SubPcs. In these species, a more pronounced pyramidal geometry was calculated, whereas the introduction of C as central atom provides the required angles for a regular tetrahedron.[132-134,141] Additional theoretical investigations on SubPcs in which the central boron had been replaced by different trivalent atoms (*i.e.* Al, Ga, In, Sc and Y) revealed that the degree of openness of the cone depends on the nature of the central species.[140] Recently, Be-SubPcs complexes were shown to be thermodynamically stable in the gas phase.[138,139] Their absorption spectra were found to be similar to those of boron-containing analogues, unlike Al-, Ga-, Zn- and Ni-SubPcs which revealed red-shifted absorptions.[137,138,141]

---

[125] V. Ferro, J. G. a. de la Vega, R. González-Jonte, L. Poveda, *J. Mol. Struct. (Theochem)* **2001**, *537*, 223-234.
[126] X. D. Gong, H. M. Xiao, H. Tian, *J. Mol. Struct. (Theochem)* **2002**, *593*, 93-100.
[127] V. Ferro, L. Poveda, C. Claessens, R. González-Jonte, J. García de la Vega, *Int. J. Quantum Chem* **2003**, *91*, 369-375.
[128] A. M. Lamsabhi, M. Yáñez, O. Mó, C. Trujillo, F. Blanco, I. Alkorta, J. Elguero, E. Caballero, M. S. Rodríguez-Morgade, C. G. Claessens, *J. Porphyrins Phthalocyanines* **2011**, *15*, 1220-1230.
[129] G. Li, S. Zheng, *Spectrochim. Acta, Part A* **2019**, *222*, 117180.
[130] X. Chen, W. Chen, S. Zheng, *J. Porphyrins Phthalocyanines* **2018**, *22*, 670-678.
[131] C. Azarias, M. n. Pawelek, D. Jacquemin, *J. Phys. Chem. A* **2017**, *121*, 4306-4317.
[132] Y. J. Yang, Z. M. Su, *Int. J. Quantum Chem* **2005**, *103*, 54-59.
[133] D. Zdravkovski, M. Milletti, *J. Mol. Struct. (Theochem)* **2005**, *717*, 85-89.
[134] Y. Yang, *Chem. Phys. Lett.* **2011**, *511*, 51-56.
[135] Y. Yang, *Polyhedron* **2012**, *42*, 249-257.
[136] Y. Yang, *Polyhedron* **2012**, *33*, 310-318.
[137] M. M. Montero-Campillo, A. M. Lamsabhi, O. Mó, M. Yáñez, *ChemPhysChem* **2013**, *14*, 915-922.
[138] M. M. Montero-Campillo, A. M. Lamsabhi, O. Mó, M. Yáñez, *J. Phys. Chem. A* **2016**, *120*, 4845-4852.
[139] M. M. Montero-Campillo, O. Mó, M. Yáñez, *Can. J. Chem.* **2016**, *94*, 1015-1021.
[140] M. J. Waters, D. Hashemi, G. Shi, E. Kioupakis, J. Kieffer, *J. Electron. Mater.* **2019**, *48*, 2962-2970.
[141] W. Chen, S. Peng, S. Zheng, *Spectrochim. Acta, Part A* **2020**, *229*, 118018.

Organization of SubPcs

Organization in the solid state

The organization of adjacent SubPc units within a crystal lattice can be described in terms of mutual arrangement of the π-surfaces (*i.e.* concave-concave, convex-convex or concave-convex) and mutual arrangement of the isoindole units constituting the SubPc macrocycle (namely head-to-head, tail-to-tail, and head-to-tail).[34] A concave-to-axial ligand motif can also be found in the crystalline solid state. Six observed solid-state arrangements of adjacent SubPc molecules are displayed in Figure 6.

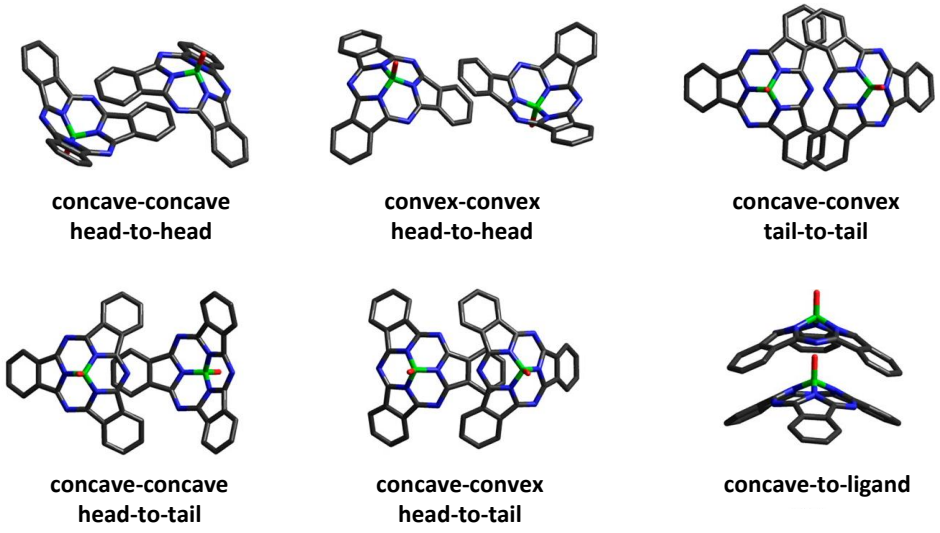

Figure 6. Observed arrangements of adjacent SubPc units in the solid state. Adapted from ref. 8.

Both axial and peripheral substituents affect the organization of SubPcs within the crystal. In this regard, it is worth to mention the work of the group of Bender, which reported a series of systematic studies on the solid-state arrangement of SubPcs.[53,62,64,67,88,142-147]

---

[142] A. S. Paton, A. J. Lough, T. P. Bender, *CrystEngComm* **2011**, *13*, 3653-3656.
[143] A. S. Paton, G. E. Morse, A. J. Lough, T. P. Bender, *CrystEngComm* **2011**, *13*, 914-919.
[144] J. S. Castrucci, M. G. Helander, G. E. Morse, Z.-H. Lu, C. M. Yip, T. P. Bender, *Cryst. Growth Des.* **2012**, *12*, 1095-1100.
[145] A. S. Paton, G. E. Morse, A. J. Lough, T. P. Bender, *Cryst. Growth Des.* **2013**, *13*, 5368-5374.
[146] E. Bukuroshi, J. Vestfrid, Z. Gross, T. P. Bender, *New J. Chem.* **2019**, *43*, 16730-16737.
[147] E. Bukuroshi, S. Wong, T. Mudigonda, K. Nova, A. Dumont, D. Holst, Z.-H. Lu, T. P. Bender, *Mol. Sys. Des. Eng.* **2021**, *6*, 308-326.

Organization in thin films

Thin films of SubPcs have been obtained both by vapor deposition[148,149] and by solution-processing techniques, such as spin coating.[150-153] In addition, the supramolecular organization of different SubPcs in Langmuir monolayers and Langmuir-Blodgett films has been investigated, revealing different dispositions at the gas/water interface, (*i.e.* edge-on *versus* side-on) as a function of the nature of the peripheral and axial substituents.[77] In comparison with Pcs, these contracted porphyrinoids show a lower degree of intermolecular interactions, probably due to their conical structure.

Organization in liquid crystalline phases

By virtue of their structure, SubPcs constitute good candidates for the obtention of columnar mesophases. In this regard, axially chlorinated SubPcs bearing long (*i.e.* C_{10}-C_{18}) thioalkyl chains have been studied at the end of last century, showing enantiotropic liquid crystalline behavior.[154] In particular, the investigated C_{10} and C_{12} derivatives exhibited mesomorphic behavior at room temperature. More recently, the organization of SubPc-F species functionalized with peripheral aryl-ethynyl or aryl-amide substituents has been thoroughly investigated by Torres, González-Rodríguez, Extebarria, Kemerink and co-workers.[91,155-157] Remarkably, these derivatives arrange in a non-centrosymmetric fashion, resulting in liquid crystalline materials that can be aligned in the presence of electric fields and that show permanent or switchable polarization. The assembly of a SubPc-F derivative bearing six C_{12} thioalkyl chains into a non-centrosymmetric columnar mesophase has also been reported.[24]

[148] C. Mattheus, W. Michaelis, C. Kelting, W. Durfee, D. Wöhrle, D. Schlettwein, *Synth. Met.* **2004**, *146*, 335-339.
[149] I.-H. Ryu, J. Kim, S.-G. Yim, J. *Nanoelectron. Optoelectron.* **2010**, *5*, 191-194
[150] G. Rojo, A. Hierro, M. Díaz-García, F. Agulló-López, B. Del Rey, A. Sastre, T. Torres, *Appl. Phys. Lett.* **1997**, *70*, 1802-1804.
[151] G. Rojo, F. Agulló-López, B. Del Rey, T. Torres, *J. Appl. Phys.* **1998**, *84*, 6507-6512.
[152] Y. Ren, A. M. Hiszpanski, Y.-L. Loo, *Chem. Mater.* **2015**, *27*, 4008-4014.
[153] Y. Shu, J. Wang, Y. Tian, X. Liang, S. Lin, B. Ma, *Adv. Mater. Interfaces* **2016**, *3*, 1600179.
[154] S. H. Kang, K. Kim, Y.-S. Kang, W.-C. Zin, G. Olbrechts, K. Wostyn, K. Clays, A. Persoons, *Chem. Commun.* **1999**, 1661-1662.
[155] J. Guilleme, E. Cavero, T. Sierra, J. Ortega, C. L. Folcia, J. Etxebarria, T. Torres, D. González-Rodríguez, *Adv. Mater.* **2015**, *27*, 4280-4284.
[156] A. V. Gorbunov, M. García Iglesias, J. Guilleme, T. D. Cornelissen, W. C. Roelofs, T. Torres, D. González-Rodríguez, E. W. Meijer, M. Kemerink, *Sci. Adv.* **2017**, *3*, e1701017.
[157] M. J. Mayoral, T. Torres, D. González-Rodríguez, *J. Porphyrins Phthalocyanines* **2020**, *24*, 33-42.

Organization on surfaces

SubPcs have been shown to adsorb over both non-metallic and metallic surfaces. A preferential Cl-down orientation (*i.e.*, with the axial chlorine pointing towards the surface) was found on Si(111)-(7 x 7)[158] and KBr(001)[159] surfaces as well as upon deposition of SubPcs onto some metallic substrates, such as Ag(111).[160-162] In a more recent study, two distinct configurations (namely Cl-down and Cl-up) of SubPcs on an Ag(100) surface were observed.[163] On the other hand, when deposited on Au(111), SubPc molecules tend to orient with the Cl atom pointing out of the substrate.[164,165] This Cl-up orientation is further stabilized in the presence of peripheral thioether ligands, as a consequence of the high affinity between sulfur and gold.[165] Interestingly, Cu(111) surfaces are less prone to induce a specific SubPc orientation, which was exploited to investigate the STM-triggered flip-flop switching of adsorbed SubPc arrays.[166-168] The self-assembly of SubPc-Cl on Cu(111) was recently investigated by means of a combination of STM and DFT studies by Monti, Zojer and co-workers.[169] In this work, two distinct adsorption configurations were observed, which were assigned to Cl-up molecules and dechlorinated DeCl-up molecules. In contrast to what reported in previous studies, no evidence was found for Cl-down molecules. As a matter of fact, the latter configuration was found to be unstable and thus unlikely to occur in the investigated conditions (Figure 7).

In general, the organization of SubPc molecules over metal surfaces strongly depends on coverage and deposition temperature.[160-162,170-172] Although further investigation is needed to

---

[158] H. Yanagi, D. Schlettwein, H. Nakayama, T. Nishino, *Phys. Review B* **2000**, *61*, 1959-1964.
[159] L. Nony, E. Gnecco, A. Baratoff, A. Alkauskas, R. Bennewitz, O. Pfeiffer, S. Maier, A. Wetzel, E. Meyer, C. Gerber, *Nano Lett.* **2004**, *4*, 2185-2189.
[160] S. Berner, M. Brunner, L. Ramoino, H. Suzuki, H.-J. Güntherodt, T. Jung, *Chem. Phys. Lett.* **2001**, *348*, 175-181.
[161] H. Suzuki, S. Berner, M. Brunner, H. Yanagi, D. Schlettwein, T. A. Jung, H.-J. Güntherodt, *Thin Solid Films* **2001**, *393*, 325-328.
[162] S. d. Berner, M. De Wild, L. Ramoino, S. Ivan, A. Baratoff, H.-J. Güntherodt, H. Suzuki, D. Schlettwein, T. Jung, *Phys. Review B* **2003**, *68*, 115410.
[163] P. J. Whiteman, J. F. Schultz, Z. D. Porach, H. Chen, N. Jiang, *J. Phys. Chem. C* **2018**, *122*, 5489-5495.
[164] S. Mannsfeld, H. Reichhard, T. Fritz, *Surf. Sci.* **2003**, *525*, 215-221.
[165] H. Yanagi, H. Mukai, M. Nair, *Thin Solid Films* **2006**, *499*, 123-128.
[166] H. Yanagi, K. Ikuta, H. Mukai, T. Shibutani, *Nano Lett.* **2002**, *2*, 951-955.
[167] H. Yanagi, K. Ikuta, *Surf. Sci.* **2005**, *581*, 9-16.
[168] Y. Hisao, *Macroheterocycles* **2019**, *12*, 244-254.
[169] N. Ilyas, S. S. Harivyasi, P. Zahl, R. Cortes, O. T. Hofmann, P. Sutter, E. Zojer, O. L. Monti, *J. Phys. Chem. C* **2016**, *120*, 7113-7121.
[170] V. Petrauskas, S. Lapinskas, E. Tornau, *J. Chem. Phys.* **2004**, *120*, 11815-11821.
[171] V. Petrauskas, E. Tornau, S. Lapinskas, *Acta Phys. Pol., A* **2005**, *107*, 388-391.
[172] N. Jiang, Y. Wang, Q. Liu, Y. Zhang, Z. Deng, K.-H. Ernst, H.-J. Gao, *Phys. Chem. Chem. Phys.* **2010**, *12*, 1318-1322.

better elucidate the solid-state arrangement of SubPcs on metallic substrates, it can be said that, with some exceptions,[173] an epitaxial coverage over the complete surface is generally observed.

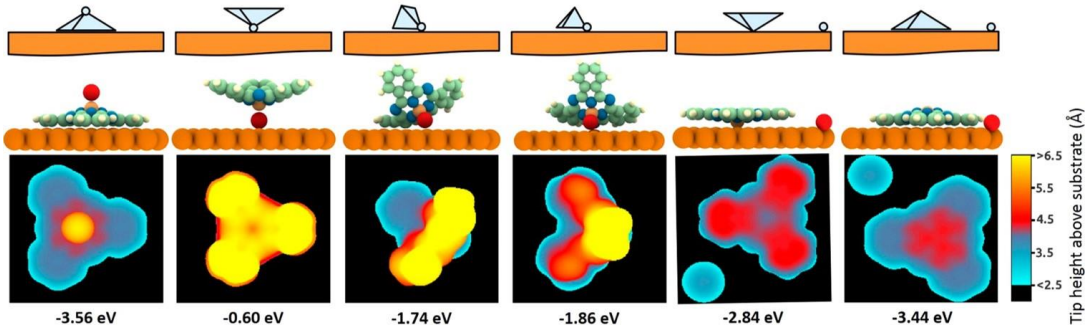

Figure 7. Adsorption configurations of SubPc-Cl on Cu(111) investigated by DFT by Monti, Zojer and co-workers with the corresponding simulated STM images and calculated adsorption energies. Adapted from ref. 169.

Organization in solution

Despite the low tendency of SubPcs towards aggregation, self-assembly in solution can be favored upon proper functionalization of the axial and peripheral positions of the macrocycle. The formation of non-centrosymmetric supramolecular polymers of a C_3-symmetric SubPc-F functionalized at the periphery with three aryl-amide substituents was reported in 2015 by González-Rodríguez, Torres, Ortí and co-workers.[105] In this work, columnar assemblies of SubPc units were shown to form through a cooperative supramolecular polymerization process driven by a combination of non-covalent interactions (*i.e.*, H-bonding between the peripheral amide groups, π-π stacking and dipolar interactions between axial B-F bonds). More recently, further studies on the solution self-assembly of this SubPc derivative disclosed a dual-mode chiral self-assembly (namely, as a dimer or as a columnar polymer) which depends on the nature of the solvent (namely, aromatic *versus* aliphatic).[174] Remarkably, each of the two SubPc enantiomers showed a strong preference to associate with itself in the dimer regime, whereas an alternate stacking order along the columns was found to be favored in the polymer regime.

[173] M. Trelka, A. Medina, D. Ecija, C. Urban, O. Gröning, R. Fasel, J. M. Gallego, C. G. Claessens, R. Otero, T. Torres, *Chem. Commun.* **2011**, *47*, 9986-9988.
[174] M. J. Mayoral, J. Guilleme, J. Calbo, J. Aragó, F. Aparicio, E. Ortí, T. Torres, D. González-Rodríguez, *J. Am. Chem. Soc.* **2020**, *142*, 21017-21031.

Applications of SubPcs

The outstanding structural, optical and electronic features of SubPcs, along with the increasing understanding of the morphology of SubPc-based molecular materials and control of the bulk properties of these derivatives, gave rise during the last decades to applications in many technologically relevant fields. On the other hand, the cone-shaped structure of these contracted porphyrinoids, and the consequent low tendency towards aggregation, along with their intense absorption and emission close to the therapeutic window and their long triplet lifetimes (on the order of 10^2 μs), which result in high singlet oxygen quantum yields, enable the use of SubPcs in biomedical research. In this context, SubPcs have been investigated in both imaging and therapy applications.

Applications in OSCs

During the last decade and a half, SubPcs have been widely studied in the frame of molecular photovoltaics, emerging as a class of high performing materials for the preparation of organic solar cells (OSCs). Notably, by virtue of their tunable redox characteristics, these macrocycles can be employed as both donor and acceptor materials.

Since the pioneering work of Thompson, Forrest and co-workers,[175] H_{12}SubPc-Cl has been extensively investigated as donor material in planar heterojunction (PHJ) photovoltaic devices in combination with C_{60} as acceptor counterpart,[176-179] reaching efficiencies above 5%.[180] In addition to the extensive research on the H_{12}SubPc-Cl/C_{60} couple, the donor capability of other SubPcs with different axial substituents (*e.g.*, F,[181] pentafluorophenoxy[182] and *para*-substituted aryl groups[88]) as well as that of μ-oxo SubPc dimer[183] and SubNc derivatives[184] have been

[175] K. L. Mutolo, E. I. Mayo, B. P. Rand, S. R. Forrest, M. E. Thompson, *J. Am. Chem. Soc.* **2006**, *128*, 8108-8109.
[176] H. Gommans, D. Cheyns, T. Aernouts, C. Girotto, J. Poortmans, P. Heremans, *Adv. Funct. Mater.* **2007**, *17*, 2653-2658.
[177] N. Wang, J. D. Zimmerman, X. Tong, X. Xiao, J. Yu, S. R. Forrest, *Appl. Phys. Lett.* **2012**, *101*, 133901.
[178] K. Cnops, B. P. Rand, D. Cheyns, P. Heremans, *Appl. Phys. Lett.* **2012**, *101*, 143301.
[179] C.-F. Lin, S.-W. Liu, C.-C. Lee, J.-C. Hunag, W.-C. Su, T.-L. Chiu, C.-T. Chen, J.-H. Lee, *Sol. Energy Mater. Sol. Cells* **2012**, *103*, 69-75.
[180] J. Golder, C. W. Lin, C. T. Chen, *J. Chin. Chem. Soc.* **2019**, *66*, 1550-1560.
[181] S. Morris, D. Bilby, M. Sykes, H. Hashemi, M. Waters, J. Kieffer, J. Kim, M. Shtein, *Org. Electron.* **2014**, *15*, 3660-3665.
[182] G. E. Morse, J. L. Gantz, K. X. Steirer, N. R. Armstrong, T. P. Bender, *ACS Appl. Mater. Interfaces* **2014**, *6*, 1515-1524.
[183] J. S. Castrucci, R. K. Garner, J. D. Dang, E. Thibau, Z.-H. Lu, T. P. Bender, *ACS Appl. Mater. Interfaces* **2016**, *8*, 24712-24721.
[184] K. L. Sampson, G. E. Morse, T. P. Bender, *ACS Appl. Energy Mater.* **2018**, *1*, 2490-2501.

investigated in PHJ architectures. Non-fullerene acceptors such as copper hexadodecafluoro-Pc,[185] truxenone derivatives,[186] and *N*-ethyl barbituric acid bithiophene[187] have also been explored in devices based on SubPcs as donor materials.

On the other hand, the use of SubPcs as acceptors allows to overcome the drawbacks associated with fullerenes which prevent the production of cost-effective and high-performance devices. For the preparation of such fullerene-free solar cells (including the so-called "all-SubPc-based devices"), different SubPc derivatives have been employed (*e.g.* peripherally halogenated[90,92,188-191] and cyanated[92] SubPcs, axially aryloxy-[182] and aryl-substituted[88] SubPcs, H_{12}SubPc-Cl,[191-193] SubPc fused dimers[194] and μ-oxo dimers[183]) in combination with suitable donors, such as SubPcs,[90,182,188,194] subnapthalocyanines (SubNcs),[90,92,189] Pcs,[90,92,193] α-sexithiophene,[88,183,191] pentacene,[90,190] tetracene,[190] and rubrene.[192] Interestingly, a record-breaking power conversion efficiency (PCE) of 8.4% was reached by Cnops *et al.* by exploiting long-range exciton energy transfer within a three-layer device architecture (Figure 8).[195] In this system, excitons generated in the outer wider-bandgap SubPc acceptor are transferred to the smaller-bandgap SubNc acceptor and subsequently dissociated at the interface with the donor (*i.e.* α-sexithiophene).

SubPcs have been extensively investigated also in bulk-heterojunction (BHJ) photovoltaic devices,[196] leading to outstanding efficiencies as both donor and acceptor material. In 2017, an efficiency of 4% was reached using Cl_6SubPc-Cl as acceptor and PTB7-Th as donor material in a solution-processed BHJ device, as reported by Zango *et al*.[58] An alternative approach to

[185] J. Yang, S. Schumann, R. Hatton, T. Jones, *Org. Electron.* **2010**, *11*, 1399-1402.
[186] C. B. Nielsen, E. Voroshazi, S. Holliday, K. Cnops, B. P. Rand, I. McCulloch, *J. Mater. Chem. A* **2013**, *1*, 73-76.
[187] P. Sullivan, G. E. Collis, L. A. Rochford, J. F. Arantes, P. Kemppinen, T. S. Jones, K. N. Winzenberg, *Chem. Commun.* **2015**, *51*, 6222-6225.
[188] P. Sullivan, A. Duraud, l. Hancox, N. Beaumont, G. Mirri, J. H. Tucker, R. A. Hatton, M. Shipman, T. S. Jones, *Adv. Energy Mater.* **2011**, *1*, 352-355.
[189] B. Verreet, K. Cnops, D. Cheyns, P. Heremans, A. Stesmans, G. Zango, C. G. Claessens, T. Torres, B. P. Rand, *Adv. Energy Mater.* **2014**, *4*, 1301413.
[190] N. Beaumont, J. S. Castrucci, P. Sullivan, G. E. Morse, A. S. Paton, Z.-H. Lu, T. P. Bender, T. S. Jones, *J. Phys. Chem. C* **2014**, *118*, 14813-14823.
[191] D. S. Josey, J. S. Castrucci, J. D. Dang, B. H. Lessard, T. P. Bender, *ChemPhysChem* **2015**, *16*, 1245-1250.
[192] Y. Lin, J. Zhong, X. Yan, L. Li, *J. Mater. Sci.: Mater. Electron.* **2017**, *28*, 9167-9173.
[193] A. I. Koptyaev, M. Khamdoush, A. N. Fedoseev, V. V. Travkin, G. L. Pakhomov, *Macroheterocycles* **2018**, *11*, 412-417.
[194] B. Verreet, B. P. Rand, D. Cheyns, A. Hadipour, T. Aernouts, P. Heremans, A. Medina, C. G. Claessens, T. Torres, *Adv. Energy Mater.* **2011**, *1*, 565-568.
[195] K. Cnops, B. P. Rand, D. Cheyns, B. Verreet, M. A. Empl, P. Heremans, *Nat. Commun.* **2014**, *5*, 3406.
[196] R. Pandey, Y. Zou, R. J. Holmes, *Appl. Phys. Lett.* **2012**, *101*, 033308.

peripheral halogenation for the preparation of SubPc-based acceptor materials for BHJ solar cells consists in the functionalization of the SubPc macrocycle with perylene diimide (PDI) moieties[197,198] or imide groups[199] In this regard, a PDI-fused SubPc afforded in 2019 the impressive record efficiency of 7.53% in combination with PBDBT-2F as donor.[198]

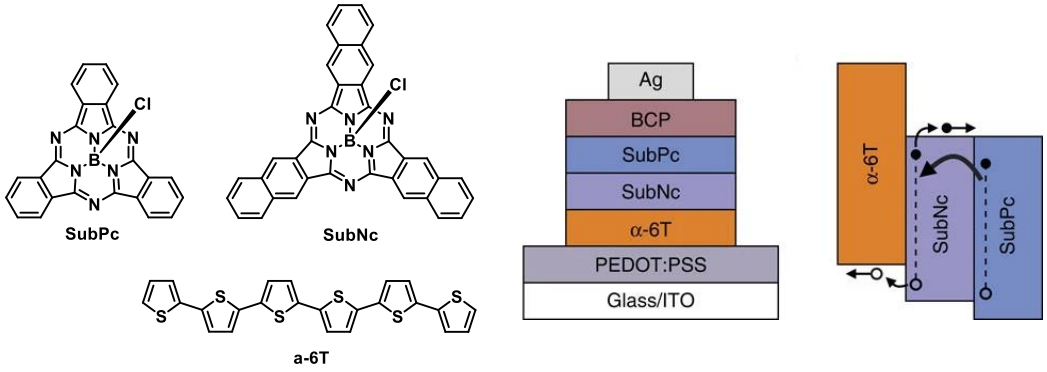

Figure 8. Left: Molecular structure of the active materials investigated by Cnops *et al.* Middle: Schematic representation of the device architecture. Right: Energy-level diagram of the active layers illustrating the two-step exciton dissociation mechanism. Adapted from ref. 195.

Although to a lesser extent, SubPcs have also been employed as sensitizers in dye-sensitized solar cells (DSSCs).[57,200,201] A respectable PCE of 5% was obtained by exploiting exciton energy transfer within a supramolecular system composed of three ZnPc sensitizer units and a pyridine-substituted SubPc, in which the latter acts as light harvester and energy donor (Figure 9).[60] Finally, the use of SubPcs as hole-transporting materials in perovskite solar cells has also been explored.[202,203]

[197] H. Hang, Z. Zhang, X. Wu, Y. Chen, H. Li, W. Wang, H. Tong, L. Wang, *J. Mater. Chem. C* **2018**, *6*, 7141-7148.
[198] T. Huang, H. Chen, J. Feng, A. Zhang, W. Jiang, F. He, Z. Wang, *ACS Materials Letters* **2019**, *1*, 404-409.
[199] X. Huang, M. Hu, X. Zhao, C. Li, Z. Yuan, X. Liu, C. Cai, Y. Zhang, Y. Hu, Y. Chen, *Org. Lett.* **2019**, *21*, 3382-3386.
[200] M. Urbani, F. A. Sarı, M. Grätzel, M. K. Nazeeruddin, T. Torres, M. Ince, *Chem. Asian J.* **2016**, *11*, 1223-1231.
[201] H. Gotfredsen, T. Neumann, F. E. Storm, A. V. Muñoz, M. Jevric, O. Hammerich, K. V. Mikkelsen, M. Freitag, G. Boschloo, M. B. Nielsen, *ChemPhotoChem* **2018**, *2*, 976-985.
[202] G. Sfyri, C. V. Kumar, G. Sabapathi, L. Giribabu, K. S. Andrikopoulos, E. Stathatos, P. Lianos, *RSC Adv.* **2015**, *5*, 69813-69818.
[203] F. Wang, X. Liu, E. Rezaee, H. Shan, Y. Zhou, Z.-X. Xu, *R. Soc. open sci.* **2018**, *5*, 180617.

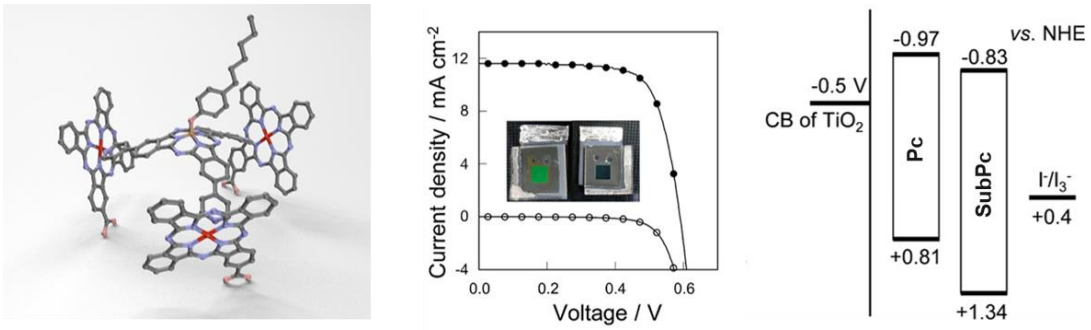

Figure 9. Left: Schematic representation of the supramolecular SubPc-Pc system adsorbed onto TiO_2 investigated by Kimura and co-workers. Middle: Photocurrent voltage obtained with a DSSC based on this supramolecular complex under standard global AM 1.5 solar condition (filled dots) and dark current (empty dots). Left: Energy level diagrams of TiO_2, the Pc derivative, the SubPc derivative, and I^-/I_3^-. Adapted from ref. 60.

Applications in OLEDs and OFETs

Since the proof-of-concept paper published by Torres and co-workers in 2007,[123] SubPcs have shown to be a promising class of emitters with a remarkably narrow emission width and excellent electrical performances in OLEDs.[34,84,204-210] In this regard, noteworthy is the work of the group of Bender. Bender and co-workers studied the impact of fluorination on luminescence,[34] reported a class of SubPc-phthalimide derivatives that, by virtue of their bipolar electrochemical characteristics, can act as both n-type and p-type charge carriers and emitters (Figure 10),[84] presented the first solution-processed organic electronic devices featuring SubPc-containing polymers as functional materials,[208] and investigated SubPcs as dopant emitters in combination with different hosts.[206,210]

[204] Y.-H. Chen, J.-H. Chang, G.-R. Lee, I.-W. Wu, J.-H. Fang, C.-I. Wu, T.-W. Pi, *Appl. Phys. Lett.* **2009**, *95*, 133302.
[205] Y.-H. Chen, Y.-J. Chang, G.-R. Lee, J.-H. Chang, I.-W. Wu, J.-H. Fang, S.-H. Hsu, S.-W. Liu, C.-I. Wu, T.-W. Pi, *Org. Electron.* **2010**, *11*, 445-449.
[206] M. G. Helander, G. E. Morse, J. Qiu, J. S. Castrucci, T. P. Bender, Z.-H. Lu, *ACS Appl. Mater. Interfaces* **2010**, *2*, 3147-3152.
[207] Y.-H. Chen, Y.-J. Cheng, G.-R. Lee, C.-I. Wu, T.-W. Pi, *Org. Electron.* **2011**, *12*, 562-565.
[208] B. H. Lessard, K. L. Sampson, T. Plint, T. P. Bender, *J. Polym. Sci. Part A: Polym. Chem.* **2015**, *53*, 1996-2006.
[209] Z. Ma, S. Liu, S. Hu, J. Yu, *J. Lumin.* **2016**, *169*, 29-34.
[210] T. G. Plint, B. H. Lessard, T. P. Bender, *Opt. Mater.* **2018**, *75*, 710-718.

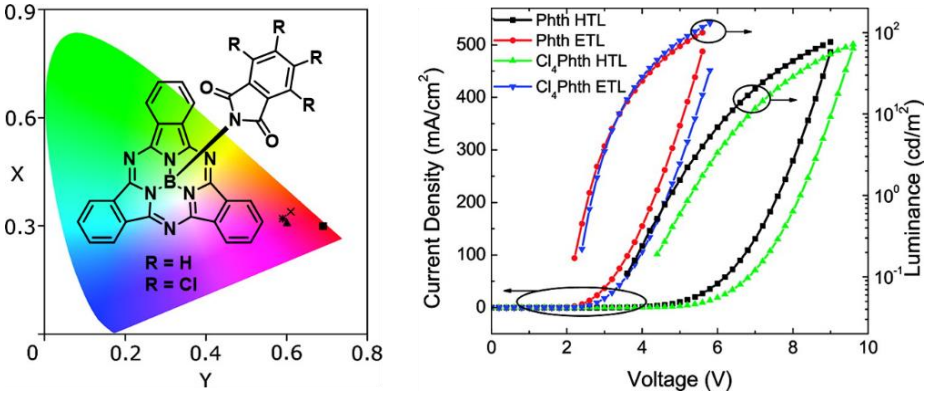

Figure 10. Left: Molecular structure of the SubPc-phthalimide derivatives investigated by Bender and co-workers and CIE color coordinates (symbol; *x, y*) for the light emission produced by the OLED devices. Right: Luminance and current density as a function of voltage for OLED devices including SubPc-phthalimide species as a hole transport layer (HTL) and an electron transport layer (ETL). Adapted from ref. 84.

SubPcs have also been investigated as components of organic field effect transistors (OFETs), which constitute the basic building blocks for many flexible integrated circuits and displays.[211-214] In this connection, it is worth to mention that electron mobilities of the order of 10^{-5}-10^{-3} cm^2 V^{-1} s^{-1} have been determined for vapor-deposited or drop-casted thin films of unsubstituted, halogenated and cyanated SubPcs.[44,144,211]

Applications in NLO

By virtue of their delocalized 14π-electron system, SubPcs have been intensively investigated as NLO materials.[215-217] Despite being first studied in terms of third harmonic generation, subsequent investigations focused on second-order nonlinear optical responses, in light of the intrinsic asymmetry of these molecules. As a matter of fact, SubPcs showed quadratic hyperpolarizability β values comparable with the best values obtained with other organic

[211] T. Yasuda, T. Tsutsui, *Mol. Cryst. Liq. Cryst.* **2006**, *462*, 3-9.
[212] C. K. Renshaw, X. Xu, S. R. Forrest, *Org. Electron.* **2010**, *11*, 175-178.
[213] X. Tong, S. R. Forrest, *Org. Electron.* **2011**, *12*, 1822-1825.
[214] J. Li, W. Shi, L. Shu, J. Yu, *J. Mater. Sci.: Mater. Electron.* **2015**, *26*, 8301-8306.
[215] G. De La Torre, P. Vazquez, F. Agulló-López, T. Torres, *J. Mater. Chem.* **1998**, *8*, 1671-1683.
[216] G. De La Torre, P. Vázquez, F. Agulló-López, T. Torres, *Chem. Rev.* **2004**, *104*, 3723-3750.
[217] M. A. Díaz-García, *J. Porphyrins Phthalocyanines* **2009**, *13*, 652-667.

molecules, mostly associated with the octupolar contribution.[154,218-223] Regarding third-order optical nonlinearities, cubic susceptibilities χ^3 values three times higher than those reported for Pcs in the same frequency range have been reported.[224-226]

Other technological applications

In addition to the applications described above, SubPcs have been employed in many other technological fields. The optical recording performances[227-229] and resistive memory behavior[97] of SubPc thin films have been investigated. Moreover, these chromophores have been employed for the preparation of electrochromic materials,[25] or as acceptors in the construction of H_2-evolving photocathodes.[230] SubPcs and SubPc dimers have been integrated as catalysts in $Li/SOCl_2$ batteries.[231,232] Recently, the use of SubPc derivatives in the growing field of photoredox catalysis has also been explored.[85,233] Moreover, SubPcs have been studied as fluorogenic and chromogenic probes for anion (*i.e.* cyanide and fluoride) sensing.[234-237] Interestingly, SubPc derivatives have also been used as stoppers for rotaxanes, where they allow to tune the slippage behavior of the ring unit.[238]

---

[218] A. Sastre, T. Torres, M. Díaz-García, F. Agulló-López, C. Dhenaut, S. Brasselet, I. Ledoux, J. Zyss, *J. Am. Chem. Soc.* **1996**, *118*, 2746-2747.
[219] B. Del Rey, U. Keller, T. Torres, G. Rojo, F. Agulló-López, S. Nonell, C. Marti, S. Brasselet, I. Ledoux, J. Zyss, *J. Am. Chem. Soc.* **1998**, *120*, 12808-12817.
[220] G. Olbrechts, K. Wostyn, K. Clays, A. Persoons, S. H. Kang, K. Kim, *Chem. Phys. Lett.* **1999**, *308*, 173-175.
[221] G. Olbrechts, K. Clays, K. Wostyn, A. Persoons, *Synth. Met.* **2000**, *115*, 207-211.
[222] C. G. Claessens, D. González-Rodríguez, T. Torres, G. Martín, F. Agulló-López, I. Ledoux, J. Zyss, V. R. Ferro, J. M. García de la Vega, *J. Phys. Chem. B* **2005**, *109*, 3800-3806.
[223] H. M. Kim, B. R. Cho, *J. Mater. Chem.* **2009**, *19*, 7402-7409.
[224] M. A. Díaz-García, F. Agulló-López, A. Sastre, T. Torres, W. E. Torruellas, G. I. Stegeman, *J. Phys. Chem.* **1995**, *99*, 14988-14991.
[225] Z. Liang, F. Gan, Z. Sun, X. Yang, L. Ding, Z. Wang, *Opt. Mater.* **2000**, *14*, 13-17.
[226] Z.-J. Liang, F.-L. Tang, F.-X. Gan, Z.-R. Xun, X.-H. Yang, L.-E. Ding, Z.-G. Wang, *Wuli Xuebao* **2000**, *49*, 252-255.
[227] Y. Wang, F. Gan, *Chin. Sci. Bull.* **2001**, *46*, 2013-2015.
[228] Y. Wang, D. Gu, F. Gan, *Phys. Status Solidi A* **2001**, *186*, 71-77.
[229] W.-F. Cao, H.-Y. Tu, J. Wang, H. Tian, Y. Wang, D. Gu, F. Gan, *Dyes and pigments* **2002**, *54*, 213-219.
[230] A. Morozan, T. Bourgeteau, D. Tondelier, B. Geffroy, B. Jousselme, V. Artero, *Nanotechnology* **2016**, *27*, 355401.
[231] R. Guo, Z. Dong, B. Xu, C. Song, Z. Li, J. Zhao, S. Zhang, *ECS Electrochemistry Letters* **2014**, *3*, A36.
[232] R. Guo, Z. Dong, B. Xu, C. Song, Z. Li, J. Zhao, S. Zhang, *J. Solid State Electrochem.* **2015**, *19*, 345-353.
[233] K. Matsuzaki, T. Hiromura, E. Tokunaga, N. Shibata, *ChemistryOpen* **2017**, *6*, 226-230.
[234] S. Xu, K. Chen, H. Tian, *J. Mater. Chem.* **2005**, *15*, 2676-2680.
[235] J. V. Ros-Lis, R. Martínez-Máñez, J. Soto, *Chem. Commun.* **2005**, 5260-5262.
[236] E. Palomares, M. V. Martínez-Díaz, T. Torres, E. Coronado, *Adv. Funct. Mater.* **2006**, *16*, 1166-1170.
[237] J. B. Arockiam, J. S. Park, *Spectrochim. Acta, Part A* **2019**, *207*, 112-117.
[238] Y. Kage, S. Shimizu, G. Kociok-Köhn, H. Furuta, G. D. Pantoş, *Org. Lett.* **2020**, *22*, 1096-1101.

Biomedical applications

Of particular interest, although less explored, is the application of SubPcs in the biomedical area. SubPcs have been investigated as photosensitizers in PDT[239] against bacteria[28,106,240] and carcinoma cells.[241,242] The use of SubPcs as fluorescent probes for imaging applications has also been explored.[243-246] Remarkably, the dual role of a series of SubPc derivatives as fluorescent probes for optical imaging and therapy of cancer has been recently investigated by de la Escosura, Torres, Juarranz de la Fuente and co-workers.[247] 2D and 3D imaging of different cancer cell lines revealed that the subcellular localization of the photosensitizer depends on the nature of the axial substituent (Figure 11). In addition, the investigated SubPcs showed excellent photocytotoxicities, which were found to be affected by the localization the SubPc photosensitizer.

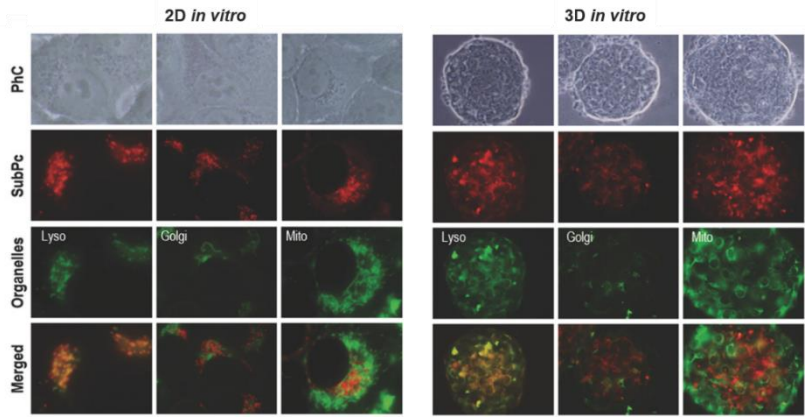

Figure 11. Subcellular localization of a SubPc bearing an axial pyrene-containing hydrophobic group in 2D cultures and 3D cultures of SCC-13 cells after 18 h of incubation. Adapted from ref. 247.

---

[239] C. M. Allen, W. M. Sharman, J. E. Van Lier, *J. Porphyrins Phthalocyanines* **2001**, *5*, 161-169.
[240] I. Ozturk, A. Tunçel, M. Ince, K. Ocakoglu, M. Hoşgör-Limoncu, F. Yurt, *J. Porphyrins Phthalocyanines* **2018**, *22*, 1099-1105.
[241] H. Xu, X.-J. Jiang, E. Y. Chan, W.-P. Fong, D. K. Ng, *Org. Biomol. Chem.* **2007**, *5*, 3987-3992.
[242] F. Yurt, F. A. Sarı, M. Ince, S. G. Colak, O. Er, H. M. Soylu, C. C. Kurt, C. B. Avci, C. Gunduz, K. Ocakoglu, *J. Photochem. Photobiol. A* **2018**, *367*, 45-55.
[243] Y. Bernhard, P. Winckler, R. Chassagnon, P. Richard, É. Gigot, J.-M. Perrier-Cornet, R. A. Decréau, *Chem. Commun.* **2014**, *50*, 13975-13978.
[244] Y. Bernhard, P. Winckler, J.-M. Perrier-Cornet, R. A. Decréau, *Dalton Trans.* **2015**, *44*, 3200-3208.
[245] R. L Calandrino, K. J McAuliffe, L. E Dolmage, E. R Trivedi, *Molecules* **2019**, *24*, 3832.
[246] F. Yurt, M. Ince, O. Er, H. M. Soylu, K. Ocakoglu, O. Yilmaz, *Photodiagnosis Photodyn. Ther.* **2019**, *26*, 361-365.
[247] E. van de Winckel, M. Mascaraque, A. Zamarrón, Á. Juarranz de la Fuente, T. Torres, A. de la Escosura, *Adv. Funct. Mater.* **2018**, *28*, 1705938.

Donor-acceptor systems for solar energy conversion

The energy issue

The increasing global energy consumption, the progressive depletion of fossil fuels, and the climate change associated with their massive use are major issues in modern world.

In 2018, world energy supply exceeded 14000 million tons of oil equivalents (Mtoe).[248] More importantly, due to population growth and economic development, the global energy demand is expected to rise significantly in the next decades.[249,250]

Global economy is based on fossil fuels as primary energy source. As a matter of fact, about 81% of world energy supply in 2018 came from oil, coal and natural gas (Figure 12).[248] Thus, as the current consumption rate is considerably higher than formation rate, fossil fuel reserves are destined to run out shortly. On the basis of global reserves-to-production ratios, it was estimated that world proved oil, natural gas and coal reserves in 2019 accounted for respectively 50, 49.8 and 132 years of current production.[251]

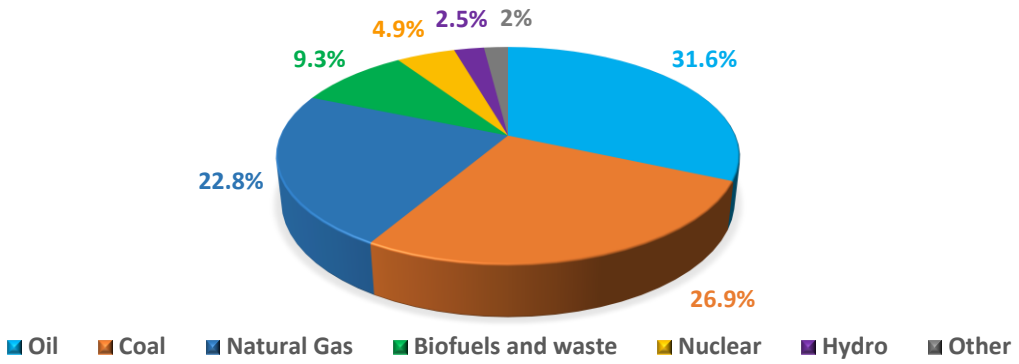

Figure 12. 2018 Source share of total energy supply (total: 14282 Mtoe).[248]

On the other hand, the enormous increase in greenhouse gas emissions related to the use of fossil fuels is the main cause of global warming. During the last years, annual carbon dioxide emissions attributable to the consumption of oil, natural gas and coal for combustion-related activities were estimated to exceed 33000 million tons (Mt).[248,251] According to the

[248] IEA (2020), Key World Energy Statistics 2020, IEA, Paris.
[249] R. F. Service, *Science* **2005**, *309*, 548-551.
[250] Commission of the European Communities. COM(2006) 105 final. Green paper: A European strategy for sustainable, competitive and secure energy, SEC(2006) 317.
[251] BP Statistical Review of World Energy, **2020**.

Intergovernmental Panel in Climate Change (IPCC), the globally averaged combined land and ocean surface temperature data show a warming of 0.85 °C over the period 1880-2012, and a substantially higher temperature increase is expected by the end of the century if an effective global climate change mitigation policy is not implemented.[252]

In summary, current global trends in energy supply are both economically and environmentally unsustainable. As a consequence, the replacement of fossil fuels by alternative energy sources constitutes one of the most urgent challenges of our time.[253]

One of the most promising and sustainable approaches to cover the global energy demand in the long term is the use of solar energy. As a matter of fact, every hour Earth receives enough solar energy at its surface to supply world energy needs for one year.[254] In the frame of solar energy conversion, different approaches should be distinguished.[255] In photovoltaics, direct light-to-electrical energy conversion is realized in optoelectronic devices (*i.e.* solar cells) by exploiting the photovoltaic effect.[256] As an alternative, solar energy can be converted into stored chemical energy in the form of fuel in photosynthetic systems.

In the development of devices able to efficiently harvest, convert and store sunlight, organic chemistry plays a key role, as it constitutes a fundamental tool for the design and synthesis of molecular ensembles with tailored structural, electrochemical, and photophysical features. In this regard, natural photosynthetic systems represent a source of inspiration for the design of synthetic models for sunlight conversion. Thus, many efforts have been dedicated to the understanding of the processes taking place in natural photosynthesis, with the final aim to produce efficient artificial devices for solar-based energy production.

[252] IPCC, 2014: *Climate Change 2014: Synthesis Report. Contribution of Working Groups I, II and III to the Fifth Assessment Report of the Intergovernmental Panel on Climate Change* [Core Writing Team, R.K. Pachauri and L.A. Meyer (eds.)]. IPCC, Geneva, Switzerland, 151 pp.
[253] V. Balzani, N. Armaroli, *Energy for a sustainable world: from the oil age to a sun-powered future*, John Wiley & Sons, **2010**.
[254] Q. Schiermeier, J. Tollefson, T. Scully, A. Witze, O. Morton, *Nature* **2008**, *454*, 816-823.
[255] R. Eisenberg, D. G. Nocera, *Inorg. Chem.* **2005**, *44*, 6799-6801.
[256] A. E. Becquerel, *C. R. Hebd. Seances Acad. Sci.* **1839**, *9*, 561-567.

Natural photosynthesis

In chlorophyll-based natural photosynthesis,[257,258] solar energy is converted into chemical energy through cascades of energy and electron transfer events that are triggered by photoexcitation and ultimately lead to the synthesis of carbohydrates. Natural photosynthesis can be conveniently divided into four distinct phases.[258]

In the first phase, light is absorbed by the antenna system, and excitation energy is eventually delivered to the reaction center through a series of sequential energy transfer processes (Figure 13). The antenna system consists of different protein complexes in which chlorophyll and other pigments (*e. g.* carotenoids) are specifically associated with proteins and precisely oriented in a unique structure. Energy collection in photosynthetic systems can be visualized by exploiting the analogy of an energy funnel. Peripheral antenna complexes generally absorb light at shorter wavelengths than do those at the core. As a consequence, sequential energy transfers from higher-energy to lower-energy pigments eventually deliver excitation energy to the proximity of the photochemical reaction center. In the final step, excitation energy is transferred to a special pair of chlorophyll-like pigments which are located within the latter.

In the second phase of the photosynthetic process, primary electron transfer takes place from the excited special pair to a nearby electron acceptor molecule in the reaction center, generating an ion-pair.

In the third phase, a series of extremely rapid secondary electron transfer processes spatially separate the oxidized and reduced species, thus reducing charge recombination rate by orders of magnitude. In oxygenic photosynthetic organisms, which include plants, algae and cyanobacteria, two reaction center complexes (*i.e.* Photosystems I and II) are involved in a non-cyclic electron transfer chain. In Photosystem II, water is oxidized to molecular oxygen, which is released as a waste product. The extracted electrons are transported through a quinone and the cytochrome b_6f complex to Photosystem I, where, in a second light-induced electron transfer event, nicotinamide adenine dinucleotide phosphate ($NADP^+$) is reduced to NADPH. In parallel, protons are pumped across the membrane, generating an electrochemical proton gradient which drives the synthesis of adenosine triphosphate (ATP).

[257] B. Alberts, A. Johnson, J. Lewis, M. Raff, K. Roberts, P. Walters, *Molecular biology of the cell*, Garland Science **2007**

[258] R. E. Blankenship, *Molecular mechanisms of photosynthesis*, Wiley, **2014**.

The final phase consists in the synthesis and export of stable high-energy products. In this phase, NADPH and ATP, high-energy compounds of intermediate stability, are employed to power the reactions of the Calvin-Benson cycle, which finally lead to the conversion of CO_2 into sugars.

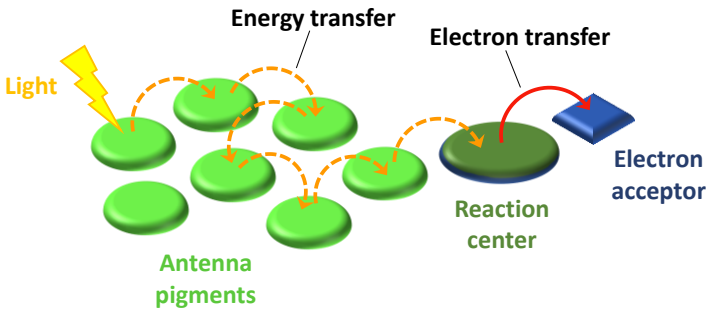

Figure 13. Cartoon illustrating the first events taking place in natural photosynthesis.

Light harvesting, excitation energy transduction and photoinduced electron transfer lie at the core of solar energy conversion in natural photosynthesis. The photophysical and electrochemical features of the molecules involved, which are determined by their intrinsic nature as well as by their environment, along with their organization within the photosynthetic system, govern the kinetics and thermodynamics of the processes that are triggered by photoexcitation, determining, in turn, the efficiency of solar energy conversion.[259-263]

On one hand, the inherent properties and ring-like organization of photosynthetic antenna pigments around the reaction center ensure the panchromatic absorption of solar light and the efficiency of energy transfer, which occurs with minimal losses. On the other hand, the electrochemical characteristics of the individual electron donor and acceptor units as well as their arrangement within the reaction center determine the effectiveness of the primary electron transfer process and the secondary events that successfully compete with charge recombination, leading to photochemical quantum yields near unity.

[259] V. Balzani, A. Credi, M. Venturi, *ChemSusChem* **2008**, *1*, 26-58.
[260] D. Gust, T. A. Moore, A. L. Moore, *Acc. Chem. Res.* **2009**, *42*, 1890-1898.
[261] I. McConnell, G. Li, G. W. Brudvig, *Chem. Biol.* **2010**, *17*, 434-447.
[262] Y. Tachibana, L. Vayssieres, J. R. Durrant, *Nat. Photonics* **2012**, *6*, 511-518.
[263] J. Barber, P. D. Tran, *J. R. Soc. Interface* **2013**, *10*, 20120984.

D-A systems as models for artificial solar energy conversion

As discussed above, the extraordinary performances observed in natural photosynthesis are based on a sophisticated optimization and synergy of photon-and charge-management. In this connection, a molecular understanding and control of the primary events taking place in photosynthetic systems as well as a deep comprehension of their mutual interplay is of fundamental importance to enable advances in the field of artificial solar energy conversion.

During the last decades, many efforts have been dedicated to the development of artificial, nature-mimicking systems in order to disclose the fundamental principles governing the processes at the basis of photosynthesis and to control the factors that ultimately influence the effectiveness of these events at the molecular level.[259-270] The final goal is the construction of synthetic devices capable of efficiently converting solar light into other energy sources, such as electrical energy or stored chemical energy.[264]

Due to the intrinsic complexity of natural photosynthetic systems, a modular approach is often employed, which consists in the design, preparation, and study of structurally simpler synthetic models with the aim to reproduce only one or a few of the fundamental steps occurring in natural photosynthesis. In this context, particular attention has been focused in enhancing light harvesting and tuning the kinetics and yields of photoinduced energy and electron transfer processes. In their most simple version, such multicomponent assemblies consist in an energy/electron donor unit (D) and an energy/electron acceptor unit (A) linked by means of covalent or supramolecular interactions. In these donor-acceptor (D-A) systems, photoexcitation of the donor or the acceptor moiety can result in either electron or energy transfer between the two units (Figure 14).

---

[264] A. F. Collings, C. Critchley, *Artificial photosynthesis: from basic biology to industrial application*, John Wiley & Sons, **2007**.
[265] D. Gust, T. A. Moore, A. L. Moore, *Acc. Chem. Res.* **1993**, *26*, 198-205.
[266] C. Herrero, B. Lassalle-Kaiser, W. Leibl, A. W. Rutherford, A. Aukauloo, *Coord. Chem. Rev.* **2008**, *252*, 456-468.
[267] M. Hambourger, G. F. Moore, D. M. Kramer, D. Gust, A. L. Moore, T. A. Moore, *Chem. Soc. Rev.* **2009**, *38*, 25-35.
[268] J. Barber, *Chem. Soc. Rev.* **2009**, *38*, 185-196.
[269] D. Gust, T. A. Moore, A. L. Moore, *Faraday Discuss.* **2012**, *155*, 9-26.
[270] B. D. Sherman, M. D. Vaughn, J. J. Bergkamp, D. Gust, A. L. Moore, T. A. Moore, *Photosynth. Res.* **2014**, *120*, 59-70.

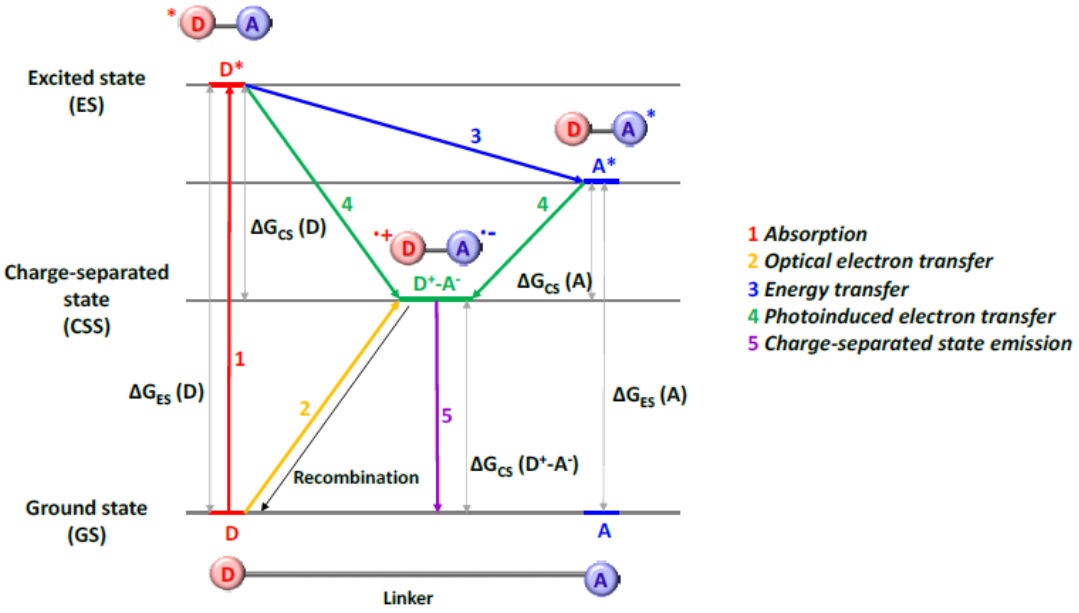

Figure 14. Schematic representation of the possible photophysical events occurring in a D-A system.

Many covalent or non-covalent, energy and/or electron D-A systems have been designed and synthesized over the decades. For the preparation of such multicomponent ensembles, a large variety of molecular building blocks has been employed, such as porphyrinoids and fullerenes to cite a couple.[271-276]

By virtue of their outstanding structural, photophysical and electrochemical properties, SubPcs have been widely used for the preparation of D-A models. An overview of SubPc-based D-A systems is given further on in this Introduction.

[271] P.-C. Lo, X. Leng, D. K. Ng, *Coord. Chem. Rev.* **2007**, *251*, 2334-2353.
[272] D. González-Rodríguez, G. Bottari, *J. Porphyrins Phthalocyanines* **2009**, *13*, 624-636.
[273] F. D'Souza, O. Ito, *Chem. Commun.* **2009**, 4913-4928.
[274] G. Bottari, G. de la Torre, D. M. Guldi, T. Torres, *Chem. Rev.* **2010**, *110*, 6768-6816.
[275] G. de la Torre, G. Bottari, M. Sekita, A. Hausmann, D. M. Guldi, T. Torres, *Chem. Soc. Rev.* **2013**, *42*, 8049-8105.
[276] G. Bottari, G. de la Torre, D. M. Guldi, T. Torres, *Coord. Chem. Rev.* **2021**, *428*, 213605.

From basic investigation on D-A systems towards applied research

As stated above, basic research in D-A systems allows for a deep understanding of the fundamental principles governing energy and electron transfer and the factors that control their efficiency and dynamics. Such a knowledge is of paramount importance for the developing of efficient artificial photosynthetic devices. Besides the preparation of solar-to-fuel systems, multicomponent D-A ensembles can also serve as models for the construction of solar-to-electricity devices, namely photovoltaic (or solar) cells. More in general, the study of the processes taking place in D-A systems is of key importance for their implementation in the expanding fields of molecular electronics and optoelectronics.

Focusing on SubPcs, besides fundamental investigation on SubPc-based D-A systems, a step forward towards more applied research in the frame of solar energy conversion has been taken through the study of SubPc-based photovoltaic devices. As a matter of fact, SubPcs have been integrated as molecular materials in several types of solar cells, including PHJ and BHJ OSCs, DSSC and perovskite solar cells. A detailed dissertation on the applications of SubPcs in photovoltaics goes beyond the aim of this Thesis. An overview of this topic has been given above in this Introduction.

At the basis of both photosynthesis and photovoltaics are the photophysical events triggered by light absorption. In the following section, a simple introduction to the basic principles underlying the main photophysical processes activated by photoexcitation is given.

General photophysical concepts

The Jablonski diagram

The relative energies of the electronic states of an organic molecule as well as the possible transitions between them can be illustrated in a state energy diagram, also known as Jablonski diagram (Figure 15).[277-279] In a Jablonski diagram, the vertical coordinate represents the potential energy of the system, whereas the horizontal coordinate has no physical meaning. Electronic states are represented by horizontal lines that are arranged in vertical order to indicate the relative energies. Usually, only the ground state and the lowest-energy excited states are displayed. Vibrational levels associated with each electronic state are also commonly represented and are arranged vertically in order of increasing energy.

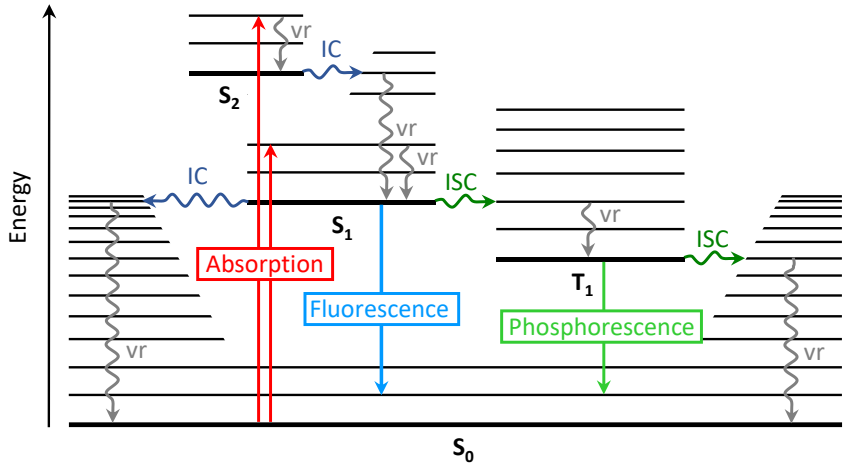

Figure 15. Jablonski diagram for an organic molecule, depicting the electronic ground state and the lowest-lying excited states as well as possible photophysical interstate transitions. Vibrational levels are represented by thin lines, except for the v = 0 levels, which are represented by thick lines. Radiative transitions are indicated by straight arrows, whereas radiationless transitions and vibrational relaxation are represented by wavy arrows. IC = internal conversion; ISC = intersystem crossing, vr = vibrational relaxation.

Interstate photophysical transitions can be radiative or radiationless processes.[278] Radiative processes include spin-allowed singlet-singlet photon absorption, spin-allowed singlet-singlet

[277] B. Wardle, *Principles and applications of photochemistry*, Wiley, **2009**.
[278] N. J. Turro, V. Ramamurthy, J. C. Scaiano, *Modern molecular photochemistry of organic molecules*, University Science Books, **2010**.
[279] V. Balzani, P. Ceroni, A. Juris, *Photochemistry and photophysics: concepts, research, applications*, Wiley, **2014**.

photon emission (known as fluorescence) and spin-forbidden singlet-triplet photon emission (referred to as phosphorescence). Normally, fluorescence and phosphorescence take place from the lowest vibrational level of the lowest singlet excited state (S_1) and from the lowest vibrational level of the lowest triplet excited state (T_1), respectively.[277] On the other hand, radiationless transitions occur between isoenergetic vibrational levels of different electronic states and include the spin-allowed non-radiative transition between states of equal spin multiplicity and the spin-forbidden non-radiative transition between states of different spin multiplicity. The former is termed internal conversion (IC), whereas the latter is named intersystem crossing (ISC).

Generally, electronically excited states are generated as "vibrationally-hot" species ($v > 0$).[277] The excess vibrational energy is dissipated as heat by collisions of vibrationally excited species with surrounding molecules. This process, which involves transitions between a vibrationally-excited level and the $v = 0$ level within a given electronic state, is known as vibrational relaxation. As vibrational relaxation is among the fastest processes occurring in the excited state, all the other processes usually take place from thermally equilibrated excited states.[279]

Besides photophysical transitions between electronic states of a single molecule, additional photophysical processes can take place as a consequence of either intermolecular interactions between different molecules or intramolecular interactions between different moieties of the same molecule. Some of these processes, which involve more than one molecular entity, are described below.

Absorption complexes and exciplexes formation

In particular cases, two or more molecules (or molecular moieties) can participate in cooperative absorption or emission. In these cases, the absorption or emission arises from ground-state or excited-state complexes of a specific stoichiometry, which are commonly formed by two molecular entities.[278] When two molecules act cooperatively to absorb a photon, an absorption complex exists in the ground state, which is responsible for the absorption. On the other hand, if two different molecules act cooperatively to emit a photon to a dissociative ground state, an exciplex exists. Thus, whereas absorption complexes possess some stability in their ground states, exciplexes do not.

Both absorption complexes and exciplexes present some significant spectroscopic features. Absorption complexes are commonly characterized by a new absorption band which is bathochromically shifted with respect to the absorptions of the individual molecular components. In contrast, exciplexes usually exhibit a new structureless emission band that is

located at longer wavelengths than the fluorescence emission of each molecular component. Moreover, in both absorption complexes and exciplexes, a concentration dependence of the intensity of the new absorption or emission bands is commonly observed.

When the molecular components of the exciplex are the same, the excited molecular complex is referred to as an excimer. Therefore, the term “exciplex” is employed only in the case of excited-state complexes formed by different molecular components. Commonly, exciplexes are formed when an electronically excited electron acceptor (or donor) molecule interacts with an electron donor (or acceptor) ground-state molecule, and their stability comes from delocalization of excitation energy accompanied by some charge transfer (CT) character.[279] Thus, exciplexes are polar species, and their emission is affected by solvent polarity.[277] As a matter of fact, an increase in solvent polarity results in the lowering of the energy level of the exciplex, while allowing also the stabilization of charged species formed by electron transfer. As a consequence, a decrease in the intensity of exciplex emission is observed in polar solvents, along with a shift of the corresponding fluorescence maximum to even higher wavelengths.

Electron transfer

In photoinduced electron transfer, an electron is transferred between an electronically excited molecule and a ground-state species.[277] Since electron transfer occurs by electron-exchange interactions, orbital overlap is required.

As it simultaneously possesses a half-filled LUMO and a half-filled HOMO, an excited-state species is both a better electron donor and a better electron acceptor than the corresponding molecule in its ground state.[278] Thus, an electronically excited molecule may act either as electron donor or as electron acceptor, depending on the electron-accepting or electron-donating ability of the partner molecule. In the first case, an electron is transferred from the LUMO of the donor to the LUMO of the acceptor (Equation 1, Figure 16). In the second case, electron transfer takes place from the HOMO of the donor to the HOMO of the acceptor (Equation 2).

$$D^{*} + A \rightarrow D^{\cdot+} + A^{\cdot-} \qquad \text{(Eq. 1)}$$

$$D + A^{*} \rightarrow D^{\cdot+} + A^{\cdot-} \qquad \text{(Eq. 2)}$$

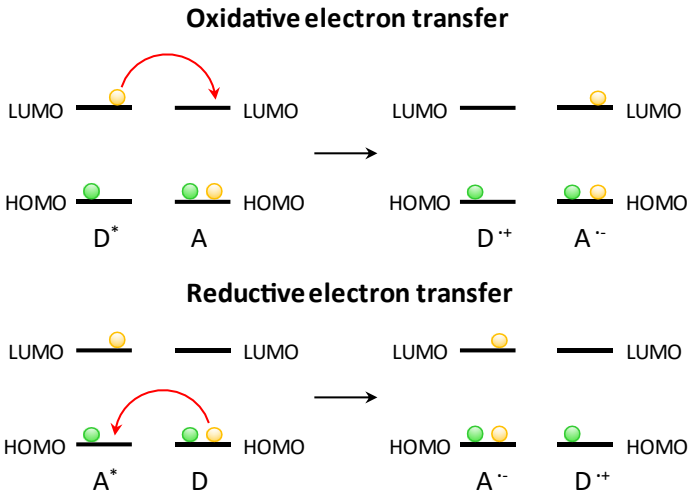

Figure 16. Schematic frontier orbital representation of electron transfer from an excited donor (oxidative electron transfer) or to an excited acceptor (reductive electron transfer).[277]

In the context of the Marcus theory of electron transfer, the potential energy surfaces on which electron transfer takes place can be represented by two bidimensional parabolic curves which intersect at the transition state (‡)(Figure 17a).[277] Thus, the free energy of activation ($\Delta G^{\neq}$) can be expressed as:

$$\Delta G^{\neq} = \frac{(\Delta G^{0} + \lambda)^{2}}{4\lambda} \qquad \text{(Eq. 3)}$$

where ΔG^{0} is the free energy change of the electron transfer event, which is a measure of the driving force of the overall process, and λ is the reorganization energy, which corresponds to the sum of the inner-sphere (bond lengths and bond angles of the two reaction partners) and outer-sphere (coordinates defining the arrangement of solvent molecules around the reacting pair) reorganization energies.

According to the collision theory, the rate constant of electron transfer (k_{et}) is given by:

$$k_{et} = A e^{\frac{-\Delta G^{\neq}}{RT}} \qquad \text{(Eq. 4)}$$

Upon combining Equations 3 and 4, the kinetics of electron transfer can be related to the thermodynamic driving force of the process.

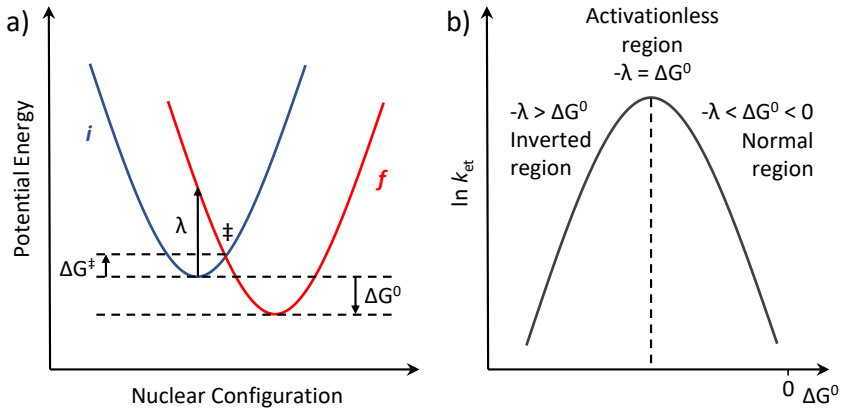

Figure 17. a) Potential energy description of an electron-transfer reaction. *i* and *f* indicate the initial and final states of the system. b) Dependence of the electron-transfer rate on the thermodynamic driving force according to the Marcus theory.

In particular, the Marcus theory predicts three distinct kinetic regions depending on the driving force of the process: 1) a normal region for small driving forces ($-\lambda < \Delta G^0 < 0$) in which the rate of electron transfer increases as the driving force increases; 2) an activationless region ($-\lambda = \Delta G^0$) in which a change in the driving force has a negligible effect in the electron-transfer rate; 3) an ''inverted'' regime ($-\lambda > \Delta G^0$) in which the rate of electron transfer decreases as the driving force increases (Figure 17b).[277]

Energy transfer

Along with electron transfer, energy transfer constitutes one of the most important interactions between an excited-state molecule and a ground-state molecule. It involves the transfer of energy from an electronically excited donor (D^*) to an acceptor in its ground state (A). As a result, the energy donor relaxes back to the ground state (D), while an electronically excited state of the acceptor (A^*) is generated (Equation 5).[277]

$$D^* + A \rightarrow D + A^* \qquad \text{(Eq. 5)}$$

In contrast with electron transfer, in energy transfer processes the excited species is always the donor, whereas the ground-state molecule can be exclusively the acceptor.[278]

Energy transfer processes are usually named according to the multiplicity of D^* and A^*, being singlet-singlet energy transfer (Equation 6) and triplet-triplet energy transfer (Equation 7) common examples.[277]

$$^1D^* + {}^1A \rightarrow {}^1D + {}^1A^* \quad \text{(Eq. 6)}$$

$$^3D^* + {}^1A \rightarrow {}^1D + {}^3A^* \quad \text{(Eq. 7)}$$

The most common energy transfer processes between organic molecules take place by two distinct types of mechanisms, namely the dipole-dipole mechanism and the electron exchange mechanism (Figure 18).[278]

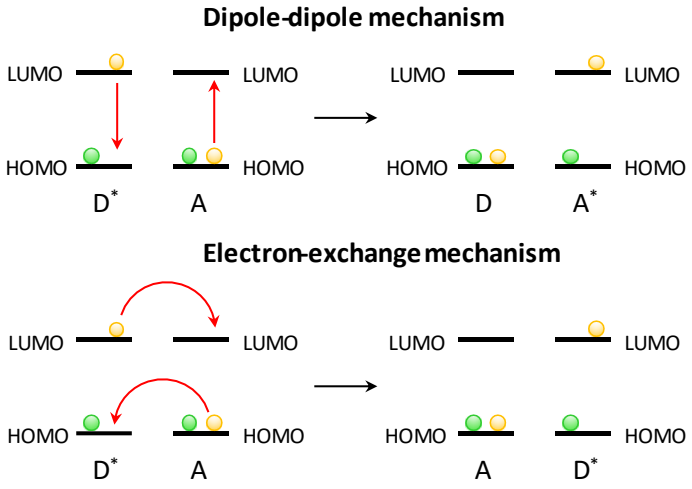

Figure 18. Schematic frontier orbital representation of the dipole-dipole and the electron-exchange mechanisms of energy transfer.

Dipole-dipole energy transfer, also known as Coulombic energy transfer or Förster resonance energy transfer (FRET), results from the interaction between the transition dipole associated with the relaxation of D^* to D and the transition dipole produced by the simultaneous electronic excitation of A to A^*.[277]

The rate constant of FRET depends, among others, on the spectral overlap between the fluorescence spectrum of the donor and the absorption spectrum of the acceptor, the size of the oscillating transition dipoles, the spatial separation between the donor and the acceptor and their relative orientation.[278] FRET can only take place if spin multiplicity is conserved, as only spin conserving transitions are associated with large transition dipoles.[277] Thus, singlet-singlet energy transfer *via* the Coulombic mechanism is plausible, as neither the donor nor the acceptor undergoes a change in multiplicity. On the other hand, triplet-triplet energy transfer requires both donor and acceptor to undergo a change in multiplicity. Therefore, it cannot occur through the dipole-dipole mechanism.

The constant rate of FRET falls off as the inverse sixth power of the distance between the donor and the acceptor.[277] Thus, dipole-dipole energy transfer is a relatively long-range process, since it can be significant even at distances of the order of 10 nm. By virtue of this distance-dependence, FRET is widely used as molecular ruler to estimate distances between chromophores, and has found extensive application in the study of the structural features of biological macromolecules.

On the other hand, electron exchange energy transfer (also referred to as Dexter energy transfer) requires orbital overlap between D^* and A.[278] In particular, energy transfer by the exchange mechanism can be regarded as a simultaneous double electron transfer, one electron moving from the LUMO of the donor to the LUMO of the acceptor and the other from the HOMO of the acceptor to the HOMO of the donor (Figure 18). In order for Dexter energy transfer to occur, the overall spin states before and after the process need to have common components.[277] This enables the electron exchange mechanism to be operative in triplet-triplet energy transfer.[279]

Since it involves orbital overlap, electron exchange energy transfer is a short-range mechanism, which requires a close approach (approximately 1-1.5 nm) between the donor and the acceptor.[277] As a matter of fact, the rate constant for Dexter energy transfer falls off as an exponential function of the distance between the donor and the acceptor.[278] As for FRET, the rate of energy transfer by the exchange mechanism is also directly related to the spectral overlap integral. However, in Dexter energy transfer the extinction coefficient of the $A \rightarrow A^*$ transition is not included in the computation of the latter.

Singlet fission

Singlet fission is a process in which an organic molecule in an excited singlet state shares its excitation energy with a neighboring molecule in its ground state to form a pair of correlated triplets with overall singlet character. Subsequently, the correlated triplet pair separates into two individual triplets (Equation 8).[280,281]

$$S_1 + S_0 \leftrightarrows {}^1(T_1T_1) \leftrightarrows T_1 + T_1 \qquad \text{(Eq. 8)}$$

Due to the overall singlet nature of the correlated triplet pair, the first step is spin allowed and can be considered a form if IC, whereas the second step involves a change in spin multiplicity and thus represents the ISC part of SF.

[280] M. B. Smith, J. Michl, *Chem. Rev.* **2010**, *110*, 6891-6936.
[281] M. B. Smith, J. Michl, *Annu. Rev. Phys. Chem.* **2013**, *64*, 361-386.

Many efforts have been dedicated to the elucidation of the mechanism of the SF process, which is still debated. However, a detailed discussion on this topic goes beyond the scope of this Thesis. Several reviews can be referred to for this purpose.[280-286] In general terms, two main mechanistic pathways have been identified for SF. On one hand, conversion of ($S_1 + S_0$) into $^1(T_1T_1)$ can take place by a direct mechanism. On the other hand, formation of $^1(T_1T_1)$ can occur *via* the involvement of a CT intermediate.

For exoergic (or, at least, isoergic) SF to take place, the energy of the lowest singlet excited state must be greater than or equal to twice the energy of the lowest triplet state:

$$E(S_1) \geq 2E(T_1) \qquad \text{(Eq. 9)}$$

This thermodynamic requirement limits the number of chromophores able to undergo SF. Among others, diphenylisobenzofurans, rylenes and acenes have been studied as SF materials.[280,281,283] Pentacene and its derivatives are at the forefront of investigations on SF, since they fulfill the energetic requirement thus rendering the process exoergic and unidirectional. An overview of SF in pentacenes, with a special focus on the investigation of intramolecular SF in dimeric pentacene derivatives, is given in the second Chapter of this Thesis.

Triplet-triplet annihilation

Commonly, the energy gap between the lowest triplet excited state (T_1) of a molecule and its ground state (S_0) is larger than the energy gap between the lowest singlet excited state (S_1) and the lowest triplet excited state (T_1). If this condition is fulfilled, when two triplets encounter, the available electronic excitation energy is high enough to promote one of the two species into an excited singlet state (S_1), provided that the other one relaxes to its ground state (Equation 10).[278]

$$T_1 + T_1 \rightarrow S_1 + S_0 \qquad \text{(Eq. 10)}$$

This process, in which two triplets interact to produce an excited singlet and a ground-state singlet, is referred to as triplet-triplet annihilation (TTA). Thus, TTA - which occurs via Dexter energy transfer mechanism and therefore requires orbital overlap - constitutes the reverse process of singlet fission.

[282] N. Monahan, X.-Y. Zhu, *Annu. Rev. Phys. Chem.* **2015**, *66*, 601-618.
[283] D. Casanova, *Chem. Rev.* **2018**, *118*, 7164-7207.
[284] A. Japahuge, T. Zeng, *ChemPlusChem* **2018**, *83*, 146-182.
[285] H. Kim, P. M. Zimmerman, *Phys. Chem. Chem. Phys.* **2018**, *20*, 30083-30094.
[286] K. Miyata, F. S. Conrad-Burton, F. L. Geyer, X.-Y. Zhu, *Chem. Rev.* **2019**, *119*, 4261-4292.

Subphthalocyanine-based D-A systems

The outstanding structural, photophysical and electrochemical properties of SubPcs, along with their versatility in terms of chemical modification of the macrocycle, render them ideal candidates for the preparation of D-A multicomponent systems.[8] As mentioned above in this Introduction, SubPcs are characterized by strong absorptions in the UV-vis region, with extinction coefficients on the order of 5-6·10^4 M^{-1} cm^{-1} and excitation energies above 2.0 eV. Moreover, by virtue of their rigid, non-planar structure, they feature intense fluorescence emission, small Stokes shifts and low reorganization energies. Notably, their photophysical and electrochemical properties can be easily tuned by proper functionalization of the macrocycle.[120] On the other hand, the multiple options for functionalization at either the axial or the peripheral positions of the macrocycle, as well as their π-conjugated bowl-shaped structure, allow for the integration of SubPcs in a variety of covalent and supramolecular multicomponent ensembles.

Remarkably, SubPcs can act either as donors or as acceptors in both energy and electron D-A systems. Their role within the multicomponent system can be tailored by tuning the substitution pattern of the SubPc chromophore, the electronic properties of the molecular counterpart, the nature of the spacer, the polarity of the solvent and/or the energy of the incident radiation. Hereafter, an overview of SubPc-based D-A models is reported, and some significative examples are discussed.

SubPc-based energy D-A systems

Due to their energetically high-lying singlet excited states, SubPcs commonly act as energy-donor antenna units towards fullerenes, Pcs, Ps, SubPc fused dimers, properly functionalized BODIPYs and azaBODIPYs, among others. On the other hand, they usually play the role of energy acceptors when linked to chromophores with higher singlet excitation energies, such as BODIPYs and polycyclic aromatics. Oligomeric SubPc systems in which different SubPcs act as either energy donor or energy acceptor have also been described.[287]

SubPcs as energy donors

Among the energy acceptors employed in the construction of SubPc-based D-A systems, fullerenes represent the most explored as a result of the good spectral matching between the two chromophores and the multiple functionalization options offered by this class of carbon allotropes.[274,276]

[287] M. Morisue, W. Suzuki, Y. Kuroda, *Tetrahedron Lett.* **2012**, *53*, 313-316.

In a pioneering work of Torres, Guldi and Echegoyen of 2002, a series of covalent SubPc-C_{60} systems axially linked through *ortho*-, *meta*-, and *para*-phenoxy spacers was presented (Figure 19).[288] In these dyads, the efficiency of energy transfer was found to be regulated by the nature of the isomeric spacer.[289] In 2004, control over energy *versus* electron transfer kinetics in a series of analogous *meta*-derivatives was reached through proper functionalization of the SubPc periphery.[121] As a matter of fact, in the presence of electron-withdrawing substituents, SubPc singlet energy transduction was found to be the dominating deactivation mechanism. About a decade later, energy transfer to the fullerene was revealed to be not the only deactivation pathway of photoexcited electron-deficient SubPcs in axially linked SubPc-C_{60} systems.[290] In this work, competition between energy transfer and electron transfer was regulated through selective population of the first or the second SubPc-centered singlet excited by tuning the excitation wavelength.

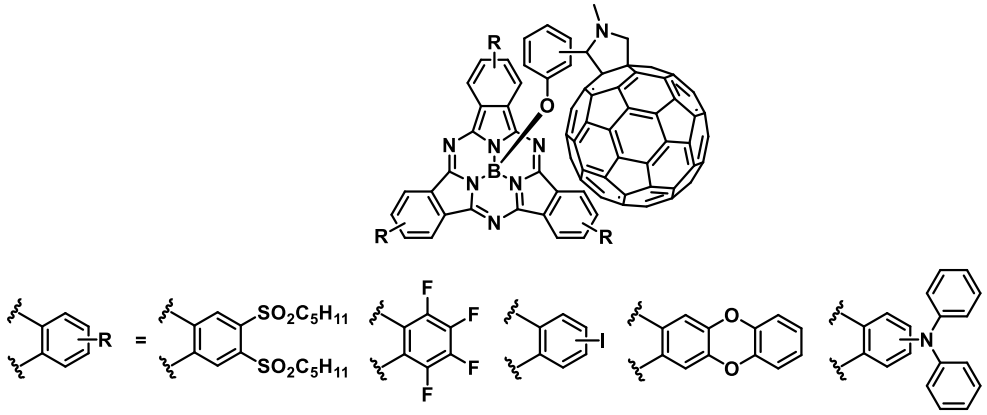

Figure 19. Structure of axially linked SubPc-C_{60} dyads investigated by Torres, Guldi, Echegoyen, Akasaka and co-workers.[121,288-290]

Energy transfer was found to take place also in peripherally connected SubPc-C_{60} systems, as long as the two units are not strongly electronically coupled.[108] Besides in covalent systems, exciton energy transduction to fullerenes has been investigated also in SubPc-fullerene supramolecular assemblies.[54,291]

[288] D. González-Rodríguez, T. Torres, D. M. Guldi, J. Rivera, L. Echegoyen, *Org. Lett.* **2002**, *4*, 335-338.
[289] D. González-Rodríguez, T. Torres, M. Á. Herranz, L. Echegoyen, E. Carbonell, D. M. Guldi, *Chem. Eur. J.* **2008**, *14*, 7670-7679.
[290] M. Rudolf, O. Trukhina, J. Perles, L. Feng, T. Akasaka, T. Torres, D. M. Guldi, *Chem. Sci.* **2015**, *6*, 4141-4147.
[291] I. Sánchez-Molina, C. G. Claessens, B. Grimm, D. M. Guldi, T. Torres, *Chem. Sci.* **2013**, *4*, 1338-1344.

In most SubPc-fullerene systems undergoing excitation energy transduction, formation of the C_{60} singlet excited state by singlet-singlet energy transfer from the SubPc unit triggers a sequence of C_{60}-centered ISC and triplet-triplet energy transfer to afford the SubPc triplet excited state. To prevent back energy transfer *via* electron exchange, direct covalent connection between the two chromophores should be avoided in order to minimize the orbital overlap, while allowing dipole-dipole interactions at the basis of Förster-type energy transduction. Such a control has been reached by exploiting diazobenzene and cyanoazulene bridges.[292,293]

Porphyrins[294,295] and phthalocyanines[122,296] have also been employed as energy-accepting units in SubPc-based D-A models.[275] Very recently, energy transfer has been observed to take place upon selective excitation of the SubPc monomers in an all-SubPc system featuring a SubPc fused dimer covalently linked through axial ethynyl spacers to the peripheral positions of two SubPc units (Figure 20).[101] The extension of the π-conjugated system in the dimeric SubPc species results in a red-shift of the absorption and emission features with respect to monomeric SubPcs, rendering energy transfer from the monomer-centered singlet excited state (2.09 eV) to the dimer-centered singlet excited state (1.77 eV) feasible.

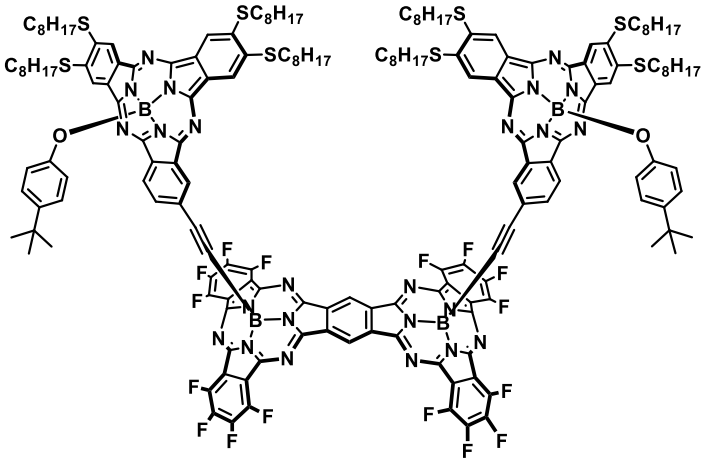

Figure 20. Structure of the all-SubPc system presented by Zango *et. al.*[101]

[292] J.-H. Kim, M. E. El-Khouly, Y. Araki, O. Ito, K.-Y. Kay, *Chem. Lett.* **2008**, *37*, 544-545.
[293] J. S. Lissau, A. Viñas Muñoz, H. Gotfredsen, M. Jevric, M. B. Nielsen, T. I. Sølling, *J. Phys. Chem. A* **2018**, *122*, 6683-6692.
[294] M. E. El-Khouly, D. K. Ju, K. Y. Kay, F. D'Souza, S. Fukuzumi, *Chem. Eur. J.* **2010**, *16*, 6193-6202.
[295] G. Bressan, A. N. Cammidge, G. A. Jones, I. A. Heisler, D. Gonzalez-Lucas, S. Remiro-Buenamañana, S. R. Meech, *J. Phys. Chem. A* **2019**, *123*, 5724-5733.
[296] R. Menting, D. K. Ng, B. Röder, E. A. Ermilov, *Phys. Chem. Chem. Phys.* **2012**, *14*, 14573-14584.

Despite singlet excited energies of BODIPY dyes are usually higher than that of SubPcs, the former can be converted into good energy acceptors in SubPc-based D-A systems upon proper functionalization of the pyrrolic rings. As a matter of fact, the introduction of styryl functionalities in the α positions of the BODIPY core results in a substantial bathochromic shift of the absorption features, rendering the spectral matching between SubPc emission and BODIPY absorption rather favorable.[71,297-300]

Aza-BODIPY dyes, which exhibit red-shifted spectral features with respect to BODIPY analogues, have also been investigated as energy acceptors in D-A systems based on SubPcs by the group of D'Souza (Figure 21).[301,302] Interestingly, control over the deactivation cascade in aza-BODIPY-containing multicomponent systems could been reached by tuning both excitation wavelength and solvent polarity.

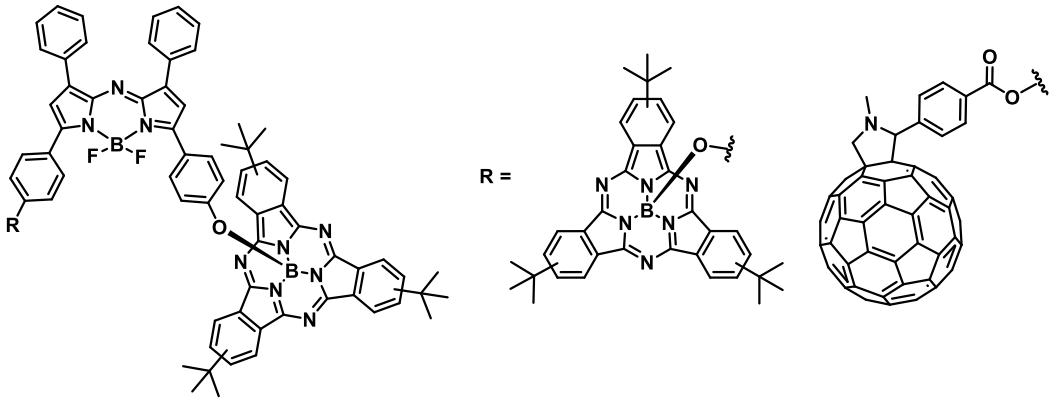

Figure 21. Structure of the SubPc-based triads investigated by D'Souza and co-workers.[301,302]

[297] J.-Y. Liu, H.-S. Yeung, W. Xu, X. Li, D. K. Ng, *Org. Lett.* **2008**, *10*, 5421-5424.
[298] R. Ziessel, G. Ulrich, K. J. Elliott, A. Harriman, *Chem. Eur. J.* **2009**, *15*, 4980-4984.
[299] D. Hablot, A. Sutter, P. Retailleau, R. Ziessel, *Chem. Eur. J.* **2012**, *18*, 1890-1895.
[300] S. Çetindere, B. Çoşut, S. Yeşilot, M. Durmuş, A. Kılıç, *Dyes and Pigments* **2014**, *101*, 234-239.
[301] H. B. Gobeze, V. Bandi, F. D'Souza, *Phys. Chem. Chem. Phys.* **2014**, *16*, 18720-18728.
[302] V. Bandi, F. P. D'Souza, H. B. Gobeze, F. D'Souza, *Chem. Commun.* **2016**, *52*, 579-581.

SubPcs as energy acceptors

Although in energy D-A systems SubPcs have been mainly employed as donors, a few ensembles have been reported in which these macrocycles act as energy acceptors in the presence of a suitable photoactive counterpart.

In this regard, some axially linked BODIPY-SubPc conjugates have been investigated, showing energy transfer to the SubPc fragment upon photoexcitation of the BODIPY moiety.[74,297] Truxene and pyrene derivatives have also been employed as energy acceptor units in SubPc-based D-A systems.[86]

SubPc-based electron D-A systems

In the presence of a proper molecular partner, electron transfer events can be triggered by photoexcitation in SubPc-based D-A models. In these systems, the role of the SubPc unit (*i.e.* electron donor *versus* electron acceptor) is determined by the electronic features of the macrocycle - which mainly depend on the nature of the ring substituents - and the redox characteristics of the molecular counterpart.

Besides SubPc-containing hetero-arrays, a few all-SubPc conjugates have been reported in which the SubPc macrocycle acts either as electron donor or as electron acceptor depending on its peripheral substitution pattern.[41,303,304] In this context, a push-pull fused dimer featuring an electron-rich *t*-butyl-functionalized half and an electron-poor chlorinated half was presented by Zango *et al.*[41] In this system, spectral evidence of formation of a CT polarized state along with an energetically lower-lying delocalized singlet excited state were found.

SubPcs as electron donors

Fullerenes cover a central role as electron acceptor partners for SubPcs in the construction of D-A systems by virtue of their unique redox and structural properties such as their favorable reduction potentials and their characteristic low reorganization energies, which promote the formation of long-lived excited states.

The photophysical behavior of axially linked SubPc-C_{60} dyads undergoing photoinduced electron transfer has been thoroughly explored by the groups of D'Souza, Torres, Echegoyen and

[303] S. Mori, N. Ogawa, E. Tokunaga, N. Shibata, *Dalton Trans.* **2015**, *44*, 19451-19455.
[304] S. Mori, N. Ogawa, E. Tokunaga, S. Tsuzuki, N. Shibata, *Dalton Trans.* **2016**, *45*, 908-912.

Guldi.[121,289,305-309] Electron transfer was found to take place in the presence of peripheral catechoxy,[121] amino,[121,289] arylthio,[308] 4-iodophenoxy,[307] pyrene[306] and phenothiazine[305,309] functionalities. Notably, π-π stacking between graphene and peripheral pyrene units results in enhanced charge separation (CS) and charge recombination (CR) kinetics, mainly due to the tuning of the free energy of the processes.[306] On the other hand, long-lived charge-separated states (CSSs) were generated by exploiting an energy-transfer cascade through the introduction of a phenoxy spacer between phenothiazine substituents and the SubPc core, allowing the distancing of the generated charges and the consequent slowdown of the CR kinetics.[305,309]

In peripherally linked SubPc-C_{60} dyads, the nature of the spacer was found to determine the degree of orbital overlap between the SubPc and C_{60} π-surfaces and, in turn, the deactivation pathway upon photoexcitation, being electron transfer the dominating scenario in shorter-spaced dyads.[108]

In a supramolecular D-A system featuring an electron-withdrawing SubPc fused dimer functionalized at the axial positions with two monomeric electron-rich alkylthio SubPcs (Figure 20), evidence of sequential CS (from a SubPc monomer to the SubPc dimer) and charge shift (from the SubPc dimer to fullerene) were found upon photoexcitation of the SubPc dimer in the presence of either C_{60} or C_{70}.[101] On the other hand, excitation of the monomeric SubPc units led to an energy transfer deactivation scenario (*vide supra*)

azaBODIPYs can also act as electron acceptors in SubPc-based D-A systems.[301,302] In a triad featuring two SubPc units covalently linked to an azaBODIPY moiety, a (SubPc)$SubPc^{\bullet+}$-$azaBODIPY^{\bullet-}$ CSS was generated either upon population of the azaBODIPY singlet excited state by direct photoexcitation or energy transfer from the photoexcited SubPc in toluene (*vide supra*), or directly from deactivation of the SubPc singlet excited state in more polar solvents (Figure 21).[301]

Electron transfer to naphthalene-[310] or perylene-diimmides[311] has also been reported.

[305] C. B. Kc, G. N. Lim, M. E. Zandler, F. D'Souza, *Org. Lett.* **2013**, *15*, 4612-4615.
[306] C. B. KC, G. N. Lim, F. D'Souza, *Angew. Chem. Int. Ed.* **2015**, *54*, 5088-5092.
[307] C. B. Kc, G. N. Lim, F. D'Souza, *Chem. Eur. J.* **2016**, *22*, 13301-13311.
[308] R. Cantu, H. B. Gobeze, F. D'Souza, *J. Porphyrins Phthalocyanines* **2016**, *20*, 987-996.
[309] C. B. Kc, G. N. Lim, F. D'Souza, *Chem. Asian J.* **2016**, *11*, 1246-1256.
[310] M. E. El-Khouly, J.-H. Kim, J.-H. Kim, K.-Y. Kay, S. Fukuzumi, *J. Phys. Chem. C* **2012**, *116*, 19709-19717.
[311] C. Romero-Nieto, J. Guilleme, J. Fernández-Ariza, M. S. Rodríguez-Morgade, D. González-Rodríguez, T. Torres, D. M. Guldi, *Org. Lett.* **2012**, *14*, 5656-5659.

SubPcs as electron acceptors

In the construction of D-A systems in which SubPcs exhibit electron accepting features, ferrocene represents the most exploited building block.[312]

In this context, several axially linked SubPc-Fc dyads have been reported in which the kinetics of electron transfer have been tuned through proper design of the linker connecting the chromophores (Figure 22).[75,124,310,313,314] A Fc-SubPc-C_{60} triad have also been reported.[110] Interestingly, when ferrocene is covalently linked to the peripheral position of the macrocycle, the short distance imposed by the substitution pattern, along with the strong perturbation of the SubPc conjugated systems, turn heavy atom-induced ISC the dominating quenching mechanism over CS.[59]

Porphyrinoids[275] and corroles have also been employed as electron donor in both covalent[61,122,294,315,316] and supramolecular[317,318] SubPc-based D-A models. In many of these systems, the electron-accepting abilities of the SubPc unit have been enhanced by functionalization of the macrocycle with peripheral electron-withdrawing substituents.[61,122,315,316,318] In some of these models, the SubPc acts as final electron acceptor of a cascade of excitation energy transduction and/or electron transfer events, which leads to CSS lifetimes on the orders of nanoseconds or tens of nanoseconds.[61,318]

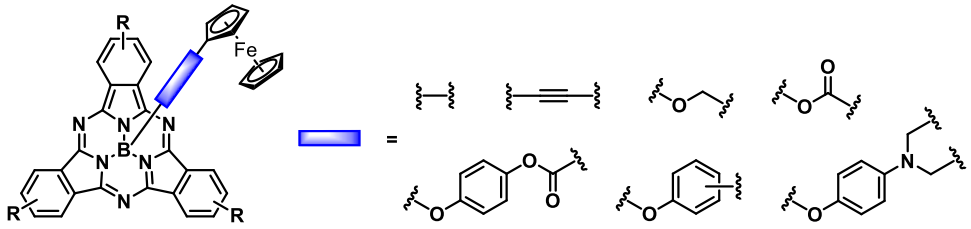

Figure 22. Investigated structures of SubPc-Fc dyads.[75,124,310,313,314]

[312] A. Vecchi, P. Galloni, B. Floris, S. V. Dudkin, V. N. Nemykin, *Coord. Chem. Rev.* **2015**, *291*, 95-171.
[313] E. Maligaspe, M. R. Hauwiller, Y. V. Zatsikha, J. A. Hinke, P. V. Solntsev, D. A. Blank, V. N. Nemykin, *Inorg. Chem.* **2014**, *53*, 9336-9347.
[314] M. E. El-Khouly, M. A. El-Kemary, A. El-Refaey, K.-Y. Kay, S. Fukuzumi, *J. Porphyrins Phthalocyanines* **2016**, *20*, 1148-1155.
[315] M. E. El-Khouly, J. B. Ryu, K.-Y. Kay, O. Ito, S. Fukuzumi, *J. Phys. Chem. C* **2009**, *113*, 15444-15453.
[316] L. C. K. Viswanath, L. D. Shirtcliff, S. Krishnan, K. D. Berlin, *Dyes and Pigments* **2015**, *112*, 283-289.
[317] M. E. El-Khouly, *Phys. Chem. Chem. Phys.* **2010**, *12*, 12746-12752.
[318] B. Berionni Berna, B. Platzer, M. Wolf, G. Lavarda, S. Nardis, P. Galloni, T. Torres, D. M. Guldi, R. Paolesse, *Chem. Eur. J.* **2020**, *26*, 13451-13461.

Interestingly, fullerenes can act as electron donors towards SubPcs upon tuning the electronic characteristics of both the chromophoric units. In this context, the groups of Torres, Guldi and Akasaka reported in 2015 a couple of conjugates featuring a strong electron accepting SubPc linked through the axial position to a $La_2@C_{80}$ moiety.[290,319] In these derivatives, the energetically low-lying $(La_2@C_{80})^{\bullet+}$-$SubPc^{\bullet-}$ CSS can be easily accessed from the SubPc singlet excited state. On the other hand, population of the SubPc second singlet excited state in analogous SubPc-C_{60} conjugates is required to generate the higher lying $C_{60}^{\bullet+}$-$SubPc^{\bullet-}$ radical ion pair, whereas upon population of the SubPc-centered first singlet excited state an energy transfer scenario is operative (*vide supra*).

The photophysical properties of SubPcs linked to triphenylamine,[315,320] phenotiazine,[305,309,311] oligothiophenes,[321] polymethine-cyanine[322] and extended tetrathiafulvalenes [323] units have also been investigated, revealing the occurrence of electron transfer to the SubPc chromophore.

[319] L. Feng, M. Rudolf, O. Trukhina, Z. Slanina, F. Uhlik, X. Lu, T. Torres, D. M. Guldi, T. Akasaka, *Chem. Commun.* **2015**, *51*, 330-333.
[320] A. Medina, C. G. Claessens, G. A. Rahman, A. M. Lamsabhi, O. Mó, M. Yáñez, D. M. Guldi, T. Torres, *Chem. Commun.* **2008**, 1759-1761.
[321] C. E. Mauldin, C. Piliego, D. Poulsen, D. A. Unruh, C. Woo, B. Ma, J. L. Mynar, J. M. Frechet, *ACS Appl. Mater. Interfaces* **2010**, *2*, 2833-2838.
[322] C. R. Nieto, J. Guilleme, C. Villegas, J. L. Delgado, D. González-Rodríguez, N. Martin, T. Torres, D. M. Guldi, *J. Mater. Chem.* **2011**, *21*, 15914-15918.
[323] C. Romero-Nieto, A. Medina, A. Molina-Ontoria, C. G. Claessens, L. Echegoyen, N. Martín, T. Torres, D. M. Guldi, *Chem. Commun.* **2012**, *48*, 4953-4955.

General Objectives

The aim of this Thesis is the preparation and study of novel SubPc-based systems in view of their potential application in solar energy conversion technologies.

Chapter 1 is devoted to the synthesis and study of a series of novel SubPc-based D-A systems incorporating photoactive and axially chiral tetracyanobuta-1,3-diene (TCBD)-aniline units at the axial and/or peripheral positions of the macrocycle. On one hand, the structural features of these derivatives will be analyzed, and interconversion between stereoisomers will be investigated. In this connection, the potential of some of these conjugates as light-responsive molecular switches will be probed. On the other hand, the electrochemical and photophysical properties of these derivatives will be studied in order to investigate the electronic interactions both in the ground and in the excited states. The study of such interactions in D-A systems is of crucial importance for their implementation in technological fields related to light-to-electrical energy conversion.

The goal of **Chapter 2** is the design and synthesis of novel multicomponent systems integrating a light harvesting unit, that is, a SubPc, and a SF chromophore, namely a pentacene dimer, as well as the study of the photophysical processes triggered by photoexcitation of the former. The final aim is the realization of a synergy between panchromatic absorption and singlet fission. Two different series of rationally designed models will be prepared and investigated, differing in the peripheral substitution pattern of the SubPc macrocycle or in the molecular spacer connecting the two units, with the purpose to modulate the interchromophoric interactions. The panchromatic activation of SF constitutes a promising strategy to enhance photon management in molecular photovoltaics.

Chapter 3 is aimed to the efficient optical resolution of inherently chiral SubPcs and to the study of the solid-state and on-surface organization of the racemic and enantiopure species, in view of the potential application of optically pure SubPcs as molecular materials in electronic and optoelectronic technologies.

Specific objectives to be met in the research will be listed in each Chapter.

Chapter 1

(TCBD-aniline)-Functionalized Subphthalocyanines: Stereoisomerism and Photophysical Properties

1.1 Introduction and background

As mentioned in the Introduction of this Thesis, electron D-A ensembles constitute extremely valuable systems for applications in technological fields related to artificial photosynthesis and molecular (opto)electronics. Their properties render them interesting candidates for applications in OLEDs,[324,325] OSCs,[326] DSSCs[327] and NLO,[328] among others.

Despite having been extensively investigated over the past decades, the interest in push-pull systems is still growing.[329] In the search for novel D-A ensembles, increasing interest has been focused during the last decade and half on 1,1,4,4-tetracyanobuta-1,3-diene (TCBD) as active unit. TCBD is an electron-withdrawing moiety which constitutes an intriguing building block for the preparation of non-planar push-pull systems.[330-332] Non-planar chromophores present different advantages in terms of physical properties over their planar analogues, which render them highly appealing as functional materials for application in optoelectronic devices.[331-333] First of all, they are generally more soluble than their planar counterparts. Moreover, non-planarity prevents aggregation in the solid state and generally favors a feasible sublimation without decomposition, enabling the preparation of crystalline thin films by vapor deposition. In light of these characteristics, the development of non-planar push-pull architectures for device applications constitutes nowadays an extremely active and rapidly expanding area of research.

Donor-substituted TCBD derivatives can be readily prepared by means of [2+2]-cycloaddition between tetracyanoethylene (TCNE) and an electron-rich alkyne, followed by electrocyclic ring opening of the initially formed cyclobutene (Scheme 4).[334] TCBD-based push-pull chromophores featuring *N*,*N*-dimethylaniline donors were first investigated by Diederich and co-workers in 2005, revealing efficient intramolecular CT interactions between the donor moieties and the

[324] W. Brütting, J. Frischeisen, T. D. Schmidt, B. J. Scholz, C. Mayr, *Phys. Status Solidi A* **2013**, *210*, 44-65.
[325] Y. Liu, C. Li, Z. Ren, S. Yan, M. R. Bryce, *Nat. Rev. Mater.* **2018**, *3*, 1-20.
[326] K. A. Mazzio, C. K. Luscombe, *Chem. Soc. Rev.* **2014**, *44*, 78-90.
[327] J. N. Clifford, E. Martínez-Ferrero, A. Viterisi, E. Palomares, *Chem. Soc. Rev.* **2011**, *40*, 1635-1646.
[328] S. Barlow, S. R. Marder, in *Functional Organic Materials: Syntheses, Strategies and Applications*, T. J. J. Müller, U. H. F. Bunz Eds., Wiley-VCH, Weinheim, Germany, **2006**, pp. 393-437.
[329] R. Gompper, H. U. Wagner, *Angew. Chem. Int. Ed.* **1988**, *27*, 1437-1455.
[330] M. Kivala, F. Diederich, *Acc. Chem. Res.* 2009, 42, 235-248.
[331] S.-i. Kato, F. Diederich, *Chem. Commun.* **2010**, *46*, 1994-2006.
[332] B. Breiten, I. Biaggio, F. Diederich, *CHIMIA* **2010**, *64*, 409-413.
[333] R. García, J. Calbo, R. Viruela, M. Á. Herranz, E. Ortí, N. Martín, *ChemPlusChem* **2018**, *83*, 300-307.
[334] T. Michinobu, F. Diederich, *Angew. Chem. Int. Ed.* **2018**, *57*, 3552-3577.

TCBD acceptor.[335] After this seminal report, "click chemistry"-type[336] [2+2] cycloaddition-retroelectrocyclization (CA-RE) reaction of TCNE with electron donor-activated alkynes has been largely exploited for the integration of the TCBD framework into different multicomponent systems. The structural, optical, and electronic properties of these derivatives have been deeply investigated by the group of Diederich and many other groups. In this context, several donor moieties have been investigated and, in some cases, both donor and acceptor units have been introduced to modulate the photophysical properties of the systems.

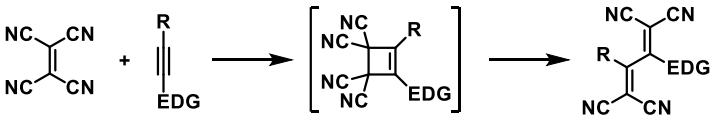

Scheme 4. Reaction between TCNE and an alkyne substituted with an electron-donating group (EDG) to afford the corresponding donor-substituted TCBD derivative.

The TCBD moiety have been linked to dimethylaniline,[333,337-341] triphenylamine,[342,343] Fc,[341,344,345] phenothiazine,[346,347] carbazole,[348] arenes,[349] azulene,[350] BODIPY,[347,351] aza-BODIPY,[342]

[335] T. Michinobu, J. C. May, J. H. Lim, C. Boudon, J.-P. Gisselbrecht, P. Seiler, M. Gross, I. Biaggio, F. Diederich, *Chem. Commun.* **2005**, 737-739.
[336] H. C. Kolb, M. Finn, K. B. Sharpless, *Angew. Chem. Int. Ed.* **2001**, *40*, 2004-2021.
[337] T. Michinobu, C. Boudon, J. P. Gisselbrecht, P. Seiler, B. Frank, N. N. Moonen, M. Gross, F. Diederich, *Chem. Eur. J.* **2006**, *12*, 1889-1905.
[338] S. i. Kato, M. Kivala, W. B. Schweizer, C. Boudon, J. P. Gisselbrecht, F. Diederich, *Chem. Eur. J.* **2009**, *15*, 8687-8691.
[339] M. Yamada, P. Rivera-Fuentes, W. B. Schweizer, F. Diederich, *Angew. Chem. Int. Ed.* **2010**, *49*, 3532-3535.
[340] F. Tancini, F. Monti, K. Howes, A. Belbakra, A. Listorti, W. B. Schweizer, P. Reutenauer, J. L. Alonso-Gómez, C. Chiorboli, L. M. Urner, *Chem. Eur. J.* **2014**, *20*, 202-216.
[341] M. Yamada, F. Tancini, M. Sekita, D. M. Guldi, C. Boudon, J.-P. Gisselbrecht, M. N. Alberti, W. B. Schweizer, F. Diederich, *Fuller. Nanotub. Car. N.* **2014**, *22*, 99-127.
[342] D. Pinjari, A. Z. Alsaleh, Y. Patil, R. Misra, F. D'Souza, *Angew. Chem. Int. Ed.* **2020**, *59*, 23697-23705.
[343] Y. Rout, Y. Jang, H. B. Gobeze, R. Misra, F. D'Souza, *J. Phys. Chem. C* **2019**, *123*, 23382-23389.
[344] C. Dengiz, B. Breiten, J.-P. Gisselbrecht, C. Boudon, N. Trapp, W. B. Schweizer, F. Diederich, *J. Org. Chem.* **2015**, *80*, 882-896.
[345] A. V. a. Muñoz, H. Gotfredsen, M. Jevric, A. Kadziola, O. Hammerich, M. B. Nielsen, *J. Org. Chem.* **2018**, *83*, 2227-2234.
[346] R. Sharma, M. B. Thomas, R. Misra, F. D'Souza, *Angew. Chem. Int. Ed.* **2019**, *58*, 4350-4355.
[347] M. Poddar, Y. Jang, R. Misra, F. D'Souza, *Chem. Eur. J.* **2020**, *26*, 6869-6878.
[348] S. i. Kato, H. Noguchi, S. Jin, Y. Nakamura, *Asian J. Org. Chem.* **2016**, *5*, 246-256.
[349] P. S. Marqués, J. M. A. Castán, B. Raul, G. Londi, I. Ramirez, M. Pshenichnikov, D. Beljonne, K. Walzer, M. Blais, M. Allain, *Chem. Eur. J.* **2020**, *26*, 16422-16433.
[350] T. Shoji, S. Ito, *Chem. Eur. J.* **2017**, *23*, 16696-16709.
[351] G. Ulrich, A. Barsella, A. Boeglin, S. Niu, R. Ziessel, *ChemPhysChem* **2014**, *15*, 2693-2700.

porphyrin,[339,352] truxene,[346] diketopyrrolopyrrole,[353] benzothiadiazole,[343] benzothiazole,[354] and fullerene[339,341] derivatives. These systems exhibit intriguing physicochemical features which render them particularly interesting for optoelectronic applications. Hereafter, the most remarkable properties of donor-substituted TCBD derivatives as well as some significative examples of D-A systems featuring TCBD as electron-accepting unit are described.

Single-crystal X-ray diffraction analysis of many TCBD-containing derivatives evidenced that the TCBD framework is highly non-planar. As a matter of fact, a substantial twist between the planes of the two dicyanovinyl (DCV) moieties is observed. A typical example is a *N*,*N*-dimethylaniline-substituted TCBD derivative, which features a torsional angle of -96.7°, corresponding to a quasi-orthogonal arrangement of the two DCV planes (Figure 23).[331]

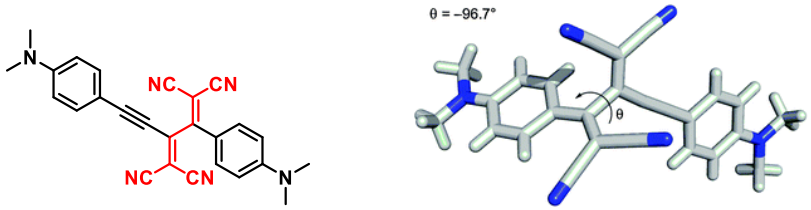

Figure 23. Chemical structure and X-ray crystal structure of a *N*,*N*-dimethylaniline-substituted TCBD. Adapted from ref. 331.

In some TCBD-based derivatives, the hindered rotation around the central buta-1,3-diene C-C single bond converts the latter in a chiral axis. Remarkably, the enantiomers of a TCBD-based push-pull system featuring a direct linkage between the TCBD moiety and a C_{60} unit have been successfully isolated by Diederich and co-workers by means of chiral HPLC (Figure 24).[339] In this work, it was found that the presence of a single methyl group rigidly attached to the fullerene surface has a dramatic impact on the rotation around the central C-C bond of the TCBD framework, raising the corresponding kinetic barrier to such an extent that separation and chiroptical characterization of the enantiomers was made feasible for the first time. On the other hand, upon replacing the methyl group by a hydrogen or upon insertion of an acetylene spacer between the TCBD moiety and the fullerene unit, the rotation around the chiral axis becomes faster. Kinetic studies carried out by CD spectroscopy allowed to determine the activation parameters for the thermal enantiomer conversion process, affording an activation energy of 28.2 kcal mol^{-1}.

[352] D. Koszelewski, A. Nowak-Król, D. T. Gryko, *Chem. Asian J.* **2012**, *7*, 1887-1894.
[353] Y. Patil, R. Misra, *J. Mater. Chem. C* **2019**, *7*, 13020-13031.
[354] P. Gautam, R. Maragani, R. Misra, *Tetrahedron Lett.* **2014**, *55*, 6827-6830.

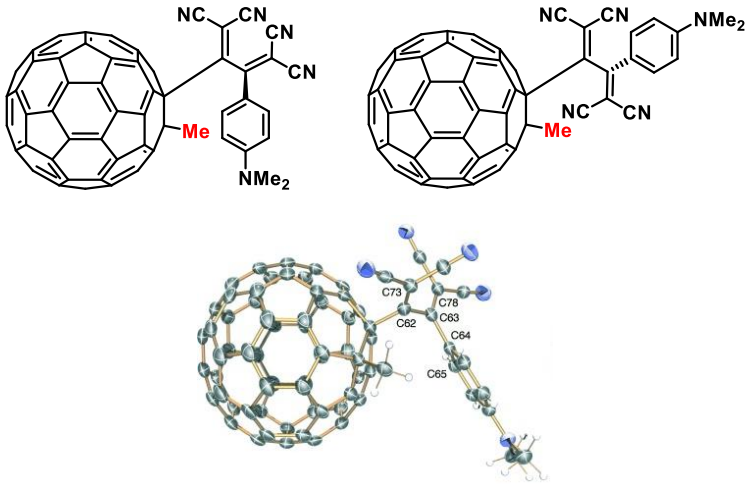

Figure 24. Chemical structure of the two enantiomers and ORTEP representation of the C_{60}-substituted TCBD derivative investigated by Diederich and co-workers. Adapted from ref. 339.

Interestingly, in some highly sterically congested TCBD-based systems (namely, C_{60} or corannulene derivatives functionalized with TCBD units), the presence of different conformers resulting from the restricted rotation around the C-C bond connecting the butadiene moiety to the linked chromophore, as well as their slow interconversion, was evidenced by variable temperature (VT)-NMR spectroscopy.[339,355]

Despite their considerable non-planarity, most of the investigated donor-substituted TCBD chromophores feature strong ground-state intramolecular CT interactions between the electron-donating moieties and the electron-withdrawing TCBD units that give rise to intense, low-energy CT absorption bands in the visible to the near infrared (NIR) region. The origin if these intramolecular CT interactions in TCBD-based push-pull chromophores featuring tetrathiafulvalene (TTF) as donor unit has been investigated by Diederich and co-workers.[338] X-ray diffraction analysis of one of the investigated derivatives showed that the TTF moiety maintains nearly fully planar π-conjugation with the neighboring DCV moiety with a torsional angle of only 1.7°, leading to strong intramolecular CT interactions in the ground state (Figure 25). Moreover, the significant bond length alternation found in the investigated derivative confirmed a substantial contribution of the charge-separated resonance structure to the ground-state geometry of the conjugate as a result of efficient intramolecular CT. The second

[355] Y.-L. Wu, M. C. Stuparu, C. Boudon, J.-P. Gisselbrecht, W. B. Schweizer, K. K. Baldridge, J. S. Siegel, F. Diederich, *J. Org. Chem.* **2012**, *77*, 11014-11026.

DCV moiety, even if twisted out of the plane up to near orthogonality, was inferred to contribute to the acceptor potency of the TCBD unit by a strong σ-inductive effect. The almost co-planarity between *N*,*N*-dimethylaniline donors and the directly attached DCV half had already been observed by the group of Diederich in their earliest report on TCBD-based push-pull chromophores.[335] Owing to such intramolecular CT interactions, TCBD-containing multicomponent systems usually exhibit panchromatic absorption in the visible region extending far into the NIR region, a relevant property for optoelectronic applications.

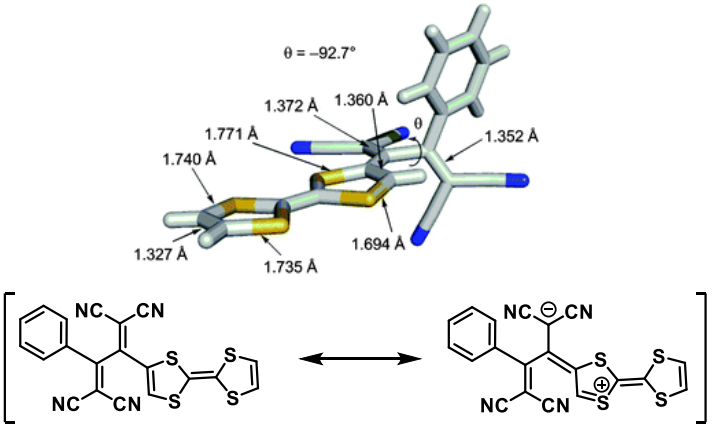

Figure 25. X-Ray crystal structure and resonance structures of a TTF-appended TCBD derivative. Adapted from ref. 331.

Moreover, in many TCBD-containing D-A molecules, excited-state interactions have been investigated, revealing the occurrence of photoinduced electron transfer resulting in the formation of CSSs.[339,341-343,346,347,356,357] In this context, Diederich, Amaroli and co-workers reported a series of Zn^{II}Ps linked to a *N*,*N*-dimethylanilino-substituted TCBD directly or through a bridging spacer and exhibiting intramolecular electron transfer upon excitation of the porphyrin unit (Figure 26).[340] Remarkably, a long-lived CSS with a lifetime of 2.3 μs was observed in the conjugate featuring the interchromophoric spacer, rendering these kind of systems appealing for application as active materials in photovoltaic devices. On the other hand, the system lacking the bridging spacer was found to undergo photoinduced CS and CR within 20 ps.

[356] M. Sekita, B. Ballesteros, F. Diederich, D. M. Guldi, G. Bottari, T. Torres, *Angew. Chem. Int. Ed.* **2016**, *55*, 5560-5564.
[357] P. Gautam, R. Misra, M. B. Thomas, F. D'Souza, *Chem. Eur. J.* **2017**, *23*, 9192-9200.

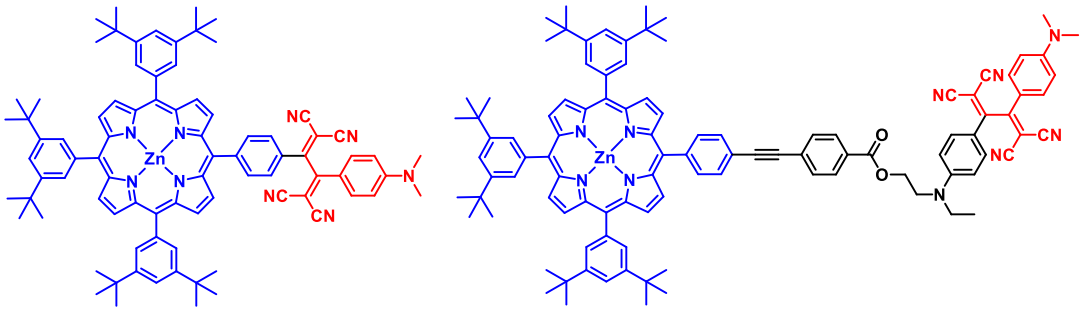

Figure 26. Multicomponent systems investigated by Diederich, Armaroli and co-workers featuring a $Zn^{II}P$ linked directly or through an interchromophoric spacer to an anilino-substituted TCBD unit.[340]

Regarding their electrochemical characteristics, TCBD-based push-pull chromophores feature an active redox behavior. Generally, the incorporation of the electron-withdrawing TCBD moiety lowers the LUMO energy level, enhancing the electron-accepting abilities of the system. The nonlinear optical properties of a number TCBD derivatives have also been studied, showing high third-order optical nonlinearities.[335,358,359] Moreover, some of these systems have been investigated as second-order NLO materials.[351,360]

By virtue of their impressive structural, photophysical and electrochemical properties, TCBD-based derivatives have been successfully employed as non-fullerene acceptors for the fabrication of BHJ OSCs giving rise to PCEs up to 9.29%.[361-365]

In 2016, our group started to investigate on porphyrinoid-containing TCBD-based conjugates by reporting two $Zn^{II}Pc$ derivatives bearing one or four TCBD-dimethylaniline groups, respectively (Figure 27).[356] The introduction of the TCBD moiety was found to have a remarkable impact on the ground- and excited-state characteristics of the investigated systems, as a consequence of the strong electronic communication between the Pc and TCBD units. In these derivatives, extremely intense ground-state CT interactions between the electron-rich ZnPc and the

[358] M. T. Beels, M. S. Fleischman, I. Biaggio, B. Breiten, M. Jordan, F. Diederich, *Opt. Mater. Express* **2012**, *2*, 294-303.
[359] Z. Pokladek, N. Ripoche, M. Betou, Y. Trolez, O. Mongin, J. Olesiak-Banska, K. Matczyszyn, M. Samoc, M. G. Humphrey, M. Blanchard-Desce, *Chem. Eur. J.* **2016**, *22*, 10155-10167.
[360] Y. Si, G. Yang, *J. Phys. Chem. A* **2014**, *118*, 1094-1102.
[361] Y. Patil, R. Misra, M. Keshtov, G. D. Sharma, *J. Phys. Chem. C* **2016**, *120*, 6324-6335.
[362] P. Gautam, R. Sharma, R. Misra, M. Keshtov, S. Kuklin, G. D. Sharma, *Chem. Sci.* **2017**, *8*, 2017-2024.
[363] Y. Patil, R. Misra, M. Keshtov, G. D. Sharma, *J. Mater. Chem. A* **2017**, *5*, 3311-3319.
[364] Y. Patil, R. Misra, R. Singhal, G. D. Sharma, *J. Mater. Chem. A* **2017**, *5*, 13625-13633.
[365] L. Bucher, N. Desbois, P. D. Harvey, C. P. Gros, R. Misra, G. D. Sharma, *ACS Appl. Energy Mater.* **2018**, *1*, 3359-3368.

electron-withdrawing TCBD give rise to low-energy absorption bands centered at 752/753 nm in benzonitrile, in addition to the high-energy TCBD-aniline transition. Moreover, a CSS is formed upon photoexcitation of either the Pc moiety or the CT ground state. These features, along with a panchromatic absorption and HOMO-LUMO gaps as low as 1.28 eV in the monosubstituted derivative, make these systems intriguing candidates for application in molecular photovoltaics.

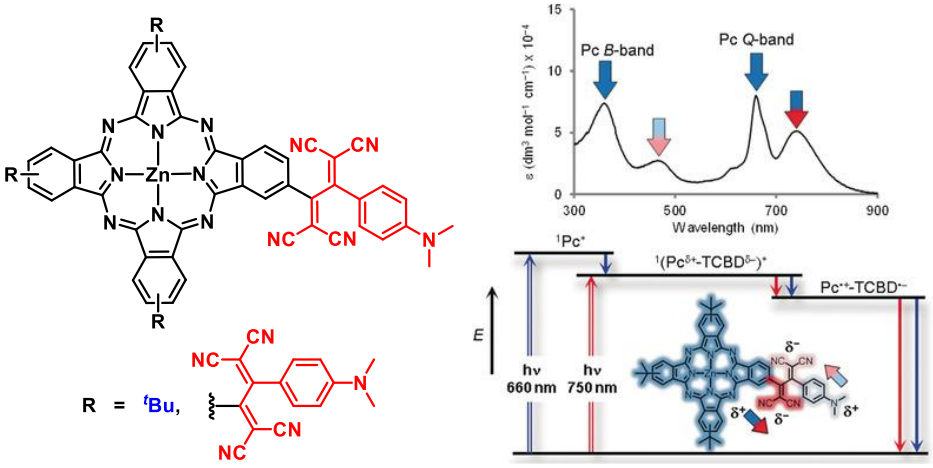

Figure 27. Structure of the Pc-TCBD conjugates investigated in our group, UV-vis absorption spectrum of the mono-substituted derivative and energy level diagram showing the energetic pathways of CR and CS after excitation of the Pc moiety or the CT ground state. Adapted from ref. 356.

These results prompted our interest in the study of TCBD-containing systems based on contracted Pc congeners, namely SubPcs, which constitutes one of the main goals of this Thesis.

During the development of this Thesis, Nielsen and co-workers presented the synthesis of a SubPc derivative bearing three *N*,*N*-dimethylanilino-substituted TCBD units in the peripheral positions.[201] In the UV-vis spectrum of this conjugate, a strong CT absorption at 466 nm in chloroform is observed due to the ground-state interactions between the aniline and the TCBD. Nevertheless, neither the stereochemical features, nor the redox properties or the excited-state interactions of this derivative were investigated. In the same year, the group of Nielsen reported the preparation of a series of SubPc derivatives bearing ferrocene-TCBD substituents at either the axial or the peripheral positions. Also in this case, perturbed absorption spectra were observed with respect to the corresponding ethynyl-ferrocene precursors, which is attributable to CT interactions.[345]

1.2 Specific objectives of Chapter 1

The main goal of this Chapter is the preparation of novel (TCBD-aniline)-functionalized SubPcs and the study of their structural, electrochemical and photophysical properties in view of their potential application as photoactive materials in technological fields related to solar energy conversion.

This Chapter is divided into three different sections.

In the **first section**, the synthesis of the target derivatives will be presented. In particular, four different SubPcs decorated at either the axial, peripheral or axial and peripheral positions of the macrocycle with TCBD-aniline moieties will be prepared (Figure 28). The introduction of the TCBD functionalities will be carried out through CA-RE reaction between the corresponding alkynyl-functionalized SubPc precursors and TCNE. In turn, the axially substituted SubPc-ethynyl-aniline derivatives will be synthesized by axial substitution reaction from the corresponding SubPc-Cl species with a Grignard reagent, whereas peripheral functionalization of the SubPc macrocycle with ethynyl-aniline moieties will be performed by palladium-catalyzed Sonogashira reaction from the starting I_3SubPc derivatives.

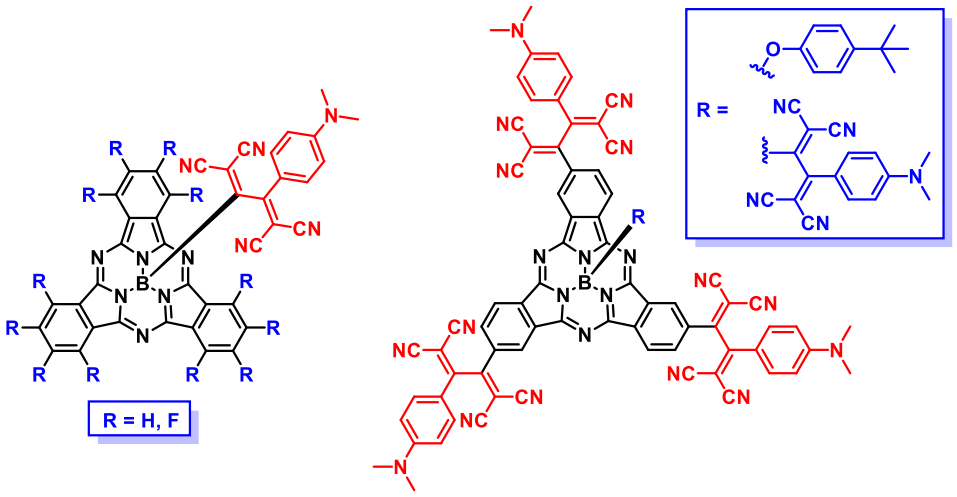

Figure 28. Structure of the (TCBD-aniline)-substituted SubPcs investigated in Chapter 1.

The design of these derivatives is aimed to study the impact of the substitution pattern of the SubPc, that is, the anchoring position of the TCBD-aniline moieties to the macrocycle, on the structural and optoelectronic properties of the derivatives. In the case of the axially substituted

SubPc-TCBD-aniline conjugates, the effect of the presence of hydrogen or fluorine atoms at the SubPc periphery will also be investigated.

The **second section** of this Chapter is dedicated to the study of the structural features of the novel (TCBD-aniline)-substituted SubPc derivatives. In particular, the organization in the crystalline solid state of the axially substituted SubPc-TCBD-aniline conjugates as well as enantiomer interconversion in solution will be thoroughly investigated. In this connection, a comparative study with a (TCBD-aniline)-functionalized SubP analogue will be performed. Stereoisomerism in the peripherally and peripherally/axially substituted conjugates will also be discussed.

The **third section** is focused on the study of the electrochemical and photophysical properties of the (TCBD-aniline)-functionalized SubPcs. The ground- and excited-state interactions within the novel SubPc derivatives will be investigated and rationalized on the basis of the SubPc functionalization pattern (namely, axial, peripheral or peripheral/axial) and, in the case of the axially substituted SubPc-TCBD-aniline conjugates, on the basis of the electronic characteristics of the SubPc macrocycle.

1.3 Results and discussion

Based on the results that will be presented in this Chapter, four manuscripts have been elaborated and published as:

- K. A. Winterfeld, G. Lavarda, J. Guilleme, M. Sekita, D. M. Guldi, T. Torres, G. Bottari, Subphthalocyanines axially substituted with a tetracyanobuta-1,3-diene-aniline moiety: synthesis, structure, and physicochemical properties, *J. Am. Chem. Soc.* **2017**, *139*, 5520-5529.
- K. A. Winterfeld,† G. Lavarda,† J. Guilleme,† D. M. Guldi, T. Torres, G. Bottari, Subphthalocyanine-tetracyanobuta-1,3-diene-aniline conjugates: stereoisomerism and photophysical properties, *Chem. Sci.* **2019**, *10*, 10997-11005.
- K. A. Winterfeld,† G. Lavarda,† K. Yoshida,† M. J. Bayerlein, K. Kise, T. Tanaka, A. Osuka, D. M. Guldi, T. Torres, G. Bottari, Synthesis and optical features of axially and peripherally substituted subporphyrins. A paradigmatic example of charge transfer versus exciplex states, *J. Am. Chem. Soc.* **2020**, *142*, 7920-7929.
- G. Lavarda, N. Bhattacharjee, G. Brancato, T. Torres, G. Bottari, Enabling racemization of axially chiral subphthalocyanine-tetracyanobutadiene-aniline enantiomers by triplet state photogeneration, *Angew. Chem. Int. Ed.* **2020**, *59*, 21224-21229.

† Shared first authorship.

1.3.1 Synthesis of (TCBD-aniline)-functionalized SubPcs

1.3.1.1 Synthesis of axially (TCBD-aniline)-substituted SubPcs

As mentioned in the Specific objectives, the aim of this Chapter is the study of the structural, electrochemical and photophysical features of novel SubPcs functionalized with TCBD-aniline moieties as a function of the substitution pattern of the macrocycle. Focusing on axially substituted SubPc-TCBD-aniline derivatives, we decided to investigate also the impact of the electronic characteristics of the SubPc macrocycle on the physicochemical properties of the system. To this end, we designed two different SubPc-TCBD-aniline species peripherally substituted with hydrogen (H_{12}SubPc) or fluorine atoms (F_{12}SubPc), in which the SubPc unit features, in principle, an electron-donor or an electron-withdrawing character, respectively.

SubPc-Cl precursors **1** and **2**, bearing hydrogen or fluorine atoms at the periphery of the macrocycle, were prepared by cyclotrimerization reaction of the corresponding phthalonitrile (namely, 1,2-dicyanobenzene or tetrafluorophthalonitrile, respectively) in the presence of BCl_3, following the procedure for the synthesis of axially chlorinated SubPcs reported by our group (Scheme 5).[22]

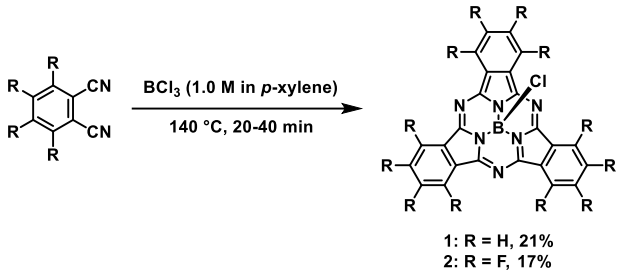

Scheme 5. Synthesis of SubPc-Cl derivatives **1** and **2**.

The preparation of the target SubPc-TCBD-aniline conjugates was carried out *via* a two-step synthesis starting from the corresponding axially chlorinated SubPcs (Scheme 6). In the first step, the axial chlorine ligand in **1** or **2** was replaced by an ethynyl-aniline group by reaction with the Grignard reagent of 4-ethynyl-*N*,*N*-dimethylaniline, which was prepared *in situ* through reaction of the corresponding terminal alkyne and ethylmagnesium bromide (EtMgBr), following the methodology presented by Ziessel and co-workers.[86] In this way, SubPc-ethynyl-aniline derivatives **3** and **4** were obtained in 56% and 62% yield, respectively. Subsequent CA-RE reaction[334] of the alkynyl-functionalized SubPcs **3** and **4** with TCNE afforded SubPc-TCBD-aniline conjugates **5** and **6**, respectively, in excellent yields (*i.e.*, 81% and 93%, respectively).

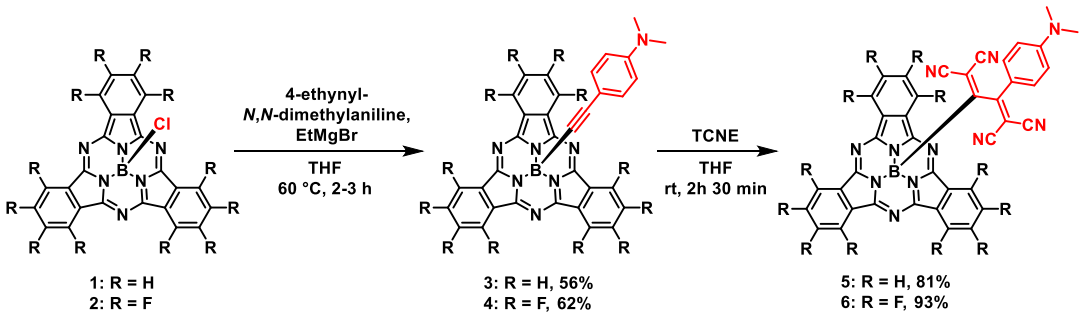

Scheme 6. Two-step synthetic route for the preparation of SubPc-TCBD-aniline derivatives **5** and **6** from the starting SubPc-Cl species **1** and **2**.

SubPc-TCBD-aniline derivatives **5** and **6** as well as SubPc-ethynyl-aniline precursors **3** and **4** were characterized by ^{1}H-NMR, ^{13}C-NMR, UV-vis and IR spectroscopy and HRMS. The ^{19}F-NMR spectra of the peripherally fluorinated derivatives **4** and **6** were also recorded. Moreover, the X-ray crystal structures of SubPc-TCBD-aniline conjugates **5** and **6** were resolved. The complete characterization of derivatives **3**-**5** is reported in the Experimental section of this Chapter.

1.3.1.2 Synthesis of peripherally and peripherally/axially (TCBD-aniline)-substituted SubPcs

To investigate the impact of the anchoring position of the TCBD-aniline groups on the stereochemical and photophysical properties of SubPc-based systems, two different (TCBD-aniline)-functionalized SubPcs bearing three or four TCBD-aniline moieties at the peripheral or peripheral and axial positions of the macrocycle were designed and synthesized.

Each of these conjugates was prepared through a few-step synthesis starting from a common SubPc precursor, namely C_3-symmetric I_3SubPc-Cl (**9**). The synthetic route followed for the preparation of the target derivatives involves the replacement of the apical halogen in SubPc **9** to afford I_3SubPcs **10** and **11**, the subsequent peripheral functionalization with ethynyl-aniline units to yield (ethynyl-aniline)$_3$SubPcs **12** and **13** and, finally, the CA-RE reaction[334] of the peripheral (in **12**) or peripheral and axial (in **13**) ethynyl-aniline groups with TCNE to afford the corresponding TCBD-containing conjugates **14** and **15**. The synthetic steps for the preparation of conjugates **14** and **15** are illustrated in Scheme 7. Henceforward in this Chapter, the *M* enantiomer of SubPcs **9**-**15** will be arbitrary represented, although it should be considered that each of these derivatives is formed as a racemic mixture of *M* and *P* enantiomers due to the inherent chirality of the SubPc core (please refer to section 1.3.2.2 for further details).

For the synthesis of (TCBD-aniline)$_3$SubPc-OAr **14** (Ar = *p*-^{t}BuPh), the apical chlorine substituent in I_3SubPc-Cl **9** was replaced by a 4-*tert*-butylphenoxy moiety by axial substitution reaction in the presence of the corresponding phenol in refluxing toluene. Then, I_3SubPc-OAr **10** was reacted with 4-ethynyl-*N*,*N*-dimethylaniline in a three-fold palladium-catalyzed Sonogashira coupling reaction which afforded (ethynyl-aniline)$_3$SubPc-OAr **12** in 79% yield. Finally, **12** was subjected to a three-fold CA-RE reaction in the presence of TCNE, obtaining conjugate **14** in 77% yield. For the preparation of (TCBD-aniline)$_3$SubPc-TCBD-aniline **15**, I_3SubPc-Cl **9** was reacted with the Grignard reagent of 4-ethynyl-*N*,*N*-dimethylaniline, which was formed *in situ* by treatment of the corresponding ethynyl derivative with EtMgBr, to afford I_3SubPc-ethynyl-aniline **11** in 59% yield. The latter was then subjected to a three-fold palladium-catalyzed Sonogashira reaction with 4-ethynyl-*N*,*N*-dimethylaniline which led to (ethynyl-aniline)$_3$SubPc-ethynyl-aniline **13** in 87% yield. Finally, a four-fold CA-RE reaction between **13** and TCNE afforded (TCBD-aniline)$_3$SubPc-TCBD-aniline **15** in 40% yield.

Conjugates **14** and **15** as well their novel precursors were full characterized by ^{1}H-NMR, ^{13}C-NMR, UV-vis, IR and HRMS techniques. The characterization of these derivatives is reported in the Experimental section of this Chapter.

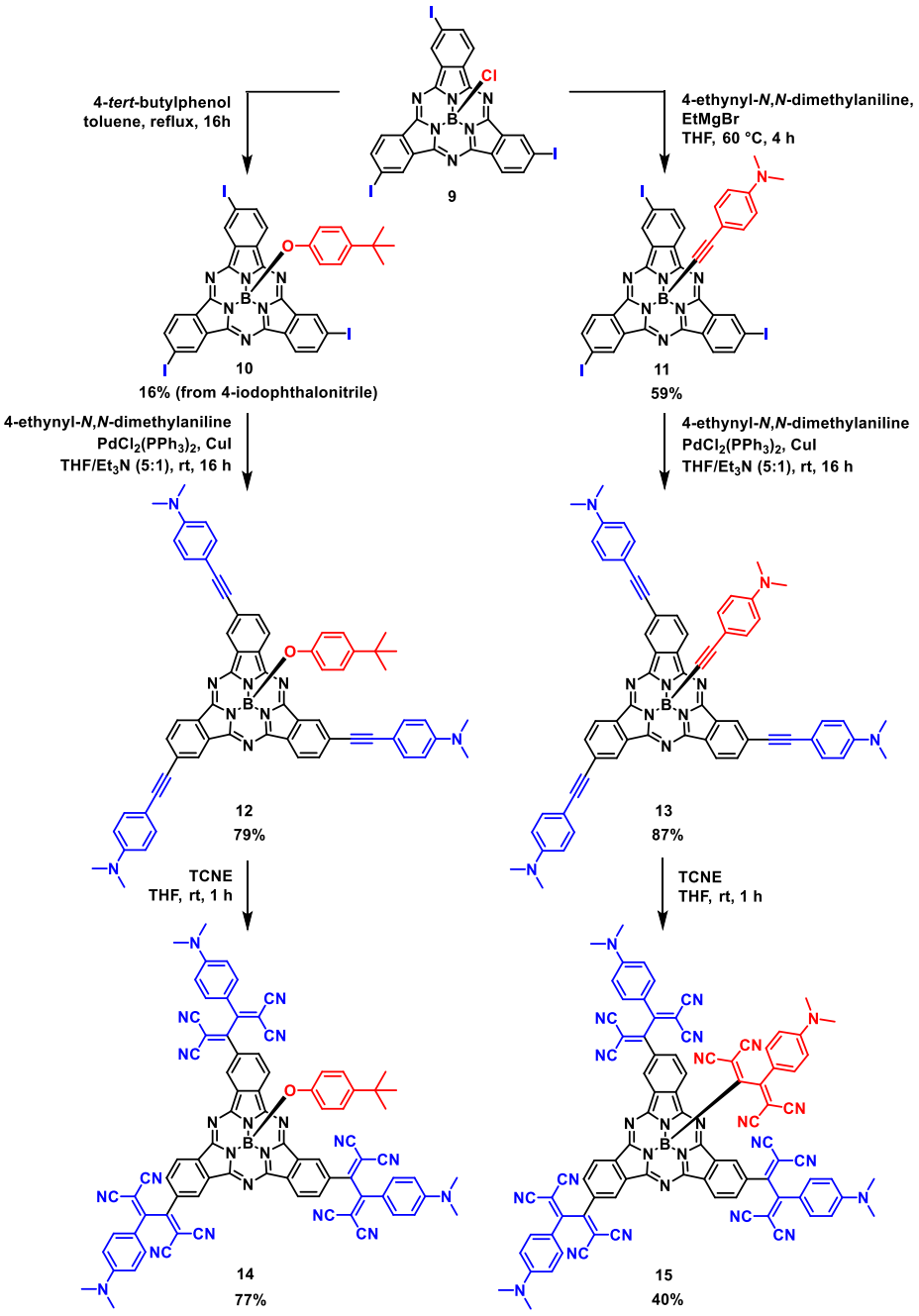

Scheme 7. Synthetic route for the preparation of (TCBD-aniline)SubPc-OAr and (TCBD-aniline)SubPc-TCBD-aniline derivatives **14** and **15** from SubPc-Cl precursor **9**.

1.3.2 Structural properties of (TCBD-aniline)-functionalized SubPcs

1.3.2.1 Structural properties of axially (TCBD-aniline)-substituted SubPcs

Crystal structure and solid-state arrangement of SubPc-TCBD-aniline derivatives 5 and 6

Single crystals of SubPc-TCBD-aniline **5** and **6** suitable for X-ray diffraction analysis were obtained by slow diffusion of *n*-hexane into a chloroform solution of the corresponding SubPc.

The crystal structures of both conjugates show that the axial TCBD unit is highly non-planar, with a torsion angle (θ) between the four carbon atoms constituting the butadiene backbone of 83.9° and 85.9° for **5** and **6**, respectively (Figure 29). The non-planarity of the TCBD framework had previously been observed in other TCBD-based compounds.[335,337] Due to the hindered rotation around the central C-C bond of the butadiene moiety and the non-planar geometry adopted by the two DCV halves, the C-C central bond of the TCBD framework constitutes a chiral axis. As a consequence, both **5** and **6** are obtained as a mixture of two atropisomers (namely, R_a-**5** and S_a-**5**, and R_a-**6** and S_a-**6**, respectively), which are related by an enantiomeric relationship. Both the R_a and the S_a species are observed in the crystal structures of SubPc-TCBD-aniline **5** and **6** (Figure 29).

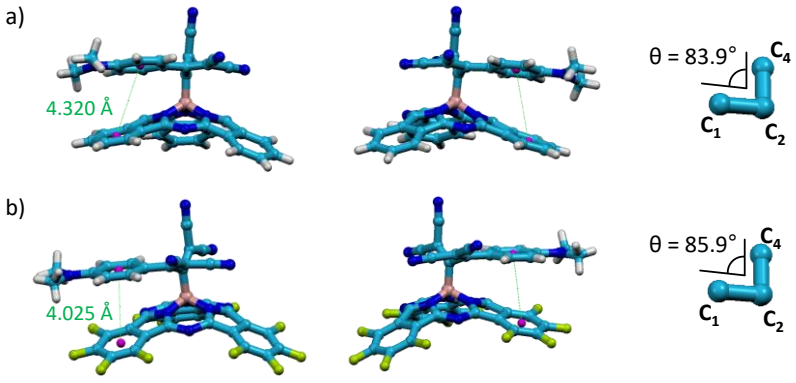

Figure 29. Lateral views of the X-ray crystal structure of (left) atropisomer R_a and (middle) atropisomer S_a within the crystal structure of (a) H_{12}SubPc-TCBD-aniline **5** and (b) F_{12}SubPc-TCBD-aniline **6**. (Right) Torsion angle (θ) between the four carbon atoms constituting the butadiene backbone of atropisomer R_a in the X-ray crystal structure of (a) H_{12}SubPc-TCBD-aniline **5** and (b) F_{12}SubPc-TCBD-aniline **6**. The C_3 atom in the butadiene backbone has been eclipsed by the C_2 atom for the sake of clarity.

Interestingly, in both derivatives, the axial aniline moiety and one of the SubPc isoindole units adopt a vicinal and quasi-parallel arrangement (Figure 29). As a matter of fact, distance values of 4.320 Å and 4.025 Å between the centroid of the aniline six-membered aromatic ring and the

centroid of the vicinal isoindolic benzene ring can be determined from the crystal structures of **5** and **6**, respectively. This geometrical feature is important to rationalize some aspects of the photophysical behavior of these conjugates that will be discussed in section 1.3.3.1.

Although SubPc-TCBD-aniline conjugates **5** and **6** possess similar geometrical features in terms of molecular structure, their crystal packing is significantly different. In particular, whereas H_{12}SubPc-TCBD-aniline **5** units organize in the form of heterochiral dimers with a head-to-head, concave-concave arrangement (Figure 30),[34] F_{12}SubPc-TCBD-aniline **6** molecules arrange in a concave-convex fashion, forming heterochiral columnar stacks which run both parallel and antiparallel between them depending on the considered direction (Figures 31 and 32). A similar solid-state arrangement of H_{12}SubPc and F_{12}SubPc derivatives, organizing in dimeric and columnar structures, respectively, had previously been observed by the group of Bender.[62]

Heterochiral dimers within the crystal lattice of H_{12}SubPc-TCBD-aniline **5** are linked together through π-stacking interactions (Figure 30). Additionally, two CN···H(aniline aryl ring) interactions can be observed between each SubPc unit within a dimer and a SubPc of opposite chirality in a vicinal dimeric structure.

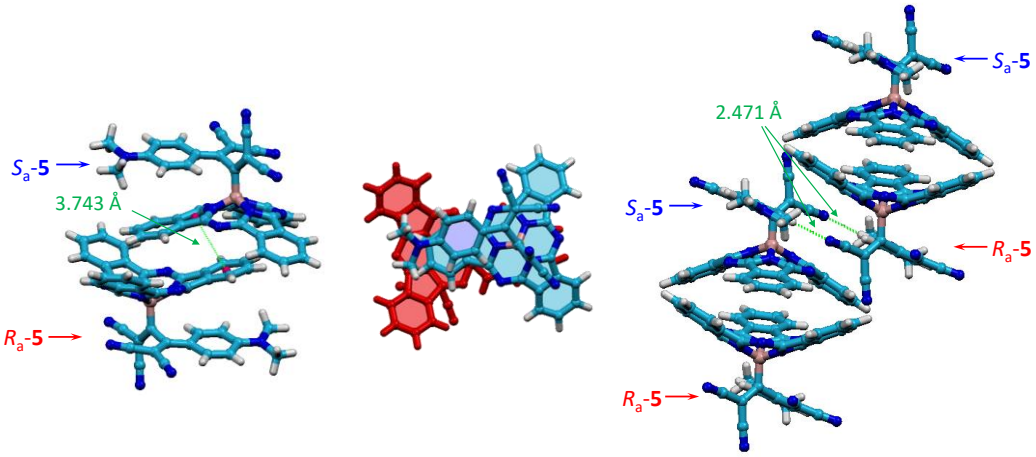

Figure 30. (Left) Lateral and (middle) top view of a heterochiral dimer within the X-ray crystal structure of H_{12}SubPc-TCBD-aniline **5**. In the top view, the R_a atropisomer has been colored in red in order to facilitate the visualization of the dimer. (Right) Lateral view of a portion of the X-ray crystal structure of H_{12}SubPc-TCBD-aniline **5** showing the interactions between two vicinal heterochiral dimers.

Turning to F_{12}SubPc-TCBD-aniline **6**, stabilizing intermolecular CN···B interactions between stacked SubPcs of opposite chirality are discernible within the heterochiral columns (Figure 31).

Moreover, π-stacking, F···H(aniline methyl group), and CN···H(aniline methyl group) interactions between F_{12}SubPc-TCBD-aniline molecules belonging to adjacent antiparallel columns can be observed.

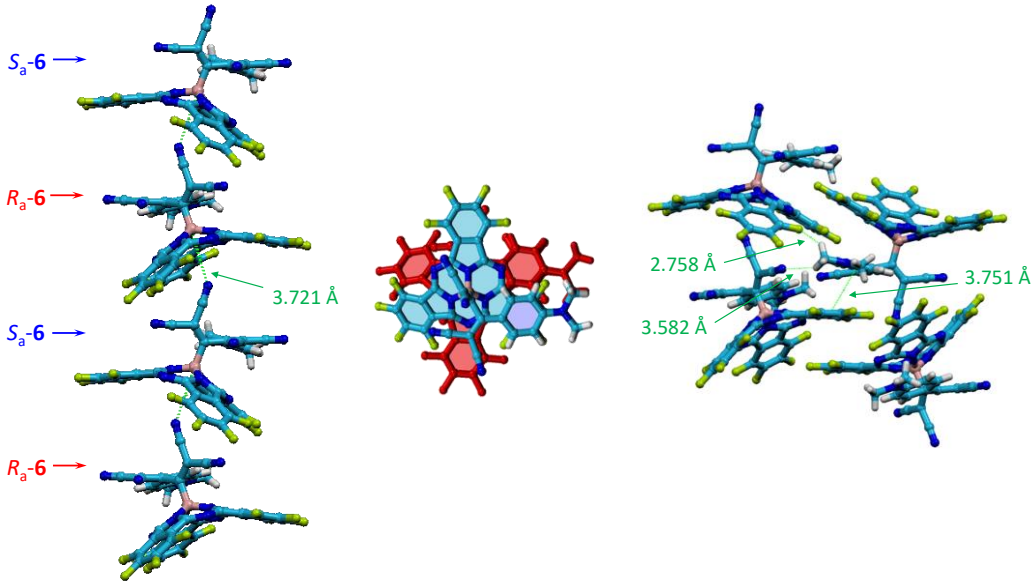

Figure 31. (Left) Lateral and (middle) top view of a portion of a heterochiral column within the X-ray crystal structure of F_{12}SubPc-TCBD-aniline **6** showing the interactions between SubPcs within the column. In the top view, the R_a atropisomer has been colored in red in order to facilitate the visualization of the columnar stack. (Right) Lateral view of a portion of the X-ray crystal structure of F_{12}SubPc-TCBD-aniline **6** showing the interactions between SubPcs in adjacent antiparallel columns.

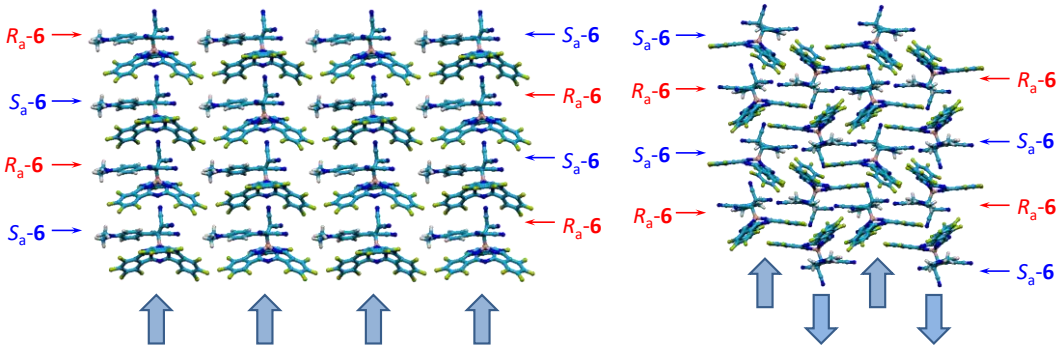

Figure 32. Two lateral views of a portion of the X-ray crystal structure of F_{12}SubPc-TCBD-aniline **6** showing the (left) parallel and (right) antiparallel arrangement adopted by adjacent columns.

Analysis of the chiral elements of SubPc-TCBD-aniline derivatives 5 and 6.

As already mentioned, as a consequence of the restricted rotation around the central C-C bond of the TCBD unit and the quasi-orthogonal arrangement of the two DCV moieties, each of the SubPc-TCBD-aniline derivatives **5** and **6** is axially chiral. The method followed for the assignment of the R_a or S_a configuration to each enantiomer of **5** and **6** is illustrated in Figure 33.

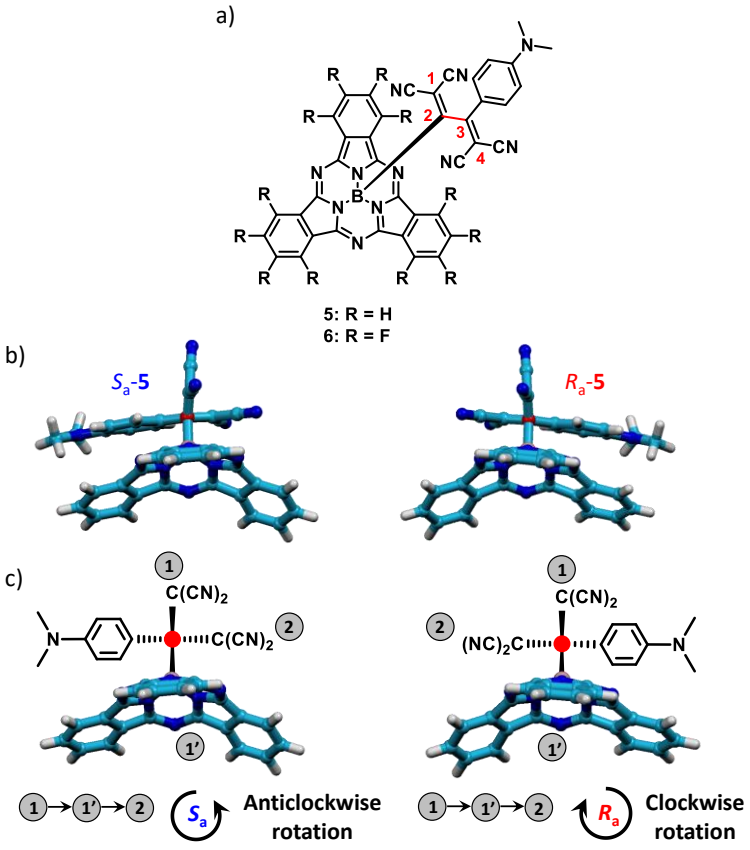

Figure 33. a) General structure of SubPc-TCBD-aniline **5** and **6**. b) X-ray crystal structure of the two enantiomers found in the crystal structure of H_{12}SubPc-TCBD-aniline **5**. c) Assignment of the absolute configuration to each enantiomer.

The stereochemical labels R_a and S_a can be assigned through the following rules. 1) The axially chiral derivative is placed so to have its chiral axis viewed end-on (regardless of the direction one sight down the chiral axis, the same stereodescriptor R_a or S_a will be obtained), with the two substituents linked to the C_2 atom and the two substituents linked to the C_3 atom perpendicular

between them. 2) Between the two substituents linked to the C_2 atom (in this case, a DCV moiety and the SubPc), group priorities are assigned following the Cahn-Ingold-Prelog (CIP) rules used for tetrahedral stereocenters. The same is done for the two substituents linked to the C_3 atom (in this case, a DCV moiety and the dimethylaniline group). 3) The R_a or S_a configuration is determined as a function of the clockwise (R_a) or anticlockwise (S_a) rotation when moving from the group with the highest priority between the two linked to the C_2 atom (1) to the group with the lowest priority between the two linked to the C_2 atom (1') and then to the group with the highest priority between the two attached to the C_3 atom (2) (*i.e.*, 1→1'→2).

^{1}H-NMR features of SubPc-TCBD-aniline derivatives 5 and 6.

The introduction of an axially chiral moiety in **5** and **6** has a noticeable impact on the NMR features of the SubPc derivatives. In H_{12}SubPc-ethynyl-aniline **3**, the *ortho* and *meta* protons of the isoindolic benzene rings give rise in the corresponding ^{1}H-NMR spectrum to a AA'XX' system (Figure 34). In particular, as a consequence of the cone-shaped geometry of the SubPc macrocycle, the *meta* protons of each isoindolic benzene ring are enantiotopic. The same can be said for the *ortho* proton of each isoindole unit. Thus, in an achiral environment, they are chemically equivalent.

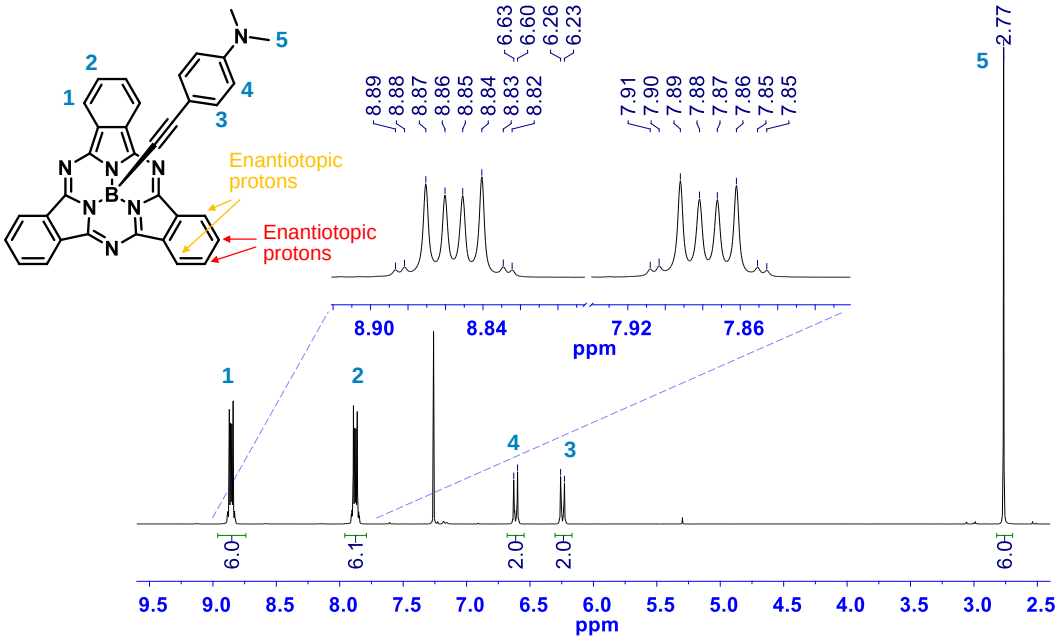

Figure 34. ^{1}H-NMR spectrum (300 MHz, $CDCl_3$) of H_{12}SubPc-ethynyl-aniline **3**. Inset: zoom of the signals of the isoindolic protons of the SubPc macrocycle.

On the contrary, in H_{12}SubPc-TCBD-aniline **5**, due to the presence of the axially chiral TCBD unit, the *meta* protons of each isoindolic benzene rings, as well as the *ortho* proton of each isoindole units, are diastereotopic between them, and thus not chemically equivalent. As a consequence, an ABXY pattern can be found in the ^{1}H-NMR spectrum of this derivative (Figure 35). A similar effect is observed in the ^{19}F-NMR spectra of F_{12}SubPc-ethynyl-aniline **4** and F_{12}SubPc-TCBD-aniline **6.**

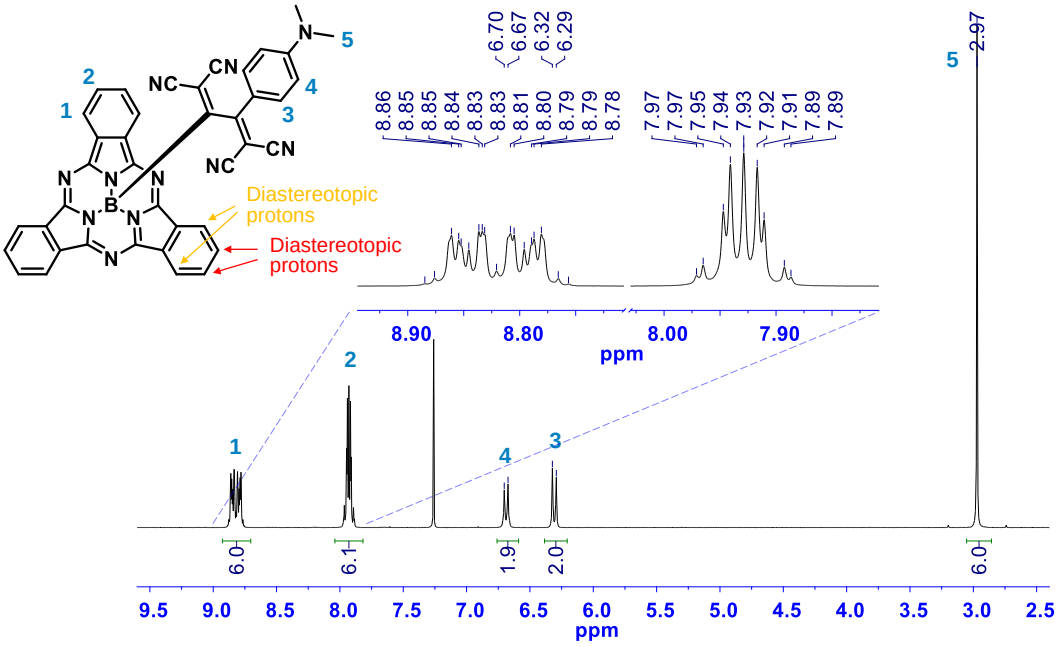

Figure 35. ^{1}H-NMR spectrum (300 MHz, $CDCl_3$) of H_{12}SubPc-TCBD-aniline **5**. Inset: zoom of the signals of the isoindolic protons of the SubPc macrocycle.

Optical resolution of SubPc-TCBD-aniline derivatives 5 and 6 and characterization of the isolated enantiomers.

In order to investigate the solid-state arrangement of the enantiopure species and to study the racemization process, we attempted the optical resolution of axially chiral SubPc-TCBD-aniline conjugates **5** and **6**. Upon systematic probing and tuning of the eluting conditions (namely, eluting solvent mixture, flow rate, and temperature), the R_a and S_a atropisomers of SubPc-TCBD-aniline **5** and **6** were successfully separated by semipreparative chiral HPLC. The corresponding chromatograms show for both derivatives two well-resolved peaks with a 1:1 peak area ratio (Figures 36 and 37). Despite the large number of TCBD-based derivatives described in literature,

only in one case the optical resolution of an axially chiral TCBD-containing species had been reported, as mentioned in the Introduction and background of this Chapter.[339] The effective optical resolution of SubPc-TCBD-aniline **5** and **6**, along with the purity of the enantiopure species, suggest that, in the employed conditions, the isolated atropisomers are configurationally stable. On the other hand, the percentage areas of the peaks corresponding to the pure enantiomers in the chromatograms of SubPc-TCBD-aniline **5** and **6** (namely, 50.1% and 49.9%, and 50.2% and 49.8%, respectively) indicate that both these derivatives are synthesized as racemic mixtures, that is, CA-RE reaction of the precursor ethynyl-species in the presence of TCNE is not enantioselective.

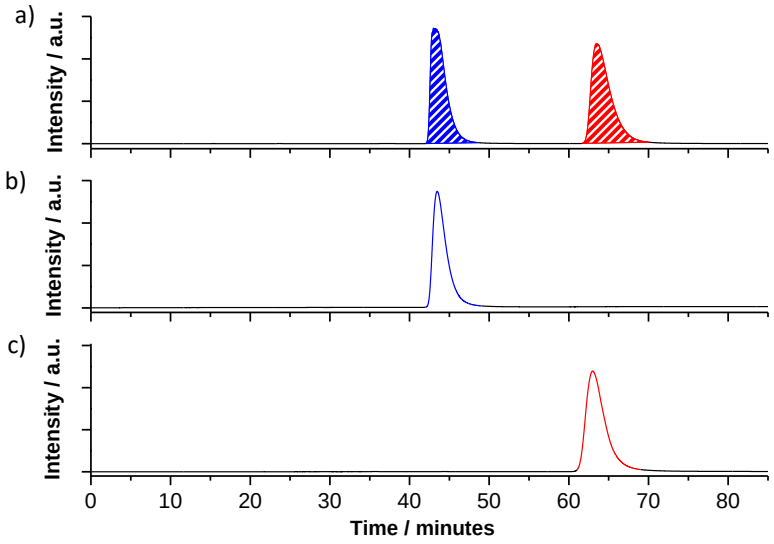

Figure 36. a) HPLC chromatogram of racemic H_{12}SubPc-TCBD-aniline **5**. The percentage areas of the first and second peaks are 50.1% and 49.9%, respectively. b,c) HPLC chromatograms of the isolated atropisomers. HPLC conditions: eluting solvent mixture = toluene/*n*-hexane/ethyl acetate 80:17:3 (v/v/v); flow rate = 1.2 mL min^{-1}; temperature = 10 °C; detection wavelength = 580 nm).

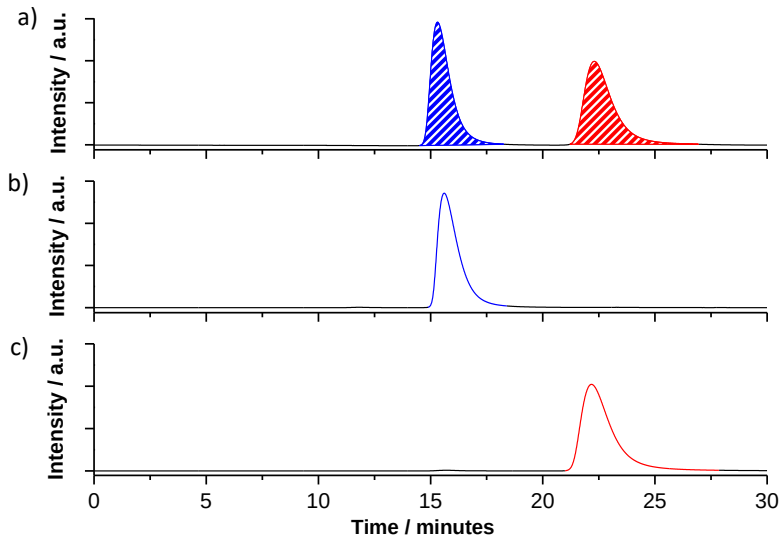

Figure 37. a) HPLC chromatogram of racemic F_{12}SubPc-TCBD-aniline **6**. The percentage areas of the of the first and second peaks are 50.2% and 49.8%, respectively. b,c) HPLC chromatograms of the isolated atropisomers. HPLC conditions: eluting solvent = toluene; flow rate = 2.5 mL min^{-1}; temperature = 10 °C; detection wavelength = 580 nm).

The mirror-image circular dichroism (CD) spectra of the isolated atropisomers of **5** and **6** provide conclusive evidence of the enantiomeric relationship between the separated species (Figure 38).

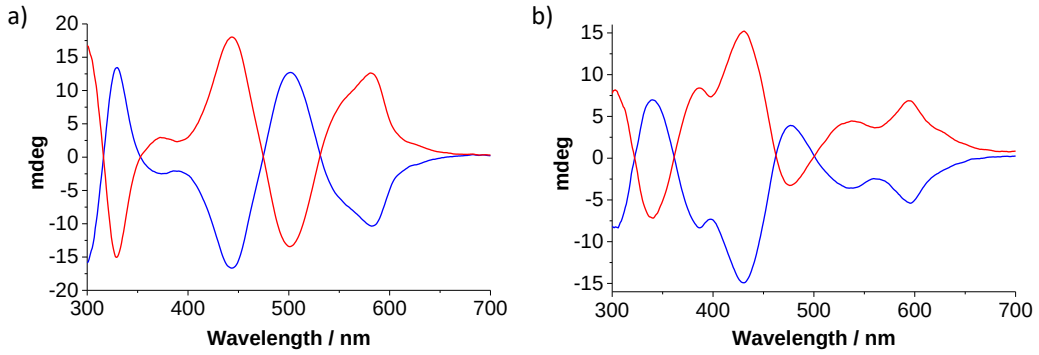

Figure 38. CD spectra of the first eluted (blue) and second eluted (red) atropisomers of a) H_{12}SubPc-TCBD-aniline **5** and b) F_{12}SubPc-TCBD-aniline **6** in $CHCl_3$ (c = 3.5 × 10^{-5} M).

Single crystals of the first eluted atropisomer of H_{12}SubPc-TCBD-aniline **5** and the second eluted atropisomer of F_{12}SubPc-TCBD-aniline **6** were obtained by slow diffusion of *n*-pentane or *n*-

hexane, respectively, into a chloroform solution of the corresponding SubPc derivative. Upon resolution of the X-ray crystal structure of the enantiopure species, the absolute configuration of each atropisomers could be unequivocally assigned. As a matter of fact, the first eluted species of **5** was determined to be the S_a-**5** enantiomer, whereas the second eluted species of **6** was found to correspond to the R_a-**6** enantiomer. The unambiguous determination of the absolute configuration of enantiopure TCBD-based species is unprecedent in literature.

From a comparison between the X-ray crystal structures of the enantiopure species and the corresponding racemates it can be observed that, whereas evident structural similarities are discernible at the molecular level, the solid-state arrangement features appreciable differences (Figure 39). S_a-**5** arranges in the solid state to form homochiral dimers, which feature a longer SubPc-to-SubPc distance (*i.e.*, 4.26 Å *versus* 3.74 Å) in comparison with that found in the heterochiral dimers within the crystal structure of racemate **5** (Figure 30). On the other hand, the X-ray crystal structure of atropisomer R_a-**6** shows the formation of homochiral columnar stacks which run both parallel and antiparallel between them, as observed for racemate **6** (Figure 31). However, in the enantiopure species, a straighter alignment of the SubPc units within the columns and a shorter intermolecular CN···B distance between stacked molecules (*i.e.*, 3.32 Å *versus* 3.72 Å) are observed.

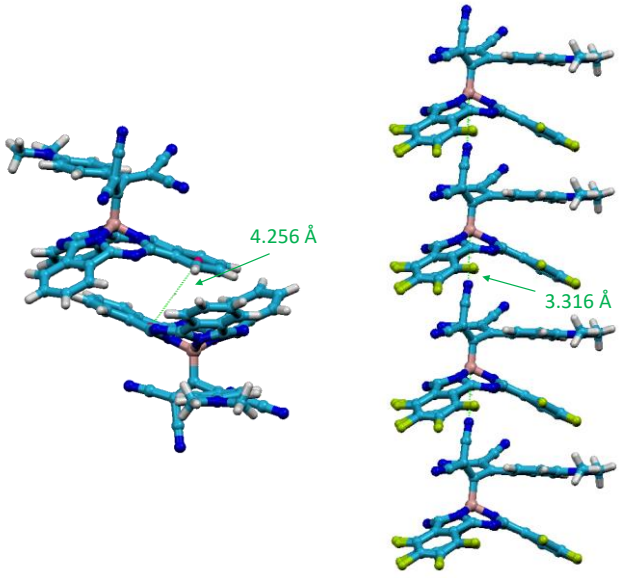

Figure 39. Left: Lateral view of a homochiral dimer within the X-ray crystal structure of H_{12}SubPc-TCBD-aniline S_a-**5**. Right: Lateral view of a portion of a homochiral column within the X-ray crystal structure of F_{12}SubPc-TCBD-aniline R_a-**6**.

Study of enantiomer conversion in SubPc-TCBD-aniline derivatives 5 and 6.

After having carried out the effective optical resolution of racemic SubPc-TCBD-aniline derivatives **5** and **6**, and once studied the organization of the enantiopure species in the solid state, the racemization behavior of **5** and **6** was investigated.

First of all, the thermal stability of optically pure samples of **5** and **6** (*i.e.*, S_a-**5** and S_a-**6**) was probed. To this end, temperature-controlled CD measurements were performed over time with non-degassed (*i.e.*, air-saturated) solutions of S_a-**5** and S_a-**6** in toluene. Surprisingly, negligible changes were observed in the CD spectra upon heating each solution at 80 °C for 3 hours (Figure 40, blue and turquoise spectra), thus indicating no appreciable racemization.

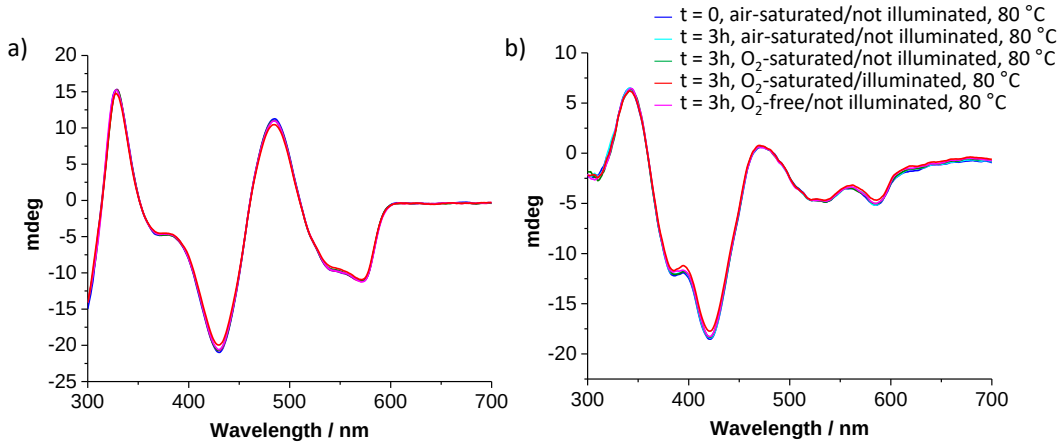

Figure 40. CD spectra of a) H_{12}SubPc-TCBD-aniline S_a-**5** and b) F_{12}SubPc-TCBD-aniline S_a-**6** in toluene ($c = 5 \times 10^{-5}$ M). Experimental conditions for both graphs are indicated in the legend in b).

The observed configurational stability of S_a-**5** and S_a-**6** is in contrast with what reported in literature for an analogous derivative featuring a TCBD-aniline moiety covalently linked to a C_{60} unit, for which a complete thermal-induced racemization had been observed (Figure 24).[339] From a comparison between the structural parameters of the S_a atropisomer within the X-ray crystal structures of **5**, **6** and the C_{60}-TCBD-aniline conjugate reported in literature,[339] it can be observed that no substantial differences are present in terms of bond lengths, bond angles and torsion angle of the TCBD unit (Figure 41 and Table 1). Such a similarity between the structural features of the axially chiral unit suggests that the different racemization behavior observed for the SubPc-based derivatives **5** and **6** with respect to the analogous C_{60}-TCBD-aniline conjugate does not arise from structural factors.

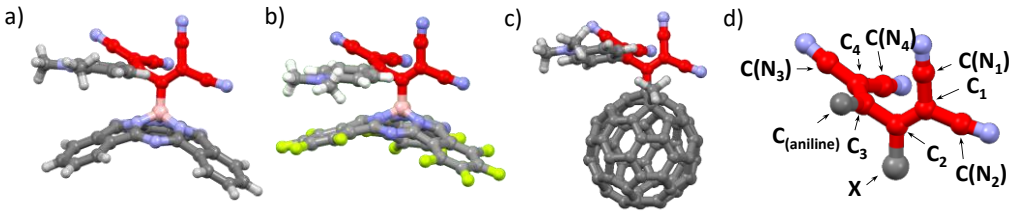

Figure 41. Molecular structure of the S_a atropisomer of a) H_{12}SubPc-TCBD-aniline **5**, b) F_{12}SubPc-TCBD-aniline **6**, c) the C_{60}-TCBD-aniline derivative investigated by Diederich and co-workers,[339] as found in the X-ray crystal structure of their respective racemates. The TCBD carbon atoms have been colored in red for the sake of clarity. d) Labels on TCBD carbon atoms and adjacent atoms used in Table 1. X stands for B atom in SubPcs **5** and **6**, or C atom in C_{60}-TCBD-aniline.

Table 1. Selected bond lengths, bond angles, and torsion angles in the S_a atropisomer of H_{12}SubPc-TCBD-aniline **5**, F_{12}SubPc-TCBD-aniline **6**, and C_{60}-TCBD-aniline[339] as determined from the X-ray crystal structures of the respective racemates.

		5	**6**	**C_{60}-TCBD-aniline**
Bond length (Å)	C_1-C_2	1.337	1.331	1.360
	C_2-C_3	1.497	1.482	1.494
	C_3-C_4	1.381	1.382	1.358
	C_1-$C(N_1)$	1.442	1.451	1.449
	C_1-$C(N_2)$	1.444	1.469	1.437
	C_4-$C(N_3)$	1.430	1.454	1.438
	C_4-$C(N_4)$	1.446	1.454	1.438
	C_2-X	1.663	1.665	1.547
	C_3-$C_{(aniline)}$	1.427	1.443	1.473
Bond angle (°)	$C(N_1)$-C_1-$C(N_2)$	114.15	110.97	114.66
	$C(N_1)$-C_1-C_2	121.82	124.82	120.79
	$C(N_2)$-C_1-C_2	123.95	124.20	124.54
	C_1-C_2-X	126.10	124.97	124.79
	C_1-C_2-C_3	118.43	120.14	117.89
	X-C_2-C_3	115.31	114.89	117.05
	C_2-C_3-$C_{(aniline)}$	117.53	117.29	119.95
	C_2-C_3-C_4	113.56	114.95	119.27
	$C_{(aniline)}$-C_3-C_4	128.75	127.39	122.78
	C_3-C_4-$C(N_3)$	127.33	124.91	122.48
	C_3-C_4-$C(N_4)$	119.35	119.14	122.59

	$C(N_3)$-C_4-$C(N_4)$	113.24	115.95	114.91
Torsion angle (°)	C_1-C_2-C_3-C_4	83.99	85.92	74.15

With the aim to elucidate the origin of the unforeseen slowdown of thermal racemization in SubPc-TCBD-aniline derivatives **5** and **6**, additional studies were carried out. To this purpose, the effect of external stimuli, namely O_2 and light, on the racemization process of enantiopure **5** and **6** species was investigated.

For the realization of CD measurements upon continuous illumination, a custom-made set-up was fabricated (Figure 42). To prevent the "external" heating of the enantiomer's solution during the temperature-controlled racemization experiments, a white light LED lamp with a negligible emission in the NIR region of the solar spectrum was employed. Moreover, the cuvette containing the sample was illuminated perpendicularly to the CD light beam reaching the CD detector, in order to prevent illumination from affecting the recording of the CD spectra.

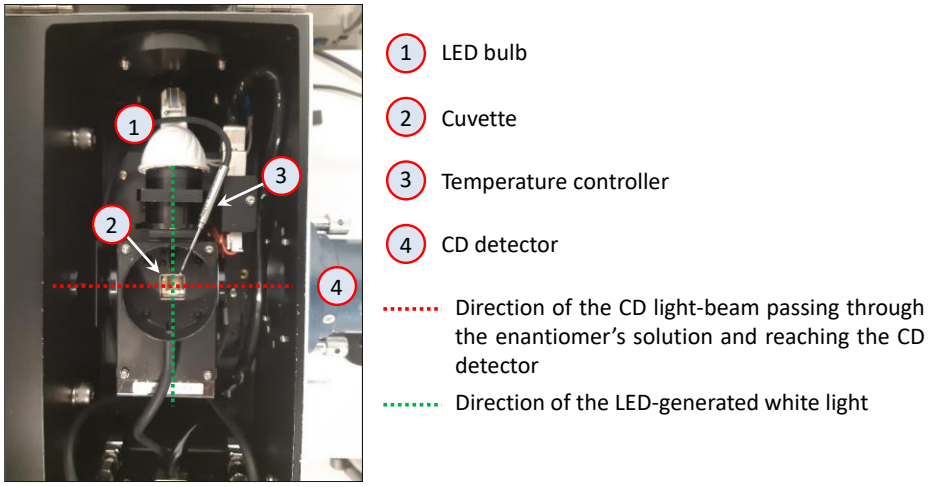

Figure 42. Picture of the custom-made CD set-up used for CD measurements upon illumination.

First, illuminated and not illuminated O_2-saturated, as well as not illuminated O_2-free toluene solutions of S_a-**5** and S_a-**6** were heated at 80 °C and their CD spectra recorded over time. In all cases, negligible changes in the CD spectra were found, as previously observed for not illuminated air-saturated toluene solutions (*vide supra*) (Figure 40, green, red and magenta spectra).

Then, CD experiments were carried out with illuminated, O_2-free toluene solutions of S_a-**5** and S_a-**6** at 80 °C. Under these conditions, a dramatic increasing of the racemization rate was observed for both species (Figure 43).

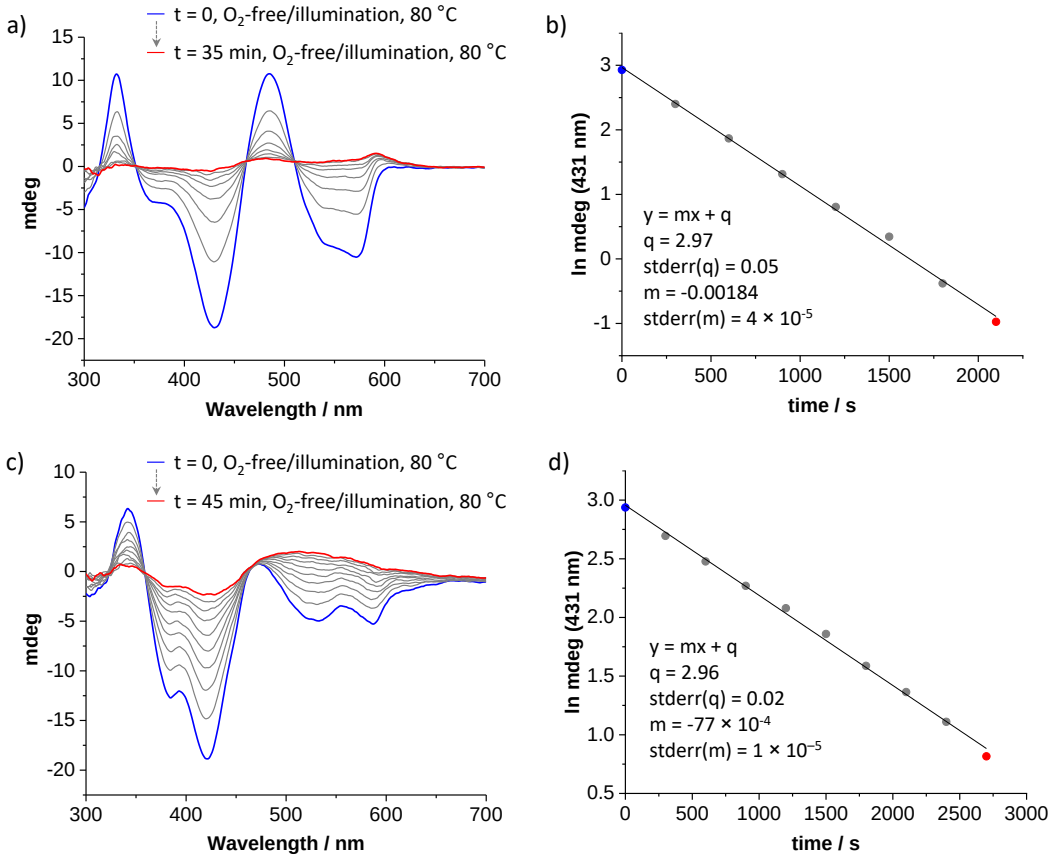

Figure 43. a,c) CD spectra of illuminated and O_2-free toluene solutions of atropisomer S_a of (a) H_{12}SubPc-TCBD-aniline **5** and (c) F_{12}SubPc-TCBD-aniline **6** in toluene ($c = 5 \times 10^{-5}$ M) heated at 80 °C over time. b,d): Linear fitting of the variation of the CD absorbance in a,b) monitored at 431 nm as a function of time. Inset in b,d): Intercept (q) and slope (m) of the linear fitting with associated standard errors.

In order to determine the activation parameters for the racemization process, photoracemization of S_a-**5** and S_a-**6** was monitored at different temperatures (namely, 60, 65, 70, 75 and 80 °C) over time. The kinetic parameters of the process were determined exploiting the Arrhenius and Eyring formalisms (Equations 11 and 12, respectively):

$$\ln k = \ln A - \frac{E_a}{RT} \quad \text{(Eq. 11)}$$

$$\ln\frac{k}{T} = -\frac{\Delta H^{\ddagger}}{RT} + \ln\frac{k_B}{h} + \frac{\Delta S^{\ddagger}}{R} \quad \text{(Eq. 12)}$$

where k is the rate constant of the process at the absolute temperature T, A is the pre-exponential factor, R is the gas constant (*i.e.*, 1.986 x 10^{-3} Kcal mol^{-1} K^{-1}), k_b is the Boltzmann constant (*i.e.*, 1.381 x 10^{-23} J K^{-1}), h is the Planck constant (*i.e.*, 6.626 x 10^{-34} J s), E_a is the activation energy, and $\Delta H^{\ddagger}$ and $\Delta S^{\ddagger}$ are the enthalpy and entropy of activation, respectively.

In particular, E_a was calculated from the slope of the linear fitting in the Arrhenius plot, whereas $\Delta H^{\ddagger}$ and $\Delta S^{\ddagger}$ were obtained from the slope and the intercept of the linear fitting in the Eyring plot, respectively (Figure 44). The free Gibbs energy of activation ($\Delta G^{\ddagger}$) was calculated as:

$$\Delta G^{\ddagger} = \Delta H^{\ddagger} - T\Delta S^{\ddagger} \quad \text{(Eq. 13)}$$

The half-time at 60 °C was determined from the corresponding kinetic constant according to the equation valid for first-order reactions:

$$\tau_{1/2} = \frac{\ln 2}{k} \quad \text{(Eq. 14)}$$

The values of $\Delta H^{\ddagger}$, $\Delta S^{\ddagger}$, $\Delta G^{\ddagger}_{(25\,°C)}$, E_a and $\tau_{1/2\,(60\,°C)}$ calculated for the photoracemization of SubPc-TCBD-aniline **5** and **6** are reported in Table 1. In this context, it is worth to mention that the racemization rate constants k determined for S_a-**5** and S_a-**6** are dependent on parameters such as the samples' concentration, the illuminated section area of the solution, the intensity of the light source, and the distance of the latter from the cuvette in the CD set-up. Thus, these rate constants are not comparable to the ones reported in literature for the thermal racemization of C_{60}-TCBD-aniline.[339]

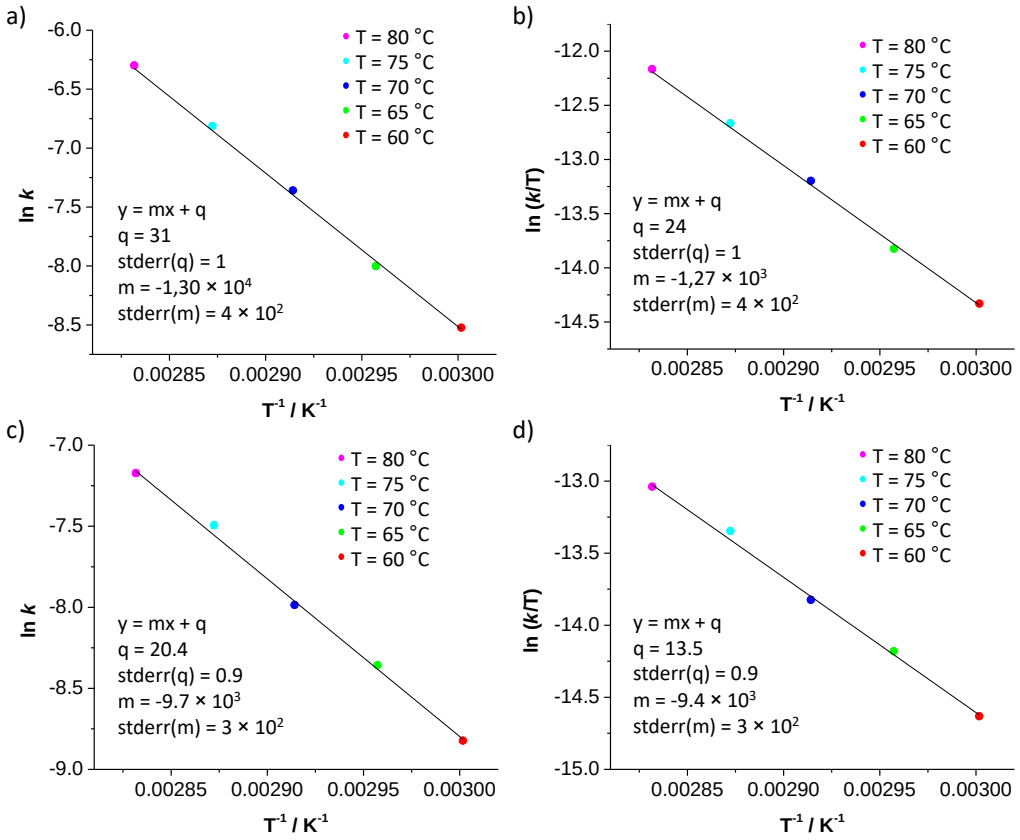

Figure 44. a,c) Arrhenius plots and b,d) Eyring plots for the photoracemization of atropisomer S_a of (a,b) H_{12}SubPc-TCBD-aniline **5** and (c,d) F_{12}SubPc-TCBD-aniline **6**. Insets: Intercept (q) and slope (m) of the linear fitting with associated standard errors.

Table 2. Kinetic parameters for the photoracemization of SubPc-TCBD-aniline derivatives **5** and **6** obtained from the Arrhenius and the Eyring plots.

	$\Delta H^{\ddagger}$ (kcal mol^{-1})	$\Delta S^{\ddagger}$ (cal mol^{-1} K^{-1})	$\Delta G^{\ddagger}_{(25\,°C)}$ (kcal mol^{-1})	E_a (kcal mol^{-1})	$\tau_{1/2\,(60\,°C)}$ (h)
5	25.2 ± 0.9	-0.116 ± 0.003	25.2 ± 0.9	25.8 ± 0.9	0.968 ± 0.004
6	18.6 ± 0.6	-20.283 ± 0.002	24.7 ± 0.6	19.3 ± 0.6	1.310 ± 0.007

In summary, CD experiments indicate that racemization of enantiopure samples of **5** and **6** is practically inhibited in not illuminated and/or O_2-saturated solutions, and significantly

accelerated upon illumination under O_2-free conditions (Figure 45). On one hand, these findings suggest that the activation barrier for the racemization of **5** and **6** is significantly higher than the amount of thermal energy provided with heating, whereas it is greatly reduced upon illumination of the sample, that is, upon promotion of the SubPc-TCBD-aniline derivative to an excited state. On the other hand, the hampering effect of O_2, a well-known triplet-state scavenger,[366] points out to the involvement of a triplet electronic state in the photoracemization process.

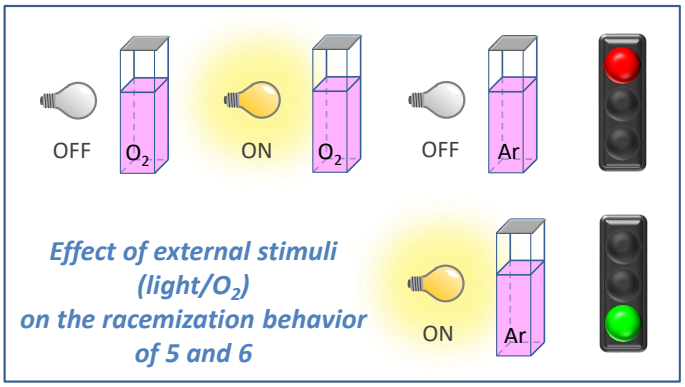

Figure 45. Cartoon depicting the effect of external stimuli (namely, light and molecular oxygen) on the racemization behavior of SubPc-TCBD-aniline derivatives **5** and **6**.

In order to shed light on the molecular mechanism leading to the racemization of SubPc-TCBD-aniline derivatives **5** and **6**, DFT B3LYP/6–31 + G(d,p) calculations were performed in collaboration with the group of Dr. Giuseppe Brancato at the Scuola Normale Superiore in Pisa, Italy. In this context, it is worth to mention that, in literature, photoracemization has been shown to take place through different mechanism, such as excited-state proton transfer,[367] photo-induced oxidation[368] or pyramidal inversion,[369] of bond breaking/formation.[370]

The energy barrier for the intramolecular rotation of one DCV unit with respect to the other around the TCBD chiral axis leading to the conversion of the S_a enantiomer into the R_a enantiomer was evaluated considering both ground (*i.e.*, S_0) and excited states (*i.e.*, S_1 and T_1).

[366] M. C. DeRosa, R. J. Crutchley, *Coord. Chem. Rev.* **2002**, *233*, 351-371.
[367] S. Ayad, V. Posey, A. Das, J. M. Montgomery, K. Hanson, *Chem. Commun.* **2019**, *55*, 1263-1266.
[368] K. Natori, T. Iwayama, O. Yamabe, Y. Kitamoto, H. Ikeda, K. Sakamoto, T. Hattori, S. Miyano, *Chirality* **2015**, *27*, 479-486.
[369] T. Machida, T. Iwasa, T. Taketsugu, K. Sada, K. Kokado, *Chem. Eur. J.* **2020**, *26*, 8028-8034.
[370] P. Wipf, W. S. Weiner, *J. Org. Chem.* **1999**, *64*, 5321-5324.

Notably, a steep increase of the ground-state energy of **5** and **6** along the isomerization coordinate (*i.e.*, the B-C_2-C_3-$C_{(aniline)}$ dihedral angle θ, see Figure 41 for atoms' labels) was observed (Figure 46). As a matter of fact, an energy barrier of 36.65 kcal mol^{-1} and 36.58 kcal mol^{-1} at 180° was calculated for **5** and **6**, respectively. This finding is in agreement with the exceptionally high thermal stability of S_a-**5** and S_a-**6** observed in CD experiments carried out with not illuminated (both O_2-saturated and O_2-free) solutions (*vide supra*).

In contrast, a significantly lower energy barrier of isomerization was calculated in the excited states with respect to S_0. In particular, the energy barrier was found to drop to approximately 15 kcal mol^{-1} upon electronic excitation of **5** and **6** (Figure 46). This trend confirms that racemization in **5** and **6** occurs through photogeneration of the corresponding excited states, as suggested by the remarkable increasing of the racemization rate of S_a-**5** and S_a-**6** observed in CD measurements performed under illumination of O_2-free solutions (*vide supra*). The formation of the electronically excited states of **5** and **6** in toluene solutions upon photoexcitation was also demonstrated by time-resolved photophysical studies, as will be discussed in section 1.3.3.1.

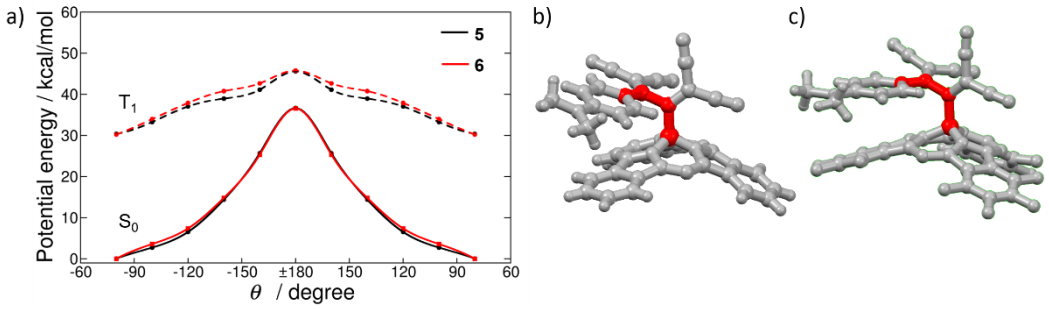

Figure 46. a) Potential energy profile of H_{12}SubPc-TCBD-aniline **5** (black line) and F_{12}SubPc-TCBD-aniline **6** (red line) as a function of the B-C_2-C_3-$C_{(aniline)}$ dihedral angle (θ) for the enantiomer conversion process computed from S_0 (solid line) and T_1 (dashed line). b,c) Computed ground state structures of (b) S_a-**5** and (c) S_a-**6**. Bonds and atoms comprising θ have been colored in red for the sake of clarity.

In light of the different racemization behavior of the C_{60}-TCBD-aniline conjugate reported by Diederich and co-workers,[339] which undergoes a complete thermal-induced racemization, comparative calculations were carried out on this derivative. In this case, a computed energy barrier of 27.9 kcal mol^{-1} was obtained in the ground state (Figure 47). This value is in very good agreement with the experimental activation barrier of C_{60}-TCBD-aniline reported in literature (*i.e.*, 28.2 ± 2.2 kcal mol^{-1}).[339] Remarkably, the ground-state activation barrier for the C_{60}-based derivative is about 9 kcal mol^{-1} lower than those calculated for SubPc-based conjugates **5** and **6**

(namely, 36.65 kcal mol^{-1} and 36.58 kcal mol^{-1}, respectively). Such a difference may explain the enhanced thermal stability of the latter towards isomerization. In this connection, it is worth to mention that an increase in the energy barrier of a few kcal/mol may lead to a significant slowdown of the rate of a chemical process. As an example, a hypothetical increase of the energy barrier for the isomerization of C_{60}-TCBD-aniline (for which a $\tau_{1/2}$ of approximately 6 h at 60 °C has been reported) by 9 kcal mol^{-1} (corresponding to the difference in the computed activation energy between C_{60}-TCBD-aniline and SubPc-TCBD-aniline derivatives **5** and **6**) would result in an increase of $\tau_{1/2}$ by a factor of 10^6.

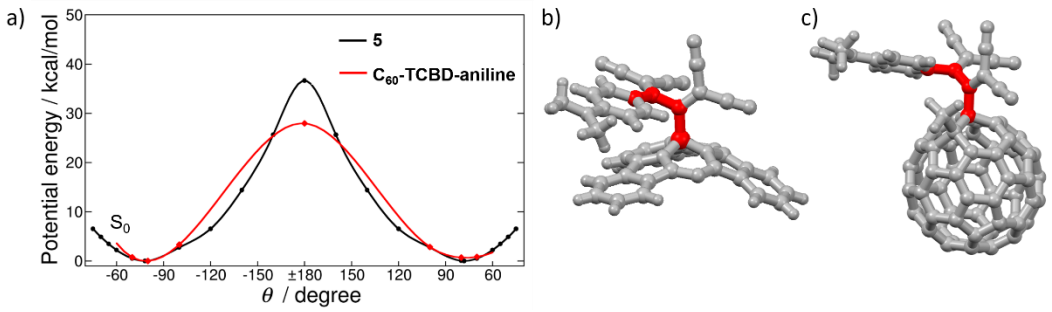

Figure 47. Ground-state potential energy profile of H_{12}SubPc-TCBD-aniline **5** (black line) and C_{60}-TCBD-aniline[339] (red line) as a function of the B-C_2-C_3-$C_{(aniline)}$ or $C_{(fullerene)}$-C_2-C_3-$C_{(aniline)}$ dihedral angle (θ). b,c) Computed ground state structures of (b) *S*$_a$-**5** and (c) *S*$_a$-C_{60}-TCBD-aniline. Bonds and atoms comprising θ have been colored in red for the sake of clarity.

Turning now to the effect of molecular oxygen on photoracemization, negligible *versus* fast racemization was observed in CD experiments carried out upon illumination of O_2-saturated and O_2-free solutions of SubPc-TCBD-aniline samples, respectively (*vide supra*). Taking into account the known role of molecular oxygen as triplet-state scavenger,[366] it is reasonable to assume that an efficient quenching of the photogenerated triplet excited state of **5** and **6** takes place in O_2-saturated solutions. Thus, the crucial role of O_2 clearly points towards a T_1-promoted photoracemization process. Nevertheless, it should be noted that similar energy barriers were provided by theoretical calculations for the isomerization of **5** and **6** from their S_1 and T_1 excited states.

In light of the aforementioned, the fact that the T_1 state promotes photoracemization more effectively than the S_1 state should be rationalized on the basis of kinetic considerations. In order for enantiomer conversions to occur, the DCV-aniline moiety should undergo a 180° rotation around the TCBD chiral axis with respect to the DCV-SubPc fragment, and the timescale of this intramolecular rearrangement has to be necessarily comparable to or shorter than the lifetime

of the SubPc excited state involved in the isomerization. Such a large intramolecular reorganization in solution likely requires several tens of picoseconds to take place. Thus, it is reasonable to assume that the above-mentioned condition is fulfilled for the T_1 species of **5** and **6** in toluene, which lifetimes are in the microsecond timescale, but not in the case of the S_1 species, which are characterized by lifetimes six order of magnitude shorter, namely, 7.5 and 3.5 ps in toluene for **5** and **6**, respectively (the photophysical characterization of **5** and **6** will be discussed more in detail in section 1.3.3.1). The involvement of triplet-state species in photoracemization processes had already been reported for binaphthyl derivatives[371] and RuII complexes,[372,373] although in these cases a different mechanism was proposed.

In order to provide additional insights on the main structural and electronic features enabling isomerization through the SubPc triplet excited state, a more extended computational investigation was performed. The lengths of the C_1-C_2, C_2-C_3 and C_3-C_4 bonds of the butadiene backbone as a function of the isomerization coordinate (namely, the B-C_2-C_3-$C_{(aniline)}$ dihedral angle θ) are reported in Figure 48.

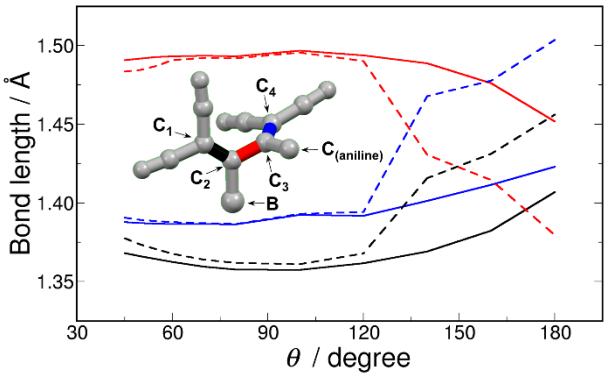

Figure 48. Length (in Å) of C_1-C_2 (black line), C_2-C_3 (red line), and C_3-C_4 (blue line) bonds in H_{12}SubPc-TCBD-aniline **5** as a function of the B-C_2-C_3-$C_{(aniline)}$ dihedral angle (θ). S_0=solid lines; T_1=dashed lines.

At the equilibrium configuration, the aniline moiety is oriented almost orthogonally with respect to the SubPc-TCBD bond (θ ≈ 80°) (Figure 41). Near this minimum-energy, non-planar geometry, the three TCBD C-C bonds in question appear very similar in both S_0 and T_1. In particular, C_1-C_2 and C_3-C_4 show a prominent double bond character, whereas C_2-C_3 exhibits a mainly single bond

[371] M. Irie, K. Yoshida, K. Hayashi, *J. Phys. Chem.* **1977**, *81*, 969-972.
[372] L. Feng, Y. Wang, *Inorg. Chem.* **2018**, *57*, 8994-9001.
[373] M. Asahara, H. Kurimoto, M. Nakamizu, S. Hattori, K. Shinozaki, *Phys. Chem. Chem. Phys.* **2020**, *22*, 6361-6369.

character. Upon increasing θ towards 180°, in the ground state the three C-C bonds smoothly converge towards a length of 1.40–1.45 Å. Such a length value is intermediate between the lengths of typical C-C single (≈1.54 Å) and double (≈1.35 Å) bonds.

Shifting to the T_1 state, an evident change in bond lengths can be observed for θ values above 120°. As a matter of fact, the C_1-C_2 and C_3-C_4 bonds acquire a single bond character (reaching, for θ = 180°, a length of 1.46 and 1.50 Å, respectively), whereas the central C_2-C_3, which initially displays a single bond character, is significantly shortened (*i.e.*, from 1.49 to 1.38 Å). These structural changes in the triplet excited state contribute at stabilizing the DCV-aniline moiety "rotor" at θ ≈ 180° with respect to the ground state, thus lowering the isomerization energy barrier. In particular, the shortening and strengthening of the C_2-C_3 bond provide further stabilization to the vertical configuration (θ ≈ 180°) of the TCBD-aniline moiety, while the elongation of both the C_1-C_2 and C_3-C_4 bonds enhances the rotational flexibility of the DCV moieties, thus facilitating the completion of the SubPc's isomerization pathway. Hence, photoinduced enantiomer conversion in conjugates **5** and **6** is achieved by lowering the energy barrier of the sterically inhibited rotation around the chiral axis. This is accomplished by rendering more favorable the sterically hindered planar configuration of the TCBD while in the excited triplet state. Thus, photoactivated isomerization in the investigated SubPc derivatives does not occur through intermediate species neither *via* bond breaking/formation, as usual for most chiral compounds.

The structural changes involving the TCBD moiety during the isomerization process are also accompanied by local electronic rearrangements, as can be deducted from the computation of the T_1-S_0 electron density difference as a function of the isomerization coordinate (Figure 49). As a matter of fact, at θ > 120°, an increase of electron density on the central C_2-C_3 bond is observed, while a planar configuration (θ ≈ 180°) is assumed by the butadiene unit.

In summary, light-triggered enantiomer conversion in SubPc-TCBD-aniline derivatives **5** and **6** exploits a peculiar mechanism enabled by triplet-state photogeneration, which makes feasible the rotation of the DCV-containing halves around the sterically hindered TCBD chiral axis.

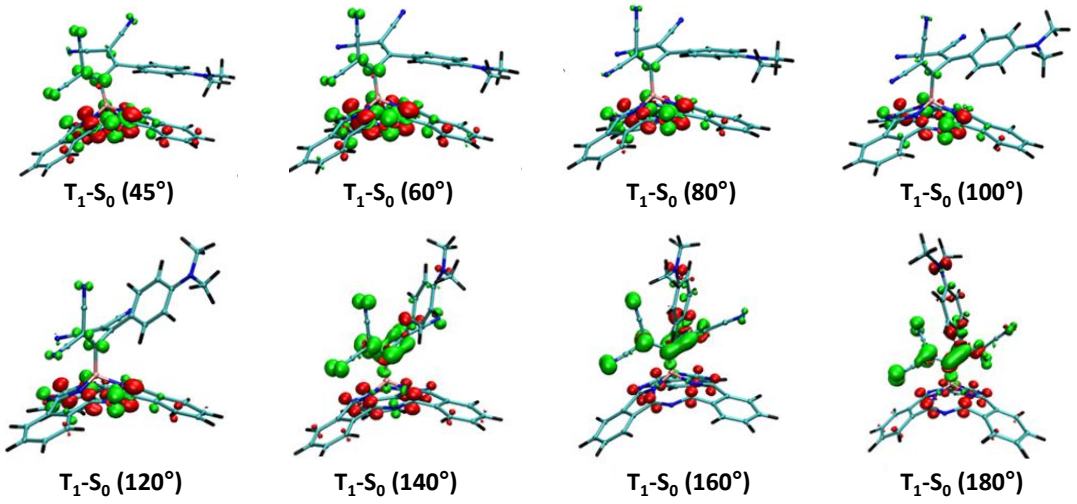

Figure 49. Electron density difference between the ground state (S_0) and first triplet (T_1) state of H_{12}SubPc-TCBD-aniline **5** at different B-C_2-C_3-$C_{(aniline)}$ dihedral angles θ. Green and red colors refer to positive and negative density changes, respectively.

Study of enantiomer conversion in SubP-TCBD-aniline 16

Given the peculiar isomerization mechanism of SubPc-TCBD-aniline derivatives **5** and **6** and with the aim to realize a comparative study, the racemization behavior of an analogous SubP conjugate bearing a TCBD-aniline moiety covalently linked to the axial position (**16**) was investigated (Figure 50). SubP-TCBD-aniline **16** was provided by the group of Prof. Atsuhiro Osuka at Kyoto University in Kyoto, Japan.

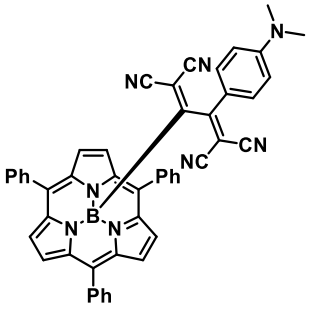

16

Figure 50. Chemical structure of SubP-TCBD-aniline **16**.

As observed for SubPc-TCBD-aniline derivatives **5** and **6**, the X-ray crystal structure of SubP-TCBD-aniline **16** shows that the TCBD unit is highly non-planar (Figure 51). As a matter of fact, a C_1-C_2-C_3-C_4 torsion angle θ of 85° is observed. Thus, two enantiomers are formed (namely, S_a-**16** and R_a-**16**), which are found in the crystal structure of **16**.

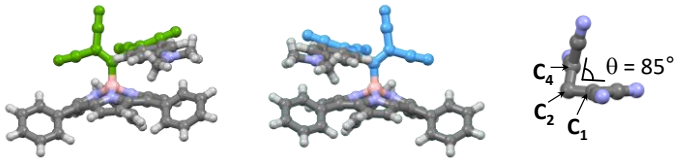

Figure 51. Lateral view of the X-ray crystal structure of (left) atropisomer R_a and (middle) atropisomer S_a within the crystal structure of SubP-TCBD-aniline **16**. Right: Torsion angle (θ) between the four carbon atoms constituting the butadiene backbone. The C_3 atom in the butadiene backbone has been eclipsed by the C_2 atom for the sake of clarity.

The optical resolution of axially chiral SubP-TCBD-aniline **16** was achieved by means of semipreparative chiral HPLC (Figure 52). The mirror-image CD spectra of the isolated species provided conclusive evidence of their enantiomeric relationship (Figure 53). In this regard, it is worth to mention that chiral HPLC separation of racemic SubPs which chirality resulted from the presence of three different aryl groups at the SubP *meso* positions has been reported by Osuka, Mori and co-workers.[374] In that work, the CD response of the enantiopure species was found to be extremely weak, which was explained on the basis of the large conformational freedom of the three aryl moieties.

[374] K. Yoshida, H. Mori, T. Tanaka, T. Mori, A. Osuka, *Eur. J. Org. Chem.* **2014**, *2014*, 3997-4004.

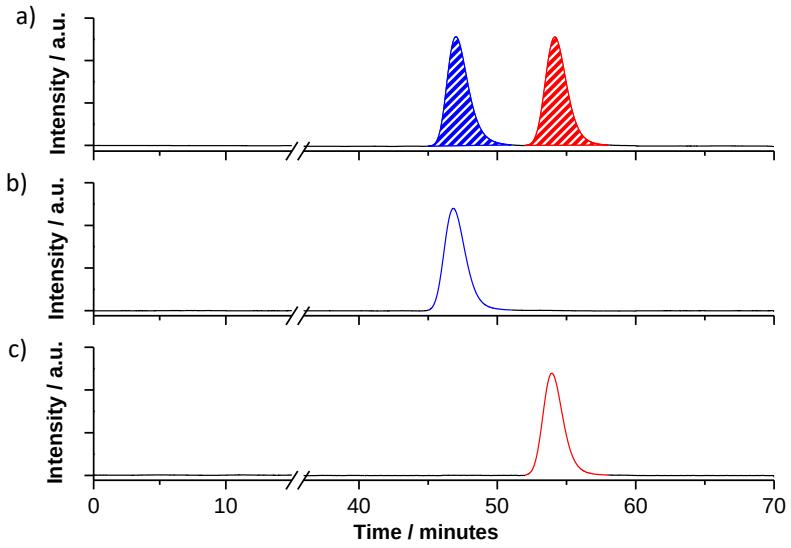

Figure 52. a) HPLC chromatogram of SubP-TCBD-aniline racemate **16**. The percentage areas of the peaks are 50.0% and 50.0%, respectively. b,c) HPLC chromatograms of the isolated atropisomers. HPLC conditions: eluting solvent mixture = toluene/*n*-hexane/ethyl acetate 85:12:3 (v/v/v); flow rate = 0.6 mL min^{-1}; temperature = 10 °C, detection wavelength = 379 nm).

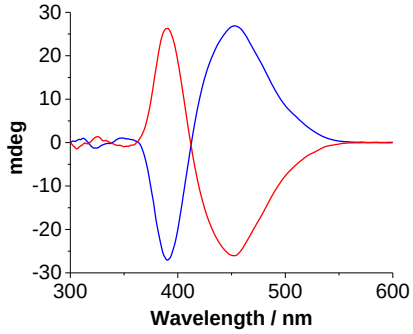

Figure 53. CD spectra of the first eluted (blue spectrum) and second eluted (red spectrum) atropisomers of SubP-TCBD-aniline **16** in toluene/*n*-hexane/THF 85:12:3 (v/v/v) (c = 2.6 × 10^{-5} M).

Once accomplished the successful chromatographic separation of the R_a and S_a enantiomers of **16**, we aimed to obtain single crystals of the isolated atropisomers in order to unambiguously assign their absolute configuration. However, any attempt to grow single crystals of the enantiopure species was unsuccessful. As a matter of fact, crystals suitable for X-ray analysis were obtained by slow evaporation of dichloromethane from a solution of optically pure SubP-

TCBD-aniline **16**. Nevertheless, X-ray diffraction measurements revealed the presence of both enantiomers in the crystal lattice, thus indicating that isomerization had took place.

The thermal stability of the enantiopure species was then investigated. To this purpose, temperature-controlled CD measurements were performed over time on air-saturated solutions of the first eluted enantiomer of **16** in the same solvent mixture employed for HPLC separation. In stark contrast with what observed for SubPc-TCBD-aniline derivatives **5** and **6**, almost complete racemization was observed upon heating the solution at 80 °C for less than an hour. Then, a kinetic study of the racemization process in **16** was performed with the aim to determine the activation parameters for enantiomer conversion. To this end, temperature-controlled CD experiments over time at five different temperature (*i.e.* 60, 65, 70, 75 and 80 °C) were performed. In this way, first-order rate constants were obtained (Figure 54). Using the Arrhenius and the Eyring formalisms (Equations 11 and 12), the kinetic parameters for the racemization process of **16** were determined (Figure 55 and Table 3).

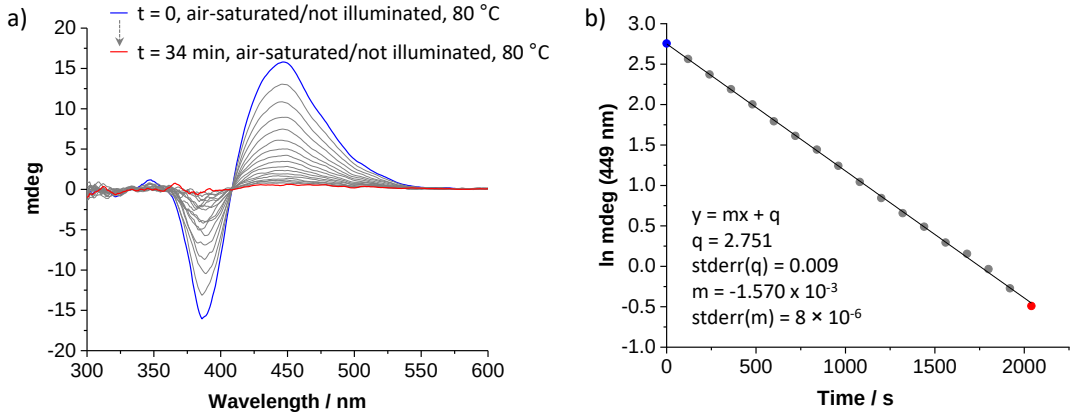

Figure 54. a) CD spectra of a solution of the first-eluted enantiomer of SubP-TCBD-aniline **16** in toluene/*n*-hexane/THF 85:12:3 (v/v/v) (c = 2.6 × 10^{-5} M) heated at 80 °C over time. b): Linear fitting of the variation of the CD absorbance in a) monitored at 449 nm as a function of time. Inset: Intercept (q) and slope (m) of the linear fitting with associated standard errors.

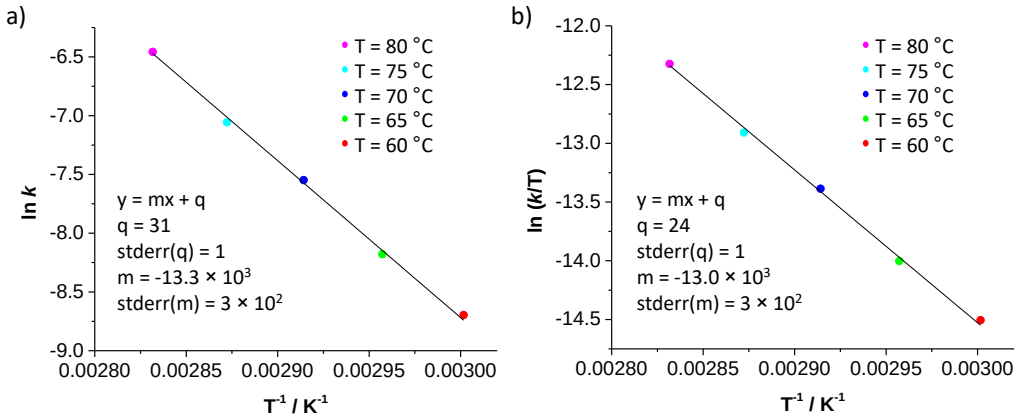

Figure 55. a) Arrhenius plot and b) Eyring plot for the racemization of the first-eluted enantiomer of SubP-TCBD-aniline **16**. Inset: Intercept (q) and slope (m) of the linear fitting with associated standard errors.

Table 3. Kinetic parameters for the racemization of SubP-TCBD-aniline **16** and C_{60}-TCBD-aniline obtained from the Arrhenius and the Eyring plots. Values relative to C_{60}-TCBD-aniline have been taken from ref. 339.

	$\Delta H^{\ddagger}$ (kcal mol^{-1})	$\Delta S^{\ddagger}$ (cal mol^{-1} K^{-1})	$\Delta G^{\ddagger}_{(25\,°C)}$ (kcal mol^{-1})	E_a (kcal mol^{-1})	$\tau_{1/2\,(60\,°C)}$ (h)
16	25.8 ± 0.7	1.467 ± 0.002	25.4 ± 0.7	26.5 ± 0.7	1.152 ± 0.006
C_{60}-TCBD-aniline	27.6 ± 2.3	9.7 ± 6.7	24.8 ± 0.3	28.2 ± 2.2	5.9 ± 2.4

From a comparison between the experimental parameters obtained for SubP-TCBD-aniline **16** and the values reported in literature for the analogous conjugate C_{60}-TCBD-aniline,[339] an evident similarity in terms of activation energies of racemization can be observed (Table 3). This is in line with the structural similarity of the TCBD moiety, *i.e.* the chiral unit involved in the racemization process, in terms of bond lengths, bond angles, and torsion angles within the crystal structure of the two TCBD-based derivatives. The experimentally observed thermal racemization SubP-TCBD-aniline **16** suggests that, in this derivative, enantiomer conversion is promoted effectively in the ground state, in contrast with what observed for SubPc-TCBD-aniline conjugates **5** and **6**.

1.3.2.2 Structural properties of peripherally and peripherally/axially (TCBD-aniline)-substituted SubPcs

Analysis of the chiral elements of (TCBD-aniline)$_3$SubPc derivatives 14 and 15

In terms of stereochemical characteristics, peripherally and peripherally/axially (TCBD-aniline)-substituted SubPcs **14** and **15** present several interesting features.

As mentioned in the Introduction of this Thesis, due to the cone-shaped geometry of the SubPc macrocycle, SubPcs prepared by cyclotrimerization reaction of non-C_{2v}-symmetric phthalonitriles are formed as a mixture of two regioisomers with C_3 and C_1 symmetry, each of which is, in turn, a racemic mixture of two enantiomers. Thus, the starting C_3-symmetric I_3SubPc-Cl **9** is inherently chiral. The same can be said for SubPcs **10-15**, which are prepared by successive functionalization of **9**, and therefore possess the same C_3-symmetric peripheral substitution pattern.

In order to assign the absolute configuration to the enantiomers of a C_3-symmetric SubPc, the following convention can be followed, which makes use of the *P*/*M* stereodescriptor system that is employed to designate the chirality of buckybowl molecules[375,376] and is based on the CIP sequence rules (Figure 56). 1) The SubPc is placed having the axial ligand pointing towards the observer. 2) The rim atoms that rank highest in priority according to the CIP rules (which for trisubstituted, C_3-SubPcs coincide with the carbon atoms bearing the peripheral substituent giving rise to the C_3-symmetric substitution pattern) are identified and considered as points of origin. 3) For each point of origin, the two rim atoms attached to this point are compared, and the same is done, if necessary, for subsequent atoms attached thereto, until two rim atoms that lie the same number of positions away from the point of origin on the clockwise and counterclockwise paths are found that differ in CIP priority. 4) If the direction of travel from the point of origin to the rim atom with higher CIP priority is clockwise, the SubPc is designated as *P*; if the direction of travel is anticlockwise, the SubPc is designated as *M*.

[375] M. A. Petrukhina, K. W. Andreini, L. Peng, L. T. Scott, *Angew. Chem. Int. Ed.* **2004**, *43*, 5477-5481.
[376] K. Kanagaraj, K. Lin, W. Wu, G. Gao, Z. Zhong, D. Su, C. Yang, *Symmetry* **2017**, *9*, 174.

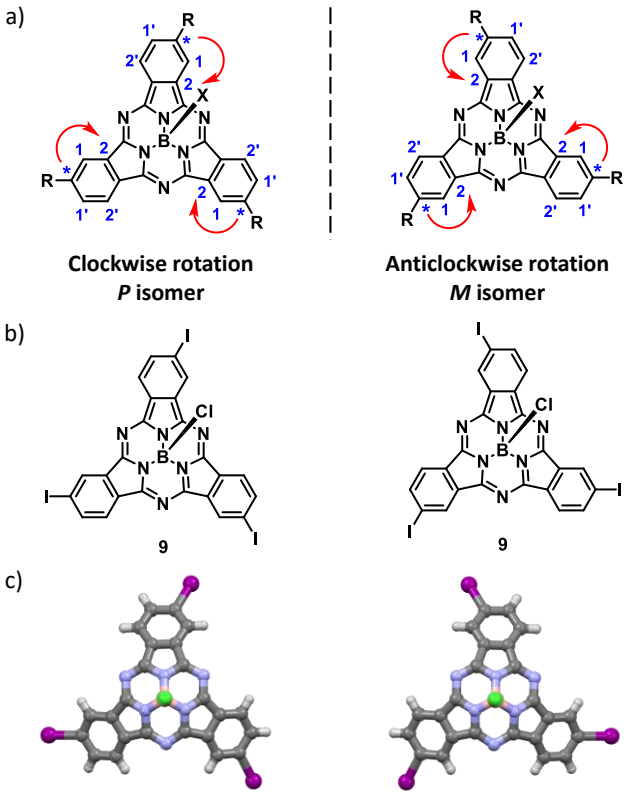

Figure 56. a) Convention for the assignment of the *P* or *M* configuration to a C_3-symmetric SubPc. The rim atoms that rank highest in priority (points of origin) are marked with an asterisk. Whereas 1 and 1' have the same priority according to the CIP rules, 2 ranks higher in priority with respect to 2'. b) Chemical structure and c) molecular modelling structure of the (left) *P* and (right) *M* enantiomers of C_3-symmetric I_3SubPc-Cl **9**.

In addition to the inherent chirality of C_3-symmetric SubPcs, the introduction of three or four TCBD moieties in conjugates **14** and **15**, respectively, brings new stereogenic elements. On one hand, each TCBD unit possesses a chiral axis arising from the restricted rotation around the central C-C bond of the butadiene framework and the quasi-orthogonal arrangement of the two DCV halves, as mentioned above in this Chapter. Thus, each of the three peripheral (in **14**) or the four peripheral and axial (in **15**) TCBD units can adopt a R_a or S_a configuration. The convention for the assignment of the R_a and S_a stereochemical labels to axially chiral TCBD-based derivatives has been described in section 1.3.2.1 (Figure 33). On the other hand, due to the non-planar geometry of the SubPc macrocycle, the rotation around the C-C single bonds connecting

the three peripheral TCBD groups to the SubPc benzene rings in **14** and **15** may give rise to different conformers.

Taking all the above-mentioned stereochemical features into account, several stereoisomeric species are expected for **14** and **15**. A simplified model is proposed herein to visualize these possible stereoisomers (Figure 57). 1) For each derivative, both the *M* and *P* enantiomers are considered; 2) each of the three peripheral TCBD units is represented as a red arrow pointing up (which means that the *N*,*N*-dimethyl-aniline moiety linked to the TCBD is pointing to the same side to which the SubPc axial ligand points to) or a blue arrow pointing down (which means that the *N*,*N*'-dimethyl-aniline moiety linked to the TCBD is pointing to the opposite side to which the SubPc axial ligand points to); 3) the arrows, pointing either up or down, are filled with either orange or green color depending on the S_a or R_a configuration of the TCBD unit, respectively. Using this model (and thus taking into account only two possible conformations for each peripheral TCBD unit), 24 pairs of enantiomers can be identified for (TCBD-aniline)$_3$SubPc-OAr **14**. In the case of (TCBD-aniline)$_3$SubPc-(TCBD-aniline) **15** this value doubles due to the presence of an additional TCBD at the SubPc axial position, which can feature either a S_a or a R_a configuration.

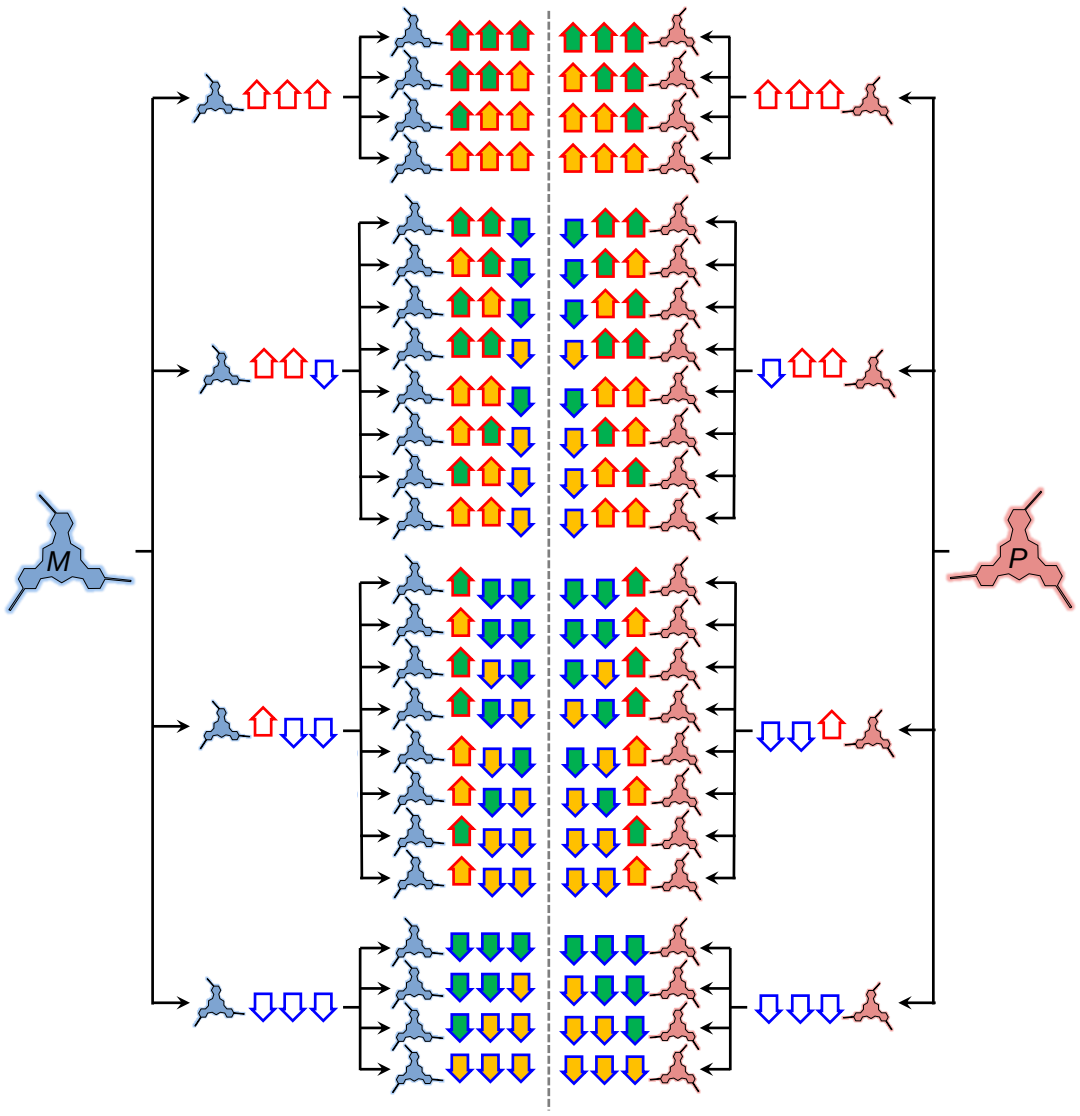

Figure 57. Cartoon representing the possible stereoisomers of (TCBD-aniline)$_3$SubPc-OAr **14**.

As an example, the four possible conformers of the S_a,S_a,S_a isomer of *P*-(TCBD-aniline)$_3$SubP-OAr **14** resulting from the 180° rotation of each of the three TCBD units around the C-C bond connecting the butadiene moiety to the SubPc macrocycle are depicted in Figure 58.

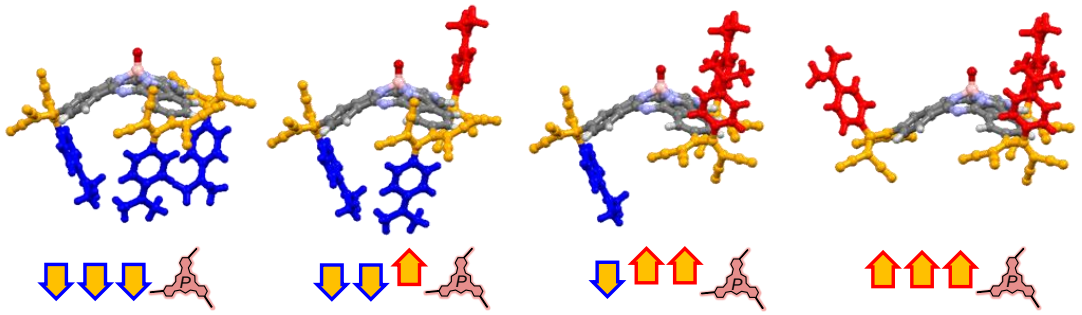

Figure 58. Molecular modelling structures (top) and cartoon representation (bottom) of four possible conformers of the S_a,S_a,S_a isomer of *P*-(TCBD-aniline)$_3$SubPc-OAr **14** originating from the 180° rotation of each of the three peripheral TCBD units around the C-C bond connecting the TCBD to the SubPc. For the sake of clarity, the SubPc axial ligand has been omitted, except for the oxygen atom.

As another example, three possible isomers of the S_a,S_a,S_a isomer of *P*-(TCBD-aniline)$_3$SubPc-OAr **14** featuring the three *N*,*N*-dimethyl-aniline moieties pointing to the opposite side to which the SubPc axial ligand points to, resulting from the configurational inversion (from S_a to R_a) of each of the three peripheral TCBD units are presented in Figure 59. In this case, each S_a to R_a TCBD inversion is accompanied by the change of the side to which the *N*,*N*-dimethyl-aniline points to (*i.e.*, from opposite to the SubPc axial ligand, to the same side).

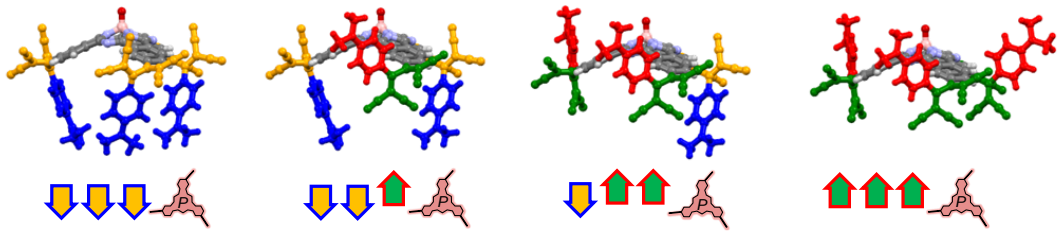

Figure 59. Molecular modelling structures (top) and cartoon representation (bottom) of the S_a,S_a,S_a isomer of *P*-(TCBD-aniline)$_3$SubPc-OAr **14** and the three possible configurational isomers resulting from the configurational inversion (from S_a to R_a) of each of the three peripheral TCBD units. For the sake of clarity, the SubPc axial ligand has been omitted, except for the oxygen atom.

The stereoisomers of *P*-(TCBD-aniline)$_3$SubPc-OAr **14** could, in principle, interconvert between them by S_a/R_a configurational inversion, and/or rotation around the C-C single bonds connecting the TCBD units to the SubPc. The same holds for the stereoisomers of *M*-(TCBD-aniline)$_3$SubPc-OAr **14**. In *P*-(TCBD-aniline)$_3$SubPc-TCBD-aniline **15** and *M*-(TCBD-aniline)$_3$SubPc-TCBD-aniline **15**, configurational inversion of the axial TCBD moiety should also be taken into account.

^{1}H-NMR features of (TCBD-aniline)$_3$SubPc derivatives 14 and 15

As mentioned above, a large number of stereoisomers are expected for both (TCBD-aniline)$_3$SubPc-OAr **14** and (TCBD-aniline)$_3$SubPc-TCBD-aniline **15** as a consequence of the inherent chirality of the SubPc macrocycle, the axial chirality of the TCBD units and the rotation of the peripheral TCBD moieties around the C-C bonds connecting the butadiene framework to the SubPc. Nevertheless, the ^{1}H-NMR spectrum of **14** in deuterated chloroform at room temperature is quite sharp and signals present the expected multiplicity (Figure 60). This is likely a result of the rapid interconversion between different stereoisomers. In other words, this experimental evidence suggests that, under these conditions, (i) the R_a/S_a interconversion of the TCBD units is fast on the NMR timescale, and (ii) the conformational flexibility of the peripheral TCBD moieties is high. Similar considerations can be drawn for **15**, although in this case two set of signals can be distinguished due to the presence of the additional axially chiral TCBD-aniline unit in the SubPc axial position (Figure 61).

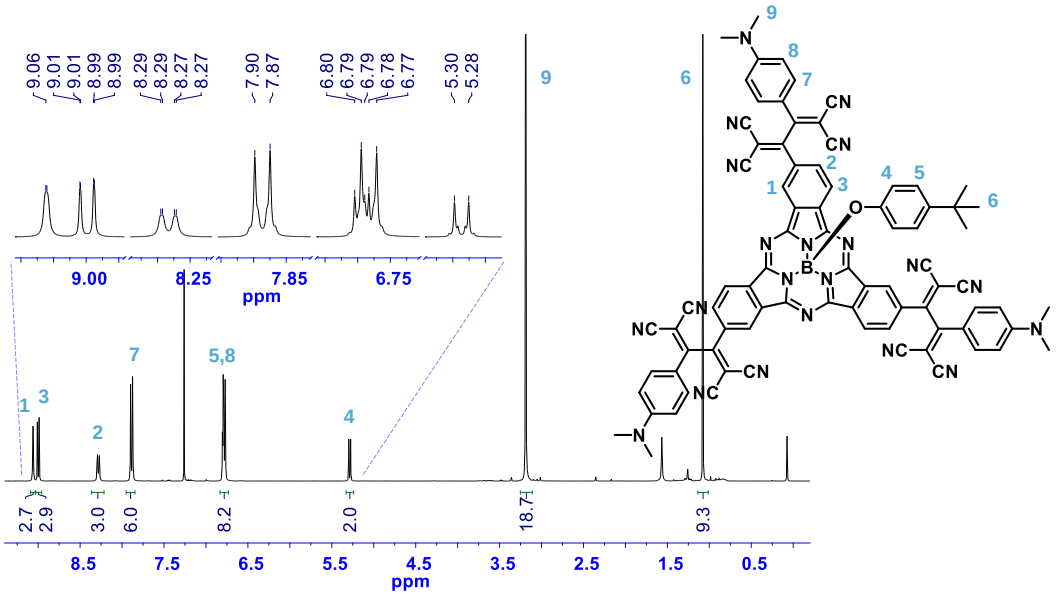

Figure 60. ^{1}H-NMR spectrum (400 MHz, $CDCl_3$) of (TCBD-aniline)$_3$SubPc-OAr **14**. Inset: zoom of the aromatic protons' peaks.

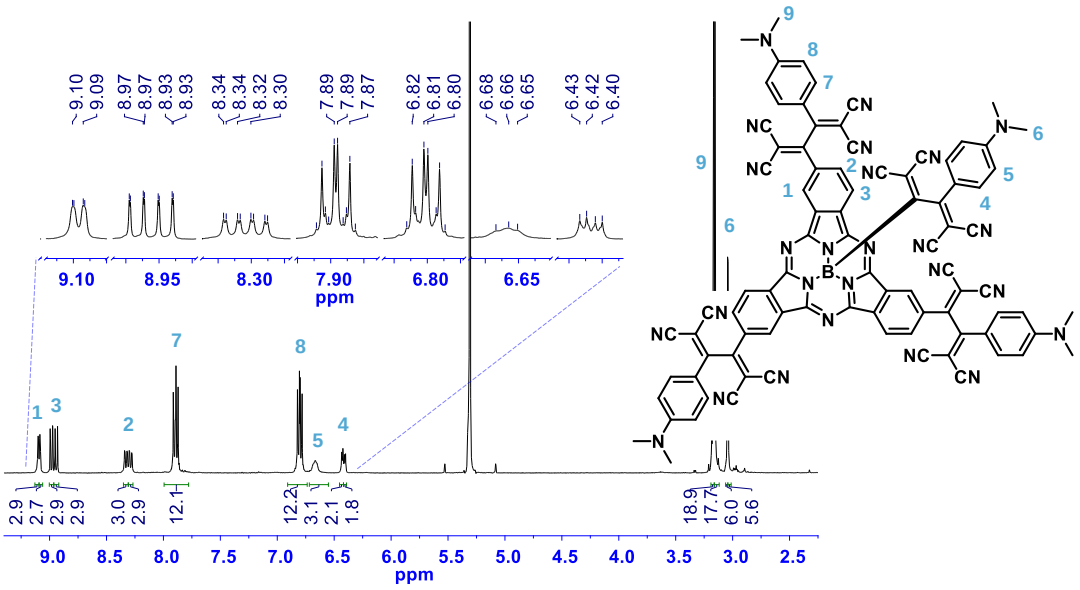

Figure 61. ^{1}H-NMR spectrum (400 MHz, CD_2Cl_2) of (TCBD-aniline)$_3$SubPc-TCBD-aniline **15**. Inset: zoom of the aromatic protons' peaks.

The assignment of the signals in the ^{1}H-NMR spectra of derivatives **14** and **15** was performed with the help of H-H NOESY experiments. As an example, the H-H NOESY spectrum of derivative **14** showing the correlations between the peripheral protons of the SubPc macrocycle, between the protons of the *N*,*N*-dimethylaniline moieties and between the protons of the *t*-butylphenoxy ligand is shown in Figure 62. In the ^{1}H-NMR spectra of (TCBD-aniline)$_3$SubPc-OAr **14** (Figure 60), the aromatic protons of the isoindolic benzene rings of the SubPc macrocycle give rise to the typical pattern expected for peripherally trisubstituted, C_3-symmetryc SubPcs. As expected, the aromatic protons of the axial aryloxy group (*i.e.*, 4 and 5) are shifted upfield due to the diatropic ring current of the SubPc macrocycle. The correlation between two of the aromatic protons of each peripheral *N*,*N*-dimethylaniline moiety (*i.e.*, 8) with the methyl protons allowed to assign the aromatic protons of the aniline groups. The same could be done for the axial *t*-butylphenoxy substituent. Similar considerations can be done for (TCBD-aniline)$_3$SubPc-TCBD-aniline **15**.

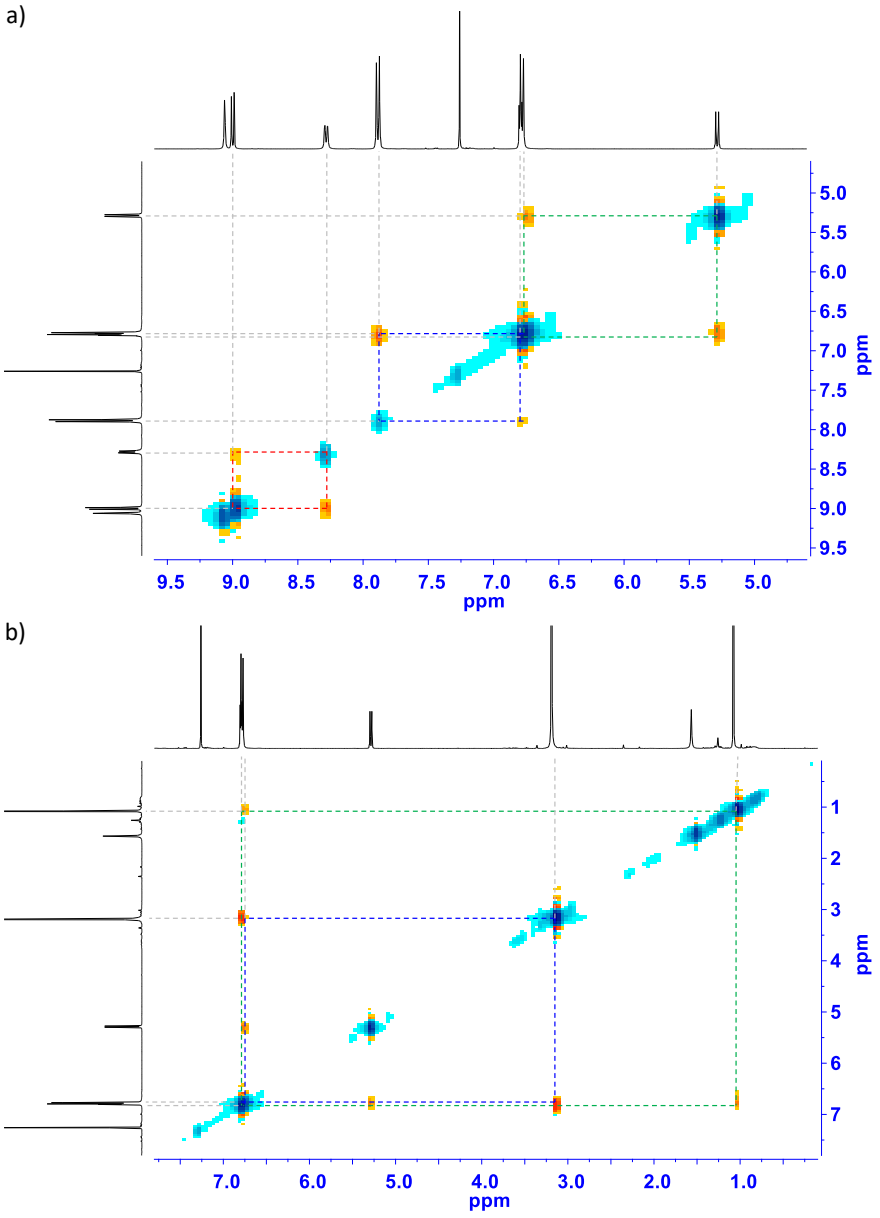

Figure 62. Zoom of the region between a) 9.6 ppm and 4.6 ppm and b) 7.8 ppm and 0.1 ppm of the H-H NOESY NMR spectrum (400 MHz, $CDCl_3$) of (TCBD-aniline)$_3$SubPc-OAr **14** showing the correlations between the peripheral protons of the SubPc macrocycle (red dashed lines), the protons of the *N*,*N*-dimethylaniline moieties (blue dashed lines) and the protons of the *t*-butylphenoxy ligand (green dashed lines).

In order to further investigate the interconversion between stereoisomers in **14** and **15**, low-temperature ^{1}H-NMR experiments were carried out. These measurements led to a rather different scenario with respect to that observed in room-temperature ^{1}H-NMR experiments. As a matter of fact, upon decreasing the temperature, an increase in multiplicity, broadening, and shifting of the NMR signals were observed (Figures 63 and 64). Such findings suggest that the interconversion between different stereoisomers in **14** and **15** is significantly slowed down upon lowering the temperature, thus resulting in the coexistence, on the NMR timescale, of many magnetically distinct species. A similar effect had been reported in literature for corannulene derivatives peripherally functionalized with two or five TCBD units.[355]

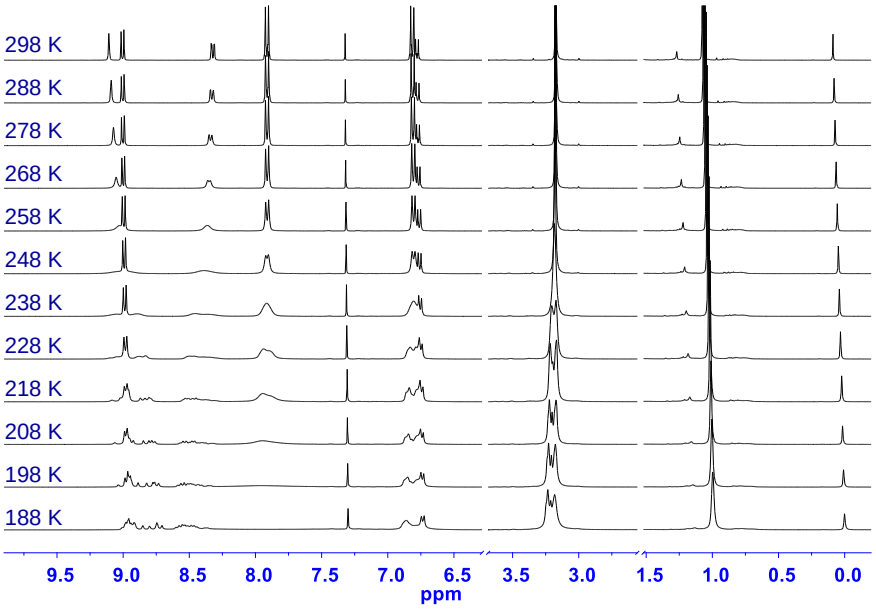

Figure 63. VT ^{1}H-NMR spectra (400 MHz, CD_2Cl_2) of (TCBD-aniline)$_3$SubPc-OAr **14**.

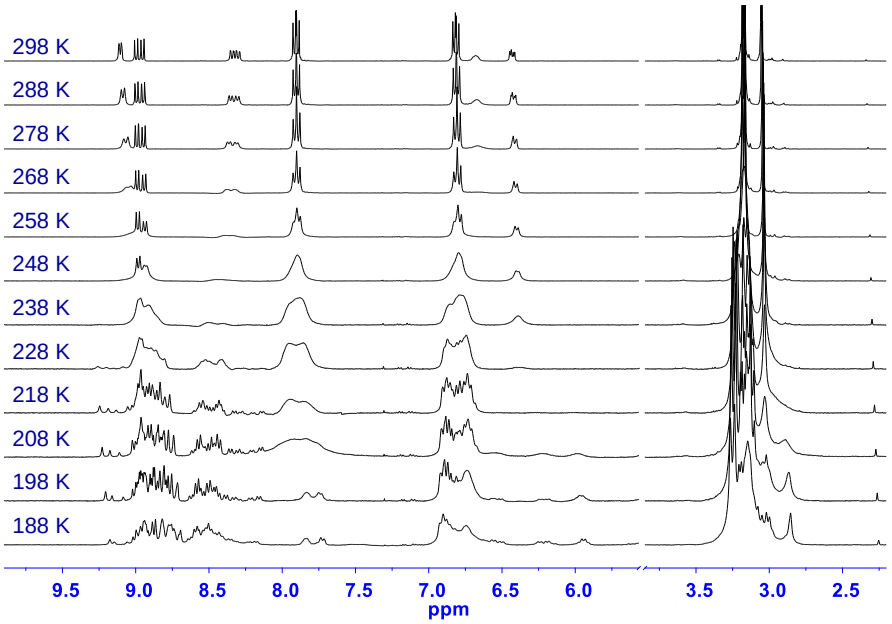

Figure 64. VT ^{1}H-NMR spectra (400 MHz, CD_2Cl_2) of (TCBD-aniline)$_3$SubPc-TCBD-aniline **15**.

1.3.3 Electrochemical and photophysical properties of (TCBD-aniline)-functionalized SubPcs

As mentioned in the Introduction of this Thesis, the study of the interchromophoric interactions within photoactive D-A systems is of fundamental importance for implementing these conjugates in technologically relevant fields related to solar energy conversion. Thus, with the aim to shed light on the intramolecular interactions both in the ground and in the excited states within the novel (TCBD-aniline)-functionalized SubPc conjugates synthesized, the electrochemical and photophysical features of derivatives **5**, **6**, **14** and **15** and their precursors were investigated. These studies were performed in collaboration with the research group of Prof. Dirk Guldi at Friedrich-Alexander University Erlangen-Nürnberg in Erlangen, Germany.

1.3.3.1 Electrochemical and photophysical properties of axially (TCBD-aniline)-substituted SubPcs

Electrochemical features of SubPc-TCBD-aniline derivatives 5 and 6

The redox properties of SubPc-TCBD-aniline conjugates **5** and **6** and their SubPc-ethynyl-aniline precursors **3** and **4** were probed by means of cyclic voltammetry (CV) and square wave voltammetry (SWV). A Ph-TCBD-aniline derivative was employed as reference compound for the electrochemical study of **5** and **6** (Figure 65). This species features two TCBD-centered, one-electron reductions at -0.94 and -1.26 V and an aniline-centered oxidation at +0.92 V.[356] The electrochemical data for derivatives **3**-**6** and the Ph-TCBD-aniline reference are summarized in Table 4.

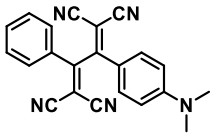

Figure 65. Chemical structure of the Ph-TCBD-aniline derivative employed as reference compound for the electrochemical studies.

First of all, the electrochemical features of the peripherally hydrogenated SubPc derivatives **3** and **5** were investigated. For H_{12}SubPc-ethynyl-aniline **3,** two one-electron reductions at -1.46 and -2.03 V as well as three one-electron oxidations at +0.38, +0.46, and +1.00 V are observed. Whereas the first oxidation is aniline-centered, all the other redox processes occur at the H_{12}SubPc moiety.

Table 4. Electrochemical oxidation and reduction data (V *versus* Fc^+/Fc) for derivatives **3**-**6** and Ph-TCBD-aniline reference[356] detected by SWV at room temperature in 0.2 M (for **3**-**6**) and 0.1 M (for the Ph-TCBD-aniline reference) solutions of *n*-Bu_4NPF_6 in DCM.

	E_{ox}^3	E_{ox}^2	E_{ox}^1	E_{red}^1	E_{red}^2	E_{red}^3	E_{red}^4	E_{red}^5
3	+1.00[b]	+0.46[b]	+0.38[a]	-1.46[b]	-2.03[b]			
4		+0.98[b]	+0.47[a]	-1.04[b]	-1.62[b]	-2.20[b]		
5		+0.92[a]	+0.68[b]	-1.16[c]	-1.24[c]	-1.24[b]	-1.85[b]	
6		+0.99[b]	+0.92[a]	-0.84[b]	-1.24[c]	-1.42[c]	-1.88[b]	-2.22[b]
Ph-TCBD-aniline			+0.92[a]	-0.94[c]	-1.26[c]			

[a] Aniline-centered process. [b] SubPc-centered process. [c] TCBD-centered process.

H_{12}SubPc-TCBD-aniline **5** exhibits two one-electron reductions at -1.16 and -1.85 V, and two coalescing one-electron reductions at -1.24 V. A comparison of the redox features of **5** with those of the reference Ph-TCBD-aniline derivative suggests that the first two reductions in **5** occur at the TCBD unit. In particular, it is reasonable to assume that the first reduction at -1.16 V is mainly centered on the DCV linked to the SubPc, whereas the second reduction at -1.24 V is centered on the DCV connected to the aniline. In this context, it is worth to mention that little, if any, electronic communication between the two DCV halves of the TCBD unit in the investigated derivatives is expected in the ground state due to their almost perpendicular arrangement, which can be observed in the X-ray crystal structure of **5** an **6** (Figure 29). On the other hand, the two reductions at -1.24 and -1.85 V are SubPc-centered. Notably, the former is anodically shifted by 0.22 V with respect to the analogous reduction in precursor **3** as a consequence of the strong electron-withdrawing effect exerted by the TCBD moiety in **5**. Electrochemical oxidation of **5** gives rise to two one-electron oxidations at +0.68 and +0.92 V. While the latter can be assigned as aniline-centered by comparison with the Ph-TCBD-aniline reference, the former occurs at the H_{12}SubPc unit.

Turing to the redox features of the peripherally fluorinated derivatives, F_{12}SubPc-ethynyl-aniline **4** undergoes three one-electron reductions at -1.04, -1.62, and -2.20 V and two one-electron oxidations at +0.47 and +0.98 V. Whereas all the reductions are SubPc-centered, the first and second oxidations involve the aniline and the SubPc units, respectively.

On the other hand, F_{12}SubPc-TCBD-aniline **6** exhibits an aniline-centered and a SubPc-centered one-electron oxidation at +0.92 and +0.99 V, respectively. In contrast with what observed for **5**, the latter occurs in **6** at the same potential as in precursor **4**, suggesting that the electron-withdrawing TCBD exerts in **6** no profound perturbation of the oxidative features of the SubPc

macrocycle. Turning to the reductive region of F_{12}SubPc-TCBD-aniline **6**, five one-electron reductions at -0.84, -1.24, -1.42, -1.88, and -2.22 V are observed. The first, fourth and fifth processes occur at the SubPc, whereas a comparison with the reductions of the reference Ph-TCBD-aniline indicates that the second and third reductions involve the TCBD unit. In particular, the peaks at -1.24 and -1.42 V can be assigned to the reduction of the DCV moiety linked to the aniline and the reduction of the DCV half connected the F_{12}SubPc, respectively. Compared to precursor **4**, the first F_{12}SubPc-centered reduction in **6** is anodically shifted by 0.20 V, similarly to what observed when comparing the H_{12}SubPc-centered reductions in **5** and **3**. This anodic shift is due to the direct linkage of the electron-accepting TCBD to the SubPc, which renders the macrocycle in **6** more electron-deficient.

From a comparison between the redox features of **5** and **6**, several considerations can be made. On one hand, the SubPc-centered oxidation is subjected to an anodic shift (0.31 V) when moving from **5** to **6**, which proves the higher ionization potential of the fluorinated SubPc in comparison with the hydrogenated macrocycle. On the other hand, an anodic shift (0.40 V) of the first SubPc-centered reductions is observed when turning from **5** and **6**. This finding is in sound agreement with the anodic shift (0.42 V) found when shifting from **3** to **4**, and results from the significantly higher electron affinity of F_{12}SubPc with respect to H_{12}SubPc. At this point, it is interesting to notice that the first reduction and oxidation events in **5** and **6** occur at different locations. In **5**, the first reduction and oxidation are TCBD- and H_{12}SubPc-centered, respectively, whereas in **6**, they are F_{12}SubPc- and aniline-centered, respectively. Taking into account that the first reduction and oxidation in **3** and **4** are located at SubPc and aniline, respectively, as observed for **6**, it can be inferred that the different redox behavior of **5** and **6** is a direct consequence of the different electronic effects exerted by the TCBD moiety in the two conjugates, which ultimately depend on the electronic character of the SubPc macrocycle.

Finally, the electrochemical HOMO-LUMO band gap for **3**-**6**, which corresponds to the approximate energy level of the radical ion pair state, was determined as the difference between the first oxidation and first reduction potentials. As a matter of fact, values of 1.84, 1.51, 1.84 and 1.76 were determined for **3**, **4**, **5** and **6**, respectively. For all the investigated derivatives, HOMO−LUMO band gap values are lower than their respective singlet excited state energies, which can be determined from photophysical measurements as will be described below. This finding suggests that, in principle, photoinduced CS is feasible for all these conjugates.

Photophysical features of SubPc-TCBD-aniline derivatives 5 and 6

Once studied the electrochemical characteristics of the axially substituted SubPc-TCBD-aniline conjugates and their SubPc-ethynyl-aniline precursors, the photophysical features of derivatives **3**-**6** were investigated by means of steady-state and time-resolved spectroscopic measurements.

Steady-state absorption studies

First of all, the absorption characteristics of SubPc-TCBD-aniline conjugates **5** and **6** and SubPc precursors **1**-**4** were studied in order to investigate the interactions in the ground state. The UV-vis spectra of SubPc-ethynyl-aniline conjugates **3** and **4** in toluene show a noticeable similarity with the ones of starting SubPc-Cl **1** and **2**, suggesting negligible ground-state interactions between the SubPc unit and the axial ethynyl-aniline moiety (Figure 66). In particular, SubPc-ethynyl-aniline derivatives **3** and **4** feature strong Q-band absorptions at 567 and 576 nm, respectively, along with less intense Soret-band absorptions at 304 and 303 nm, respectively.

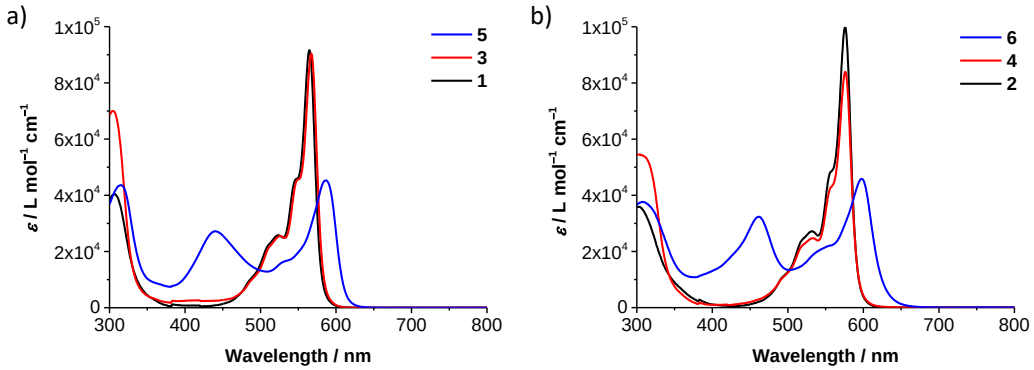

Figure 66. Steady-state absorption spectra of a) H_{12}SubPc derivatives **5**, **3** and **1** and b) F_{12}SubPc derivatives **6**, **4** and **2** in toluene. Absorption spectra of SubPc-TCBD-aniline conjugates **5** and **6** are in blue, absorption spectra of SubPc-ethynyl-aniline conjugates **3** and **4** are in red and absorption spectra of SubPc-Cl derivatives **1** and **2** are in black.

In contrast, the absorption spectra of SubPc-TCBD-aniline conjugates **5** and **6** exhibit significant differences with respect to the spectra of their respective SubPc precursors. First of all, additional absorption features can be observed at 440 and 461 nm, respectively (Figure 66). These transitions are attributable to ground-state CT interactions between the electron-donating aniline and the electron-withdrawing TCBD. As mentioned in the Introduction and background of this Chapter, CT absorption bands are commonly observed in TCBD-aniline push-pull derivatives.[331,340,356] Two of the possible resonance structures of a generic TCBD-aniline

conjugate are shown in Figure 67. In this connection, it is important to notice that, due to the large torsional angle existing between the four carbon atoms constituting the butadiene backbone in **5** and **6** (*i.e.*, 83.9° and 85.9°, respectively) that can be determined from the X-ray crystal structure of the two derivatives (Figure 29), the electron-donating aniline moiety linked to the butadiene framework can only present resonance with the almost co-planar electron-accepting DCV half, but not with the DCV half connected to the SubPc macrocycle.[338]

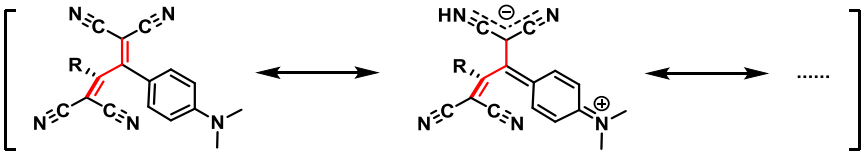

Figure 67. Two of the possible resonance structures of a generic TCBD-aniline derivative.

The CT nature of the additional transition observed in the UV-vis spectra of **5** and **6** was further confirmed by UV-vis measurements in solvents of different polarity, which revealed a positive solvatochromism of the band in question. As a matter of fact, a bathochromic shift of the CT absorption maximum in **5** and **6** was observed upon shifting from toluene (*i.e.*, 440/461 nm) to chlorobenzene (*i.e.*, 450/467 nm), anisole (*i.e.*, 451/470 nm) and benzonitrile (*i.e.*, 459/473 nm). (Figure 68).

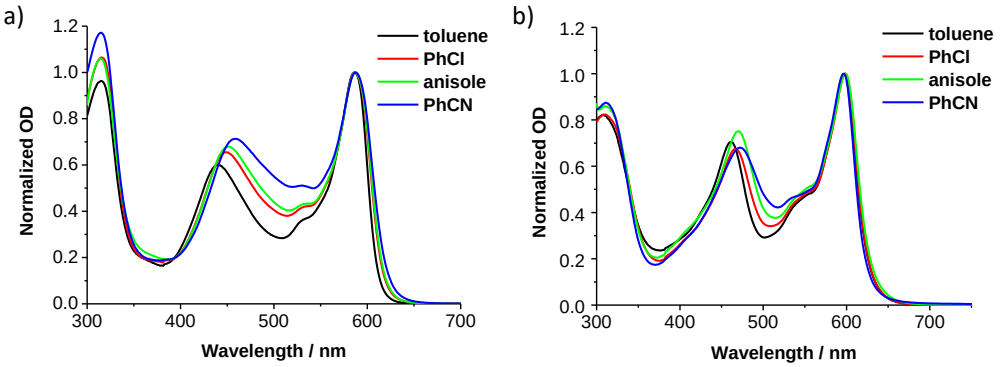

Figure 68. Normalized (with respect to the SubPc Q-band) steady-state absorption spectra of a) H_{12}SubPc-TCBD-aniline **5** and b) F_{12}SubPc-TCBD-aniline **6** in toluene (black), chlorobenzene (red), anisole (green), and benzonitrile (blue).

In addition to the presence of such ground-state absorptions attributable to the highly polarized TCBD-aniline moiety, Q-band absorptions in the UV-vis spectra of SubPc-TCBD-aniline derivatives **5** and **6** are significantly red-shifted (*i.e.*, 20 and 22 nm, respectively) and slightly

broadened with respect to the corresponding transitions in SubPc-ethynyl-aniline precursors **3** and **4** (Figure 66). As a matter of fact, for **5** and **6** Q-band maxima are observed in toluene at 587 and 598 nm, respectively. This finding is particularly remarkable considering that usually the position of the main absorptions in SubPc UV-vis spectra is mainly dictated by the nature of the peripheral substituents, whereas the axial ligand has only a slight influence on the absorption features of the macrocycle.[8] To rule out any possible correlation of the observed Q-band redshift with aggregation of **5** and **6** in solution, UV-vis measurements at different concentrations were carried out. The lack of any appreciable change in the position and shape of the main absorptions in dilution assays indicates that the bathochromic shift of the Q band observed in **5** and **6** is likely due to ground-state intramolecular electronic communications between the SubPc and the axial TCBD moiety rather than to intermolecular electronic effects.

Moreover, a slight broadening of the Q band in the UV-vis spectra of **5** is observed upon increasing solvent polarity, whereas the low-energy transition in **6** lacks any dependence on the nature of the solvent (Figure 68). A possible rationale includes an underlying ground CT state between the electron-donating SubPc moiety and the electron-withdrawing TCBD unit in **5** (*vide infra*). On the other hand, the lack of ground-state CT interactions between the fluorinated SubPc and TCBD in **6** could be explained on the basis of the electron-withdrawing nature of the macrocycle.

Steady-state fluorescence studies

To shed light on the excited-state interactions, fluorescence studies were performed on derivatives **3**-**6**. For the determination of fluorescence quantum yields (ϕ_F), a F_{12}SubPc axially substituted with a phenoxy ligand and showing a solvent-independent ϕ_F of 0.17 was used as reference (Figure 69).[319] The most relevant data from the fluorescence measurements carried out on SubPcs **3**-**6** are summarized in Table 5.

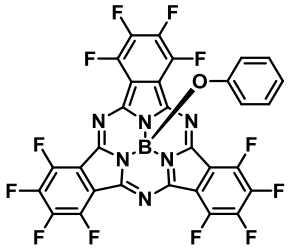

Figure 69. Chemical structure of the F_{12}SubPc-OPh derivative used as reference compound for ϕ_F measurements.

Table 5. Fluorescence quantum yields and emission maxima of SubPc-ethynyl-aniline precursors **3** and **4** and SubPc-TCBD-aniline derivatives **5** and **6** in solvents of different polarity.

	3		**4**		**5**		**6**	
solvent	**ϕ_F / %**	**λ_{max} / nm**	**ϕ_F / %**	**λ_{max} / nm**	**ϕ_F / %**	**λ_{max} / nm**	**ϕ_F / %**	**λ_{max} / nm**
toluene	15.67	574	0.02	683	0.77	583	$< 10^{-3}$	675
PhCl	4.73	577	0.14	685	0.60	584	$< 10^{-3}$	680
anisole	1.38	576	0.02	586	0.52	584	$< 10^{-3}$	710
PhCN	0.50	578	0.03	584	0.06	584	$< 10^{-3}$	~610

The emission spectra of SubPc-ethynyl-aniline conjugates **3** and **4** in toluene are the mirror images of the respective absorption spectra with maxima at 574 and 583 nm, respectively, and small Stokes shifts of 7 nm (Figure 70). Remarkably, significant differences between **3** and **4** can be observed in terms of fluorescence quantum yields. For **3**, a ϕ_F of 0.16 was calculated in toluene, which is nearly identical to that of the F_{12}SubPc-OPh reference compound, whereas a significant fluorescence quenching (*i.e.*, 97%) is observed when shifting to benzonitrile, in which a ϕ_F value of 5×10^{-3} was determined. On the other hand, a fluorescence quenching of more than 99% with respect to the F_{12}SubPc-OPh reference compound is observed for **4** in all the investigated solvents, with ϕ_F values ranging from 2×10^{-4} (toluene and anisole) to 1.4×10^{-3} (chlorobenzene). Singlet excited state energies were calculated by means of Equation 15:

$$E = 2\frac{hc}{\lambda_{max}(abs) + \lambda_{max}(em)} \qquad \text{(Eq. 15)}$$

where λ_{max}(abs) is the absorption maximum at the longest wavelength and λ_{max}(em) is the fluorescence maximum at the shortest wavelength. In this way, energy values of 2.17 and 2.14 eV were determined for **3** and **4**, respectively. As the energy of the singlet excited state of aniline (*i.e.*, 4.30 eV)[377] is higher than that of the SubPc, energy transfer from the SubPc unit to the aniline moiety is unfeasible. Thus, the fluorescence quenching observed for **3** in a polar solvent such as benzonitrile and for **4** in all the investigated solvents is likely to be due to an intramolecular CS event. In line with this conclusion, the stronger quenching observed for **4** with respect to **3** in low-polar solvents such as toluene can be rationalized considering that F_{12}SubPc is a much stronger electron acceptor than H_{12}SubPc, which results in more favorable CS thermodynamics in **4** than in **3**.

[377] K. Kimura, H. Tsubomura, S. Nagakura, *Bull. Chem. Soc. Jpn.* **1964**, *37*, 1336-1346.

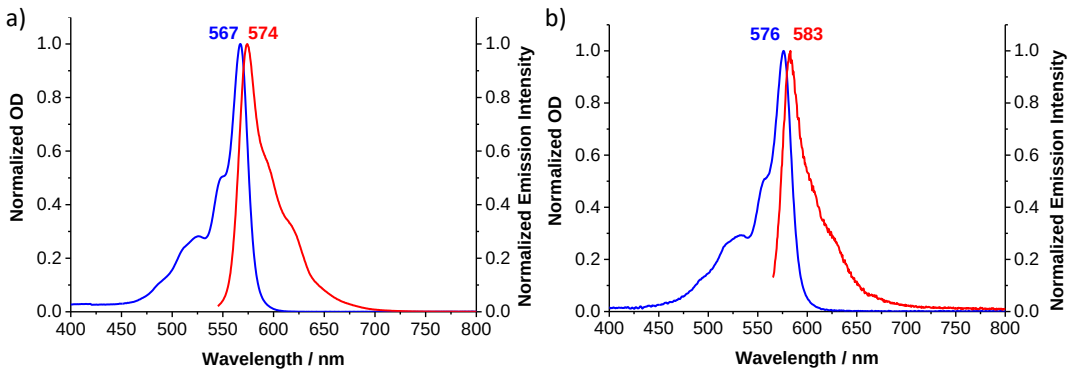

Figure 70. Normalized absorption (blue) and fluorescence spectra (red) of a) H_{12}SubPc-ethynyl-aniline **3** (λ_{ex} = 530 nm, c = 1.24 × 10^{-6} M) and b) F_{12}SubPc-ethynyl-aniline **4** (λ_{ex} = 550 nm, c = 7.53 × 10^{-6} M) in toluene.

Turning to SubPc-TCBD-aniline derivative **5**, an "inverted" Stokes shift of 3 nm is determined when comparing the SubPc Q-band absorption and fluorescence maxima (*i.e.*, 587 and 584 nm, respectively) (Figure 71a). To shed light on such unusual behavior, an excitation spectrum of **5** (λ_{em} = 630 nm) was recorded in toluene. A comparison between the excitation and absorption spectra of **5** reveals that the SubPc Q-band is blue-shifted (15 nm) in the former (Figure 71b). Moreover, a negligible contribution from the TCBD−aniline CT band to the emission at 630 nm is observed. Such differences between excitation and absorption spectra are not observed in the case of SubPc-ethynyl-aniline derivatives **3** and **4**. Notably, a good matching in terms of position and shape of the Q band can be observed between the excitation spectrum of **5** and the absorption spectra of precursors H_{12}SubPc-ethynyl-aniline **3** and H_{12}SubPc-Cl **1** (Figure 72a). Worthy of notice is also the reasonable red shift (*i.e.*, 12 nm) observed when comparing the SubPc excitation and emission band maxima of **5** (Figure 72b). Taking all these experimental findings into account, it is reasonable to assume that the SubPc Q-band in the absorption spectrum of **5** results from an overlap of two transitions, namely, a "pure" SubPc Q-band and a CT absorption band. A ground-state CT interaction between the SubPc unit and the TCBD moiety in **5**, which is likely to be responsible for such CT absorption band, had already been postulated in the context of solvent-dependent absorption studies (Figure 68a). The observed quenching of the fluorescence emission of **5** when moving from toluene (ϕ_F = 7.7 × 10^{-3}) to a more polar solvent such as benzonitrile (ϕ_F = 6 × 10^{-4}) (Table 5) further supports a push-pull effect between the SubPc and the TCBD unit.

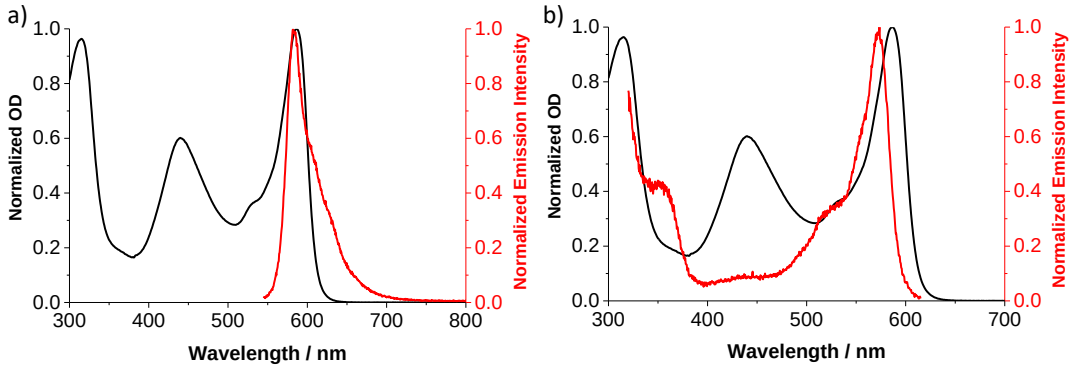

Figure 71. a) Normalized steady-state absorption (black) and emission spectra (red) of H_{12}SubPc-TCBD-aniline **5** (λ_{ex} = 530 nm, c = 2.05 × 10^{-6} M) in toluene. b) Normalized steady-state absorption (black) and excitation spectra (red) of H_{12}SubPc-TCBD-aniline **5** (λ_{em} = 630 nm, c = 1.09 × 10^{-6} M) in toluene.

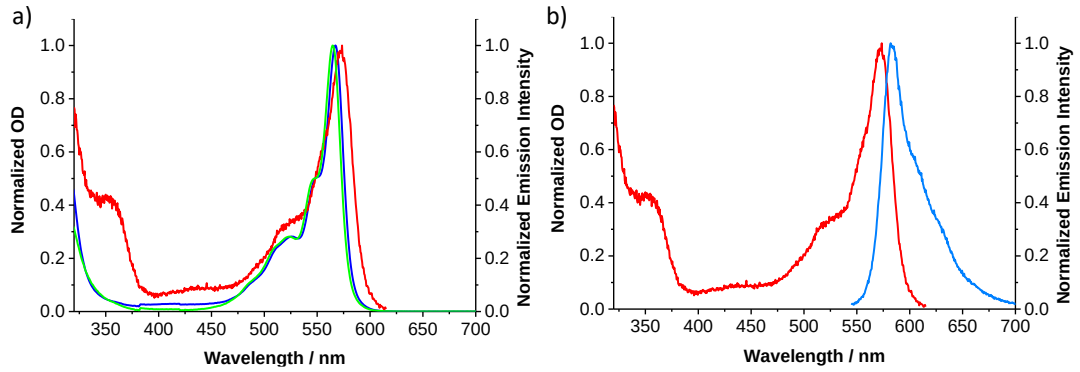

Figure 72. Normalized excitation spectrum of H_{12}SubPc-TCBD-aniline **5** (red, λ_{em} = 630 nm, c = 1.09 × 10^{-6} M) in toluene compared to a) the normalized steady-state absorption spectra of H_{12}SubPc-ethynyl-aniline **3** (blue) and H_{12}SubPc-Cl **1** (light green) in toluene, and b) the fluorescence spectrum of H_{12}SubPc-TCBD-aniline **5** (light blue, λ_{ex} = 530 nm, c = 2.05 × 10^{-6} M) in toluene.

On the other hand, the fluorescence spectrum of F_{12}SubPc-TCBD-aniline **6** in toluene is dominated by a broad, featureless low-energy band maximizing at 675 nm with a shoulder at around 612 nm (Figure 73a). These emission features are red-shifted with respect to the SubPc Q-band absorption by 77 and 14 nm, respectively. Moreover, in contrast to what observed for **5**, the excitation spectrum of **6** (λ_{em} = 680 nm) strongly resembles its absorption spectrum (Figure 73b).

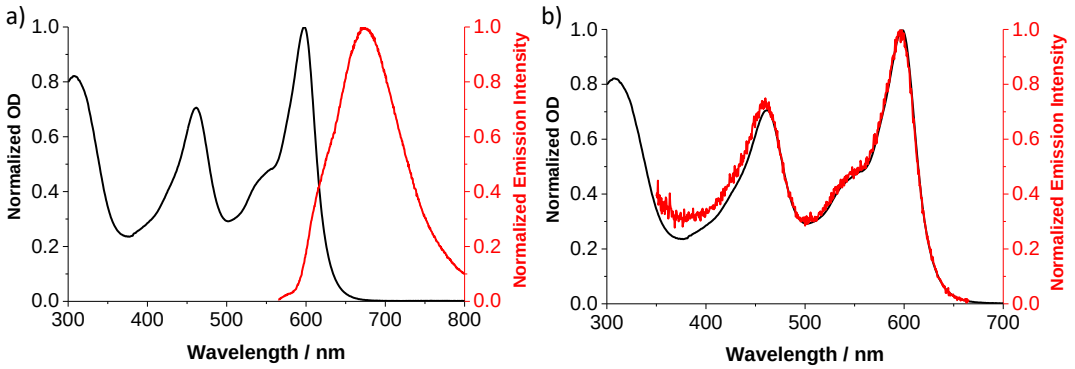

Figure 73. a) Normalized steady-state absorption (black) and fluorescence spectra (red) of F_{12}SubPc-TCBD-aniline **6** (λ_{ex} = 550 nm, c = 8.90 × 10^{-6} M) in toluene. b) Normalized steady-state absorption (black) and excitation spectra (red) of F_{12}SubPc-TCBD-aniline **6** (λ_{em} = 680 nm, c = 1.09 × 10^{-6} M) in toluene.

In order to shed light on the origin of the dual fluorescence observed in the emission spectrum of **2**, solvent-dependent studies were carried out (Figure 74). On one hand, the increasing solvent polarity when shifting from toluene to benzonitriles has a negligible effect on the position of the higher-energy emission. The lack of solvent dependence and the relatively small Stokes shift observed suggest that this fluorescence stems from a non-polar excited state, such as the locally excited SubPc state. On the other hand, a strong quenching (>99%) and a large red shift (namely, 35 nm) of the intense, lower-energy emission band are observed upon increasing solvent polarity from toluene to anisole (Figure 74 and Table 5). Such an intense fluorescence quenching and strong positive solvatochromism of the broad and featureless low-energy emission, along with the lack of any ground CT state absorptions (*vide supra*), infer the formation of a polarized excited complex (*i.e.*, an exciplex). As mentioned in the Introduction of this Thesis, exciplexes result from electrostatic interactions between closely spaced electron donors and electron acceptors in their excited and ground states through a partial CT.[279,378] Thus, exciplexes are transient CT species, in which a partial redistribution of charge density from the electron donor to the electron acceptor occurs resulting in the formation of a polarized excited D-A complex, namely $(D^{\delta+}\text{-}A^{\delta-})^*$. In this context, it is important to notice that exciplexes differ significantly from radical ion pair species, namely $D^{\cdot+}\text{-}A^{\cdot-}$, in which a charge has been fully transferred from D to A. In a non-polar medium, the non-fluorescent $D^{\cdot+}\text{-}A^{\cdot-}$ state is generally higher in energy than the fluorescent $(D^{\delta+}\text{-}A^{\delta-})^*$ state due to Coulomb stabilization of the latter (Figure 75). Thus, the $(D^{\delta+}\text{-}A^{\delta-})^*$ species is formed more likely than the radical ion pair species.

[378] J. Verhoeven, *Pure Appl. Chem.* **1996**, *68*, 2223-2286.

The situation is reversed in more polar media, in which, due to stronger solvation and stabilization of $D^{\cdot+}$-$A^{\cdot-}$, the latter falls energetically below the $(D^{\delta+}$-$A^{\delta-})^*$ state. As a consequence, a decrease in the intensity and a bathochromic shift of the exciplex emission is commonly observed in polar solvents.

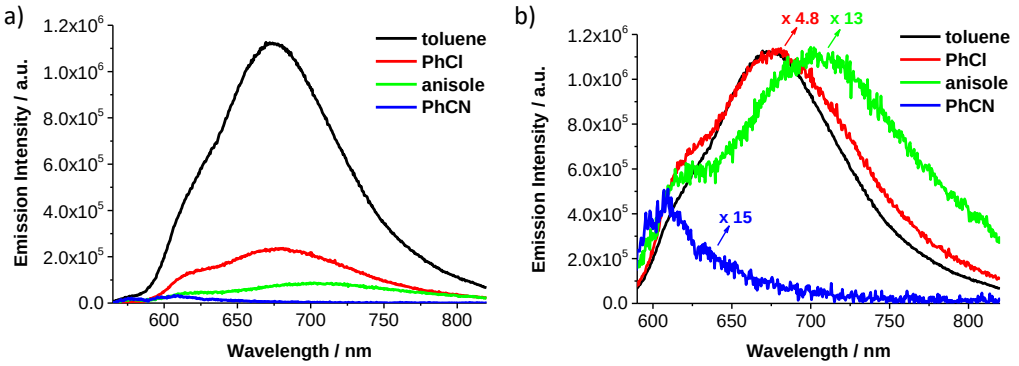

Figure 74. a) Fluorescence and b) normalized fluorescence spectra of F_{12}SubPc-TCBD-aniline **6** (λ_{ex} = 550 nm, OD_{ex} ≈ 0.2) in toluene (black), chlorobenzene (red), anisole (green), and benzonitrile (blue).

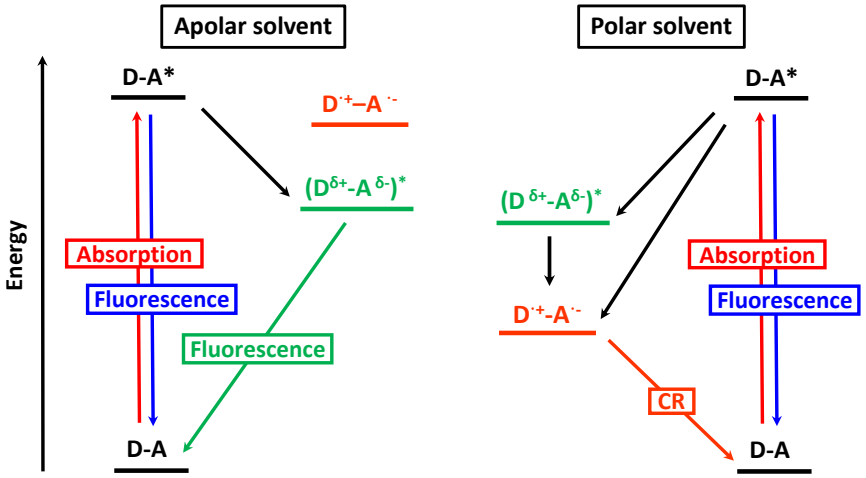

Figure 75. Schematic energy level diagrams showing the relative energies of $(D^{\delta+}$-$A^{\delta-})^*$ exciplex species and $D^{\cdot+}$-$A^{\cdot-}$ radical ion pair species in apolar and polar solvents.

Excitation studies further support the exciplex hypothesis. As mentioned above, the excitation spectrum of **6** strongly resembles its absorption spectrum, that is, regardless of photoexciting the SubPc Q-band or the TCBD-aniline CT band, a radiative state is generated (Figure 73b). As a

matter of fact, we hypothesize that ground-state and excited-state interactions between the SubPc and the TCBD−aniline moiety are involved.

Finally, additional support for the exciplex hypothesis comes from the X-ray crystal structure of **6**, which shows a nearly parallel and vicinal arrangement of the aniline moiety with respect to F_{12}SubPc, as discussed in section 1.3.2.1 (Figure 29b). As a result, an intramolecular orbital overlap between the electron-rich aniline and the electron-withdrawing fluorinated macrocycle is feasible in the excited state, which gives rise to a partial CT from the former to the latter resulting in the formation of a $[(\text{SubPc-TCBD})^{\delta-}\text{-aniline}^{\delta+}]^*$ species.

At this point, it is worth to mention that the formation of an excited dimer species (*i.e.*, an excimer) through interactions between identical molecular entities of **6** can be ruled out on the basis of different considerations. First of all, excimer fluorescence is concentration-dependent, whereas for **6** the broad, featureless fluorescence is already observed at concentrations lower than 10^{-6} M (Figure 76). In addition, the maximum wavelength of excimer emission is usually only weakly solvent-dependent,[278] whereas in the case of **6**, a strong effect of solvent polarity is observed (Figure 74). Finally, the low tendency towards aggregation of SubPcs in solution should also be considered.

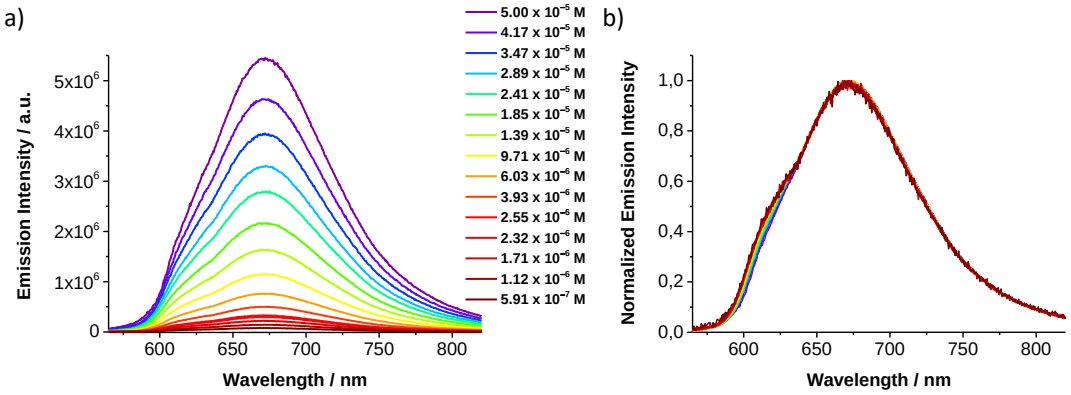

Figure 76. a) Fluorescence and b) normalized fluorescence spectra of F_{12}SubPc-TCBD-aniline **6** (λ_{ex} = 550 nm) at different concentrations in toluene.

Transient absorption studies

The excited-state deactivation pathways of SubPc-TCBD-aniline derivatives **5** and **6** and their SubPc-ethynyl-aniline precursors **3** and **4** were investigated by means of femtosecond and nanosecond transient absorption measurements.

Upon 550 nm photoexcitation of H_{12}SubPc-ethynyl-aniline **3** in toluene, transient maxima at 433, 612, and 635 nm as well as transient minima at 525 and 568 nm are discernible, along with a broad differential absorption spanning from 650 to 900 nm (Figure 77a,b). These features relate to the SubPc singlet excited state $^1(S_1)$ (2.17 eV), which converts *via* ISC into the corresponding triplet excited state $^3(T_1)$ within 1.9 ns. SubPc $^3(T_1)$ state signatures include maxima at 460 and 610 nm as well as minima at 525 and 570 nm.

Interestingly, a different deactivation mechanism of the SubPc $^1(S_1)$ state is observed upon increasing solvent polarity. In anisole, the decay of the singlet excited state is accompanied by the formation of maxima at 455, 612, and 678 nm as well as minima at 525 and 570 nm (Figure 77c,d). These transients resemble the spectral changes obtained upon electrochemical reduction of **3** in spectroelectrochemical measurements. Thus, an electron transfer from the aniline moiety to the SubPc unit to afford the metastable $H_{12}SubPc^{\cdot-}$-ethynyl-aniline$^{\cdot+}$ radical ion pair state (1.84 eV) is postulated. A similar deactivation pathway is observed also in chlorobenzene and benzonitrile. As a matter of fact, CS occurs rapidly (*i.e.*, within 95 ps in chlorobenzene, 73 ps in anisole, and 9.4 ps in benzonitrile), whereas CR is one order of magnitude slower (namely, 579 ps in chlorobenzene, 200 ps in anisole, and 56 ps in benzonitrile). In nanosecond experiments, maxima at 455 and 610 nm and minima at 530 and 570 nm, which attest the formation of the SubPc $^3(T_1)$ state, can be observed.

The energy level diagrams of H_{12}SubPc-ethynyl-aniline **3** reflecting the energetic pathways in toluene and chlorobenzene after excitation of the hydrogenated SubPc are depicted in Figure 78.

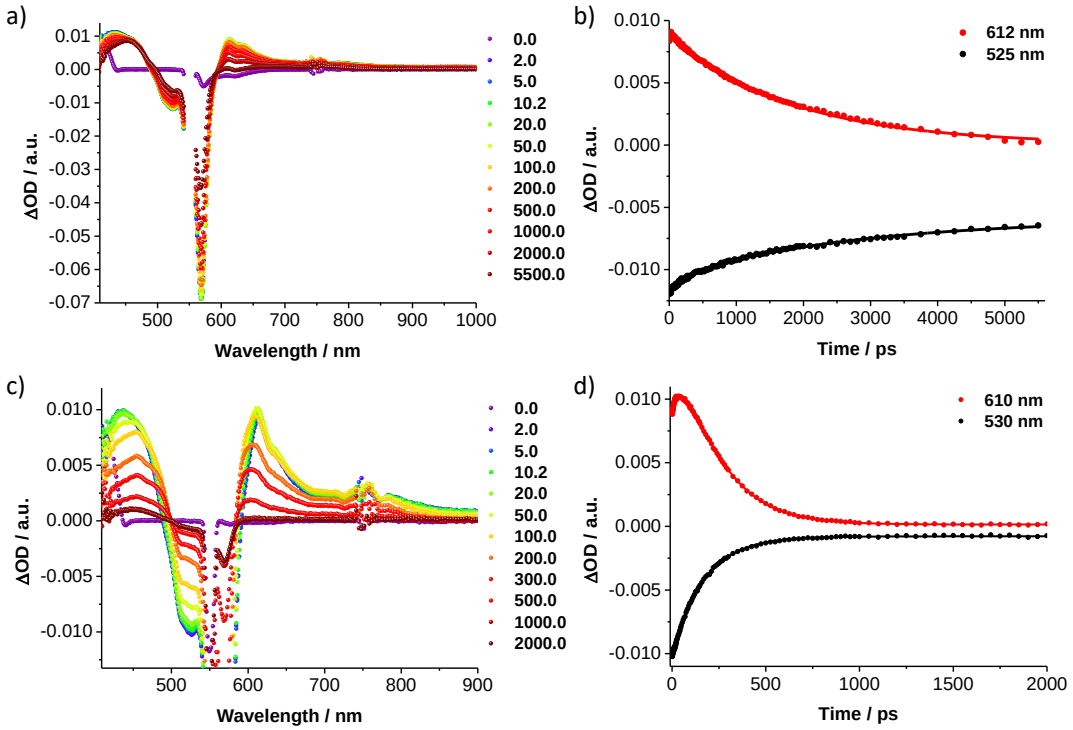

Figure 77. a,c) Differential absorption spectra (visible and near-infrared) obtained upon femtosecond flash photolysis (550 nm) of H_{12}SubPc-ethynyl-aniline **3** (c = 2 × 10^{-5} M) in a) toluene and c) anisole with several time delays between (a) 0 and 5500 ps and (c) 0 and 2000 ps at room temperature. b,d) Time-absorption profiles of the spectra shown in (a) and (c) monitoring b) ISC and d) the CS and CR processes.

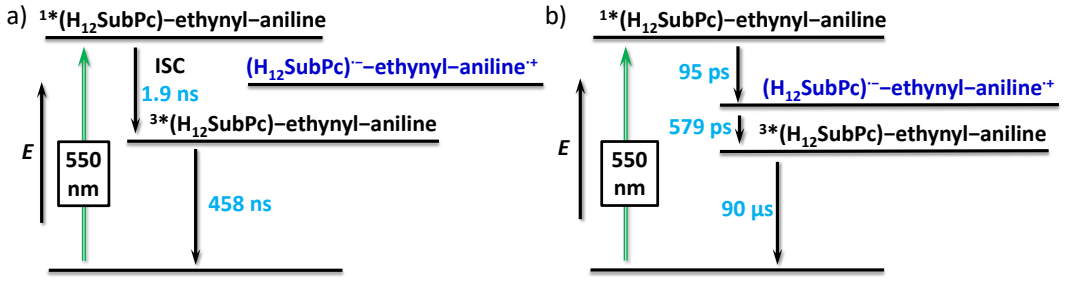

Figure 78. Energy level diagrams of H_{12}SubPc-ethynyl-aniline **3** reflecting the energetic pathways in a) toluene, and b) chlorobenzene after excitation of the H_{12}SubPc (λ_{ex} = 550).

Upon excitation at 550 nm of F_{12}SubPc-ethynyl-aniline **4** in toluene, transient maxima at 479, 504, 614, 675, and 755 nm as well as minima at 535 and 576 nm are observed. These features attest the formation of the SubPc $^1(S_1)$ state (Figure 79a,b). After that, a slight increase of the intensity of the 504 and 675 nm maxima is observed, along with a monoexponential decay of all transients. Although in light of the electrochemical studies carried out on **4** (*vide supra*) an intramolecular CS could be inferred, a comparison with the literature and the transient features of the $F_{12}SubPc^{\cdot-}$ radical anion (namely, a distinct maximum at 594 nm and a minimum at 517 nm) fails to corroborate this hypothesis.[290] On the other hand, the observed signatures match the spectral features seen observed upon reduction of F_{12}SubPc-Cl **2** in spectroelectrochemical measurements. In light of the aforementioned, the observed transients can be assigned to a polarized $F_{12}SubPc^{\delta-}$-ethynyl-aniline$^{\delta+}$ CT excited state. The latter exhibits ultrafast formation and decay kinetics (*i.e.*, 4.9/44 ps in toluene, 4.4/15 ps in chlorobenzene, and 4.3/11 ps in anisole), and deactivates directly into the singlet ground state (Figure 80a).

In a more polar solvent such as benzonitrile, a different scenario is observed. In particular, the initially formed transient features (namely, maxima at 579, 501, 620, 644 and 755 nm and minima at 535 and 577 nm) do not decay, but rather transform into new transients including a sharp maximum at 594 nm as well as a minimum at 517 nm (Figure 79c,d). The latter can be related to the formation of the $F_{12}SubPc^{\cdot-}$ radical anion.[290] Thus, an intramolecular CS involving the SubPc $^1(S_1)$ state (2.14 eV) to afford the $F_{12}SubPc^{\cdot-}$-ethynyl-aniline$^{\cdot+}$ radical ion pair state (1.51 eV) is inferred. In particular, three lifetimes were derived from multiwavelength and global analyses, namely, 1.2, 4.6, and 13 ps. The first one is attributed to the deactivation of the SubPc $^1(S_1)$ to the polarized $F_{12}SubPc^{\delta-}$-ethynyl-aniline$^{\delta+}$ CT state. The latter subsequently converts into the fully separated $F_{12}SubPc^{\cdot-}$-ethynyl-aniline$^{\cdot+}$ radical ion pair state, which finally deactivates to the singlet ground state (Figure 80b).

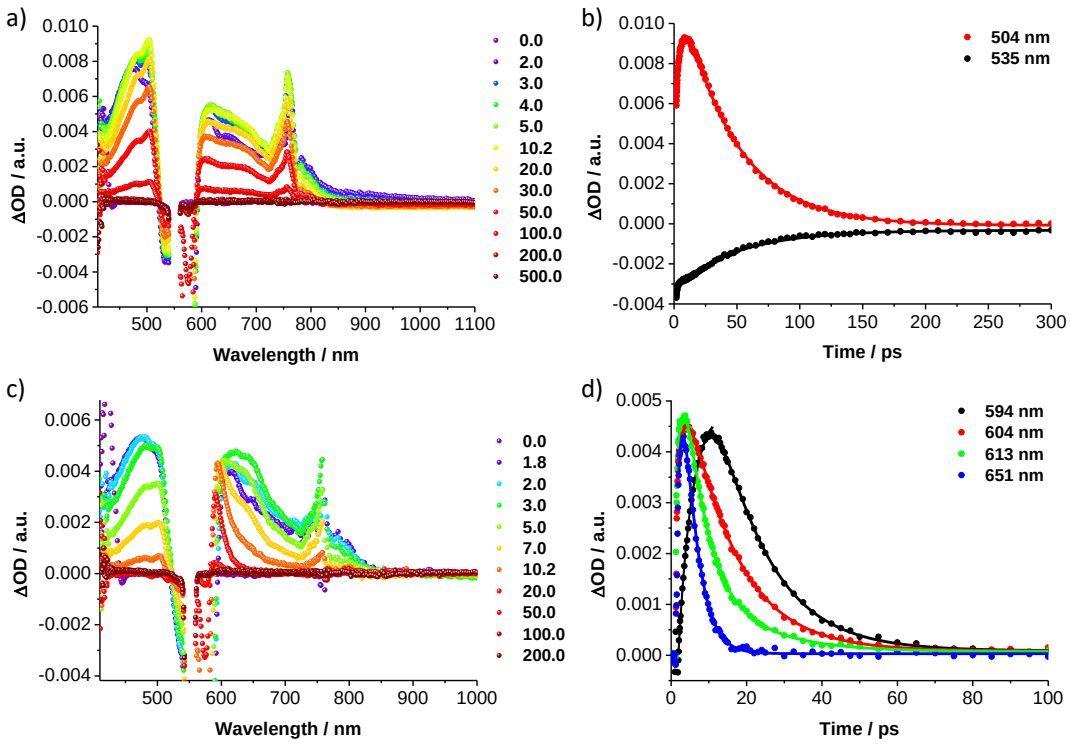

Figure 79. a,c) Differential absorption spectra (visible and near-infrared) obtained upon femtosecond flash photolysis (550 nm) of F_{12}SubPc-ethynyl-aniline **4** (c = 2 × 10^{-5} M) in a) toluene and c) benzonitrile with several time delays between (a) 0 and 5500 ps and (c) 0 and 2000 ps at room temperature. b,d) Time-absorption profiles of the spectra shown in (a) and (c) monitoring the formation and decay of the polarized CT state.

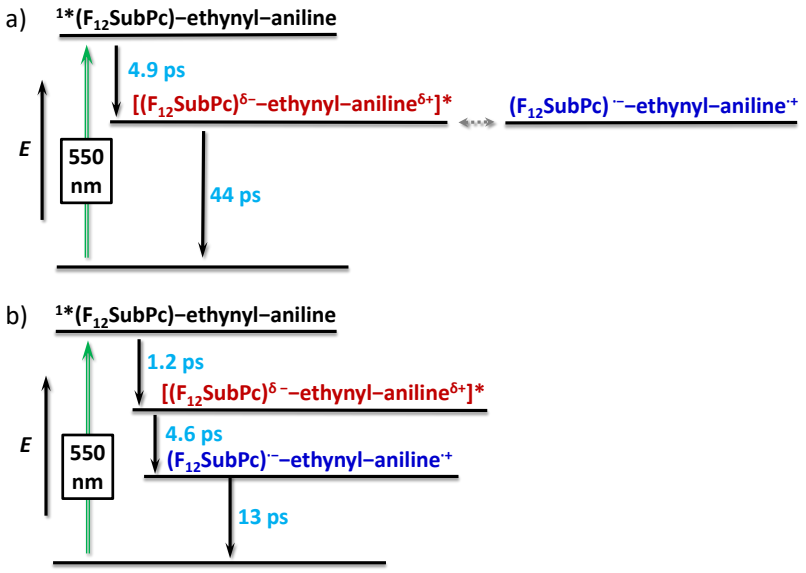

Figure 80. Energy level diagrams of F_{12}SubPc-ethynyl-aniline **4** reflecting the energetic pathways in a) toluene and b) benzonitrile after excitation of the F_{12}SubPc (λ_{ex} = 550).

In the case of **5**, several transient features are discernible after 550 nm laser excitation in toluene. On one hand, transient maxima at 635 and 786 nm together with a broad absorption extending into the NIR are assigned to the SubPc $^1(S_1)$ state (2.15 eV). On the other hand, transient minima at 439 and 588 nm stem from the bleaching of the ground CT absorption band between SubPc and the axial TCBD. Notably, while the broad absorption reaching the NIR decreases, maxima at 515 and 635 nm increase and a new featureless transient around 660 nm arises with monoexponential kinetics. The new signature at 660 nm and the bleaching are related to the one-electron reduced TCBD, as can be deducted from spectroelectrochemical measurements carried out on the reference Ph-TCBD-aniline derivative (Figure 65). In light of these findings, an electron transfer from H_{12}SubPc to TCBD to afford the metastable $H_{12}SubPc^{\cdot+}$-$TCBD^{\cdot-}$-aniline radical ion pair (1.84 eV) is inferred. A similar deactivation pathway is observed in chlorobenzene, anisole and benzonitrile (Figure 81). Ultrafast CS and CR kinetics (*i.e.*, 7.5/82 ps in toluene, 7.3/24 ps in chlorobenzene, 5.6/23 ps in anisole, and 2.9/16 ps in benzonitrile) were determined by multiwavelength and global analysis. At longer times, new transients at 574 and 620 nm are observed, indicating the formation of the SubPc triplet excited state as a minor deactivation pathway. Interestingly, photoexcitation of **5** at 458 nm affords the same kinetics observed when exciting the sample at 550 nm. Thus, it can be stated that, regardless of exciting

into the SubPc Q-band absorption or into the TCBD-aniline CT transition, the $H_{12}SubPc^{\cdot+}$-$TCBD^{\cdot-}$-aniline state is populated (Figure 82).

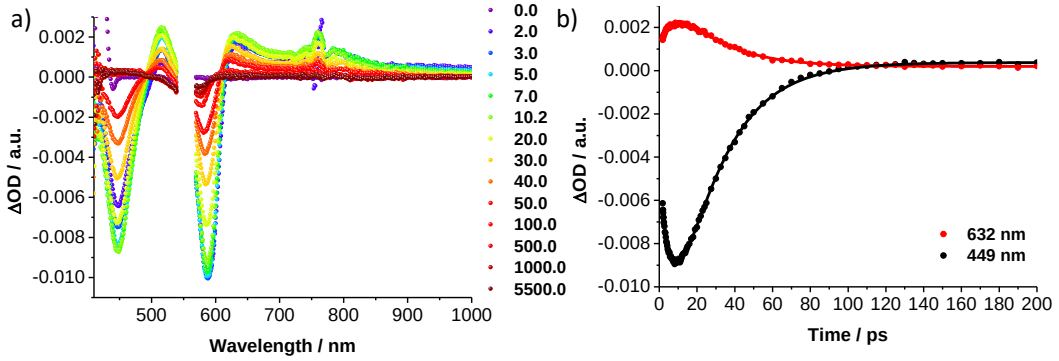

Figure 81. a) Differential absorption spectra (visible and near-infrared) obtained upon femtosecond flash photolysis (550 nm) of H_{12}SubPc-TCBD-aniline **5** (c = 2 × 10^{-5} M) in anisole with several time delays between 0 and 5500 ps at room temperature. b) Time-absorption profiles of the spectra shown in (a) monitoring the CS and CR processes.

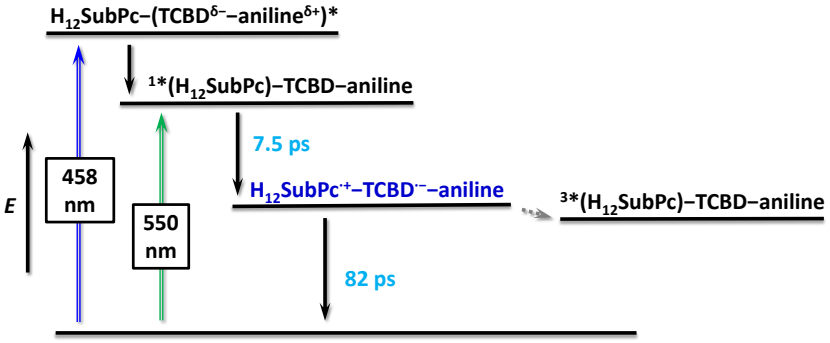

Figure 82. Energy level diagram of H_{12}SubPc-TCBD-aniline conjugate **5** reflecting the energetic pathways in toluene after excitation of the H_{12}SubPc (λ_{ex} = 550) and the TCBD-aniline ground CT state (λ_{ex} = 458 nm).

Turning to F_{12}SubPc-TCBD-aniline **6**, 550 nm excitation in toluene results in the instantaneous formation of a series of fingerprint absorptions of the $^1(S_1)$ state of F_{12}SubPc (2.05 eV), including a transient maximum at 786 nm, a broad absorption extending into the NIR region, and a transient minimum at 598 nm. The decay of these transients is accompanied by the formation of new maxima at 500, 660, and 742 nm and a minimum at 460 nm. Importantly, the underlying dynamics, which are strictly monoexponential, are linked to each other. Whereas the transients

at 500 and 742 nm are attributable to the $F_{12}SubPc^{\bullet-}$ radical anion, the broad feature around 660 nm is related to the $TCBD^{\bullet-}$ radical anion, as indicated by spectroelectrochemical measurements on F_{12}SubPc-Cl **2** and the Ph-TCBD-aniline reference. This indicate that the negative charge is likely to be delocalized over the SubPc and the TCBD frameworks. The bleaching of the ground-state TCBD-aniline CT band absorption at 460 nm, which reflects the TCBD reduction and/or the aniline oxidation (as deducted from spectroelectrochemical studies on the Ph-TCBD-aniline reference derivative), further supports such an electronic distribution. In light of these findings, the formation of a $[(F_{12}SubPc\text{-}TCBD)^{\delta-}\text{-}aniline^{\delta+}]^{*}$ exciplex species is postulated. A similar deactivation pathway is observed also in chlorobenzene and anisole (Figure 83). As a matter of fact, multiwavelength and global analysis yielded formation and decay kinetics of 3.5/1300 ps in toluene, 4.7/648 ps in chlorobenzene, and 4.3/505 ps in anisole, which are quite close to those obtained by time-resolved fluorescence measurements (*i.e.*, 1.3 ns in toluene, 0.6 ns in chlorobenzene, and 0.5 ns in anisole). At the end of the femtosecond experiments, maxima at 443, 488, and 660 nm and minima at 467, 535, and 598 nm are still observed. These long-lived transients can be attributed, as confirmed by complementary nanosecond experiments, to the SubPc $^{3}(T_1)$ state.

On the other hand, the lack of any radiative exciplex feature is observed in benzonitrile. This lead to hypothesize that, in this solvent, an $(F_{12}SubPc\text{-}TCBD)^{\bullet-}\text{-}aniline^{\bullet+}$ radical ion pair state (1.76 eV) is formed with CS and CR kinetics of 3.5 and 61 ps, respectively.

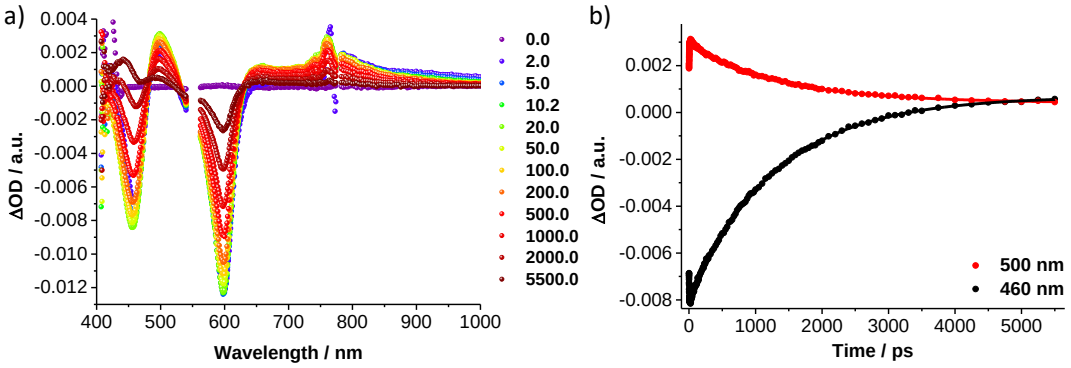

Figure 83. a) Differential absorption spectra (visible and near-infrared) obtained upon femtosecond flash photolysis (550 nm) of F_{12}SubPc-TCBD-aniline **6** ($c = 2 \times 10^{-5}$ M) in chlorobenzene with several time delays between 0 and 5500 ps at room temperature. b) Time-absorption profiles of the spectra shown in (a) monitoring the exciplex formation and decay processes.

To sum up, two different scenarios take place upon photoexcitation of **6** depending on the polarity of the solvent. In low polar solvents, the SubPc $^1(S_1)$ state deactivates forming a $[(F_{12}SubPc\text{-}TCBD)^{\delta-}\text{-}aniline^{\delta+}]^*$ exciplex species, which decays to the ground state through the energetically lower-lying SubPc $^3(T_1)$ state (Figure 84a). In contrast, in high polar solvents, the SubPc $^1(S_1)$ state mainly deactivates by populating the $(F_{12}SubPc\text{-}TCBD)^{\cdot-}\text{-}aniline^{\cdot+}$ radical ion pair state. The latter lies energetically below the exciplex state and the SubPc $^3(T_1)$ state, and transforms directly into the ground state (Figure 84b). Upon 458 nm photoexcitation, the same kinetics are observed in all the investigated solvents, which indicates that the formation of the exciplex and/or the radical ion pair state also proceeds upon excitation of the TCBD-aniline ground-state CT band.

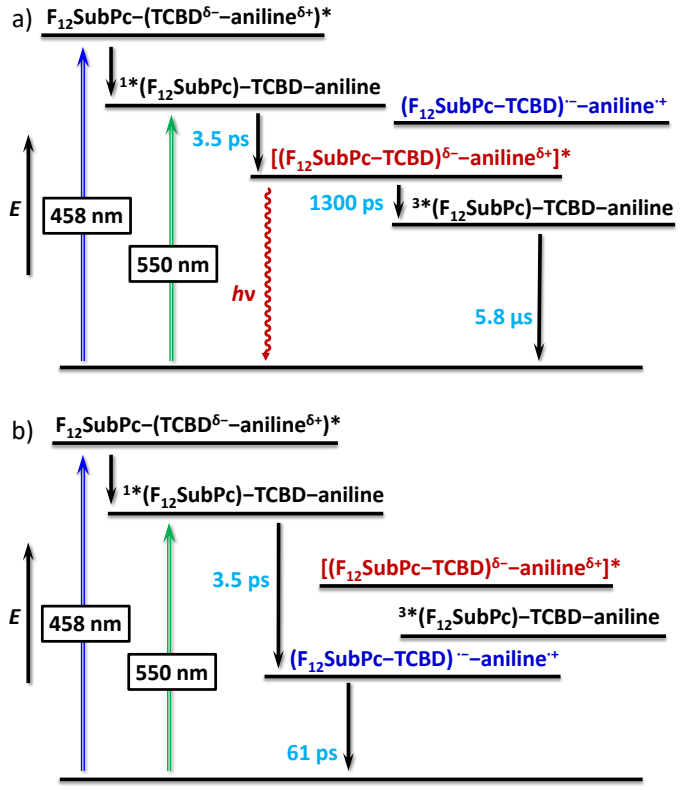

Figure 84. Energy level diagrams of F_{12}SubPc-TCBD-aniline conjugate **6** reflecting the energetic pathways in (a) toluene and (b) benzonitrile after excitation of the F_{12}SubPc (λ_{ex} = 550 nm) and TCBD-aniline band (λ_{ex} = 458 nm).

1.3.3.2 Electrochemical and photophysical properties of peripherally and peripherally/axially (TCBD-aniline)-substituted SubPcs

With the aim to investigate the interactions in the ground and excited states within the peripherally substituted derivatives, we studied the electrochemical and photophysical features of the novel (TCBD-aniline)$_3$SubPc conjugates **14** and **15** and compared them with those of the (ethynyl-aniline)$_3$SubPc-OAr precursor **12**. In this connection, it is worth to mention that (ethynyl-aniline)$_3$SubPc-OAr **12** and (ethynyl-aniline)$_3$SubPc-ethynyl-aniline **13** are expected to feature substantially identical electrochemical and photophysical characteristics, as the latter are mainly dictated by the nature of the peripheral substituent of the SubPc macrocycle and only slightly affected by the axial ligand. Thus, (ethynyl-aniline)$_3$SubPc-OAr **12** was employed as the only peripherally (ethynyl-aniline)-substituted SubPc reference for these studies.

Electrochemical features of (TCBD-aniline)$_3$SubPc derivatives 14 and 15

The electrochemical features of (ethynyl-aniline)$_3$SubPc-OAr **12**, SubPcs (TCBD-aniline)$_3$SubPc-OAr **14** and (TCBD-aniline)$_3$SubPc-TCBD-aniline **15** were probed by means of cyclic (CV) and square wave voltammetry (SWV) and compared to those of the Ph-TCBD-aniline reference[356] (Figure 65). The electrochemical data for derivatives **12**, **14** and **15** are summarized in Table 6.

Table 6. Electrochemical oxidation and reduction data (V *versus* Fc^+/Fc) for derivatives **12**, **14** and **15** and the Ph-TCBD-aniline reference[356] detected by SWV at room temperature in 0.2 M (for **12**, **14** and **15**) and 0.1 M (for Ph-TCBD-aniline) solutions of *n*-Bu_4NPF_6 in DCM.

	E_{ox}^3	E_{ox}^2	E_{ox}^1	E_{red}^1	E_{red}^2	E_{red}^3	E_{red}^4	E_{red}^5
12	+0.71[b]	+0.65[a]	+0.41[b]	-1.40[b]	-1.85[b]	-2.22[b]		
14		+0.91[a]	+0.85[b]	-0.79[d]	-1.11[d]	-1.81[b]		
15		+0.93[a]	+0.88[b]	-0.71[c]	-0.81[d]	-1.14[d]	-1.31[c]	-1.45[b]
Ph-TCBD-aniline			+0.92[a]	-0.94[d]	-1.26[d]			

[a] Aniline-centered process. [b] SubPc-centered process. [c] $TCBD_{axial}$-centered process. [d] $TCBD_{peripheral}$-centered process.

(Ethynyl-aniline)$_3$SubPc-OAr **12** exhibits three one-electron reductions at -1.40, -1.85, and -2.22 V, and two one-electron oxidations at +0.41 and +0.71 V, along with a three-electron oxidation at +0.65 V. Whereas the three-electron process is attributable to the peripheral aniline units, all the other events are SubPc-centered.

Turning to (TCBD-aniline)$_3$SubPc-OAr **14**, three reductive peaks are observable at -0.79, -1.11, and -1.81 V. Taking into account that the integrals of the first two SWV peaks are three times

higher than that of the latter, and comparing the reduction features of **14** with that of the Ph-TCBD-aniline reference,[356] it can be inferred that the first two processes involve the reduction of the TCBD units. In particular, the reduction at -0.79 V takes place at the DCV linked to the SubPc, whereas the one at -1.11 V is located at the DCV connected to the aniline, similarly to what observed for axially substituted H_{12}SubPc-TCBD-aniline **5** in section 1.3.3.1. On the other hand, the reduction at -1.81 V is SubPc-centered and is cathodically shifted (*i.e.*, 0.41 V) with respect to that of SubPc precursor **12**. This is probably due to the repulsive negative charges at the TCBD units covalently linked to the macrocycle in **14**. Regarding oxidation potentials, one one-electron oxidation peak at +0.85 V and one three-electron oxidation peak at +0.91 V can be observed. The former is SubPc-centered, whereas the latter, which matches the aniline-centered oxidation peak in the Ph-TCBD-aniline reference compound,[356] is attributable to the three peripheral aniline units.

Finally, the redox features of (TCBD-aniline)$_3$SubPc-TCBD-aniline **15** were investigated. For this derivative, five reductive processes were identified. The three-electron reductions at -0.81 and -1.14 have potentials similar to the first two reductions of **14**, and can therefore be assigned to the three peripheral DCV halves linked to the SubPc macrocycle and the three peripheral DCV halves connected to aniline moieties, respectively. On the other hand, the one-electron reductions at -0.71 and -1.31 V involve the axial TCBD unit. In particular, the former is located at the DCV adjacent to the SubPc, whereas the latter takes place at the DCV linked to the aniline. Finally, the last reduction at -1.45 V is SubPc-centered. Finally, electrochemical oxidation of **15** gives rise to a SubPc-centered one-electron oxidation at +0.88 V and an aniline-centered three-electron oxidation at +0.93 V.

Photophysical features of (TCBD-aniline)$_3$SubPc derivatives 14 and 15

Steady-state absorption studies

The absorption spectrum of (ethynyl-aniline)$_3$SubPc-OAr **12** in toluene is dominated by a sharp Q band at 601 and a less intense Soret band at 329 nm (Figure 85a). The latter is slightly broadened and more intense than in H_{12}SubPc-Cl **1**, probably due to the contribution of the aniline absorption in the UV region of the spectrum. Moreover, the Q band absorption in **12** is bathochromically shifted (*i.e.*, 36 nm) and broadened with respect to that of H_{12}SubPc-Cl, as a consequence of the extension of the SubPc π-conjugation in the (ethynyl-aniline)-substituted derivative.[8] Finally, additional bands attributable to $n \rightarrow \pi^*$ transitions stemming from the peripheral nitrogen lone pairs are observed in the absorption spectrum of **12** at 394 and 439.[111,121]

Both (TCBD-aniline)-functionalized SubPcs **14** and **15** show substantial differences in terms of absorption features with respect to (ethynyl-aniline)-substituted SubPc **12** and H_{12}SubPc-Cl **1**. For (TCBD-aniline)$_3$SubPc-OAr **14**, characteristic Q- and Soret-band absorptions are observable at 622 and 310 nm in toluene (Figure 85b). The latter band is broadened and red-shifted with respect to the Q-band of the precursor **12** and H_{12}SubPc-Cl **1** (*i.e.*, 21 and 57 nm, respectively). Moreover, an additional feature maximizing at 462 nm is present in the absorption spectrum of **14**, which correspond to a CT absorption resulting from push-pull ground state interactions between the electron-rich aniline and the electron-withdrawing TCBD units, similarly to what observed for axially-substituted derivatives **5** and **6** in section 1.3.3.1 (Figure 67).[331,340,356] The observed positive solvatochromism of this additional band further confirms the CT nature of this transition (Figure 86a). As a matter of fact, the absorption maximum of the band in question is subject to a bathochromic shift upon increasing solvent polarity from toluene (462 nm) to chlorobenzene (468 nm), anisole (470 nm) and benzonitrile (473 nm). Finally, an additional broad absorption is observed in the UV-vis spectra of **14** in toluene around 860 nm, which becomes more prominent in more polar solvents, namely chlorobenzene, anisole, and benzonitrile. Such NIR absorption is unprecedent in SubPc-based chemistry. In addition, solvent-dependent studies evidenced a slight broadening of the Q band upon increasing solvent polarity (Figure 86a). These experimental findings may be rationalized on the basis of the formation of a CT state between the electron-rich SubPc macrocycle and the electron-withdrawing TCBD units (*vide infra*).

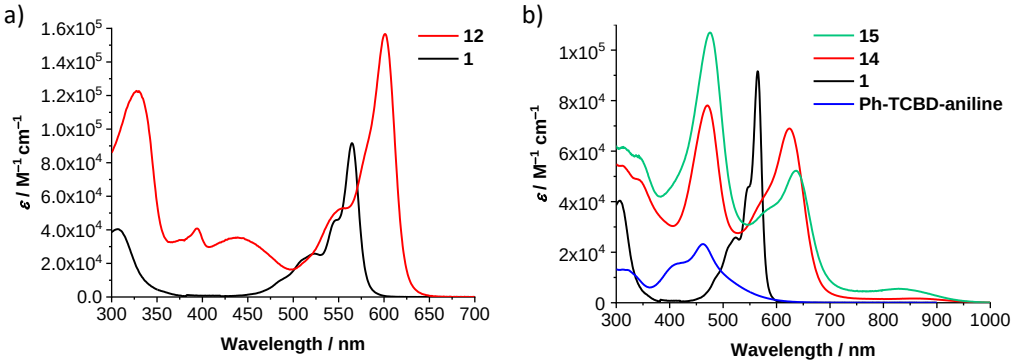

Figure 85. a) Steady-state absorption spectra of (ethynyl-aniline)$_3$SubPc-OAr **12** (red) and H_{12}SubPc-Cl **1** (black) in toluene. b) Steady-state absorption spectra of (TCBD-aniline)$_3$SubPc-TCBD-aniline **15** (green) in anisole, (TCBD-aniline)$_3$SubPc-OAr **14** (red) in anisole, H_{12}SubPc-Cl **1** (black) in toluene, and phenyl-TCBD-aniline[356] (blue) in toluene.

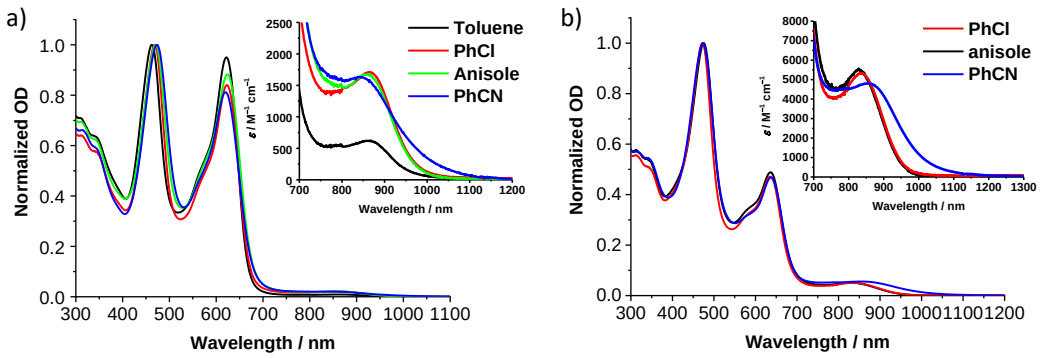

Figure 86. Normalized (with respect to the TCBD-aniline CT band) steady-state absorption spectra of a) (TCBD-aniline)$_3$SubPc-OAr **14** in toluene (black), chlorobenzene (red), anisole (green), and benzonitrile (blue) and b) (TCBD-aniline)$_3$SubPc-TCBD-aniline **15** in chlorobenzene (red), anisole (black), and benzonitrile (blue). Insets: Zoom of the steady-state absorption spectra in the region between 700 and 1200 nm.

The absorption spectrum of (TCBD–aniline)$_3$SubPc-TCBD-aniline **15** in toluene could not be recorded due to solubility issues. In anisole, Q- and Soret- band transitions are discernible at 636 and 313 nm, respectively, along with a TCBD-aniline CT absorption band at 475 nm (Figure 85b). Similarly to what observed for **14**, an additional low-energy band is present in the absorption spectrum of **15**, which maximizes at 832 nm. Remarkably, and in contrast to what observed with **14**, the TCBD-aniline CT absorption band in **15** lacks any appreciable solvatochromism (Figure 86b). However, a noticeable broadening and red-shift of the low-energy band is observed moving from anisole and chlorobenzene (*i.e.*, 832 and 838 nm, respectively) to benzonitrile (*i.e.*, 860 nm). In light of the solvent-independent nature of the TCBD-aniline CT absorption and the positive solvatochromism of the low-energy transition, it can be postulated that, in **15**, the axial TCBD enhances the electron-withdrawing effect which is exerted onto the macrocycle. Thus, the polarized CT state which is populated upon excitation in the low energy regime is more susceptible to external influences, such as solvent polarity, and, hence, subject to polarizability and energy stabilization to a larger extent with increasing solvent polarity.

Steady-state fluorescence studies

Next, fluorescence studies on **12**, **14** and **15** were carried out. For the determination of fluorescence quantum yields, F_{12}SubPc-OPh (Figure 69) was employed as reference compound.[319] Experimental data from fluorescence measurements carried out on SubPcs **12**, **14** and **15** are summarized in Table 7.

Table 7. Fluorescence quantum yields and emission maxima of (ethynyl-aniline)$_3$SubPc-OAr **12**, (TCBD-aniline)$_3$SubPc-OAr **14** and (TCBD-aniline)$_3$SubPc-TCBD-aniline **15** in solvents of different polarity.

	12		**14**		**15**	
solvent	**ϕ_F / %**	**λ_{max} / nm**	**ϕ_F / %**	**λ_{max} / nm**	**ϕ_F / %**	**λ_{max} / nm**
toluene	27	613	0.02	650	-	-
PhCl	11	624	0.02	655	$< 10^{-3}$	~666
anisole	9.6	623	0.05	658	$< 10^{-3}$	~668
PhCN	0.12	623	0.01	663	$< 10^{-3}$	~664

The fluorescence spectrum of (ethynyl-aniline)$_3$SubPc-OAr **12** in toluene is characterized by a maximum at 613 nm, which results in a Stokes shift of 12 nm (Figure 87). Remarkably, the fluorescence quantum yield of **12** is significantly affected by solvent polarity and decreases moving from toluene (0.27) to chlorobenzene (0.11), anisole (0.096) and benzonitrile (0.001) (Table 7). Similarly to what observed for derivatives **3** and **4** in section 1.3.3.1, a singlet-singlet energy transfer from the photoexcited SubPc (which singlet excited state energy of 2.04 eV can be calculated by means of Equation 15) to the aniline (4.30 eV)[377] is not feasible. Thus, the fluorescence quenching of **12** upon increasing solvent polarity could be attributed to an intramolecular CS event (*vide infra*).

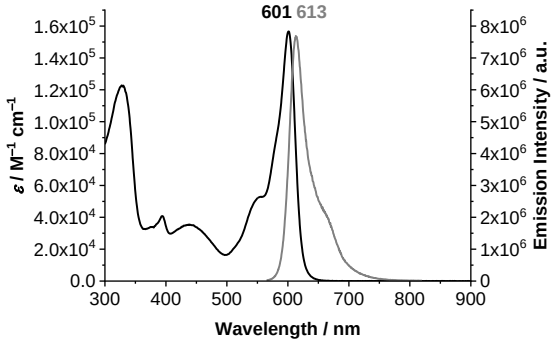

Figure 87. Steady-state absorption (black) and fluorescence spectra (grey) of (ethynyl-aniline)$_3$SubPc-OAr **12** (λ_{ex} = 550 nm) in toluene (c = 7.07 × 10^{-7} M).

With respect to precursor **12**, the fluorescence of (TCBD-aniline)$_3$SubPc-OAr **14** is broader and further shifted to the red, with a fluorescence maximum at 650 nm in toluene and a Stokes shift of 28 nm (Figure 88a). Both broadening and Stokes shift increase upon moving from toluene to

benzonitrile, in which a Stokes shift of 33 nm is observed. The ϕ_F of **14** is very low in all the investigated solvents, ranging between 1 x 10^{-4} in benzonitrile and 5 x 10^{-4} in anisole (Table 7).

A further fluorescence quenching is observed for (TCBD–aniline)$_3$SubPc-TCBD-aniline **15,** which exhibits ϕ_F values lower than 1 x 10^{-5}, corresponding to a quenching of more than 99.99% (Table 7). The Stokes shifts observed for **15** resemble that of **14**, ranging from 26 nm in benzonitrile to 32 nm in anisole (Figure 88b). The strongly quenching of fluorescence in **14** and **15** suggests a possible deactivation pathway involving an intramolecular CT process from the photoexcited SubPc to the electron-accepting TCBD moiety. In this connection, the stronger quenching observed in the case of **15** with respect to **14** could result from the presence of an additional TCBD unit at the axial position.

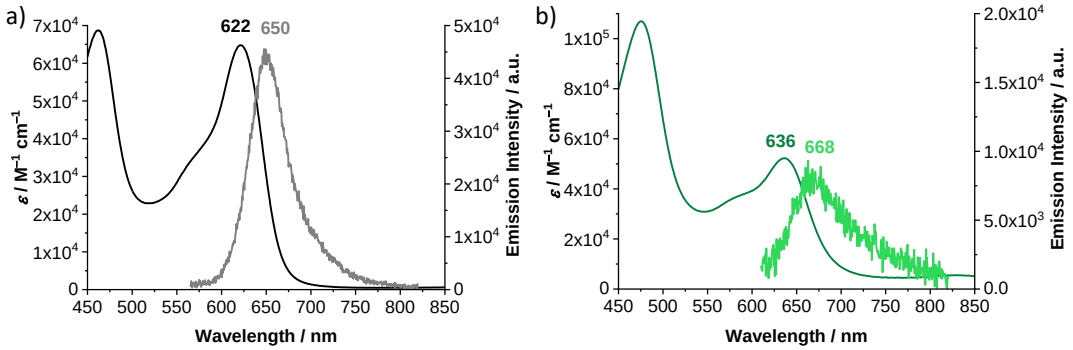

Figure 88. Steady-state absorption and fluorescence spectra of a) (TCBD-aniline)$_3$SubPc-OAr **14** (λ_{ex} = 550 nm, c = 1.24 × 10^{-6} M) in toluene and b) (TCBD-aniline)$_3$SubPc-TCBD-aniline **15** (λ_{ex} = 470 nm, c = 9.38 × 10^{-7} M) in anisole.

Transient absorption studies

Finally, femtosecond transient absorption spectroscopy studies were performed on derivatives **12**, **14** and **15**. Upon photoexcitation of (ethynyl-aniline)$_3$SubPc-OAr **12** at 550 nm in toluene, the characteristic features of the SubPc $^1(S_1)$ state (2.04 eV) are instantaneously discernible (Figure 89a,b). The latter include maxima at 501 and 690 nm with a shoulder at 657 nm and minima at 455 and 607 nm, along with a broad absorption extending far into the NIR region. The SubPc $^1(S_1)$ state then undergoes a fast vibrational relaxation within 16 ps and transforms *via* ISC within 1709 ps into the corresponding $^3(T_1)$ state, which signatures include maxima at 496 and 695 nm as well as a minimum at 604 nm.[319] In chlorobenzene and anisole, a similar deactivation scenario is observed.

In contrast, a different deactivation pathway in the form of an intramolecular CS is operative for **12** in benzonitrile. In this solvent, the deactivation of the SubPc $^1(S_1)$ state is accompanied by the formation of maxima at 516 and 673 nm, as well as a minimum at 610 nm (Figure 89c,d). As already discussed in section 1.3.3.1, these features suggest the formation of a radical anion SubPc species.[290] The metastable $SubPc^{\cdot-}[(ethynyl\text{-}aniline)_3]^{\cdot+}$ state subsequently decays to the ground state with CS and CR kinetics of 12 ps and 42 ps, respectively. Such a substantial change in the SubPc deactivation pattern upon increasing the solvent polarity can be rationalized on the basis of the redox features of derivative **12**. As a matter of fact, electrochemical measurement showed that in toluene, chlorobenzene and anisole the $SubPc^{\cdot-}[(ethynyl\text{-}aniline)_3]^{\cdot+}$ CSS is energetically higher (2.05 eV) than the SubPc $^1(S_1)$ state (2.04 eV), whereas in benzonitrile the CSS is stabilized and, thus, populated from the SubPc singlet excited state. Fluorescence studies on **12**, which evidenced a strong fluorescence quenching when moving from anisole to benzonitrile, further support this hypothesis (Table 7).

At this point, it is interesting to compare the photophysical behavior of derivative **12** with that of H_{12}SubPc-ethynyl-aniline **3**, which has been discussed in section 1.3.3.1. For the latter, transient absorption studies suggested that ISC takes place only in toluene, whereas the SubPc $^1(S_1)$ state deactivates via a CSS in chlorobenzene, anisole, and benzonitrile. Such a different trend suggests that CT from the electron-rich aniline moiety to the SubPc is more likely to occur when the former is electronically decoupled from the macrocycle as in the case of **3**, in which the aniline group is placed at the axial position of the SubPc. On the contrary, a full CS is hampered when the aniline is linked to the peripheral position of the macrocycle, and thus fully integrated in the extended π-system, as in the case of **12**.

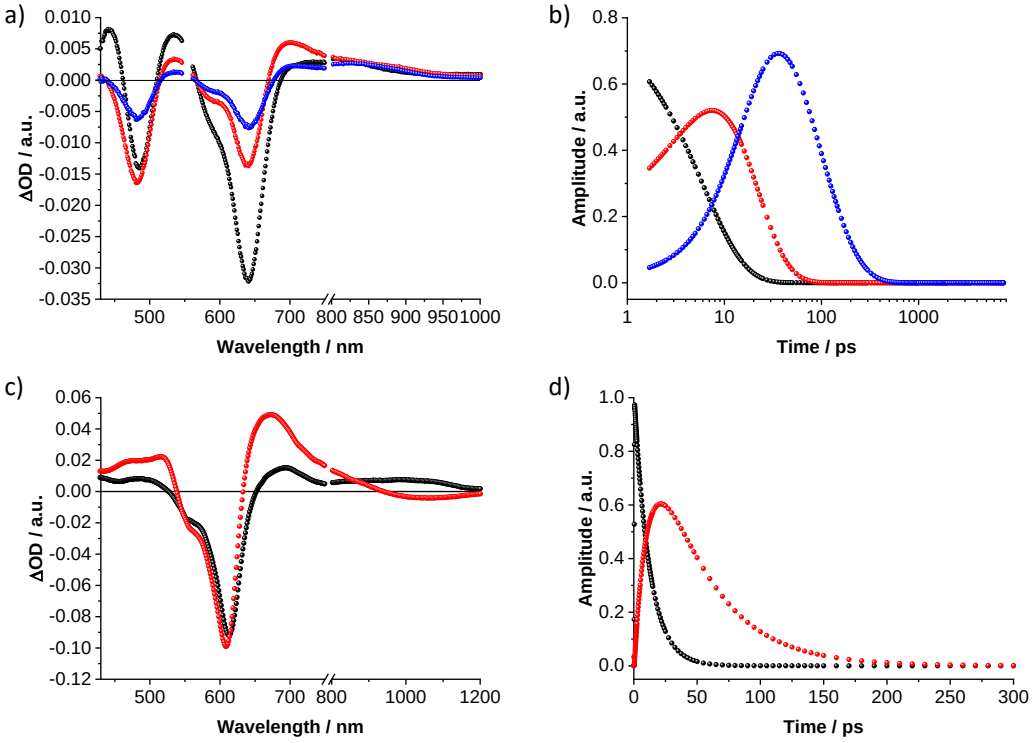

Figure 89. a,c) Evolution associated spectra and b,d) associated time-dependent amplitudes obtained upon femtosecond flash photolysis (550 nm) of (ethynyl-aniline)$_3$SubPc-OAr **12** (c = 2 × 10^{-5} M) in a,b) toluene monitoring ISC and c,d) benzonitrile monitoring CS and CR.

Turning to (TCBD-aniline)$_3$SubPc-OAr **14**, upon 550 nm excitation in anisole, transient minima at 474 and 626 nm (which are a good reflection of the ground state absorption) along with maxima at 520 and 687 nm as well as a broad absorption reaching far into the NIR are observed (Figure 90). As time progresses, several features evolve. Firstly, the broad NIR absorption and the ground state bleaching of the SubPc Q-band decrease, whereas the ground state bleaching of the TCBD-aniline CT band at 474 nm intensifies and experiences a slight blue-shift to 470 nm. Secondly, a new signature maximizing at 674 nm grows-in with monoexponential kinetics. These findings point out to the formation of the one-electron reduced form of TCBD, as suggested by spectroelectrochemical measurements on the reference Ph-TCBD-aniline derivative (Figure 65) and similarly to what observed in section 1.3.3.1. Based on these results, a CT process from the SubPc to one of the peripheral TCBD units leading to the formation of a highly polarized (SubPc$^{\delta+}$[(TCBD-aniline)$_3$]$^{\delta-}$)* species is proposed (Figure 91). The same transient absorption features were observed in toluene, chlorobenzene, and benzonitrile. As a matter of fact,

ultrafast formation and decay kinetics were determined (namely, 3.3/13 ps in toluene, 4.2/15 ps in chlorobenzene, 3.6/14 ps in anisole, and 2.0/15 ps in benzonitrile). However, it is worth to notice that the formation of a fully CSS is not observed for **14** in any of the investigated solvents.

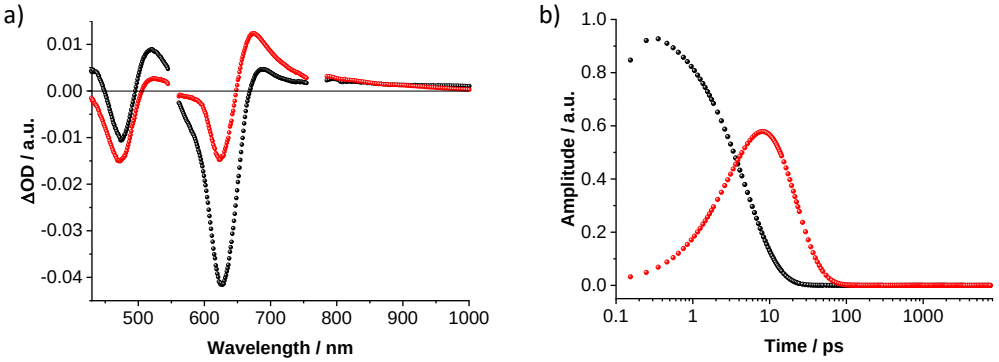

Figure 90. a) Evolution associated spectra and b) associated time-dependent amplitudes obtained by femtosecond flash photolysis (550 nm) of (TCBD-aniline)$_3$SubPc-OAr **14** (c = 2 x 10^{-5} M) in anisole monitoring formation and decay kinetics.

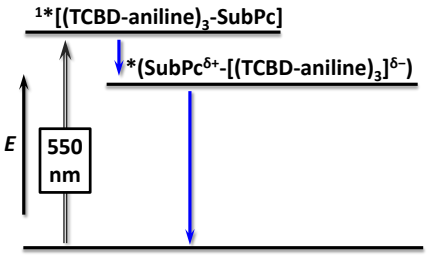

Figure 91. Energy level diagram of (TCBD-aniline)$_3$SubPc-OAr **14** in toluene, chlorobenzene, anisole, and benzonitrile reflecting the energetic pathways after excitation of SubPc (λ_{ex} = 550 nm).

Next, (TCBD-aniline)$_3$SubPc-TCBD-aniline conjugate **15** was probed. Photoexcitation of **15** at 550 nm in anisole leads to the instantaneous formation of the fingerprints of the SubPc $^1(S_1)$ state, namely sharp maxima at 441 and 534 nm, a broad maximum at 805 nm, as well as minima at 484 and 641 nm (Figure 92a,b). Remarkably, the NIR absorption in more intense than in **14**, which reflects a stronger electronic coupling between the SubPc macrocycle and the TCBD units. As time progresses, a slight hypsochromic shift (*i.e.*, from 484 to 482 nm) and an increase of the CT ground state bleaching is observed, along with a significant decay of the SubPc ground state bleaching. In parallel, a maximum at 701 nm raises with monoexponential kinetics. All these features resemble those of the highly polarized excited CT state seen for **14**. Thus, we infer that

the SubPc $^1(S_1)$ state transforms into the $(SubPc^{\delta+}\text{-}[(TCBD\text{-}aniline)_4]^{\delta-})^*$ species. In particular, formation kinetics of 3.6 ps in chlorobenzene and 4.2 ps in anisole were determined. However, global analysis reveals the presence of an additional component, which characteristics, that is, minima at 484 and 642 nm, are fingerprints of the TCBD-aniline CT and the SubPc Q-band transition, respectively. These features are complemented by transient maxima at 539 and 703 nm, as well as a broad absorption with a maximum at 836 nm. The latter can be assigned to a significant electronic interaction between the SubPc and the TCBD units, as already suggested by steady-state absorption and fluorescence measurements (*vide supra*). The 703 nm maximum and the 484 nm minimum can be assigned to the one-electron reduced form of TCBD, whereas the 642 nm minimum is a signature of the one-electron oxidized form of SubPc. In light of the aforementioned, the formation of a $SubPc^{\cdot+}\text{-}[(TCBD\text{-}aniline)_4]^{\cdot-}$ CSS is postulated. In particular, CS and CR kinetics of 20/120 ps in chlorobenzene and 17/89 ps in anisole were determined.

Interestingly, in benzonitrile, global analysis was based on a two-species kinetic model. The first species - namely, the SubPc $^1(S_1)$ state - transforms within 1.8 ps into a second species, which transient features (namely, a distinct maximum at 700 nm and a broad maximum around 825 nm) resemble those attributed to the radical cation SubPc species and radical anion TCBD species formed in chlorobenzene and anisole (Figure 92c,d). These findings indicate that in a polar solvent such as benzonitrile, the SubPc $^1(S_1)$ state transforms directly into the highly stabilized $SubPc^{\cdot+}\text{-}[(TCBD–aniline)_4]^{\cdot-}$ CSS. The latter finally deactivates to the ground state within 29 ps (Figure 93b). The observed electron-transfer process is in line with the higher intensity of the CT absorption band in the NIR region (Figure 86) and the dramatic decrease of ϕ_F (Table 7) in **15** in comparison to **14**. In this connection, it is important to notice that the different behavior observed for $(TCBD\text{-}aniline)_3$SubPc-TCBD-aniline **15** with respect to $(TCBD\text{-}aniline)_3$SubPc-OAr **14** can be related to the different substitution pattern and, in particular, to the different anchoring position of the TCBD units to the SubPc macrocycle. In particular, in the case of **15**, CS is feasible due to the presence of an electron-accepting TCBD unit at the axial position of the macrocycle. As a matter of fact, the axial TCBD-aniline is decoupled from the SubPc through the nodal plane at the boron atom, which allows for a significant stabilization of the electron transfer product. In contrast, the peripheral TCBDs are part of the SubPc's π-conjugated system. This enhances the electronic communication, but, at the same time, destabilizes the electron transfer product. Therefore, the peripheral TCBD units and the SubPc in **14** are subject to CT interactions rather than undergoing electron transfer.

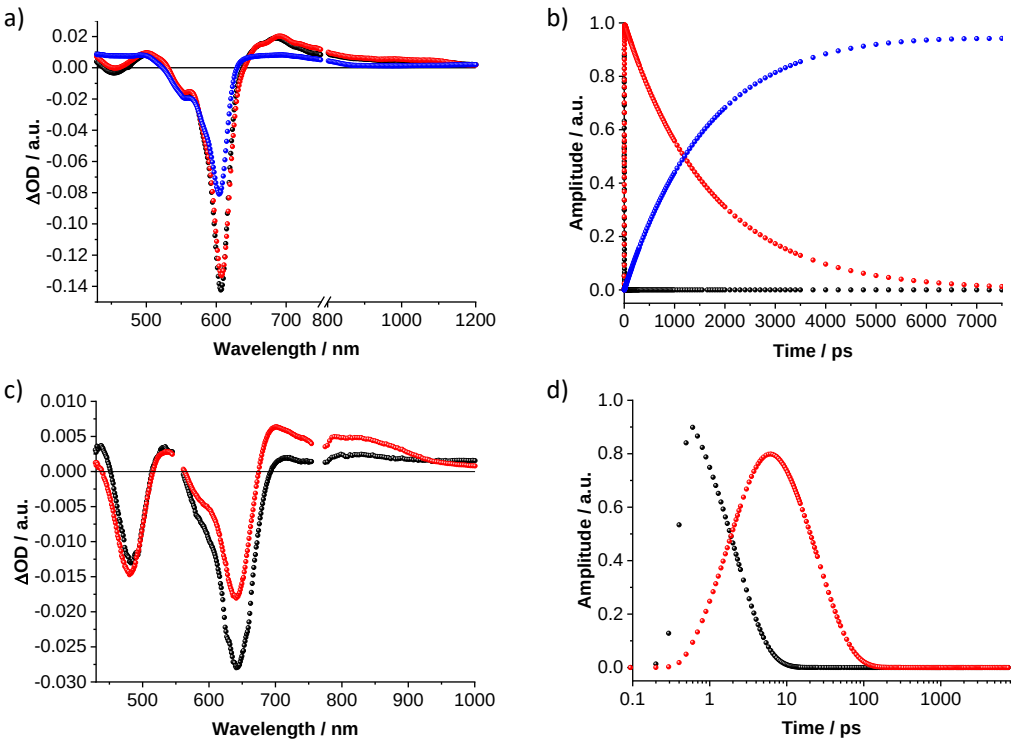

Figure 92. a,c) Evolution associated spectra and b,d) associated time-dependent amplitudes obtained upon femtosecond flash photolysis (550 nm) of (TCBD-aniline)$_3$SubPc-TCBD-aniline **15** (c = 3 × 10^{-5} M) in a,b) anisole c,d) benzonitrile monitoring formation and decay kinetics.

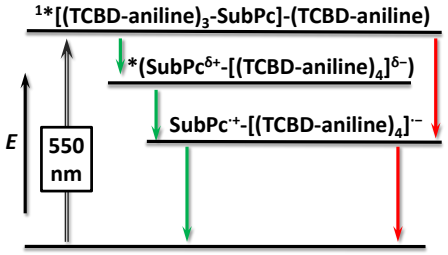

Figure 93. Energy level diagram of (TCBD-aniline)$_3$SubPc-TCBD-aniline **15** in chlorobenzene and anisole (green arrows), and benzonitrile (red arrows) reflecting the energetic pathways after excitation of the SubPc (λ_{ex} = 550 nm).

1.4 Summary and conclusions

In this Chapter, the synthesis and study of novel D-A conjugates featuring a SubPc core functionalized at the axial (**5** and **6**), peripheral (**14**), or axial and peripheral (**15**) positions with one, three or four TCBD-aniline moieties have been presented.

The target derivatives were prepared through CA-RE reaction of the corresponding ethynyl-substituted SubPcs with TCNE. In turn, the alkynyl-functionalized SubPc precursors were obtained by axial substitution reaction of axially chlorinated SubPcs with a Grignard reagent and/or palladium-catalyzed Sonogashira cross-coupling reaction from the corresponding peripherally iodinated SubPcs.

The in-depth structural, electrochemical and photophysical characterization of the novel SubPc-based derivatives provided interesting insights into their stereochemical features and the electronic interactions in the ground and excited states. In particular, the anchoring position of the TCBD-aniline units was found to have a remarkable impact on the structural and optoelectronic properties of the conjugates.

Single-crystal X-ray diffraction analysis provided useful information on the structural features of the axially substituted derivatives. A different solid-state arrangement (*i.e.*, in heterochiral dimers or heterochiral columnar stacks) was observed for H_{12}SubPc-TCBD-aniline **5** and F_{12}SubPc-TCBD-aniline **6**, respectively. Moreover, the crystal structures of both conjugates show that the TCBD moiety adopts an almost orthogonal geometry. As a consequence of the hindered rotation around the central C-C bond of the TCBD framework, SubPc-TCBD-aniline conjugates **5** and **6** are formed as racemic mixtures of two atropisomers. Both derivatives were optically resolved by means of semipreparative chiral HPLC, and X-ray diffraction analysis of the enantiopure species allowed to unambiguously assign the absolute configuration of each atropisomer, something unprecedent in TCBD-based compounds.

The racemization process in enantiopure species of SubPc-TCBD-aniline derivatives **5** and **6** was investigated by means of CD measurements and theoretical calculations. These studies revealed a light-triggered enantiomer conversion mechanism enabled by triplet-state photogeneration, which can be rationalized on the basis of energetic, structural and kinetic considerations (Figure 94). The thermal configurational stability of the isolated enantiomers of **5** and **6** is in stark contrast with what reported in literature for a C_{60}-TCBD-aniline analogue and what observed for a SubP derivative functionalized at the apical position with a TCBD-aniline unit, for which a thermal racemization was noticed. The peculiar racemization behavior of the investigated

SubPc-TCBD-aniline derivatives render them intriguing photoresponsive systems for potential applications in the fast-growing field of light-controllable molecular switches.

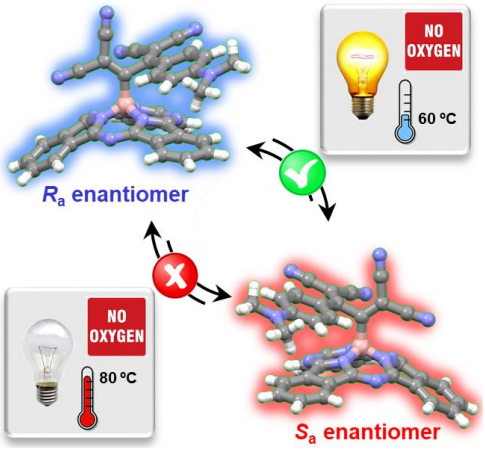

Figure 94. Graphical abstract depicting the racemization behavior of **5** and **6**.

In peripherally and peripherally/axially substituted derivatives **14** and **15**, due to the combination of the inherent chirality of the C_3-symmetric SubPc core, the axial chirality of the multiple TCBD units, and the cone-shaped structure of the SubPc macrocycle which results in the possible formation of different conformers upon rotation of the peripheral TCBD units around the C-C bonds connecting them to the SubPc benzene rings, several stereoisomers are expected. Although these species rapidly interconvert at room temperature, interconversion between different stereoisomers is significantly slowed down upon lowering the temperature, as suggested by VT-NMR experiments which evidenced the coexistence on the NMR timescale of many magnetically distinct species.

The in-depth electrochemical and photophysical characterization of the novel derivatives evidenced that the introduction of TCBD-aniline moieties has a profound impact on the optical and electronic features of SubPc-based systems.

In the case of axially functionalized derivatives **5** and **6**, the ground- and excited-state interactions are determined by the electronic characteristics of the macrocycle, which ultimately depend on the nature of the peripheral substituents. On one hand, H_{12}SubPc-TCBD-aniline **5** features ground-state CT interactions between the H_{12}SubPc and the axial TCBD moiety (Figure 95). On the other hand, an intramolecular exciplex is formed in F_{12}SubPc-TCBD-aniline **6**. This polarized CT state is a direct result of the unique geometry adopted by the latter, which allows for intramolecular interactions between the spatially close electron-rich aniline and the

F_{12}SubPc π-surface. Remarkably, the formation on exciplex species has no precedent in both SubPc- and TCBD-based chemistry. Moreover, for both axially substituted conjugates **5** and **6**, CS processes were found to take place upon photoexcitation.

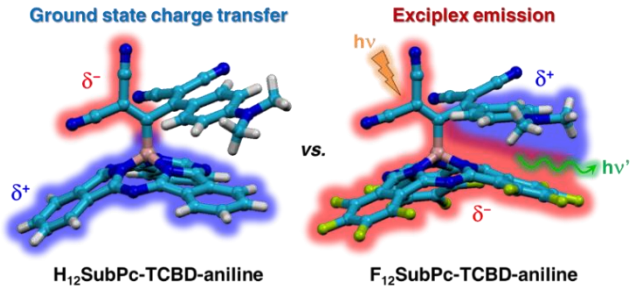

Figure 95. Graphical abstract depicting ground- and excited-state interactions in **5** and **6**.

Turning to peripherally and peripherally/axially substituted derivatives **14** and **15**, intense ground-state CT interactions between the SubPc and the electron-withdrawing TCBD units were observed, which are further enhanced in **15** due to the presence of an additional TCBD moiety at the apical position of the macrocycle. In these derivatives, photoexcitation leads to charge and/or electron transfer events, which depend on the substitution pattern of the macrocycle. In particular, the presence on an axial TCBD unit in **15** allows for the formation of a fully charge-separated species (Figure 96).

The ground- and excited-state photophysical features of the investigated systems (which include a panchromatic absorption in the visible region of the solar spectrum, ground-state CT interactions, and a photoinduced electron transfer behavior) render these derivatives promising candidates for applications in the technologically relevant field of molecular photovoltaics.

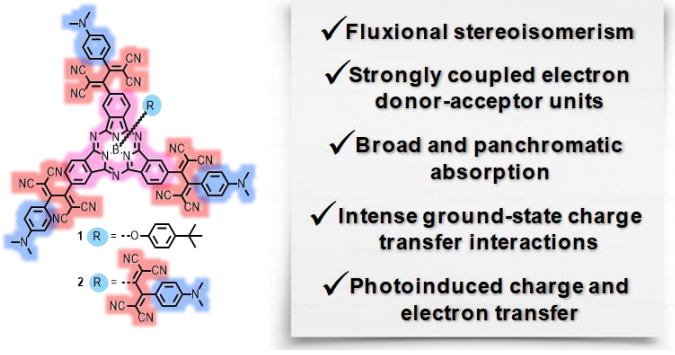

Figure 96. Graphical abstract depicting the most significative properties of derivatives **14** and **15**.

1.5 Experimental section

1.5.1 Materials and methods

Chemicals (reagent grade) and solvents (synthetic grade, anhydrous, HPLC grade, spectroscopy grade and deuterated) were purchased from Aldrich Chemical, Alfa Aesar, Acros Organics, TCI and Scharlau. Chemical reagents were used without further purification. Synthetic grade solvents were used for chemical reactions and column chromatography purifications and anhydrous solvents were used for reactions under dry conditions. Additionally, some solvents were further dried by distillation with Na/benzophenone (THF), with previously activated molecular sieves (3 or 4 Å), or with a solvent purifying system by Innovative Technology Inc. MD-4-PS. Oxygen- and moisture-sensitive reactions were carried out using standard Schlenk line techniques.

Chromatography: the monitoring of the reactions has been carried out by thin layer chromatography (TLC), employing aluminum sheets coated with silica gel type 60 F254 (0.2 mm thick, Merck). The analysis of the TLCs was carried out with a UV lamp of 254 and 365 nm. Column chromatography was performed using silica gel (230-400 mesh, 0.040-0.063 mm, Merck). Eluents are indicated for each particular case. High-performance liquid chromatography (HPLC) was performed using an Agilent 1200 equipment with a Daicel CHIRALPAK IC semi-preparative chiral column (particle size 5 µm, dimensions 10 mm ø x 250 mm). HPLC grade solvents were used. HPLC conditions for the optical resolution of H_{12}SubPc-TCBD-aniline **5**: eluting solvent mixture = toluene/*n*-hexane/ethyl acetate 80:17:3 (v/v/v); flow rate = 1.2 mL min^{-1}; temperature = 10 °C; detection wavelength = 580 nm. HPLC conditions for the optical resolution of F_{12}SubPc-TCBD-aniline **6**: eluting solvent = toluene; flow rate = 2.5 mL min^{-1}; temperature = 10 °C; detection wavelength = 580 nm. HPLC conditions for the optical resolution of SubP-TCBD-aniline **16**: eluting solvent = toluene/*n*-hexane/ethyl acetate 85:12:3 (v/v/v); flow rate = 0.6 mL min^{-1}; temperature = 10 °C; detection wavelength = 379 nm.

Nuclear Magnetic Resonance (NMR): NMR spectra were recorded with a Bruker AVANCE 300 (300 MHz), a Bruker AVANCE-II 300 (300 MHz), a BRUKER AVANCE III-HD Nanobay (300MHz), a Bruker AC-400 (400 MHz) and a Bruker DRX-500 (500 MHz) instruments in the Organic Chemistry Department of UAM, in the Interdepartmental Investigation Service of UAM or at IMDEA Nanociencia. The deuterated solvent employed is indicated for each case. Chemical shifts (δ) are reported in ppm, and coupling constants (J) are reported in hertz (Hz). For ^{1}H-NMR and ^{13}C-NMR spectra, δ are measured relative to residual solvent signals using literature reference

values.[379] The following abbreviations are used to indicate the multiplicity in ^{1}H-NMR spectra: s, singlet; d, doublet; t, triplet; q, quartet; quint, quintet; m, multiplet.

Mass Spectrometry (MS) and High-Resolution Mass Spectrometry (HRMS): Matrix Assisted Laser Desorption/Ionization-Time of Flight (MALDI-TOF) mass spectra were recorded in the Interdepartmental Investigation Service of UAM, using a Bruker ULTRAFLEX III spectrometer equipped with a Nd:YAG laser operating at 355 nm. The different matrixes employed are indicated for each spectrum. Mass spectrometry data are expressed in *m/z* units.

Steady-State Absorption and Fluorescence Spectroscopy: absorption spectra were recorded in the Organic Chemistry Department of UAM and at Friederich-Alexander University in Erlangen, employing a V660 spectrophotometer from Jasco, a Lambda 2 UV/Vis/NIR spectrophotometer from Perkin Elmer and a Cary 5000 UV/Vis/NIR spectrophotometer from Varian. Fluorescence measurements were carried out with a FluoroMax®-3 fluorometer from Horiba Jobin Yvon. Spectroscopic grade solvents were used for spectroscopic measurements.

Circular dichroism (CD) Spectroscopy: CD spectra were recorded at IMDEA Nanociencia using a JASCO V-815 spectrometer equipped with a JASCO Peltier ETCT-762 temperature controller. For CD experiments carried out upon continuous illumination, a custom-made set-up was used. Illumination was performed with a Cree XLamp® CXA3070 LED.

Transient absorption Spectroscopy: transient absorption studies in the femto- to microsecond regime were carried out at Friederich-Alexander University in Erlangen using a transient absorption pump/probe HELIOS/EOS system in combination with an amplified CPA-2101 Ti:sapphire laser (1 kHz, 150 fs pulse width, 775 nm output) from Clark-MXR Inc. The excitation wavelengths at 458 and 550 nm were generated with a non-collinear optical parameter (NOPA) from Clark-MXR Inc.

Time-correlated single photon counting (TCSPC). fluorescence lifetimes were determined at Friederich-Alexander University in Erlangen by time-correlated single photon counting (TCSPC) technique using a TemPro system from Horiba Jobin Yvon with a TBX Picosecond Photon Detection Module. The samples were excited at 461 nm by means of a pulsed NanoLED.

Infrared Spectroscopy (FT-IR): infrared spectra were recorded in the Interdepartmental Investigation Service of UAM with a Bruker IFS66v FTIR spectrometer.

[379] G. R. Fulmer, A. J. Miller, N. H. Sherden, H. E. Gottlieb, A. Nudelman, B. M. Stoltz, J. E. Bercaw, K. I. Goldberg, *Organometallics* **2010**, *29*, 2176-2179.

Cyclic Voltammetry (CV) and Square Wave Voltammetry (SWV): electrochemical measurements were performed in a single compartment glass cell with a three-electrode setup comprising a polished glassy carbon electrode as working electrode, a platinum wire as counter electrode, and a silver wire as pseudo reference electrode. The applied potential was controlled with a μAutolab III/FRA2 potentiostat from METROHM. All measurements were carried in an argon-saturated 0.2 M solution of *n*-Bu_4NPF_6 in DCM. The Fc^+/Fc redox couple was used as internal standard.

X-Ray Spectroscopy: X-Ray diffraction analysis was performed in the Interdepartmental Investigation Service of UAM with a Bruker KAPPA APEX II (X8 APEX) single-crystal diffractometer with Mo source (λ = 0.71073 Å). Data are corrected with the SADABS program. Intensities are calculated with the SAINT software. The structures are resolved and refined using the Bruker SHELXTL Software Package.

Melting point (MP): melting points were measured in open-end capillary tubes by using a Büchi 504392-S apparatus, and are uncorrected.

Theoretical calculations: Theoretical calculations were carried out using QM calculations at DFT level and its time-dependent extension (TD-DFT).[380,381] All QM calculations were performed with Gaussian09 software package.[382] Hybrid B3LYP[383,384] functional and 6-31+G(d,p) basis set were used for all calculations. Grimme's D3 damping function was included to take care of dispersion correction.[385] The implicit toluene effect was included by the conductor version of the polarizable continuum model (C-PCM).[386-388] Crystallographic structures were considered as starting point for the QM calculations.

[380] E. Runge, E. K. Gross, *Phys. Rev. Lett.* **1984**, *52*, 997-1000.
[381] M. E. Casida, in *Recent Advances In Density Functional Methods: (Part I)*, World Scientific, **1995**, pp. 155-192.
[382] M. J. Frisch, G. W. Trucks, H. B. Schlegel, G. E. Scuseria, M. A. Robb, J. R. Cheeseman, G. Scalmani, *et al.* "Gaussian 09, Revision B.01," **2009**.
[383] A. D. Becke, *The Journal of Chemical Physics* **1993**, *98*, 5648-5652.
[384] P. J. Stephens, F. J. Devlin, C. F. Chabalowski, M. J. Frisch, *J. Phys. Chem.* **1994**, *98*, 11623-11627.
[385] S. Grimme, J. Antony, S. Ehrlich, H. Krieg, *J. Chem. Phys.* **2010**, *132*, 154104.
[386] A. Klamt, G. Schurmann, *J. Chem. Soc., Perkin Trans* **1993**, *2*, 799-805.
[387] V. Barone, M. Cossi, *J. Phys. Chem. A* **1998**, *102*, 1995-2001.
[388] M. Cossi, N. Rega, G. Scalmani, V. Barone, *J. Comput. Chem.* **2003**, *24*, 669-681.

1.5.2 Synthetic procedures

1.5.2.1 Synthetic procedures for the preparation of axially (TCBD-aniline)-substituted SubPcs

Subphthalocyanine **1**[22]

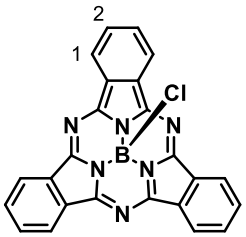

A 1.0 M solution of BCl_3 in *p*-xylene (7.8 mL, 7.8 mmol) was added to 1,2-dicyanobenzene (1.00 g, 7.8 mmol) under argon atmosphere and the mixture was refluxed for 40 min under vigorous stirring. The reaction mixture was then allowed to cool down to room temperature and flushed with argon. After evaporating the solvent under reduced pressure, heptane was added to the flask. The crude product was recovered through filtration and thoroughly washed with heptane and methanol. H_{12}SubPc-Cl **1** was obtained as a purple solid in 21% yield (237 mg).

^{1}H-NMR (300 MHz, $CDCl_3$): δ (ppm) = 8.72-8.63 (AA'XX' system, 6H; H-1), 7.88-7.78 (AA'XX' system, 6H; H-2).

UV-vis ($CHCl_3$): λ_{max} (nm) (log ε (dm^3 mol^{-1} cm^{-1})) = 565 (4.4), 529 (sh), 308 (4.1), 273 (4.1).

Subphthalocyanine **2**[22]

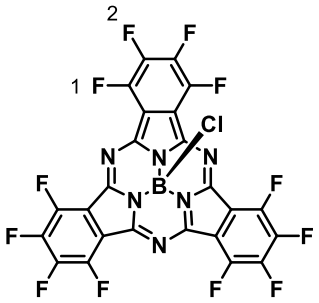

A 1.0 M solution of BCl_3 in *p*-xylene (10.0 mL, 10.0 mmol) was added to 3,4,5,6-tetrafluorophthalonitrile (2.00 g, 10.0 mmol) under argon atmosphere and the mixture was refluxed for 20 min under vigorous stirring. The reaction mixture was then allowed to cool down to room temperature and flushed with argon. After evaporating the solvent under reduced pressure, the crude was dissolved in a toluene/THF 10:1 (v/v) mixture and passed through a short silica plug. The solvent was evaporated under reduced pressure, and the product was

purified by column chromatography on silica gel using hexane/toluene 60:40 (v/v) as eluent. F_{12}SubPc-Cl **2** was obtained as a purple solid in 17% yield (366 mg).

^{19}F-NMR (471 MHz, $CDCl_3$): δ (ppm) = -137.0 (AA'XX' system, 6H; F-1), -147.7 (AA'XX' system, 6H; F-2).

UV-vis ($CHCl_3$): λ_{max} (nm) (log ε (dm^3 mol^{-1} cm^{-1})) = 574 (4.6), 556 (sh), 530 (sh), 311 (4.3), 277 (4.0).

Subphthalocyanine **3**

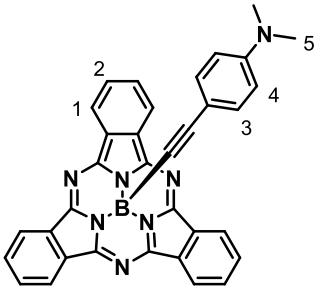

A 1.0 M solution of EtMgBr in THF (0.17 mL, 0.17 mmol) was added to a solution of 4-ethynyl-*N*,*N*-dimethylaniline (34 mg, 0.23 mmol) in degassed and anhydrous THF (4 mL) under argon atmosphere. The solution was stirred at 60 °C for 1 hour and then transferred *via* cannula to a degassed and anhydrous solution of H_{12}SubPc-Cl **1** (50 mg, 0.12 mmol) in THF (6 mL). The resulting mixture was then stirred at 60 °C until the disappearance of the SubPc-Cl starting material as confirmed by TLC (3 h). The reaction mixture was then allowed to cool down to room temperature and the solvent was evaporated under reduced pressure. The crude product was dissolved in chloroform and washed with water, and the organic phase was dried with $MgSO_4$. After filtration of the drying agent and evaporation of the solvent, the solid obtained was purified by column chromatography on silica gel using toluene/EtOAc 98:2 (v/v) as eluent. Recrystallization from a DCM/hexane mixture afforded H_{12}SubPc-ethynyl-aniline **3** as a purple solid in 56% yield (35 mg).

^{1}H-NMR (300 MHz, $CDCl_3$): δ (ppm) = 8.89-8.82 (AA'XX' system, 6H; H-1), 7.91-7.85 (AA'XX' system, 6H; H-2), 6.62 (d, $^{3}J_{H\text{-}H}$ = 9.0 Hz, 2H; H-4), 6.24 (d, $^{3}J_{H\text{-}H}$ = 9.0 Hz, 2H; H-3), 2.77 (s, 6H; H-5).

^{13}C-NMR (100.6 MHz, $CDCl_3$): δ (ppm) = 150.56, 149.78, 132.64, 131.08, 129.64, 122.18, 111.37, 109.39, 40.15.

^{11}B-NMR (96.3 MHz, $CDCl_3$): δ (ppm) = -20.84.

MS (MALDI-TOF, DCTB): *m/z* = 539.3 $[M]^+$.

HRMS: *m/z* Calculated for $[C_{34}H_{22}BN_7]$: 539.2030; Found: 539.2013.

UV-vis (toluene): λ_{max} (nm) (log ε (dm^3 mol^{-1} cm^{-1})) = 567 (4.96), 549 (sh), 526 (sh), 304 (4.85).

FT-IR (ATR): *v* (cm^{-1}) = 3052, 2857, 2801, 2168 (C≡C), 1604, 1521, 1456, 1363, 1282, 1226, 1192, 1127, 1080, 1021, 998, 946, 866, 808, 759, 733, 692, 633, 571, 531.

MP > 250 °C.

Subphthalocyanine **4**

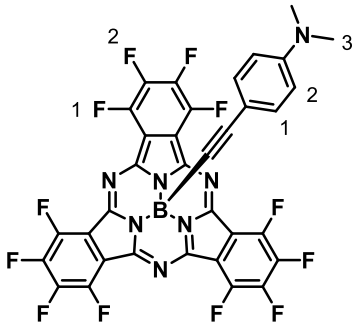

A 1.0 M solution of EtMgBr in THF (0.12 mL, 0.12 mmol) was added to a solution of 4-ethynyl-*N*,*N*-dimethylaniline (22 mg, 0.15 mmol) in degassed and anhydrous THF (3 mL) under argon atmosphere. The solution was stirred at 60 °C for 1 hour and then transferred *via* cannula to a degassed and anhydrous solution of F_{12}SubPc-Cl **2** (50 mg, 0.08 mmol) in THF (4 mL). The resulting mixture was then stirred at 60 °C until the disappearance of the SubPc-Cl starting material as confirmed by TLC (2 h). The reaction mixture was then allowed to cool down to room temperature and the solvent was evaporated under reduced pressure. The crude product was dissolved in chloroform and washed with water, and the organic phase was dried with $MgSO_4$. After filtration of the drying agent and evaporation of the solvent, the solid obtained was purified by column chromatography on silica gel using toluene/heptane 70:30 (v/v) as eluent. Recrystallization from a DCM/hexane mixture afforded F_{12}SubPc-ethynyl-aniline **4** as a purple solid in 62% yield (36 mg).

^{1}H-NMR (400 MHz, $CDCl_3$): *δ* (ppm) = 6.61 (d, $^{3}J_{H\text{-}H}$ = 9.1 Hz, 2H; H-2), 6.27 (d, $^{3}J_{H\text{-}H}$ = 9.1 Hz, 2H; H-1), 2.81 (s, 6H, H-3).

^{13}C-NMR (75.5 MHz, $CDCl_3$): *δ* (ppm) = 150.20, 147.65, 143.90, 141.30, 132.76, 115.11, 111.32, 107.76, 40.06.

^{19}F-NMR (470.6 MHz, toluene-d_8): *δ* (ppm) = -138.25–-138.42 (AA'XX' system, 6F; F-1), -150.07–-150.24 (AA'XX' system, 6F; F-2).

^{11}B-NMR (96.3 MHz, $CDCl_3$): *δ* (ppm) = -21.02.

MS (MALDI-TOF, DCTB): *m/z* = 755.2 $[M]^+$.

HRMS: *m/z* Calculated for $[C_{34}H_{10}BF_{12}N_7]$: 755.0900; Found: 755.0919.

UV-vis (toluene): λ_{max} (nm) (log *ε* (dm^3 mol^{-1} cm^{-1})) = 576 (4.92), 556 (sh), 533 (sh), 303 (4.73).

FT-IR (ATR): ν (cm^{-1}) = 2907, 2863, 2816, 2174 (C≡C), 1646, 1527, 1472, 1364, 1285, 1258, 1209, 1162, 1103, 1071, 962, 877, 819, 737, 710, 651, 592, 567, 538.

MP > 250 °C.

Subphthalocyanine **5**

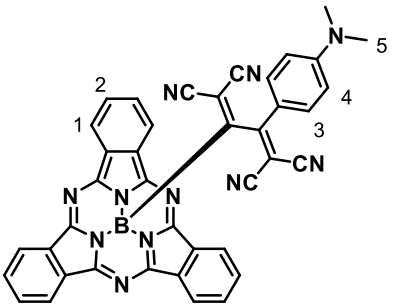

H_{12}SubPc-ethynyl-aniline **3** (22 mg, 0.04 mmol) and TCNE (6.3 mg, 0.049 mmol) were dissolved in anhydrous THF (4 mL) and the reaction mixture was stirred at room temperature until the starting SubPc was completely consumed as confirmed by TLC (2 h and 30 min). Then, the solvent was evaporated under reduced pressure and the crude product was purified by column chromatography on silica gel using toluene as eluent. Recrystallization from a DCM/hexane mixture afforded H_{12}SubPc-TCBD-aniline **5** as a red solid in 81% yield (22 mg).

^{1}H-NMR (300 MHz, $CDCl_3$): δ (ppm) = 8.88-8.76 (ABXY system, 6H; H-1), 7.97-8.89 (ABXY system, 6H; H-2), 6.69 (d, $^{3}J_{H\text{-}H}$ = 8.8 Hz, 2H; H-4), 6.31 (d, $^{3}J_{H\text{-}H}$ = 8.8 Hz, 2H; H-3), 2.97 (s, 6H; H-5).

^{13}C-NMR (75.5 MHz, $CDCl_3$): δ (ppm) = 151.19, 150.92, 130.81, 130.70, 130.29, 122.40, 122.36, 115.45, 111.29, 103.21, 93.89, 39.94.

^{11}B-NMR (96.3 MHz, $CDCl_3$): δ (ppm) = -17.33.

MS (MALDI-TOF, DCTB): *m/z* = 667.3 $[M]^+$.

HRMS: *m/z* Calculated for $[C_{40}H_{22}BN_{11}]$: 667.2154; Found: 667.2173.

UV-vis (toluene): λ_{max} (nm) (log ε ($dm^3\ mol^{-1}\ cm^{-1}$)) = 587 (4.66), 530 (sh), 440 (4.43), 315 (4.64).

FT-IR (ATR): ν (cm^{-1}) = 3061, 2924, 2908, 2203 (C≡N), 1600, 1448, 1382, 1331, 1284, 1204, 1173, 1133, 1085, 1015, 989, 947, 827, 757, 722, 693, 632, 579, 567.

XRD: Single crystals of racemate **5** and enantiopure S_a-**5** were obtained by slow diffusion of *n*-hexane or *n*-pentane in chloroform, respectively. Selected crystallographic data are summarized in Tables 8 and 9.

MP > 250 °C.

Table 8. Selected crystallographic data for racemate **5**.

Chemical formula	$C_{40.75}H_{22.50}BCl_{2.75}N_{11}$
Formula weight	774.49 g/mol
Crystalline system	Triclinic
Space group	P-1
Volume	1956.3(4) $Å^3$
Density	1.315 g cm^{-3}
Z	2
a	11.0776(14) Å
b	12.2173(13) Å
c	15.629(2) Å
α	70.044(4)°
β	85.636(4)°
γ	79.768(4)°
R	4814 data; I>2σ(I) R1 = 0.1301, wR2 = 0.3459
	all data R1 = 0.1632, wR2 = 0.3769

Table 9. Selected crystallographic data for S_a-**5**.

Chemical formula	$C_{40}H_{22}BCN_{11}O_{0.25}$
Formula weight	671.49 g/mol
Crystalline system	Orthorombic
Space group	P 21 21 21
Volume	6711.8(3) $Å^3$
Density	1.329 g cm^{-3}
Z	8
a	11.3269(3) Å
b	14.3193(3) Å
c	41.3817(12) Å
α	90°
β	90°
γ	90°
R	9815 data; I>2σ(I) R1 = 0.0399, wR2 = 0.0868
	all data R1 = 0.0617, wR2 = 0.1015

Subphthalocyanine **6**

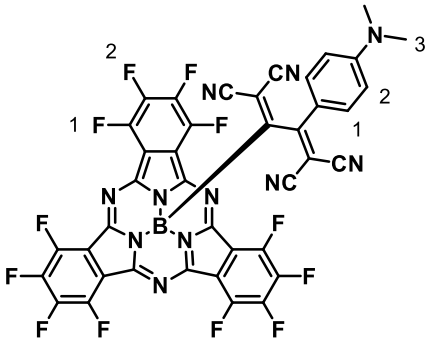

F_{12}SubPc-ethynyl-aniline **4** (30 mg, 0.04 mmol) and TCNE (6.1 mg, 0.048 mmol) were dissolved in anhydrous THF (4 mL) and the reaction mixture was stirred at room temperature until the starting SubPc was completely consumed as confirmed by TLC (2 h and 30 min). Then, the solvent was evaporated under reduced pressure and the crude product was purified by column chromatography on silica gel using a mixture of toluene/THF 90:10 (v/v) as eluent. Recrystallization from a DCM/hexane mixture afforded F_{12}SubPc-TCBD-aniline **6** as a grey solid in 93% yield (33 mg).

^{1}H-NMR (400 MHz, $CDCl_3$): δ (ppm) = 6.72 (d, $^{3}J_{H\text{-}H}$ = 7.8 Hz, 2H; H-2), 6.46 (d, $^{3}J_{H\text{-}H}$ = 7.8 Hz, 2H; H-1), 3.11 (s, 6H; H-3).

^{13}C-NMR (75.5 MHz, $CDCl_3$): δ (ppm) = 162.82, 153.64, 148.11, 144.23, 141.65, 130.90, 115.44, 114.91, 112.30, 111.60, 77.48, 77.36, 77.16, 77.16, 76.84, 40.08.

^{19}F-NMR (470.6 MHz, toluene-d_8): δ (ppm) = -136.75–-137.00 (ABXY system, 6F; F-1), -146.57–-146.69 (ABXY system, 6F; F-2).

^{11}B-NMR (96.3 MHz, $CDCl_3$): δ (ppm) = -17.53.

MS (MALDI-TOF, DCTB): *m/z* = 883.1 $[M]^+$.

HRMS: *m/z* Calculated for $[C_{40}H_{10}BF_{12}N_{11}]$: 883.1023; Found: 883.1013.

UV-vis (toluene): λ_{max} (nm) (log ε ($dm^3\ mol^{-1}\ cm^{-1}$)) = 598 (4.66), 556 (sh), 461 (4.51), 308 (4.58).

FT-IR (ATR): ν (cm^{-1}) = 2931, 2216 (C≡N), 1601, 1535, 1481, 1383, 1328, 1284, 1264, 1223, 1197, 1070, 1116, 1068, 964, 897, 829, 745, 715, 632, 593, 566.

XRD: Single crystals of racemate **6** and enantiopure R_a-**6** were obtained by slow diffusion of *n*-hexane in chloroform. Selected crystallographic data are summarized in Tables 10 and 11.

MP > 250 °C.

Table 10. Selected crystallographic data for racemate **6**.

Chemical formula	$C_{40.50}H_{10.50}BCl_{1.50}F_{12}N_{11}$
Formula weight	943.08 g/mol
Crystalline system	Monoclinic
Space group	P 1 21/n
Volume	4198.0(3) Å^3
Density	1.492 g cm^{-3}
Z	4
a	16.4663(7) Å
b	17.0450(6) Å
c	16.9234(7) Å
α	90°
β	117.894(2)°
γ	90°
R	3067 data; I>2σ(I) R1 = 0.1031, wR2 = 0.2840
	all data R1 = 0.2400, wR2 = 0.3700

Table 11. Selected crystallographic data for R_a-**6**.

Chemical formula	$C_{40.75}H_{10.75}BCl_{2.25}F_{12}N_{11}$
Formula weight	972.93 g/mol
Crystalline system	Orthorhombic
Space group	P 21 21 21
Volume	4036.1(5) Å^3
Density	1.601 g cm^{-3}
Z	4
a	8.3602(6) Å
b	20.2111(16) Å
c	23.8869(17) Å
α	90°
β	90°
γ	90°
R	4004 data; I>2σ(I) R1 = 0.1484, wR2 = 0.3648
	all data R1 = 0.2302, wR2 = 0.4047

1.5.2.2 Synthetic procedures for the preparation of peripherally and peripherally/axially (TCBD-aniline)-substituted SubPcs

4-Aminophthalonitrile **7**[389]

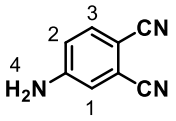

4-Nitrophthalonitrile (20.00 g, 115 mmol) was added to a mixture of MeOH (450 mL) and concentrated HCl (96 mL). Upon heating to reflux and observing the total dissolution of the solid, iron powder (22.00 g, 392 mmol) was added in small portions over 1 h. The reaction mixture was further refluxed for 1 h and then cooled down to room temperature. Cold water (600 mL) was poured onto the mixture resulting in the precipitation of a yellow-green solid which was filtered, washed with water and vacuum-dried. After recrystallization from toluene, 4-aminophthalonitrile **7** was obtained in 76% yield.

^{1}H-NMR (300 MHz, DMSO-d_6): δ (ppm) = 7.65 (d, $^3J_{H\text{-}H}$ = 8.7 Hz, 1H; H-3), 7.00 (d, $^4J_{H\text{-}H}$ = 2.5 Hz, 1H; H-1), 6.85 (dd, $^3J_{H\text{-}H}$ = 8.7 Hz, $^4J_{H\text{-}H}$ = 2.5 Hz, 1H; H-2), 6.70 (s (broad), 2H; H-4).

4-Iodophthalonitrile **8**[390]

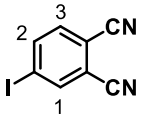

A suspension of 4-aminophthalonitrile (5.00 g, 35 mmol) in H_2SO_4 2.5 M (70 mL) was cooled to -10 °C and a solution of $NaNO_2$ (2.80 g, 39 mmol) in water (10 mL) was added dropwise under stirring. After that, the mixture was further stirred for 30 min at 0 °C and then poured over a solution of KI (6.50 g, 39 mmol) in cold water (40 mL). The resulting mixture was stirred for 45 min at room temperature. A brown solid was recovered through filtration, washed with water and dissolved in $CHCl_3$ (200 mL). This solution was then washed with a saturated solution of $Na_2S_2O_3$ (30 mL) and water (30 mL) and dried over Na_2SO_4. After filtration of the drying agent, the solvent was evaporated under reduced pressure and the yellow solid obtained was subjected to column chromatography on silica gel using DCM as eluent. 4-Iodophthalonitrile **8** was obtained as a white solid in 69% yield.

---

[389] J. Griffiths, B. Roozpeikar, *J. Chem. Soc., Perkin Trans. 1* **1976**, 42-45.

[390] S. M. Marcuccio, P. I. Svirskaya, S. Greenberg, A. Lever, C. C. Leznoff, K. B. Tomer, *Can. J. Chem.* **1985**, *63*, 3057-3069.

^{1}H-NMR (300 MHz, $CDCl_3$): δ (ppm) = 8.17 (d, $^4J_{H\text{-}H}$ = 1.6 Hz, 1H; H-1), 8.12 (dd, $^3J_{H\text{-}H}$ = 8.2 Hz, $^4J_{H\text{-}H}$ = 1.6 Hz, 1H; H-2), 7.49 (d, $^3J_{H\text{-}H}$ = 8.2 Hz, 1H; H-3).

Subphthalocyanine **9**[22,37]

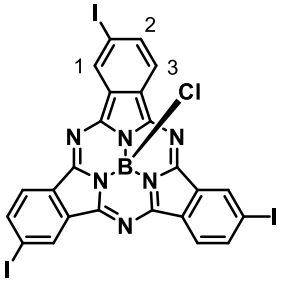

***C*$_3$-I$_3$SubPc-Cl 9**

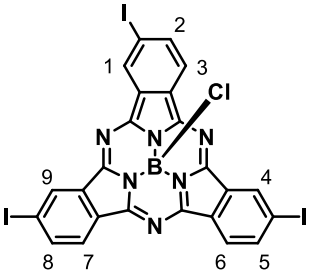

***C*$_1$-I$_3$SubPc-Cl**

A 1.0 M solution of BCl_3 in *p*-xylene (7.9 mL, 7.9 mmol) was added to 4-iodophthalonitrile **8** (2.00 g, 7.9 mmol) under argon atmosphere and the mixture was refluxed for 30 min under vigorous stirring. The reaction mixture was then allowed to cool down to room temperature and flushed with argon. After evaporating the solvent under reduced pressure, the crude product was dissolved in a toluene/THF (10:1) mixture and passed through a short silica plug. The solvent was evaporated under reduced pressure, and the product was purified by column chromatography on silica gel using toluene as eluent. During the process, the C_3 and C_1 regioisomers of I_3SubPc-Cl were separated. C_3-I_3SubPc-Cl **9** was obtained as a purple solid in 6% yield (overall yield of the C_3/C_1 mixture: 24%).

***C*$_3$-I$_3$SubPc-Cl (9):**

^{1}H-NMR (300 MHz, $CDCl_3$): δ (ppm) = 9.25 (d, $^4J_{H\text{-}H}$ = 1.2 Hz, 3H; H-1), 8.59 (d, $^3J_{H\text{-}H}$ = 8.2 Hz, 3H; H-3), 8.25 (dd, $^3J_{H\text{-}H}$ = 8.2 Hz, $^4J_{H\text{-}H}$ = 1.2 Hz, 3H; H-2).

UV-vis ($CHCl_3$): λ_{max} (nm) (log ε ($dm^3\ mol^{-1}\ cm^{-1}$)) = 570 (4.5), 520 (sh), 303 (3.9), 270 (4.1).

***C*$_1$-I$_3$SubPc-Cl:**

^{1}H-NMR (300 MHz, $CDCl_3$): δ (ppm) = 9.24-9.22 (m, 3H; H-1, H-4, H-9), 8.59-8.55 (m, 3H; H-3, H-6, H-7), 8.26-8.22 (m, 3H; H-2, H-5, H-8).

UV-vis ($CHCl_3$): λ_{max} (nm) (log ε ($dm^3\ mol^{-1}\ cm^{-1}$)) = 570 (4.5), 520 (sh), 303 (3.9), 270 (4.1).

Subphthalocyanine **10**[54]

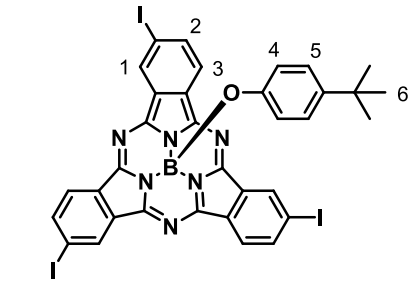

***C*$_3$-I$_3$SubPc-OAr 10 (Ar = *p*-^{t}BuPh)**

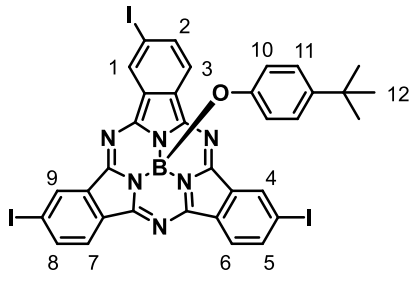

***C*$_1$-I$_3$SubPc-OAr (Ar = *p*-^{t}BuPh)**

4-*tert*-butylphenol (788 mg, 5.25 mmol) and toluene (3 mL) were added to the crude of the previous reaction and the mixture was refluxed for 16 h. The reaction mixture was then allowed to cool down to room temperature and the solvent was evaporated under reduced pressure. The crude was washed with H_2O/methanol 1:1 (v/v) and purified by column chromatography on silica gel using toluene as eluent. During the process, the C_3 and C_1 regioisomers of I_3SubPc-OAr (Ar = *p*-^{t}BuPh) were separated. C_3-I_3SubPc-OAr **10** was obtained as a purple solid in 16% yield (overall yield of the C_3/C_1 mixture: 64%).

***C*$_3$-I$_3$SubPc-OAr 10 (Ar = *p*-^{t}BuPh):**

^{1}H-NMR (400 MHz, $CDCl_3$): δ (ppm) = 9.20 (d, $^4J_{H\text{-}H}$ = 1.2 Hz, 3H; H-1), 8.54 (d, $^3J_{H\text{-}H}$ = 8.4 Hz, 3H; H-3), 8.21 (dd, $^3J_{H\text{-}H}$ = 8.4 Hz, $^4J_{H\text{-}H}$ = 1.2 Hz, 3H; H-2), 6.75 (d, $^3J_{H\text{-}H}$ = 8.8 Hz, 2H; H-5), 5.25 (d, $^3J_{H\text{-}H}$ = 8.8 Hz, 2H; H-4), 1.08 (s, 9H; H-6).

UV-vis ($CHCl_3$): λ_{max} (nm) (log ε (dm^3 mol^{-1} cm^{-1})) = 573 (4.6), 530 (sh), 340 (4.1), 317 (4.2), 277 (4.3).

***C*$_1$-I$_3$SubPc-OAr (Ar = *p*-^{t}BuPh):**

^{1}H-NMR (400 MHz, $CDCl_3$): δ (ppm) = 9.20-9.19 (m, 3H; H-1, H-4, H-9), 8.56-8.53 (m, 3H; H-3, H-6, H-7), 8.24-8.19 (m, 3H; H-5, H-8, H-2), 6.75 (d, $^3J_{H\text{-}H}$ = 8.8 Hz, 2H; H-11), 5.26 (d, $^3J_{H\text{-}H}$ = 8.8 Hz, 2H; H-10), 1.08 (s, 9H; H-12).

UV-vis ($CHCl_3$): λ_{max} (nm) (log ε (dm^3 mol^{-1} cm^{-1})) = 573 (4.6), 530 (sh), 340 (4.1), 317 (4.2), 277 (4.3).

Subphthalocyanine **11**

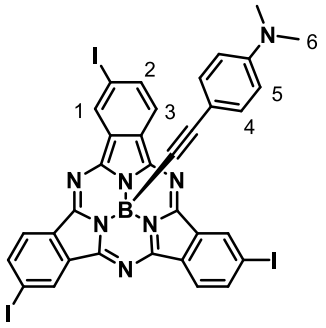

A 1.0 M solution of EtMgBr in THF (55 µL, 0.055 mmol) was added to a solution of 4-ethynyl-*N*,*N*-dimethylaniline (10.8 mg, 0.074 mmol) in degassed and anhydrous THF (1.5 mL) under argon atmosphere. The solution was stirred at 60 °C for 1 hour and then transferred *via* cannula to a degassed and anhydrous solution of I_3SubPc-Cl **9** (30 mg, 0.04 mmol) in THF (2 mL). The resulting mixture was then stirred at 60 °C until the disappearance of the SubPc-Cl starting material as confirmed by TLC (4 h). The reaction mixture was then allowed to cool down to room temperature and the solvent was evaporated under reduced pressure. The crude product was dissolved in chloroform and washed with water, and the organic phase was dried with $MgSO_4$. After filtration of the drying agent and evaporation of the solvent, the solid obtained was purified by column chromatography on silica gel using toluene/EtOAc 98:2 (v/v) as eluent. Recrystallization from a DCM/methanol mixture afforded I_3SubPc-ethynyl-aniline **11** as a blue solid in 59% yield (20 mg).

^{1}H-NMR (400 MHz, $CDCl_3$): δ (ppm) = 9.20 (d, $^4J_{H\text{-}H}$ = 0.9 Hz, 3H; H-1), 8.54 (dd, $^3J_{H\text{-}H}$ = 8.3 Hz, $^5J_{H\text{-}H}$ = 0.4 Hz, 3H; H-3), 8.19 (dd, $^3J_{H\text{-}H}$ = 8.3 Hz, $^4J_{H\text{-}H}$ = 0.9 Hz, 3H; H-2), 6.61 (d, $^3J_{H\text{-}H}$ = 9.1 Hz, 2H; H-5), 6.25 (d, $^3J_{H\text{-}H}$ = 9.1 Hz, 2H; H-4), 2.78 (s, 6H; H-6).

^{13}C-NMR (100.6 MHz, $CDCl_3$): no ^{13}C-NMR peaks were observed after a 16 h accumulation experiment.

^{11}B-NMR (96.3 MHz, $CDCl_3$): δ (ppm) = -20.82.

MS (MALDI-TOF, DCTB): *m/z* = 772.9 $[M\text{-axial ligand}]^+$, 916.9 $[M]^+$.

HRMS: *m/z* Calculated for $[C_{34}H_{19}BI_3N_7]$: 916.8929; Found: 916.8936.

UV-vis ($CHCl_3$): λ_{max} (nm) (log ε ($dm^3\ mol^{-1}\ cm^{-1}$)) = 575 (4.76), 556 (sh), 535 (4.23), 314 (4.60), 286 (sh).

FT-IR (ATR): ν (cm^{-1}) = 3067, 2855, 2799, 2164 (C≡C), 1724, 1559, 1516, 1429, 1355, 1257, 1219, 1171, 1082, 1027, 890, 818, 785, 740, 696, 647, 589, 528.

MP > 250 °C.

Subphthalocyanine **12**

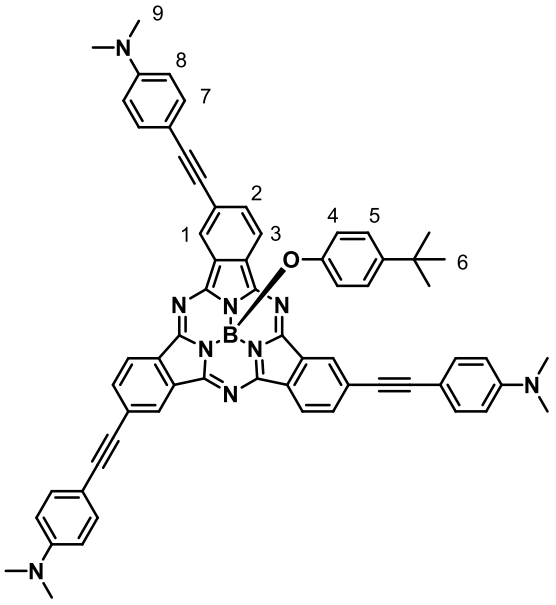

I_3SubPc-OAr **10** (30.0 mg, 0.033 mmol), $PdCl_2(PPh_3)_2$ (4.0 mg, 0.006 mmol), CuI (1.1 mg, 0.006 mmol) and 4-ethynyl-*N*,*N*-dimethylaniline (19.9 mg, 0.137 mmol) were dissolved in a degassed and anhydrous mixture of THF/Et_3N 5:1 (v/v, 3 mL) and the mixture was stirred at room temperature for 16 h. After this time, the reaction mixture was filtered through celite and the solvent was evaporated under reduced pressure. The crude was purified by column chromatography on silica gel using chloroform as eluent. Recrystallization from a DCM/methanol mixture afforded (ethynyl-aniline)$_3$SubPc-OAr **12** as a dark blue solid in 79% yield (25 mg).

^{1}H-NMR (400 MHz, $CDCl_3$): δ (ppm) = 8.95 (dd, $^4J_{H-H}$ = 1.2 Hz, $^5J_{H-H}$ = 0.8 Hz, 3H; H-1), 8.74 (dd, $^3J_{H-H}$ = 8.2 Hz, $^5J_{H-H}$ = 0.8 Hz, 3H; H-3), 7.97 (dd, $^3J_{H-H}$ = 8.2 Hz, $^4J_{H-H}$ = 1.2 Hz, 3H; H-2), 7.51 (d, $^3J_{H-H}$ = 8.9 Hz, 6H; H-7), 6.78 (d, $^3J_{H-H}$ = 8.9 Hz, 6H; H-8), 6.71 (d, $^3J_{H-H}$ =9.0 Hz, 2H, H-4), 5.35 (d, $^3J_{H-H}$ =9.0 Hz, 2H, H-5), 3.03 (s, 18H; H-9), 1.09 (s, 9H; H-6).

^{13}C-NMR (100.6 MHz, $CDCl_3$): δ (ppm) = 151.55, 150.56, 150.18, 143.77, 133.17, 132.53, 131.27, 129.24, 126.25, 125.86, 125.13, 122.14, 117.92, 112.00, 109.65, 94.23, 88.11, 77.48, 40.34, 33.97, 31.47.

^{11}B-NMR (96.3 MHz, $CDCl_3$): δ (ppm) = -14.62.

MS (MALDI-TOF, DCTB): *m/z* = 824.4 $[M\text{-axial ligand}]^+$, 937.4 $[M]^+$.

HRMS: *m/z* Calculated for $[C_{64}H_{52}BN_9O]$: 973.4388; Found: 973.4397.

UV-vis ($CHCl_3$): λ_{max} (nm) (log ε ($dm^3\ mol^{-1}\ cm^{-1}$)) = 603 (5.07), 549 (sh), 442 (4.47), 394 (4.52), 329 (5.02).

FT-IR (ATR): ν (cm^{-1}) = 3041, 2949, 2856, 2800, 2193 (C≡C), 1728, 1596, 1516, 1441, 1354, 1287, 1255, 1225, 1195, 1178, 1112, 1079, 1050 (B-O), 944, 888, 811, 775, 760, 713, 644, 607, 557, 528.

MP > 250 °C.

Subphthalocyanine **13**

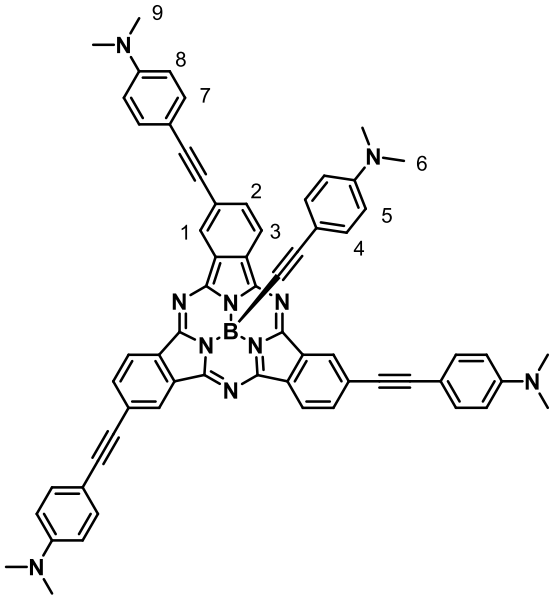

I_3SubPc-ethynyl-aniline **11** (13.0 mg, 0.014 mmol), $PdCl_2(PPh_3)_2$ (1.8 mg, 0.0026 mmol), CuI (0.5 mg, 0.0026 mmol) and 4-ethynyl-*N*,*N*-dimethylaniline (8.6 mg, 0.060 mmol) were dissolved in a degassed and anhydrous mixture of THF/Et_3N 5:1 (v/v, 3 mL) and the mixture was stirred at room temperature for 16 h. After this time, the reaction mixture was filtered through celite and the solvent was evaporated under reduced pressure. The crude was purified by column chromatography on silica gel using chloroform as eluent. Recrystallization from a DCM/methanol mixture afforded (ethynyl-aniline)$_3$SubPc-ethynyl-aniline **13** as a blue solid in 87% yield (12 mg).

^{1}H-NMR (400 MHz, $CDCl_3$): δ (ppm) = 8.96 (dd, $^4J_{H\text{-}H}$ = 1.2 Hz, $^5J_{H\text{-}H}$ = 0.8 Hz, 3H; H-1), 8.75 (dd, $^3J_{H\text{-}H}$ = 7.6 Hz, $^5J_{H\text{-}H}$ = 0.8 Hz, 3H; H-3), 7.96 (dd, $^3J_{H\text{-}H}$ = 7.6 Hz, $^4J_{H\text{-}H}$ = 1.2 Hz, 3H; H-2), 7.51 (d, $^3J_{H\text{-}H}$ = 8.9 Hz, 6H; H-7), 6.71 (d, $^3J_{H\text{-}H}$ = 8.9 Hz, 6H; H-8), 6.66 (d, $^3J_{H\text{-}H}$ =9.1 Hz, 2H, H-5), 6.26 (d, $^3J_{H\text{-}H}$ =9.1 Hz, 2H, H-4), 3.03 (s, 18H; H-9), 2.78 (s, 6H; H-6).

^{13}C-NMR (100.6 MHz, $CDCl_3$): δ (ppm) = 150.54, 150.51, 150.50, 149.81, 133.15, 132.70, 132.31, 131.17, 130.38 129.21, 125.93, 125.02, 122.01, 112.00, 111.39, 109.74, 109.37, 93.97, 88.23, 40.34, 40.15.

MS (MALDI-TOF, DCTB): *m/z* = 953.5 $[M\text{-}CH_3]^+$, 968.5 $[M]^+$, 1937.0 $[2M]^+$.

HRMS: *m/z* Calculated for $[C_{64}H_{49}BN_{10}]$: 967.4266; Found: 967.4233.

UV-vis ($CHCl_3$): λ_{max} (nm) (log ε ($dm^3\ mol^{-1}\ cm^{-1}$)) = 605 (5.38), 555 (sh), 429 (4.84), 396 (4.95), 320 (5.44).

FT-IR (ATR): *v* (cm^{-1}) = 3042, 2894, 2803, 2645, 2180 (C≡C), 2052, 1984, 1725, 1598, 1519, 1443, 1355, 1260, 1223, 1196, 1180, 1111, 1079, 1025, 945, 814, 789, 754, 712, 562, 531.

MP > 250 °C.

Subphthalocyanine **14**

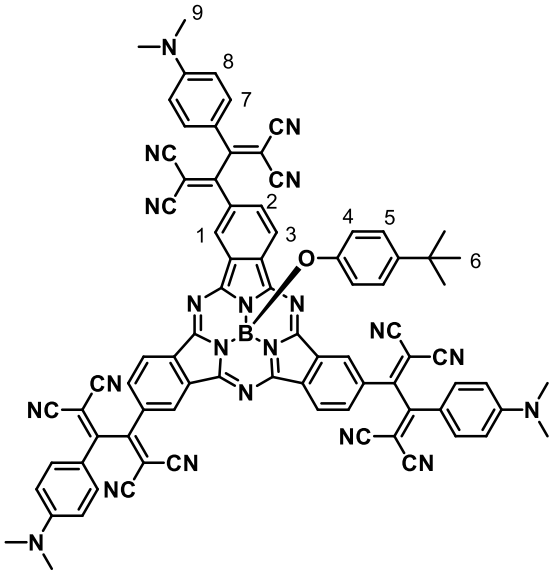

(Ethynyl-aniline)$_3$SubPc-OAr **12** (30 mg, 0.03 mmol) and TCNE (14.2 mg, 0.111 mmol) were dissolved in anhydrous THF (4 mL) and the reaction mixture was stirred for 1 h at room temperature. After this time, the solvent was evaporated under reduced pressure and the crude product was purified by column chromatography on silica gel employing $CHCl_3$/MeOH/pyridine 98.9:1:0.1 (v/v/v) as eluent. Recrystallization from a DCM/hexane mixture afforded (TCBD-aniline)$_3$SubPc-OAr **14** as a dark green solid in 76% yield (32 mg).

^{1}H-NMR (400 MHz, $CDCl_3$): δ (ppm) = 9.06 (d, $^4J_{H\text{-}H}$ = 1.1 Hz, 3H; H-1), 9.00 (dd, $^3J_{H\text{-}H}$ = 8.5 Hz, $^5J_{H\text{-}H}$ = 0.4 Hz, 3H; H-3), 8.28 (dd, $^3J_{H\text{-}H}$ = 8.5 Hz, $^4J_{H\text{-}H}$ = 1.1 Hz, 3H; H-2), 7.89 (d, $^3J_{H\text{-}H}$ = 9.4 Hz, 6H; H-

7), 6.88-6.69 (m, 8H; H-5, H-8), 5.29 (d, $^{3}J_{H\text{-}H}$ = 8.7 Hz, 2H; H-4), 3.19 (s, 18H; H-9), 1.08 (s, 9H; H-6).

^{13}C-NMR (100.6 MHz, $CDCl_3$): δ (ppm) = 167.23, 161.40, 153.50, 150.81, 150.23, 147.94, 143.39, 132.54, 132.26, 131.54, 129.85, 129.37, 124.91, 123.11, 123.08, 116.95, 116.34, 113.13, 112.35, 111.42, 110.83, 109.89, 87.98, 73.23, 39.12, 32.78, 30.11.

^{11}B-NMR (96.3 MHz, $CDCl_3$): δ (ppm) = -14.60.

MS (MALDI-TOF, DCTB): *m/z* = 1208.4 $[M\text{-axial ligand}]^+$, 1357.4 $[M]^+$.

HRMS: *m/z* Calculated for $[C_{82}H_{52}BN_{21}O]$: 1357.4757; Found: 1357.4791.

UV-vis ($CHCl_3$): λ_{max} (nm) (log ε ($dm^3\ mol^{-1}\ cm^{-1}$)) = 621 (4.83), 562 (sh), 465 (4.92), 341 (4.67), 314 (4.70).

FT-IR (ATR): ν (cm^{-1}) = 3079, 2923, 2867, 2215 (C≡N), 1734, 1602, 1486, 1444, 1381, 1344, 1254, 1212, 1172, 1137, 1064 (B-O), 943, 895, 821, 763, 742, 700, 562.

MP > 250 °C.

Subphthalocyanine **15**

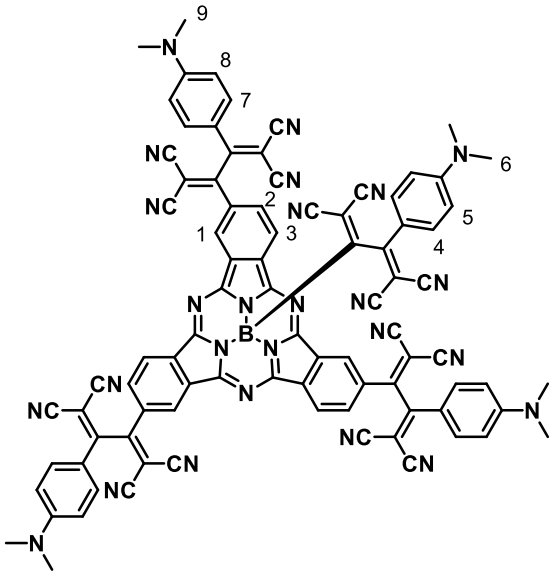

(Ethynyl-aniline)$_3$SubPc-ethynyl-aniline **13** (12.0 mg, 0.012 mmol) and TCNE (7.6 mg, 0.059 mmol) were dissolved in anhydrous THF (3 mL) and the reaction mixture was stirred for 1 h at room temperature. After this time, the solvent was evaporated under reduced pressure and the crude product was purified by column chromatography on silica gel using $CHCl_3$/MeOH/pyridine 98.9:1:0.1 (v/v/v) as eluent. Recrystallization from a DCM/hexane mixture afforded (TCDB-aniline)$_3$SubPc-TCBD-aniline **15** as a dark green solid in 40% yield (7.4 mg).

^{1}H-NMR (400 MHz, $CDCl_3$): δ (ppm) = 9.10 (d, $^{4}J_{H\text{-}H}$ = 1.6 Hz, 3H; H-1), 9.08 (d, $^{4}J_{H\text{-}H}$ = 1.6 Hz, 3H; H-3), 8.98 (dd, $^{3}J_{H\text{-}H}$ = 8.4 Hz, $^{5}J_{H\text{-}H}$ = 0.8 Hz, 3H; H-3), 8.94 (dd, $^{3}J_{H\text{-}H}$ = 8.4 Hz, $^{5}J_{H\text{-}H}$ = 0.8 Hz, 3H; H-3), 8.33 (dd, $^{3}J_{H\text{-}H}$ = 8.4 Hz, $^{4}J_{H\text{-}H}$ = 1.6 Hz, 3H; H-2), 8.29 (dd, $^{3}J_{H\text{-}H}$ = 8.4 Hz, $^{4}J_{H\text{-}H}$ = 1.6 Hz, 3H, H-2 + H-8), 7.92-7.86 (m, 12H; H-7), 6.83-6.77 (m, 12H; H-8), 6.68-6.65 (m, 4H; H-5), 6.43-6.40 (m, 4H; H-4), 3.17 (s, 18H; H-9), 3.15 (s, 18H; H-9), 3.04 (s, 6H; H-6), 3.04 (s, 6H; H-6).

^{13}C-NMR (100.6 MHz, $CDCl_3$): δ (ppm) = 168.77, 162.73, 155.43, 152.48, 152.31, 152.15, 134.89, 134.85, 133.53, 133.29, 131.71, 131.55, 131.15, 125.08, 124.92, 124.62, 118.49, 118.43, 115.05, 114.33, 113.08, 112.72, 112.27, 111.74, 90.29, 74.48, 74.44, 40.72.

^{11}B-NMR (96.3 MHz, $CDCl_3$): δ (ppm) = -16.83.

MS (MALDI-TOF, DCTB): *m/z* = 1481.4 $[M]^+$, 1504.4 $[M+Na]^+$.

HRMS: *m/z* Calculated for $[C_{88}H_{49}BN_{26}Na]$: 1504.4654; Found: 1504.4685.

UV-vis ($CHCl_3$): λ_{max} (nm) (log ε ($dm^3\ mol^{-1}\ cm^{-1}$)) = 635 (4.83), 586 (sh), 470 (5.13), 343 (4.83), 314 (4.83).

FT-IR (ATR): ν (cm^{-1}) = 3078, 2920, 2866, 2214 (C≡N), 1733, 1601, 1484, 1443, 1380, 1340, 1256, 1211, 1171, 1139, 1012, 943, 821, 779, 741, 710, 629, 560.

MP > 250 °C.

Chapter 2

Tuning Energy Transfer and Activating Singlet Fission in Subphthalocyanine-Pentacene Conjugates

2.1 Introduction and background

As discussed in the Introduction of this Thesis, the efficient conversion of sunlight into electrical energy constitutes a major challenge in modern world. In natural photosynthetic systems, the effective collection of solar light is guaranteed by successive energy transfer events between well-arranged light-harvesting antenna pigments, which funnel energy to the reaction center where a cascade of electron-transfer reactions is initiated.[257,258]

The underlying principle of solar cells is the same that is found in natural photosynthesis. Photovoltaic cells are based on the generation of electron-hole pairs by light absorption, and the subsequent separation of such charge carrier pairs. Among the factors that contribute to determine the efficiency limit in photovoltaic devices there is the loss as heat of the part of energy of absorbed photons which is in excess with respect to the cell bandgap, along with losses related to unabsorbed low-energy photons. Thus, the efficient utilization of high-energy photons represents a crucial challenge towards the optimization of the performances of solar cells. In particular, the use of high-energy photons for the production of multiple photogenerated excitons constitutes a promising strategy to enhance the efficiency of sunlight-to-electrical energy conversion.[391]

In this connection, singlet fission (SF) holds great potential towards the realization of more efficient photovoltaic devices. As mentioned in the Introduction of this Thesis, SF[280,281] involves the conversion of a singlet excited state $^1(S_1S_0)$ into two independent triplet excited states 2 x $^3(T_1)$ *via* a pair of triplet excitons $^1(T_1T_1)$, thus allowing for the generation of two excited electrons from a single photon. As such, this process constitutes a valuable means to overcome the ca. 33% Shockley-Queisser limit[392] for PCE in single-junction solar cells.[393,394] As a matter of fact, it has been proposed that the upper efficiency limit could be increased to nearly 50% in a cell which sensitizer is capable of quantitative SF, provided that the two triplets are sufficiently independent to each other to produce charge carriers separately and quantitatively.[280,393]

[391] M. C. Beard, J. C. Johnson, J. M. Luther, A. J. Nozik, *Philos. Trans. R. Soc. A* **2015**, *373*, 20140412.
[392] W. Shockley, H. J. Queisser, *J. Appl. Phys.* **1961**, *32*, 510-519.
[393] M. C. Hanna, A. J. Nozik, *J. Appl. Phys.* **2006**, *100*, 074510.
[394] A. Rao, R. H. Friend, *Nature Rev. Mater.* **2017**, *2*, 17063.

Interestingly, SF has already been implemented in solar energy conversion devices, demonstrating significant promise for boosting the efficiency of photovoltaic cells.[395-397]

In light of its potential application in photovoltaics, extensive efforts have been dedicated to the study of SF during the last decade and a half.[280-286,398] To date, several chromophores have been investigated as SF materials, although the variety of molecules undergoing SF is still rather limited.[280-283,399] Among them, pentacene and its derivatives are particularly well-suited for the study of SF, as they fulfil the thermodynamic requirement (Equation 9) rendering the process exothermic and unidirectional.

In the frame of research on SF, most studies have been realized in the solid state (namely, on molecular crystals or thin films), being acenes the most investigated materials.[283] Although in the early years SF in pentacene received much less attention than in anthracene and tetracene, during the last decade or so considerable effort has been dedicated to the study of SF in single-crystal, polycrystalline, and amorphous solids of pentacene.[280,281,283,400]

In 2013, Friend and co-workers showed in a groundbreaking report that highly efficient SF could take place in concentrated solutions of TIPS-pentacene with quantitative triplet yield (*i.e.*, 200%).[401] In the investigated conditions, an excimer intermediate is formed by collision of one singlet-excited and one ground-state molecule, which then decays in two triplets (Figure 97).

[395] J. Lee, P. Jadhav, P. D. Reusswig, S. R. Yost, N. J. Thompson, D. N. Congreve, E. Hontz, T. Van Voorhis, M. A. Baldo, *Acc. Chem. Res.* **2013**, *46*, 1300-1311.
[396] J. Xia, S. N. Sanders, W. Cheng, J. Z. Low, J. Liu, L. M. Campos, T. Sun, *Adv. Mater.* **2017**, *29*, 1601652.
[397] R. Casillas, I. Papadopoulos, T. Ullrich, D. Thiel, A. Kunzmann, D. M. Guldi, *Energy Environ. Sci.* **2020**, *13*, 2741-2804.
[398] S. Ito, T. Nagami, M. Nakano, *J. Photoch. Photobio. C* **2018**, *34*, 85-120.
[399] T. Ullrich, D. Munz, D. M. Guldi, *Chem. Soc. Rev.* **2021**, *50*, 3485-3518.
[400] M. W. Wilson, A. Rao, B. Ehrler, R. H. Friend, *Acc. Chem. Res.* **2013**, *46*, 1330-1338.
[401] B. J. Walker, A. J. Musser, D. Beljonne, R. H. Friend, *Nat. Chem.* **2013**, *5*, 1019-1024.

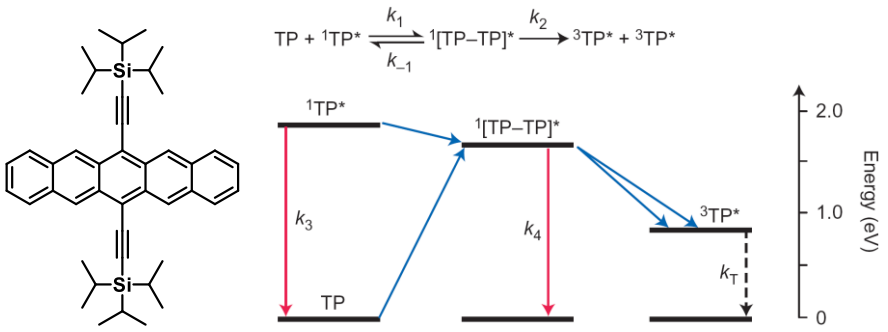

Figure 97. Structure of the TIPS-pentacene investigated by Friend and co-workers and scheme for the mechanism of SF in TIPS-pentacene solutions showing the formation on an excimer intermediate. Adapted from ref. 401.

Two years later, Zirzlmeier *et al.* reported on unprecedent intramolecular SF (i-SF) within pentacene dimers (Pnc_2) in solution.[402] In this work, a series of regioisomeric 6,6'-linked Pnc_2 derivatives tethered *via* a phenylene spacer in an *ortho*-, *meta*-, and *para*-arrangement was investigated (Figure 98). Through the different substitution patterns of the linker, geometrical control is imposed, which affects through-bond and through-space coupling between the pentacene moieties. As a matter of fact, whereas the *para*-isomer features a strong linear conjugation between the pentacene units *via* the phenylene spacer, in the cross-conjugated *meta*-derivative through-bond coupling is limited. On the other hand, the orthogonal arrangement of the phenylene group and the pentacene units in the *ortho*-phenylene-linked species prevents strong linear conjugation, while through-space interactions are favored by spatial proximity of the pentacenes. Within this series, the cross-conjugated *meta*-isomer gave the best i-SF performances, exhibiting triplet quantum yields as high as 156% in benzonitrile. Notably, in all the dimers of the series, the $^1(T_1T_1)$ state is subject to deactivation *via* TTA.

Solution-based i-SF had been observed for the first time in *para*-phenylene-linked tetracene dimers, although in that case very low i-SF quantum yields (approximately 3%) were detected.[403] Compared with SF in solutions of TIPS-pentacene reported by Friend and co-workers,[401] i-SF allows to perform experimental measurements in more diluted systems, preventing issues related to solubility, aggregation and optical density. Moreover, the targeted design of the spacer connecting the two chromophores allows to control and tune the distance, orientation,

[402] J. Zirzlmeier, D. Lehnherr, P. B. Coto, E. T. Chernick, R. Casillas, B. S. Basel, M. Thoss, R. R. Tykwinski, D. M. Guldi, *Proc. Natl. Acad. Sci. USA* **2015**, *112*, 5325-5330.
[403] A. M. Müller, Y. S. Avlasevich, W. W. Schoeller, K. Müllen, C. J. Bardeen, *J. Am. Chem. Soc.* **2007**, *129*, 14240-14250.

and electronic coupling between the two moieties, allowing for the rational investigation of the effect of different parameters on the SF process.

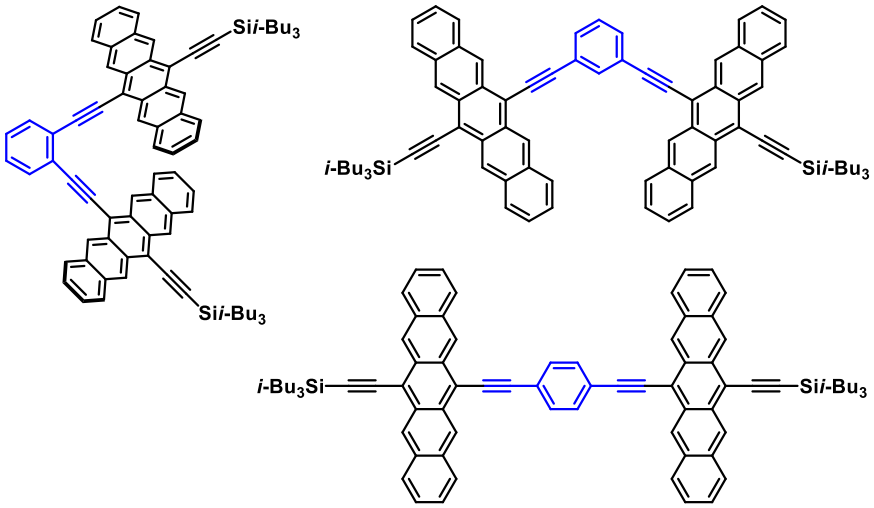

Figure 98. *Ortho*-, *meta*- and *para*-Pnc$_2$ derivatives investigated by Zirzlmeier *et al.*[402]

Considering the favorable excited-state energetics of pentacene derivatives, Pnc$_2$s[404] constitute a key tool for investigation on i-SF. In this context, numerous Pnc$_2$s have been designed, synthesized, and probed with the aim to elucidate the influence of specific structural parameters on the i-SF process. Different "anchoring" patterns have been investigated, and a wide toolbox of molecular spacers has been explored to modulate the spatial orientation and fine-tune the electronic coupling between the pentacene units, with the final aim to investigate the impact on i-SF dynamics and efficiencies and investigate the operative mechanism (Figure 99). Advances in the use of Pnc$_2$s as model systems for the investigation of i-SF have been recently reviewed by Tykwinski, Guldi and co-workers.[405,406] Here, an overview of the main recent findings is given.

[404] D. Lehnherr, R. R. Tykwinski, *Aust. J. Chem.* **2011**, *64*, 919-929.
[405] C. Hetzer, D. M. Guldi, R. R. Tykwinski, *Chem. Eur. J.* **2018**, *24*, 8245-8257.
[406] B. S. Basel, I. Papadopoulos, D. Thiel, R. Casillas, J. Zirzlmeier, T. Clark, D. M. Guldi, R. R. Tykwinski, *Trends Chem.* **2019**, *1*, 11-21.

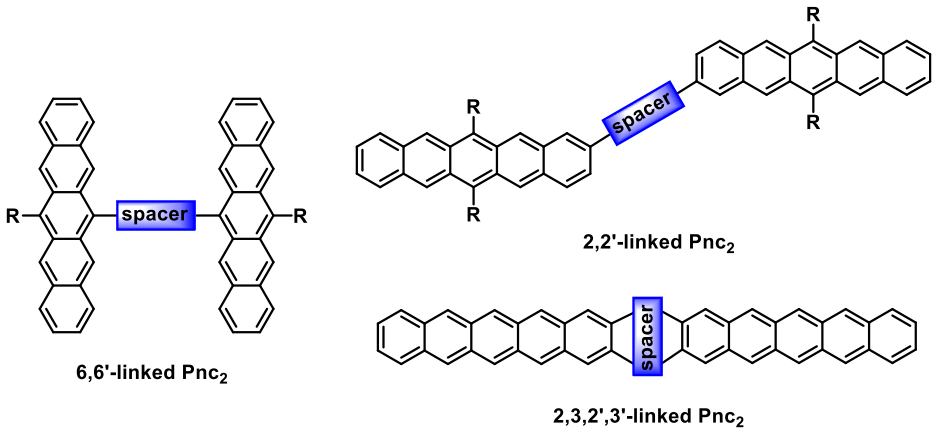

Figure 99. General molecular structure of the most investigated Pnc_2 derivatives.

The pivotal work of Zirzlmeier *et al.*[402] suggested that moderating the electronic communication between the two pentacene moieties might be an important point for i-SF. To further explore this hypothesis, two 6,6'-linked, cross-conjugated Pnc_2s featuring diethynyl- and tetraethynylethenes as spacer were explored (Figure 100).[407] In both derivatives, the cross-conjugated tether allows for electronic coupling, which is slightly stronger in the tetraethynylethene-based derivative. This study, along with the previous study on phenylene-linked pentacene dimers, evidenced that a delicate balance between through-space and through-bond coupling is of key importance towards the optimization of i-SF.[402,407]

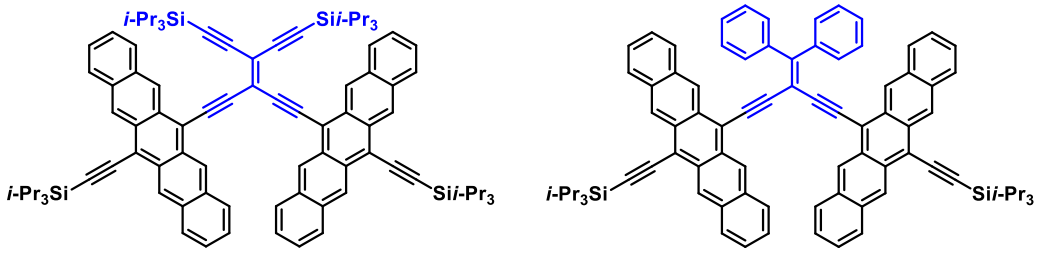

Figure 100. Cross-conjugated Pnc_2s investigated by Zirzlmeier *et al.*[402]

Non-conjugated Pnc_2s linked *via* a 1,3-diethynyladamantyl and a 1,4-diethynylbibyclo[2.2.2]octane spacer in the 6- and 6'-positions have also been investigated

[407] J. Zirzlmeier, R. Casillas, S. R. Reddy, P. B. Coto, D. Lehnherr, E. T. Chernick, I. Papadopoulos, M. Thoss, R. R. Tykwinski, D. M. Guldi, *Nanoscale* **2016**, *8*, 10113-10123.

(Figure 101).[408,409] In the former, i-SF with a triplet quantum yield of ca. 188% was detected, evidencing that neither strong through-bond coupling nor direct through-space overlap of the two pentacenes is necessary for efficient SF to take place. Remarkably, the non-conjugated spacer keeps the electronic coupling between the chromophores weak enough to allow SF to successfully compete with TTA, leading to the formation of two independent triplet excited states ($T_1 + T_1$).

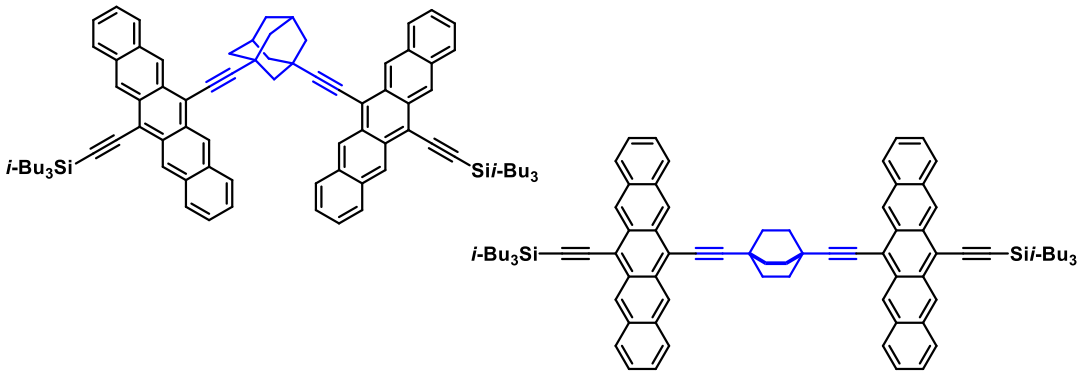

Figure 101. Non-conjugated Pnc$_2$s investigated by Basel *et al.*[408,409]

Interestingly, Pnc$_2$s featuring *meta*-phenylene and adamantyl spacers have been employed in a proof-of-concept study which showed that i-SF can be initiated from a singlet excited state accessed by two-photon absorption. This expands the spectral range for SF, allowing for the exploitation of irradiation wavelengths at which Pnc$_2$s do not exhibit linear absorption of light to enable i-SF.[410]

In addition to the study of rigid, σ-bonded spacers, the use of flexible linkers to connect the two pentacene chromophores has also been explored.[411] The influence of efficient, intramolecular π-overlap on i-SF was explored through the study of a set of Pnc$_2$s in which a xanthene linker strictly maintains the pentacene chromophores in a rigid arrangement.[412] On the other hand,

[408] B. S. Basel, J. Zirzlmeier, C. Hetzer, B. T. Phelan, M. D. Krzyaniak, S. R. Reddy, P. B. Coto, N. E. Horwitz, R. M. Young, F. J. White, *Nat. Commun.* **2017**, *8*, 1-8.
[409] B. S. Basel, J. Zirzlmeier, C. Hetzer, S. R. Reddy, B. T. Phelan, M. D. Krzyaniak, M. K. Volland, P. B. Coto, R. M. Young, T. Clark, *Chem* **2018**, *4*, 1092-1111.
[410] E. Garoni, J. Zirzlmeier, B. S. Basel, C. Hetzer, K. Kamada, D. M. Guldi, R. R. Tykwinski, *J. Am. Chem. Soc.* **2017**, *139*, 14017-14020.
[411] I. Papadopoulos, J. Zirzlmeier, C. Hetzer, Y. J. Bae, M. D. Krzyaniak, M. R. Wasielewski, T. Clark, R. R. Tykwinski, D. M. Guldi, *J. Am. Chem. Soc.* **2019**, *141*, 6191-6203.
[412] B. S. Basel, C. Hetzer, J. Zirzlmeier, D. Thiel, R. Guldi, F. Hampel, A. Kahnt, T. Clark, D. M. Guldi, R. R. Tykwinski, *Chem. Sci.* **2019**, *10*, 3854-3863.

strongly coupled, platinum-bridged Pnc_2 allowed to investigate the role of the heavy-atom effect and chirality in i-SF.[413,414] Nearly orthogonal Pnc_2 linked *via* a single C-C bond in the 6- and 6'-positions have also been investigated, showing highly efficient i-SF.[415,416]

Recently, Kunzmann *et al.* reported on i-SF in a 6,6'-linked dimeric pentacene derivative and subsequent electron injection into doped ZnO, which evolves from the energetically low-lying triplet excited state formed by i-SF, with a carrier multiplication of nearly 130% (Figure 102).[417] In the investigated dimer, a *meta*-arrangement of the two pentacenes and a carboxylate anchor were chosen to balance i-SF dynamics and charge injection. The combination of i-SF with electron injection in semiconductor photoelectrodes represents an important advance in view of the potential exploitation of SF in photovoltaics.

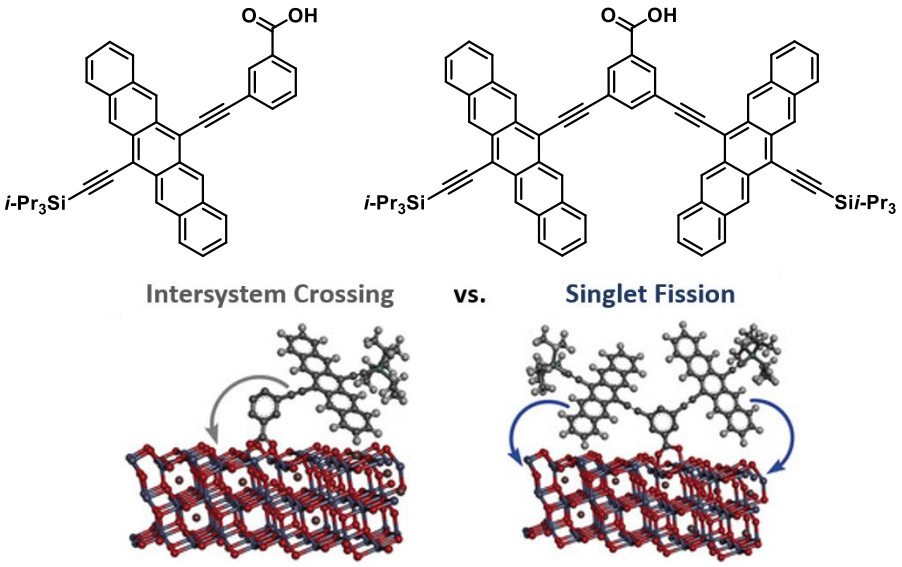

Figure 102. Structure of the monomeric and dimeric pentacene derivatives investigated by Kunzmann *et al.* and cartoon depicting electron injection into ZnO. Adapted from ref. 417.

---

[413] B. S. Basel, R. M. Young, M. D. Krzyaniak, I. Papadopoulos, C. Hetzer, Y. Gao, N. T. La Porte, B. T. Phelan, T. Clark, R. R. Tykwinski, *Chem. Sci.* **2019**, *10*, 11130-11140.
[414] I. Papadopoulos, Y. Gao, C. Hetzer, R. R. Tykwinski, D. M. Guldi, *ChemPhotoChem* **2020**, *4*, 5168-5174.
[415] S. Lukman, A. J. Musser, K. Chen, S. Athanasopoulos, C. K. Yong, Z. Zeng, Q. Ye, C. Chi, J. M. Hodgkiss, J. Wu, *Adv. Funct. Mater.* **2015**, *25*, 5452-5461.
[416] S. Lukman, K. Chen, J. M. Hodgkiss, D. H. Turban, N. D. Hine, S. Dong, J. Wu, N. C. Greenham, A. J. Musser, *Nat. Commun.* **2016**, *7*, 1-13.
[417] A. Kunzmann, M. Gruber, R. Casillas, J. Zirzlmeier, M. Stanzel, W. Peukert, R. R. Tykwinski, D. M. Guldi, *Angew. Chem. Int. Ed.* **2018**, *57*, 10742-10747.

Besides 6,6'-linked dimeric pentacene derivatives, several 2,2'-linked[418-422] and a few 2,3,2',3'-linked[422] Pnc_2s have been synthesized and probed as SF materials.[405,406] In contrast to 6,6'-linked Pnc_2 derivatives, in which i-SF takes place predominantly *via* a CT-mediated mechanism (Figure 103, step 3), experimental evidences for Pnc_2s linked *via* the 2,2' positions typically suggest a direct SF mechanism (Figure 103, step 2).[405]

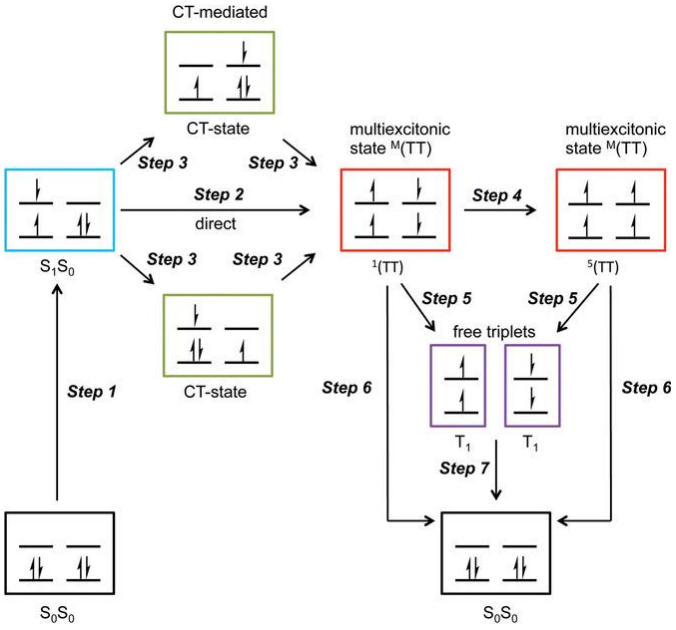

Figure 103. Depiction of the SF mechanism. Reproduced from ref. 405.

To sum up, Pnc_2s constitute a fundamental tool for research on i-SF.[405] Considerable effort has been dedicated to the study of the impact of the structural arrangement between the pentacene units on through-bond and through-space electronic communication and, in turn, on the dynamics and efficiency of i-SF, with the ultimate goal to investigate the various mechanistic

[418] S. N. Sanders, E. Kumarasamy, A. B. Pun, M. T. Trinh, B. Choi, J. Xia, E. J. Taffet, J. Z. Low, J. R. Miller, X. Roy, *J. Am. Chem. Soc.* **2015**, *137*, 8965-8972.
[419] T. Sakuma, H. Sakai, Y. Araki, T. Mori, T. Wada, N. V. Tkachenko, T. Hasobe, *J. Phys. Chem. A* **2016**, *120*, 1867-1875.
[420] E. G. Fuemmeler, S. N. Sanders, A. B. Pun, E. Kumarasamy, T. Zeng, K. Miyata, M. L. Steigerwald, X.-Y. Zhu, M. Y. Sfeir, L. M. Campos, *ACS Cent. Sci.* **2016**, *2*, 316-324.
[421] M. J. Tayebjee, S. N. Sanders, E. Kumarasamy, L. M. Campos, M. Y. Sfeir, D. R. McCamey, *Nat. Phys.* **2017**, *13*, 182-188.
[422] E. Kumarasamy, S. N. Sanders, M. J. Tayebjee, A. Asadpoordarvish, T. J. Hele, E. G. Fuemmeler, A. B. Pun, L. M. Yablon, J. Z. Low, D. W. Paley, *J. Am. Chem. Soc.* **2017**, *139*, 12488-12494.

aspects of the SF process. More in general, a variety of different chromophores have been explored as SF materials, with the aim to unravel the underlying mechanism.[280,281,283,399]

Nevertheless, much less interest has been focused on possible strategies to enhance light absorption in SF-based systems.[410] In fact, the design, synthesis and probing of targeted molecular architectures aimed to boost the efficiency of light harvesting in SF-performing systems towards an intense and ideally panchromatic absorption is practically unexplored. Such a lack of efforts in this area is rather surprising in view of the potential application of SF in photovoltaics,[393,395-397] for which the improvement of the absorption characteristics of the active molecular systems is of crucial importance.

As a matter of fact, SF normally takes place from a singlet excited state populated through photoexcitation (Figure 103, step 1). In other words, the system is initially promoted to an electronically excited state by direct absorption of light. Nevertheless, in principle, SF could be initiated from a singlet excited state accessed through alternative pathways, such as by energy transfer from a suitable donor molecular partner. The population of the singlet excited state from which SF takes place by exciton energy transduction as well as through photoabsorption would allow for the exploitation of high-energy photons to enable SF, thus expanding the spectral range for SF and improving the overall light response of the system.

2.2 Specific objectives of Chapter 2

The main objective of this Chapter is the design, synthesis and study of a series of novel SubPc-Pnc_2 conjugates in which i-SF at the Pnc_2 moiety is enabled by energy transfer from the SubPc unit, as well as the modulation of the interchromophoric interactions through proper molecular design. The final aim is the realization of a synergy between panchromatic absorption and SF, which constitutes a promising strategy towards the improvement of the efficiency of solar energy conversion in molecular photovoltaics.

This Chapter is divided into two different sections. Both are focused on the study of multicomponent systems integrating a SubPc and a Pnc_2 unit. In these conjugates, the SubPc is expected to act as light-harvesting, energy-donor antenna, whereas the Pnc_2 is expected to behave as energy acceptor and SF-performing moiety. Moreover, each section is aimed to modulate the dynamics of energy transfer through different approaches.

The first part of this Chapter is focused on tuning FRET by a modular SubPc approach, based on decorating the SubPc core with different peripheral substituents in order to tailor the optical properties of the macrocycle and, in turn, the spectral overlap between the emission of the SubPc and the absorption of the Pnc_2. In particular, we will synthesize a series of three different systems incorporating a perhydrogenated, a triphenoxy-substituted or a hexathiooctyl-substituted SubPc, in which a Pnc_2 unit is linked through a carboxylate group to the axial position of the macrocycle (Figure 104). The photophysical features of these derivatives will be investigated with the aim to probe FRET-activated i-SF and study the impact of the nature of the peripheral substituents on the dynamics of intramolecular energy transfer.

The second part of the Chapter is centered on modulating FRET by rational spacer design, that is, by tailoring the length (*i.e.*, number of aryl units) and flexibility (*i.e.*, presence or absence of a CH_2 group) of the molecular spacer connecting the energy donor SubPc and the energy acceptor Pnc_2 and, in turn, the distance and orientation between the two chromophores. To this end, we will prepare a series of four different SubPc-Pnc_2 derivatives, featuring a peripherally hydrogenated SubPc linked through the axial position to a Pnc_2 moiety *via* different bridging units (Figure 105). The effect of the structural features of the spacer on FRET (and SF) dynamics will be probed and rationalized by means of experimental measurements and theoretical calculations.

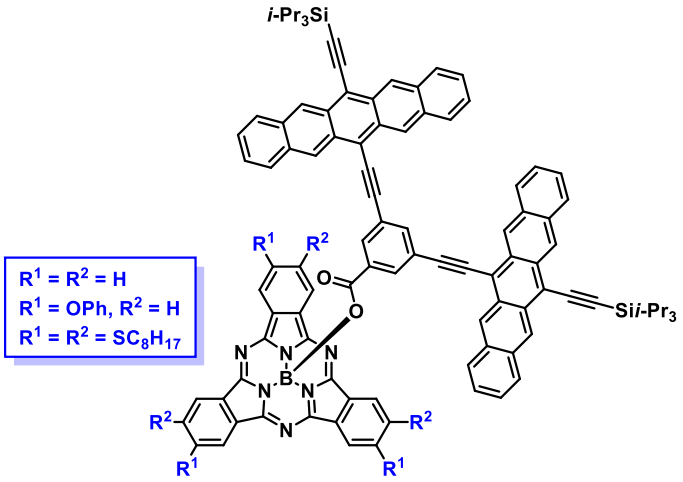

Figure 104. Structure of the SubPc-Pnc$_2$ conjugates featuring different substituents at the periphery of the SubPc macrocycle investigated in the first section of Chapter 2.

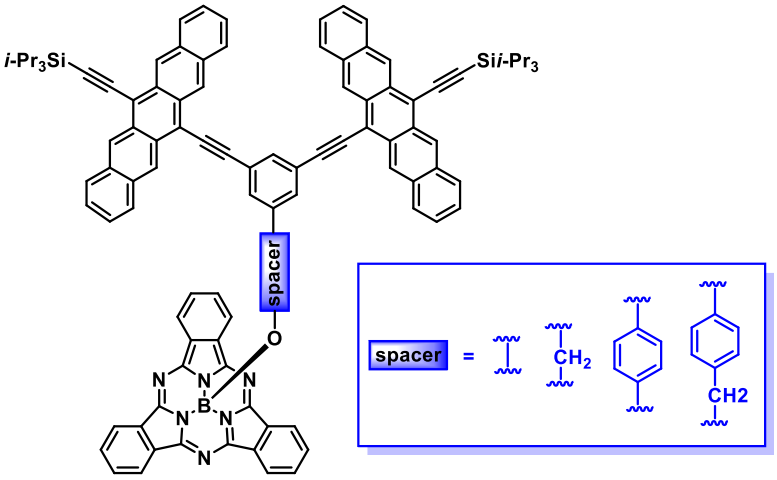

Figure 105. Structure of the SubPc-Pnc$_2$ conjugates featuring different molecular spacers investigated in the second section of Chapter 2.

2.3 Results and discussion

Based on the results that will be presented in this Chapter, two manuscripts have been elaborated and published as:

- G. Lavarda,† J. Zirzlmeier,† M. Gruber, P. R. Rami, R. R. Tykwinski, T. Torres, D. M. Guldi, Tuning intramolecular Förster resonance energy transfer and activating intramolecular singlet fission, *Angew. Chem. Int. Ed.* **2018**, *57*, 16291-16295.
- J. Zirzlmeier,† G. Lavarda,† H. Gotfredsen,† I. Papadopoulos,† L. Chen, T. Clark, R. R. Tykwinski, T. Torres, D. M. Guldi, Modulating the dynamics of Förster resonance energy transfer and singlet fission by variable molecular spacers, *Nanoscale* **2020**, *12*, 23061-23068.

† Shared first authorship.

2.3.1 Synthesis and study of SubPc-Pnc_2 conjugates featuring different peripheral substituents

2.3.1.1 Design, synthesis and characterization of SubPc-Pnc_2 conjugates featuring different peripheral substituents

As mentioned in the Introduction and Background of this Chapter, down-conversion of high-energy excitons into multiple low-energy excited states constitutes a viable strategy to overcome the Shoeckley-Queisser limit[392] which restricts efficiencies in conventional solar energy conversion schemes.[391] In this context, SF, in which a singlet exciton is transformed *via* a pair of correlated triplet excitons into two independent triplet excited states, represents a powerful means towards the optimization of the performances of photovoltaic devices.[393-397]

During the last decades, major experimental and theoretical efforts have been dedicated to the study of the mechanistic aspects of the SF process.[280-286] In particular, Pnc_2s recently emerged as the systems of choice for the investigation of i-SF.[405,406] In this context, the seminal work of Zirzlmeier *el al.*[402] on i-SF in phenylene-linked Pnc_2s triggered a plethora of studies aimed to unravel the impact of electronic communication between the pentacene units on the dynamics and efficiency of i-SF.[405,406]

Nevertheless, the improvement of light-harvesting efficiency in SF systems, that is, the realization of a broad and strong light response as is seen in natural photosynthetic centers[258] by exploiting interchromophoric interactions has never been addressed. In the frame of i-SF in Pnc_2s, enhancing the efficiency of light harvesting is highly desirable in light of the limited absorption region and the rather low extinction coefficients of Pnc_2 derivatives[404] and in view of potential applications in photovoltaics.[396,397,417] The expansion of the spectral range for SF in

such systems can be realized, in principle, by exploiting excitation energy transduction from a suitable molecular donor.

Thus, the realization of a synergy between panchromatic absorption and SF constitutes a promising and still unexplored strategy towards the optimization of solar energy conversion in photovoltaic devices.

By virtue of the outstanding optical and electronic properties of SubPcs, these chromophores are particularly interesting for light-harvesting applications. As mentioned in the Introduction of this Thesis, SubPcs are characterized by strong absorptions in the UV-vis range of the solar spectrum, high electronic excitation energies and intense fluorescence emission features.[8] These characteristics, along with the versatility of these chromophores in terms of chemical modification of both the axial and peripheral substituents and the tunability of their photophysical and electrochemical features by means of proper functionalization of the macrocycle, render SubPcs valuable energy-donor antennae for the preparation of multicomponent systems. As a matter of fact, many SubPc-based D-A ensembles have been described in which SubPcs act as energy donors in combination with different acceptor partners (*e.g.* fullerenes, Ps, Pcs, SubPc fused dimers, azaBODIPY and properly functionalized BODIPYs).[54,71,101,108,121,122,288-302]

In light of the aforementioned, we meant to explore the combination between intramolecular FRET (i-FRET) and i-SF with the aim to boost the overall light response in SF-performing systems. To this end, we designed a series of multicomponent models in which a light harvesting material, that is, a SubPc, and a SF-material, namely a Pnc$_2$, are synergically integrated. In light of the excited-state energetics of the components, singlet-singlet energy transfer from the SubPc to the Pnc$_2$ is expected to take place upon photoexcitation of the former, followed by i-SF at the Pnc$_2$ unit. As a matter of fact, energy values exceeding 2.0 eV[8] and below 1.9 eV[402,417] are typically determined for the singlet excited state of SubPcs and Pnc$_2$s, respectively.

In the designed conjugates, the chemical features of the molecular partners were targeted to accomplish three primary goals. 1) To guarantee the complementarity between the absorption of the energy donor antenna and the absorption of the acceptor moiety and, in turn, light harvesting across most of the visible range of the solar spectrum. 2) To optimize the spectral overlap between the fluorescence emission of the energy donor and the absorption of the energy acceptor and, in turn, the efficiency and the rate of i-FRET upon photoexcitation of the former. 3) To prevent intramolecular electron transfer from the SF-performing moiety to the light harvester in order to guarantee high i-SF quantum yields. 4) To ensure the efficiency of the i-SF process occurring at the acceptor moiety.

Properly functionalized SubPc chromophores allow to successfully fulfill the first three conditions, thus representing suitable molecular counterparts for Pnc_2s. As a matter of fact, the Q-band absorption of SubPcs is complementary to the long-wavelength absorption of Pnc_2s.[8,404] Moreover, SubPcs generally exhibit an intense fluorescence emission in the absorption region of Pnc_2s. In particular, the periphery of the SubPc core was decorated with different substituents in order to tune the electronic and optical properties of the macrocycle, with the double aim to prevent electron transfer and modulate the dynamics of i-FRET. In this connection, it is worth to consider that the nature of the peripheral functionalities has generally a strong impact on the photophysical and electrochemical features of SubPcs.[8,120]

On one hand, the choice of the ring substituents was aimed to enhance the electron-rich character of the macrocycle and, in turn, to suppress any electron transfer from the Pnc_2, that would result in a decreasing of the i-SF performances of the systems. It has already been observed that the competition between energy transfer and electron transfer in SubPc-based multicomponent models can be regulated by proper functionalization of the peripheral positions of the macrocycle, as discussed in the Introduction of this Thesis.[121]

On the other hand, the integration of SubPcs with different peripheral substitution patterns had as objective the fine-tuning of the interchromophoric interactions. In particular, the choice of the peripheral substituents was aimed to modulate the spectral overlap between the fluorescence emission of the SubPc and the absorption of the Pnc_2, which contributes to control the FRET rate constant.[278] In this connection, it should be considered that although both electron-donor and electron-withdrawing peripheral substituents able to extend the π-conjugation of the macrocycle produce a redshift of the Q band of the SubPc with respect to the corresponding non-substituted species, in the presence of π-donor atoms (*e.g.* oxygen, nitrogen or sulfur) linked to the isoindolic benzene ring this effect is typically stronger.[8] In particular, the bathochromic shift of the low-energy SubPc absorption increases with the π-donating ability of the heteroatom and with the number of π-donor peripheral substituents.

In light of the aforementioned, we designed three different SubPc-Pnc_2 conjugates in which the SubPc moiety is functionalized with peripheral hydrogen or electron-donor (namely, phenoxy or thioether) groups (Figure 106).

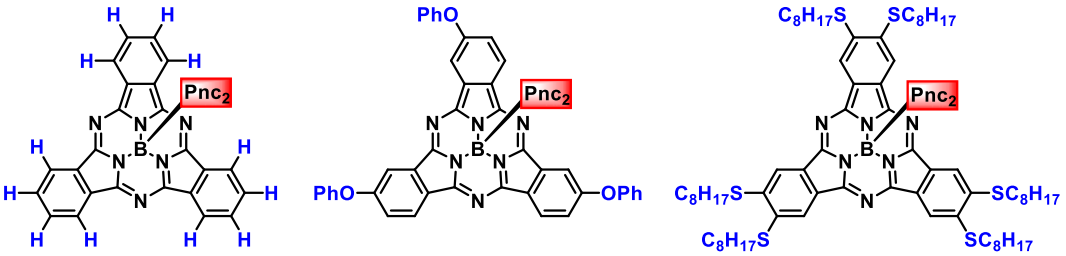

Figure 106. Peripheral substitution patterns of the SubPc unit within the different SubPc-Pnc$_2$ conjugates investigated in this section.

With respect to the SF moiety, a 6,6'-linked Pnc$_2$ bearing a *meta*-phenylene spacer functionalized with a carboxylic acid (**17**) was employed (Figure 107). Pnc$_2$ **17** was provided by the research group of Prof. Rik Tykwinski at the University of Alberta in Edmonton, Canada. The *meta*-arrangement of the pentacene moieties in Pnc$_2$ derivatives tethered *via* a phenylene spacer has already been demonstrated to assure better i-SF performances in comparison with the corresponding *ortho*- and *para*-isomers, by virtue of the limited electronic communication between the two pentacene moieties.[402] Moreover, worth of mention is a recent proof-of-concept study presented by Guldi, Tykwinski, Peukert and co-workers regarding the integration of *meta*-phenylene tethered Pnc$_2$ **17** into a DSSC, in which a 130% injection efficiency was demonstrated.[417]

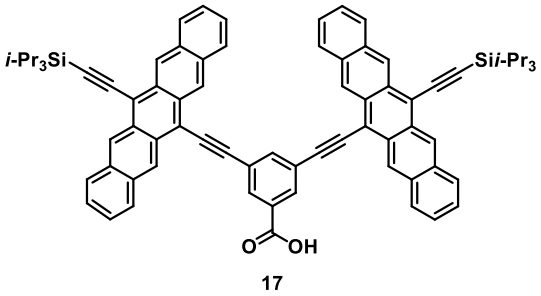

17

Figure 107. Chemical structure of Pnc$_2$ **17**.

Regarding the functionalization strategy, the axial approach was chosen for the derivatization of the SubPc unit. Substitution at the axial position bears the double advantage of preserving the electronic and optical characteristics of the macrocycle, which are mainly determined by the ring substituents, and permitting to avoid the tedious preparation of asymmetrically substituted SubPcs.

In particular, the target SubPc-Pnc_2 conjugates **26**-**28** were prepared by axial substitution reaction from the corresponding SubPc-Cl precursors (namely, H_{12}SubPc-Cl **1**, $(OPh)_3$SubPc-Cl **24** and $(SC_8H_{17})_6$SubPc-Cl **25**), as reported in Scheme 8. The latter were prepared by cyclotrimerization reaction of the corresponding starting phthalonitriles in the presence of BCl_3. At this point, it is worth to mention that the reaction of axially chlorinated SubPcs with carboxylic acids could be carried out directly by refluxing the starting SubPc precursor in a high boiling solvent in the presence of an excess of the corresponding acid.[8] Nevertheless, in light of the steric hindrance of Pnc_2 **17**, and with the aim to minimize the equivalents of nucleophile used in the reaction and use milder conditions than those employed in direct substitution reactions, axial ligand exchange was carried out *via* generation of an activated SubPc-OTf species, following a synthetic procedure previously reported in our group (Scheme 8).[48] Chlorobenzene was used as solvent owing to the poor solubility of **17** in toluene. In contrast, SubPc-Pnc_2 conjugates **26**-**28** are soluble in most common organic solvents.

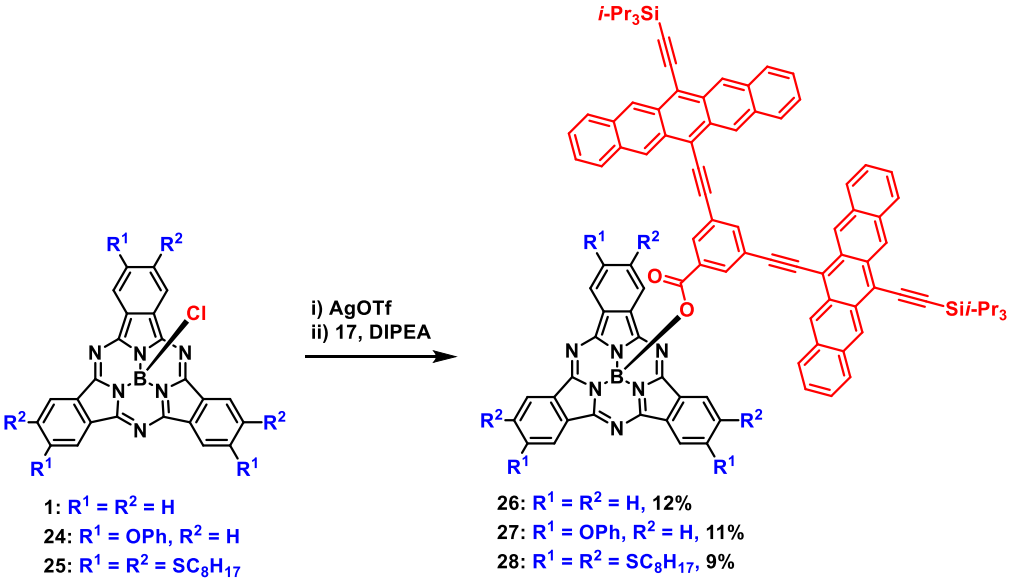

Scheme 8. Synthesis of SubPc-Pnc_2 conjugates **26**-**28** from SubPc-Cl precursors **1**, **24** and **25.**

Considerable amounts of SubPc-OH and μ-oxo-SubPc species are formed during the axial substitution reactions, suggesting the high tendency towards hydrolysis of the conjugates and their corresponding triflate-intermediates (in particular, the ones functionalized with donor substituents). Decomposition products from the Pnc_2 precursor were also found in the reaction mixture. Whereas SubPc-Pnc_2 conjugates **26** and **27** were purified by flash column

chromatography on silica gel followed by recrystallization from methanol, in the case of the hexa-thiooctyl-substituted derivative **28** purification through a short silica plug was performed in order to minimize hydrolysis, in light the higher reactivity in terms of axial substitution. In this case, additional purification of the product by means of size exclusion chromatography was required to remove any trace of SubPc-OH. Anyway, ^{1}H-NMR analysis and MS still revealed the presence of μ-oxo-SubPc species in the purified product, which could not be separated by means of size exclusion chromatography even after probing different eluents. Purification of SubPc-Pnc$_2$ **28** from the μ-oxo dimer could be finally carried out by preparative TLC. The low yields obtained in the synthesis of **26**-**28** may be rationalized on the basis of the steric hindrance of Pnc$_2$ **17**, the partial decomposition of the latter and the partial hydrolysis of the target conjugates and their precursor SubPc-OTf species during the reaction and the subsequent work-up.

All the novel SubPc-Pnc$_2$ derivatives were characterized by ^{1}H-NMR, ^{13}C-NMR, ^{11}B-NMR, UV-vis and IR spectroscopy and HRMS. Notably, in the MALDI mass spectra of **26**-**28**, signals corresponding to the dimers of the molecular structures of the investigated conjugates are detectable. A likely rationale involves π-interactions between the axial Pnc$_2$ units and their potential stacking. Unfortunately, single crystals suitable for X-ray diffraction analysis could not be obtained despite probing several crystallization conditions, probably due to the stacking between the axial moieties. The complete characterization of derivatives **26**-**28** is reported in the Experimental section of this Chapter.

The assignment of the proton signals of **26**-**28** in the corresponding ^{1}H-NMR spectra was carried out with the help of COSY and NOESY experiments. As an example, the ^{1}H-NMR spectrum of SubPc-Pnc$_2$ **26** and the corresponding H-H COSY and H-H NOESY spectra are shown in Figures 108-110. In particular, the COSY spectrum shows the correlations between the signals of the protons of the pentacene moieties (6/10 and 7/8 in Figure 108) as well as the correlations between the signals of the protons of the SubPc macrocycle (1 and 2 in Figure 108). The “inner” protons of the Pnc$_2$ unit, that is, the protons pointing towards the phenylene spacer (*e.g.*, 5 in Figure 108), can be distinguished from the outer protons, that is, the protons pointing towards the TIPS group (*e.g.*, 11 in Figure 108) by means of the NOESY spectrum, which shows the correlations between the signal corresponding to proton 5 and the signals of the phenylene bridge (blue dashed lines in Figure 110).

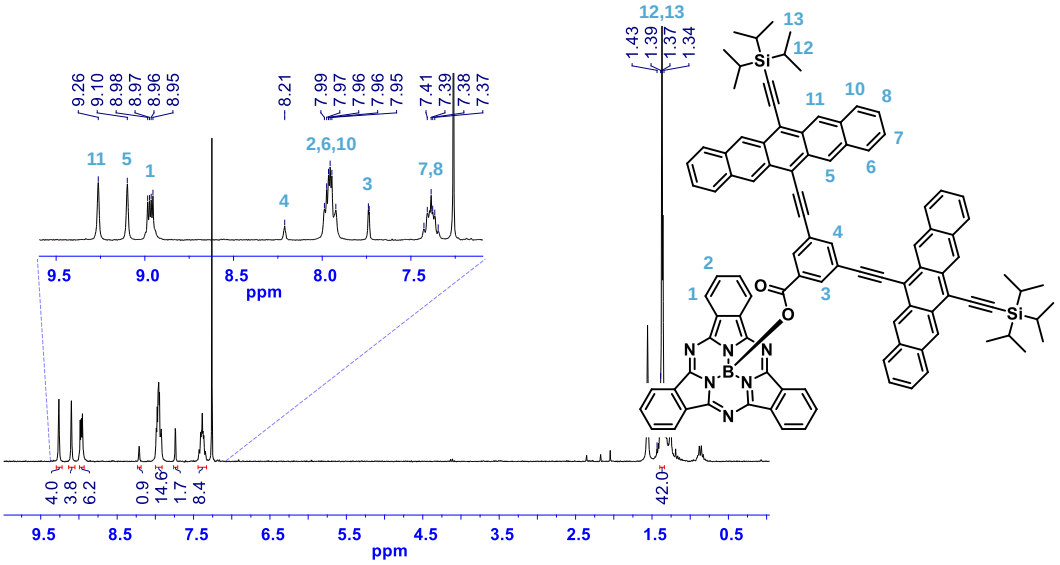

Figure 108. ^{1}H-NMR spectrum (500 MHz, $CDCl_3$) of SubPc-Pnc$_2$ **26**. Inset: zoom of the aromatic protons' peaks.

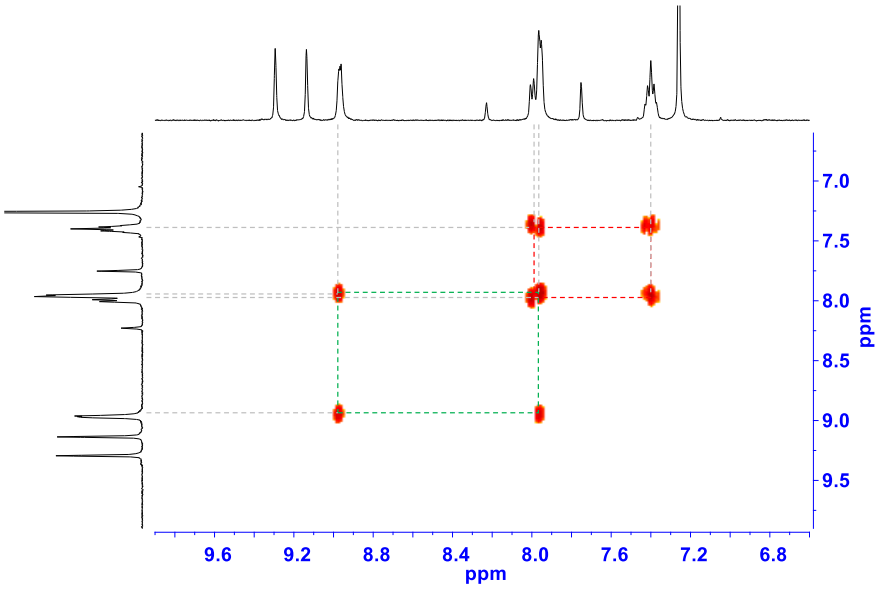

Figure 109. Zoom of the region between 9.9 ppm and 6.6 ppm of the H-H COSY NMR spectrum (500 MHz, $CDCl_3$) of **26** showing the correlations between the protons of the pentacene moieties (red dashed lines) and between the protons of the SubPc macrocycle (green dashed lines).

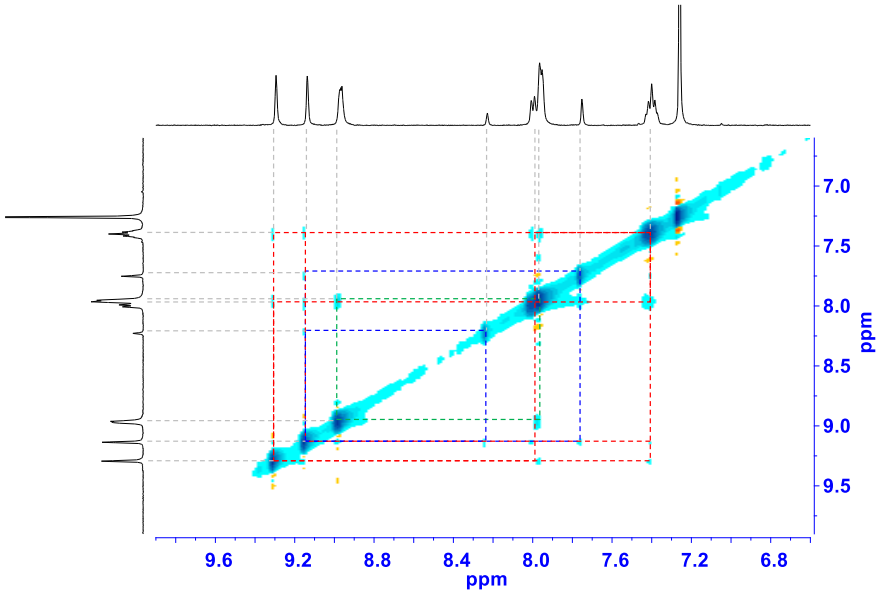

Figure 110. Zoom of the region between 9.9 ppm and 6.6 ppm of the H-H NOESY NMR spectrum (500 MHz, $CDCl_3$) of **26** showing the correlations between the protons of the pentacene moieties (red dashed lines), between the protons of the SubPc macrocycle (green dashed lines), and between the protons of the pentacene moieties and the protons of the phenylene linker (blue dashed lines).

2.3.1.2 Photophysical properties of SubPc-Pnc$_2$ conjugates featuring different peripheral substituents

Steady-state absorption and fluorescence studies as well as transient absorption measurements were carried out in order to investigate the ground- and excited-state interactions between the SubPc and Pnc$_2$ fragments in SubPc-Pnc$_2$ derivatives **26**-**29**. To this end, comparative measurements on the SubPc precursors **1**, **24** and **25** and the starting Pnc$_2$ **17** were also performed. The photophysical studies presented in this section were carried out during a predoctoral stay in the laboratory of Prof. Dirk Guldi at Friederich-Alexander University in Erlangen, Germany.

Steady-state absorption studies

The absorption spectra of SubPc-Cl precursors **1**, **24**, and **25** in toluene are dominated by a Soret band at around 320 nm and a Q band maximizing at 565, 572, and 601 nm, respectively (Figure 111). The bathochromic shift of the Q-band absorption observed when moving from the hydrogenated derivative **1** to the triphenoxy-substituted derivative **24** (*i.e.*, 7 nm) and from **24** to the hexathiooctyl-substituted derivative **25** (*i.e.*, 29 nm) is in line with the increasing electron-

donor character of the peripheral substituents. Changes in solvent polarity have only a minor impact on the absorption features of the reference SubPc-Cl species. As a matter of fact, Q-band maxima at 568, 576, and 603 nm are detected in benzonitrile for **1**, **24** and **25**, respectively.

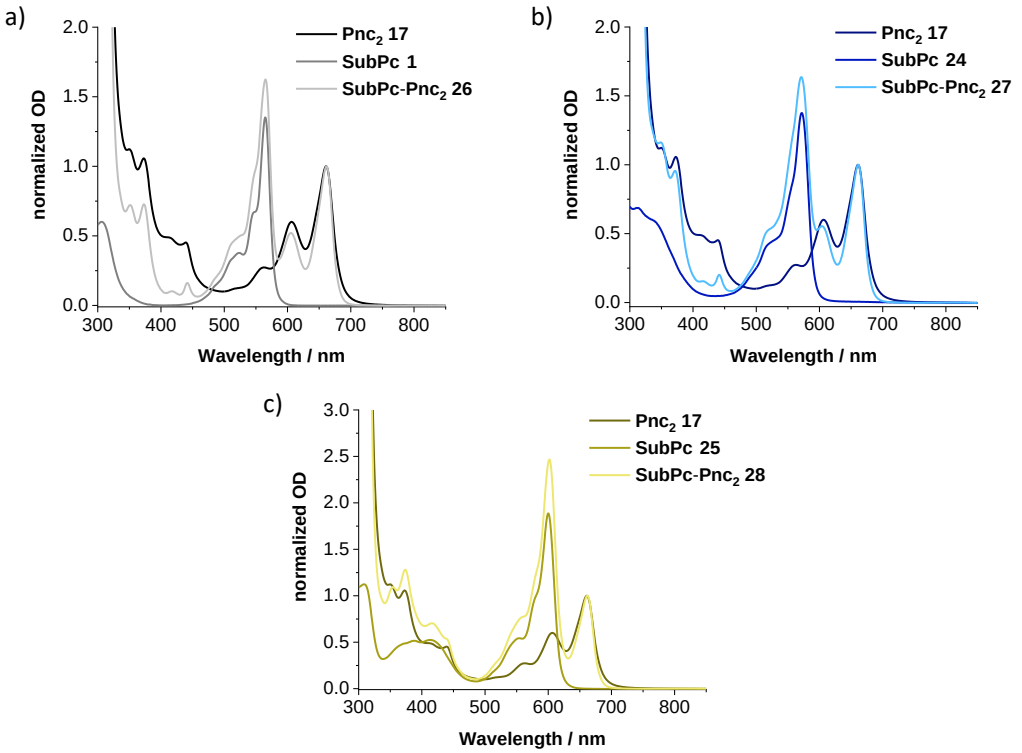

Figure 111. Steady-state absorption spectra of a) Pnc_2 **17**, SubPc-Cl **1** and SubPc-Pnc_2 **26**, b) Pnc_2 **17**, SubPc-Cl **24** and SubPc-Pnc_2 **27**, and c) Pnc_2 **7**, SubPc-Cl **25** and SubPc-Pnc_2 **28** in toluene. The absorption spectra of **26**-**28** and **17** have been normalized to the long-wavelength absorption of **17**. The absorption spectra of **1**, **24** and **25** have been corrected for the intensity of the Pnc_2-related absorption at the maximum SubPc absorption within the conjugates **26**-**28**.

For Pnc_2 **17**, short-wavelength absorptions in the 300-500 nm region along with long-wavelength absorptions featuring vibrational fine structure in the 500-750 nm region are observed both in toluene and in benzonitrile (Figure 111). In particular, long-wavelength absorption maxima at 661 and 666 nm are detected in the former and the latter solvent, respectively.

Turning to SubPc-Pnc_2 derivatives **26**-**28**, their UV-vis absorption spectra are best described as the linear superimposition of the individual components (Figure 111). This experimental finding

indicates that no, or only marginal, ground-state interactions take place between the SubPc and the Pnc$_2$ units within the three conjugates. As a matter of fact, the SubPc Q-band absorption in toluene is centered at 565, 571, and 602 nm for **26**, **27**, and **28**, respectively, whereas the long-wavelength absorption of the Pnc$_2$ maximizes around 661 nm. In benzonitrile, SubPc Q-band maxima at 568, 574 and 604 are observed for **26**, **27**, and **28**, respectively, while the long-wavelength absorption maximum of the Pnc$_2$ is centered around 667 nm. Importantly, the combined absorption features of the two components (*i.e.*, the SubPc and the Pnc$_2$) almost cover the whole visible region of the solar spectrum. In other words, the investigated SubPc-Pnc$_2$ conjugates feature a nearly panchromatic absorption.

Steady-state fluorescence studies

Next, steady-state fluorescence studies were carried out to shed light onto the excited-state interchromophoric interactions. ϕ_F values were determined using as reference compounds: 1) Rhodamine 6G in ethanol (ϕ_F = 0.95[423]) for the SubPc fluorescence in hydrogenated and tri-phenoxy-substituted derivatives, 2) a F_{12}SubPc axially substituted with a phenoxy ligand in toluene (ϕ_F = 0.17,[319] Figure 69) for the SubPc fluorescence in hexathiooctyl-subsituted derivatives, and 3) ZnPc in toluene (ϕ_F = 0.30[424]) for the Pnc$_2$ fluorescence. A summary of the most relevant photophysical properties of SubPc-Cl precursors **1**, **24** and **25**, SubPc-Pnc$_2$ conjugates **26**-**28** and Pnc$_2$ **17** obtained from steady-state fluorescence and TCSPC measurements in toluene and benzonitrile is given in Tables 12 and 13, respectively.

Upon photoexcitation of SubPc-Cl references **1**, **24** and **25** in toluene at 500 nm, that is, into the SubPc Q-band region, a rather strong fluorescence is observed with short-wavelength maxima at 573, 583, and 609 nm, and ϕ_F of 0.30, 0.31, and 0.16, respectively (Figure 112 and Table 12). The lower fluorescence quantum yield of $(S_8H_{17})_6$SubPc-Cl **25** in comparison with that determined for H_{12}SubPc-Cl **1** and $(OPh)_3$SubPc-Cl **24** can be attributed to the heavy-atom effect of sulfur, which is known to enhance ISC.[425] From TCSPC measurements, fluorescence lifetimes of 3.30 (**1**), 3.01 (**24**), and 2.47 ns (**25**) were determined. None of the fluorescence features of the SubPc-Cl references **1**, **24** and **25** changes upon increasing solvent polarity, as demonstrated by steady-state fluorescence measurements carried out in benzonitrile (Table 13).

[423] R. F. Kubin, A. N. Fletcher, *J. Lumin.* **1982**, *27*, 455-462.
[424] S. L. Murov, I. Carmichael, G. L. Hug, *Handbook of photochemistry*, CRC Press, **1993**.
[425] A. Rodríguez-Serrano, V. Rai-Constapel, M. C. Daza, M. Doerr, C. M. Marian, *Phys. Chem. Chem. Phys.* **2015**, *17*, 11350-11358.

Table 12. Fluorescence emission maxima, fluorescence quantum yields and fluorescence lifetimes of SubPc-Cl **1**, **24** and **25**, SubPc-Pnc_2 **26**-**28** and Pnc_2 **17** in toluene.

	λ_{max} / nm		ϕ_F	τ_F
Compound	**SubPc[a]**	**Pnc_2[b]**	**SubPc[a]**	**SubPc[a]**
1	573	-	0.30	3.30 ns
24	583	-	0.31	3.01 ns
25	609	-	0.16	2.47 ns
26	574	666	<0.01	<100 ps[c]
27	585	666	0.01	<100 ps[c]
28	610	666	0.01	<100 ps[c]
17	-	666	~0.02[b]	<200 ps[b,c]

[a] Values refer to the SubPc-centered fluorescence if not stated otherwise. [b] Values refer to the Pnc_2-centered fluorescence. [c] Lifetime is below the resolution limit of the TCSPC setup.

Table 13. Fluorescence emission maxima, fluorescence quantum yields and fluorescence lifetimes of SubPc-Cl **1**, **24** and **25**, SubPc-Pnc_2 **26**-**28** and Pnc_2 **17** in benzonitrile.

	λ_{max} / nm		ϕ_F	τ_F
Compound	**SubPc[a]**	**Pnc_2[b]**	**SubPc[a]**	**SubPc[a]**
1	577	-	0.27	3.04 ns
24	589	-	0.25	2.83 ns
25	615	-	0.17	3.21 ns
26	577	673	<0.01	<100 ps[c]
27	587	674	<0.01	<100 ps[c]
28	614	672	<0.01	<100 ps[c]
17	-	673	~0.02[b]	<200 ps[b,c]

[a] Values refer to the SubPc-centered fluorescence if not stated otherwise. [b] Values refer to the Pnc_2-centered fluorescence. [c] Lifetime is below the resolution limit of the TCSPC setup.

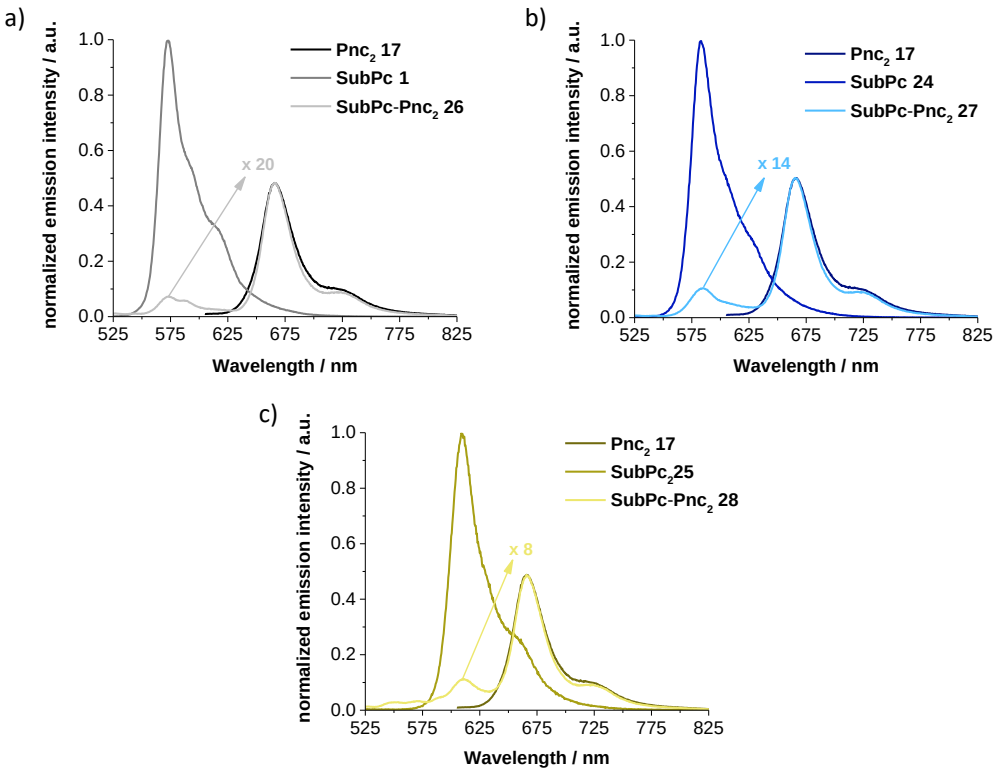

Figure 112. Steady-state fluorescence spectra (λ_{ex} = 500 nm for **1**, **24**-**28**; λ_{ex} = 590 nm for **17**) of a) Pnc$_2$ **17**, SubPc-Cl **1** and SubPc-Pnc$_2$ **26**, b) Pnc$_2$ **17**, SubPc-Cl **24** and SubPc-Pnc$_2$ **27**, b) Pnc$_2$ **17**, SubPc-Cl **25** and SubPc-Pnc$_2$ **28** in toluene. The emission spectra of Pnc$_2$ **17** have been normalized to the Pnc$_2$-related emission of SubPc-Pnc$_2$ conjugates **26**-**28** to visualize the analogy between the Pnc$_2$-related emission of **26**-**28** and the fluorescence of **17**. The depicted emission spectra of **26**-**28** have been recorded with wider entrance and exit slits compared to **1**, **24** and **25** to ensure a reasonable signal-to-noise ratio. Afterwards, the respective intensities were corrected.

Excitation of Pnc$_2$ **17** into the long-wavelength absorptions (*i.e.*, at 590 nm) leads to a fluorescence emission maximizing at 666 nm in toluene and 673 in benzonitrile, with a rather low ϕ_F of about 0.02 (Figure 112, Table 12 and Table 13). This finding is in line with the SF behavior expected for the Pnc$_2$ derivative.[417]

Remarkably, dramatic changes in the fluorescence features of SubPc-Pnc$_2$ **26**-**28** in comparison with that of SubPc-Cl references **1**, **24** and **25** are observed upon photoexcitation of the conjugates into the SubPc Q-band region (*i.e.*, at 500 nm) in toluene (Figure 112 and Table 12). On one hand, the SubPc-centered fluorescence is quenched nearly quantitatively (namely, by

more than 90%) with respect to SubPc-Cl **1**, **24** and **25**. As a matter of fact, fluorescence quantum yields of 0.01 and lower were determined for **26**-**28** for the fluorescence stemming from the singlet excited state of the SubPc unit. Moreover, fluorescence lifetimes shorter than 100 ps were determined from TCSPS measurements for such SubPc-centered emission in **26**-**28**. On the other hand, a fluorescence emission maximizing at 666 nm is observed, which is in perfect agreement with the fluorescence observed for Pnc_2 reference **17**. Similar features are observed upon 500 nm photoexcitation in benzonitrile (Table 13). Taking all these experimental findings into account, we postulate for SubPc-Pnc_2 conjugates **26**-**28** a unity efficient FRET, which takes place upon photoexcitation of the SubPc unit and funnels singlet excited-state energy from the SubPc to the Pnc_2.

Transient absorption studies

Femtosecond (fsTA) and nanosecond (nsTA) transient absorption measurements were performed with SubPc-Cl references **1**, **24** and **25**, SubPc-Pnc_2 conjugates **26**-**28** and Pnc_2 **17**. For SubPc-based systems, 530 nm was selected as the excitation wavelength, whereas for Pnc_2 **17** a 633 nm irradiation wavelength was employed.

Photoexcitation of SubPc-Cl **1**, **24** and **25** at 530 nm leads to the instantaneous formation of the typical SubPc singlet excited-state features in fsTA and nsTA experiments. As an example, for **24** in toluene a transient ground-state bleaching is observed at 575 nm (Figures 113 and 114). Additional SubPc $^1(S_1)$ state signatures include maxima at 411 and 652 nm, a shoulder at 630 nm, and a broad NIR absorption. The singlet excited state in **1**, **24** and **25** then undergoes a monoexponential decay to afford the corresponding SubPc triplet excited state, which characteristic signatures include a maximum at 419 nm together with a 450 nm shoulder and a ground-state bleaching at 572 nm. Global analysis of the spectra was performed using the model given in Equation 16, and afforded a lifetime of the SubPc singlet excited state of 3.07 ns.

$$^1(S_1) \rightarrow {}^3(T_1) \rightarrow {}^1(S_0) \qquad \text{(Eq. 16)}$$

In the respective nsTA experiments, the SubPc $^3(T_1)$ state is replaced at a longer timescale by the ground state, and the underlying lifetime is 60.01 µs (Figure 114). Almost identical deactivation patterns were observed for **1** and **25**, with lifetimes of the SubPc $^1(S_1)$ state of 3.40 ns (**1**) and 2.37 ns (**25**), and lifetimes of the SubPc $^3(T_1)$ state of 48.22 µs and 50.14 µs, respectively.

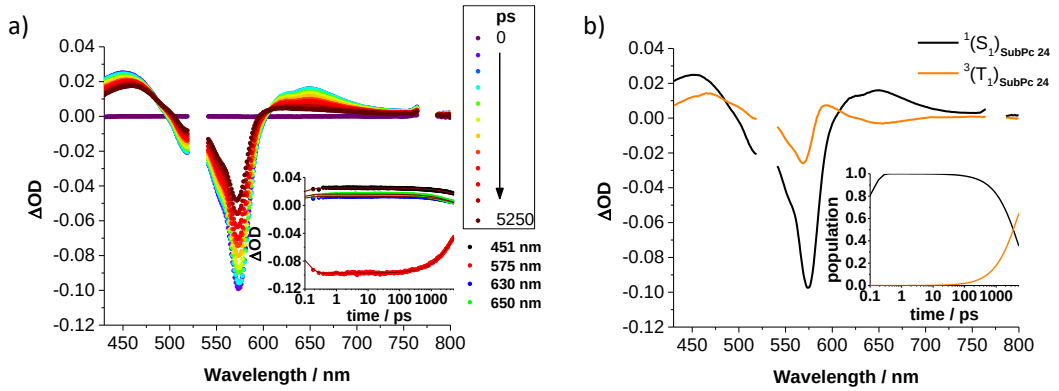

Figure 113. a) Differential absorption spectra (visible) obtained upon fsTA experiments (530 nm) of **24** in toluene with several time delays between 0 and 5250 ps at room temperature. Inset: Single wavelength kinetics at 451 (black), 575 (red), 630 (blue), and 650 nm (green) monitoring the excited-state dynamics and fits to the data (red lines). b) Evolution-associated spectra of the transient absorption data of **24** shown in (a). The black spectrum illustrates the initially formed SubPc $^1(S_1)$ state, while the orange spectrum is that of the SubPc $^3(T_1)$ state. Inset: relative populations of $^1(S_1)$ and $^3(T_1)$.

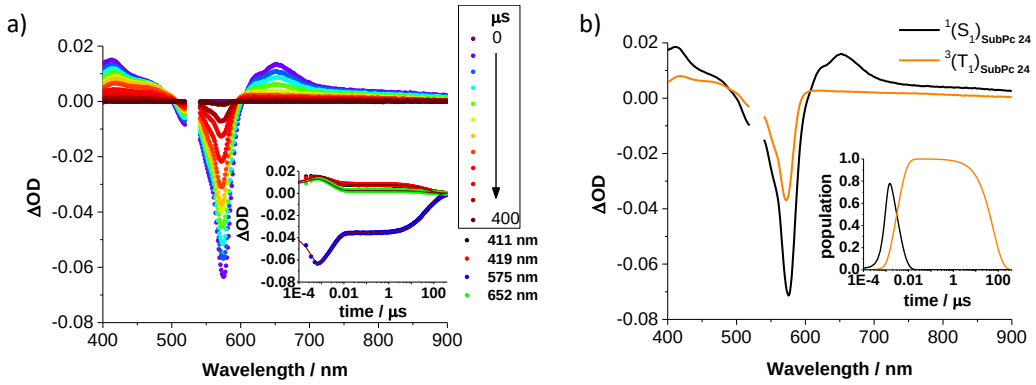

Figure 114. a) Differential absorption spectra (visible) obtained upon nsTA experiments (530 nm) of **24** in toluene with several time delays between 0 and 400 μs at room temperature. Inset: Single wavelength kinetics at 411 (black), 419 (red), 575 (blue), and 652 nm (green) monitoring the singlet excited-state and triplet excited-state dynamics and fits to the data (red lines). b) Evolution-associated spectra of the transient absorption data of **24** shown in (a). The black spectrum illustrates the initially formed SubPc $^1(S_1)$ state, while the orange spectrum is that of the SubPc $^3(T_1)$ state. Inset: relative populations of $^1(S_1)$ and $^3(T_1)$.

Upon photoexcitation of **17** at 633 nm, the immediate evolution of the singlet excited-state features is observed in fsTA measurements. In toluene, these comprise a ground-state bleaching in the 550-750 nm region along with characteristic maxima at 451 and 508 nm in the visible region and at 1386 nm in the NIR (Figure 115). The $^{1}(S_1S_0)$ state signatures are rapidly replaced by triplet excited-state maxima at 473 and 506 nm. Considering, however, that the transformation of the singlet to the triplet excited state is rapid, as it takes place on a timescale of around 200 ps, we postulate that the formation of the Pnc_2 triplet excited state occurs *via* intramolecular SF. This hypothesis is further supported by the intensification of the ground-state bleaching, which infers the formation of more than one triplet excited state per Pnc_2, that is, a correlated pair of triplet excited states (*i.e.*, $^{1}(T_1T_1)$). The $^{1}(T_1T_1)$ formation is biphasic and involves an intermediate state, in agreement with previous investigations on a *meta*-phenylene Pnc_2.[402] The mediating step is likely a singlet excited state mixed with a higher-lying CT-type state. A notable solvent dependence, which was established for the biphasic $^{1}(T_1T_1)$ formation, further supports this notion. Intramolecular TTA of $^{1}(T_1T_1)$ concludes the deactivation cascade of **17**, repopulating the electronic ground state on a timescale of 3.22 ns. The model used for the global fitting of the transient absorption data is summarized by Equation 17.

$$^{1}(S_1S_0) \rightarrow {}^{CT}(S_1S_0) \rightarrow {}^{1}(T_1T_1) \rightarrow {}^{1}(S_0S_0) \qquad \text{(Eq. 17)}$$

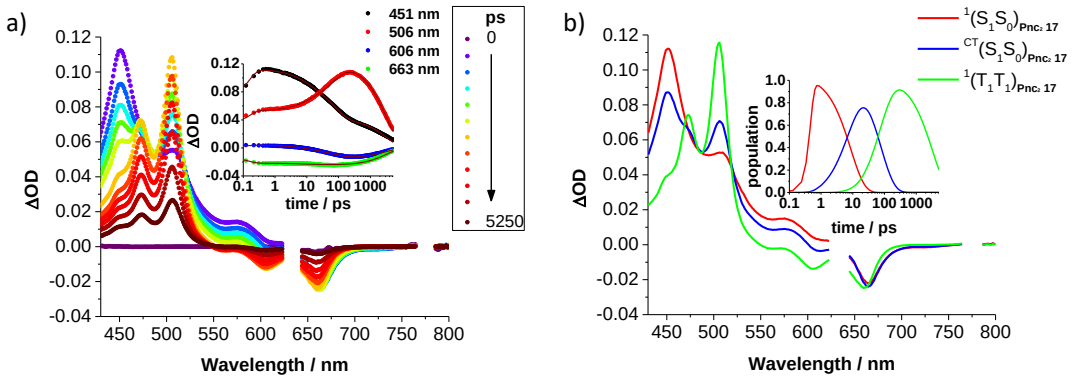

Figure 115. a) Differential absorption spectra (visible) obtained upon fsTA experiments (633 nm) of Pnc_2 **17** in toluene with several time delays between 0 and 5250 ps at room temperature. Inset: Single wavelength kinetics at 451 (black), 506 (red), 606 (blue), and 663 nm (green) monitoring the singlet excited-state ($^{1}(S_1S_0)$: 8.67 ps), intermediate state ($^{CT}(S_1S_0)$: 75.35 ps), and triplet excited-state ($^{1}(T_1T_1)$: 3.22 ns) dynamics and fits to the data (red lines). b) Evolution-associated spectra of the transient absorption data of **17** shown in (a). The red spectrum illustrates the initially formed Pnc_2 $^{1}(S_1S_0)$ state, while the blue and green spectra are those of the intermediate Pnc_2 $^{CT}(S_1S_0)$ state and the multiexcitonic Pnc_2 $^{1}(T_1T_1)$ state, respectively. Inset: relative populations of $^{1}(S_1S_0)$, $^{CT}(S_1S_0)$, and $^{1}(T_1T_1)$.

Finally, fsTA assays were performed with SubPc-Pnc$_2$ conjugates **26**-**28**. For these derivatives, the characteristic signatures of the SubPc $^1(S_1)$ state develop right after photoexcitation at 530 nm in toluene. Taking **27** as an example, these fingerprint absorptions include a transient ground-state bleaching at 574 nm along with maxima at 455 and around 650 nm, similarly to what observed for the corresponding SubPc-Cl precursor **24** (Figure 116). Remarkably, and in stark contrast with the behavior of the axially chlorinated SubPc reference **24**, the SubPc $^1(S_1)$ state in SubPc-Pnc$_2$ **27** is rapidly replaced by the $^1(S_1S_0)$ features found for **17**. In particular, the characteristic SubPc ground-state bleaching decays with the same kinetics that emerge for the ground-state bleaching of the Pnc$_2$ moiety, and all these events occur within less than 10 ps. These findings indicate that the initial population of the SubPc singlet excited state is followed by FRET to the singlet excited state of Pnc$_2$, as already suggested by steady-state fluorescence measurements which revealed for the SubPc-Pnc$_2$ conjugates a nearly quantitative quenching of the SubPc-centered emission along with the appearance of a fluorescence emission band attributable to the Pnc$_2$ unit (*vide supra*).

After population of the $^1(S_1S_0)$ state of Pnc$_2$, the stepwise deactivation of **27** is identical to that observed for Pnc$_2$ reference **17**. As a matter of fact, a two-step population of the multiexcitonic $^1(T_1T_1)$ state takes place *via* population of the intermediate $^{CT}(S_1S_0)$ state. Finally, TTA back to the ground state concludes the deactivation process. In other words, all processes that follow the FRET-induced population of the Pnc$_2$ $^1(S_1S_0)$ state are unaffected by the presence of the SubPc unit. Equation 18 was employed to fit the experimental data:

$$^1(S_1) \rightarrow {}^1(S_1S_0) \rightarrow {}^{CT}(S_1S_0) \rightarrow {}^1(T_1T_1) \rightarrow {}^1(S_0S_0) \qquad \text{(Eq. 18)}$$

Similar deactivation patterns were observed for SubPc-Pnc$_2$ **26** and **28**. A qualitative energy diagram depicting the deactivation cascade of SubPc-Pnc$_2$ conjugates **26**-**28** upon photoexcitation of the SubPc moiety is represented in Figure 117.

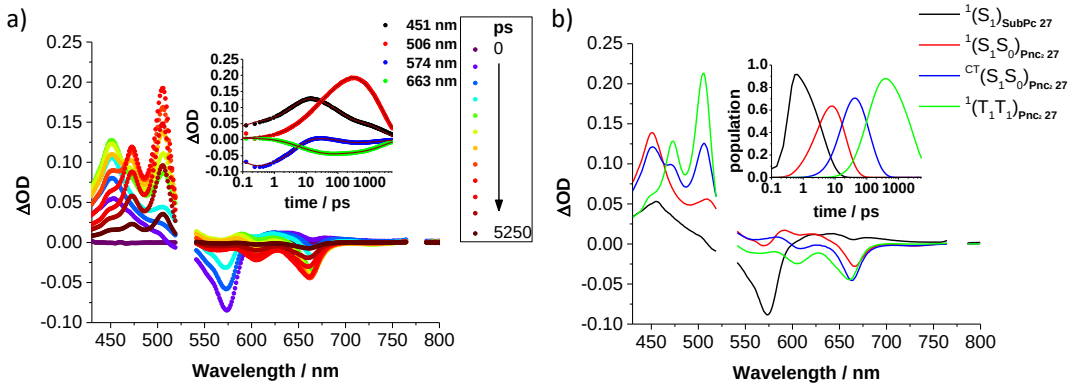

Figure 116. a) Differential absorption spectra (visible) obtained upon fsTA experiments (530 nm) of **27** in toluene with several time delays between 0 and 5250 ps at room temperature. Inset: Single wavelength kinetics at 451 (black), 506 (red), 574 (blue), and 663 nm (green) monitoring the singlet excited-state ($^1(S_1)$: 4.08 ps), singlet excited-state ($^1(S_1S_0)$: 16.84 ps), intermediate state ($^{CT}(S_1S_0)$: 108.37 ps), and triplet excited-state ($^1(T_1T_1)$: 2.89 ns) dynamics, as well as fits to the data (red lines). b) Evolution-associated spectra of the transient absorption data of **27** shown in (a). The black spectrum illustrates the initially formed SubPc $^1(S_1)$ state, while the red spectrum is the Pnc_2 $^1(S_1S_0)$ state, blue the intermediate Pnc_2 $^{CT}(S_1S_0)$ state, and green the multiexcitonic Pnc_2 $^1(T_1T_1)$ state. Inset: Relative populations of $^1(S_1)$, $^1(S_1S_0)$, $^{CT}(S_1S_0)$, and $^1(T_1T_1)$.

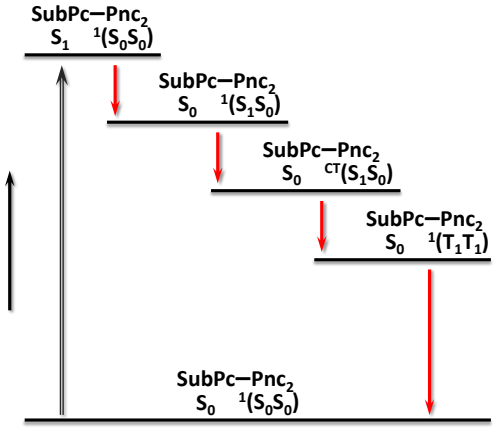

Figure 117. Qualitative energy diagram depicting the deactivation cascade of SubPc-Pnc_2 conjugates **26**-**28**. The initial population of the SubPc singlet excited state $^1(S_1)$ is followed by FRET to the singlet excited state of Pnc_2 $^1(S_1S_0)$. Population of the intermediate state $^{CT}(S_1S_0)$, subsequent SF to yield the multiexcitonic state $^1(T_1T_1)$, and TTA back to the Pnc_2 ground state conclude the deactivation process.

For SubPc-Pnc$_2$ **27** in toluene, global fitting afforded two lifetimes (namely, 16.8 and 108.4 ps) for the population of the multiexcitonic $^1(T_1T_1)$ state, which, in turn, is subject to efficient TTA to recover the ground state with a lifetime of 2.89. In benzonitrile, global fitting yielded two lifetimes of 13.2 and 80.8 ps for the population of the $^1(T_1T_1)$ state, whereas the multiexcitonic $^1(T_1T_1)$ state undergoes TTA with a lifetime of 2.50 ns. Besides on decay dynamics, solvent polarity has an influence also on the overall triplet quantum yields (TQYs) of the multiexcitonic $^1(T_1T_1)$ state. In particular, TQYs as high as 206% were determined in benzonitrile. In this connection, it is worth to mention that an error margin in the range of ±10% may be considered when determining TQYs. On the other hand, lower values (*i.e.*, as low as 157%) were obtained in toluene.

The fact that more polar solvents favor higher TQYs and shorter-lived Pnc$_2$ $^1(S_1S_0)$ states is in line with previous works on 6,6'-linked Pnc$_2$s and is commonly considered as an evidence for the CT character of the intermediate Pnc$_2$ $^{CT}(S_1S_0)$ state.[402,409] In other words, more polar solvents stabilize the Pnc$_2$ $^{CT}(S_1S_0)$ state, facilitating the population of the Pnc$_2$ $^1(T_1T_0)$ state.

A summary of the kinetic data of SubPc-Cl references **1**, **24** and **25** and SubPc-Pnc$_2$ conjugates **26**-**28** obtained from fsTA and nsTA measurements in toluene and benzonitrile, including the lifetimes of all the involved states, as well as the quantum yields of the multiexcitonic state for **26**-**28**, is reported in Tables 14 and 15.

Table 14. Summary of kinetic data of SubPc-Cl derivatives **1**, **24** and **25** and SubPc-Pnc$_2$ conjugates **26**-**28** and TQYs of **26**-**28** obtained from fsTA and nsTA in toluene.

	fsTA				nsTA		
	$^1(S_1)_{SubPc}$	$^1(S_1S_0)_{Pnc2}$	$^{CT}(S_1S_0)_{Pnc2}$	$^1(T_1T_1)_{Pnc2}$	$^1(S_1)_{SubPc}$	$^3(T_1)_{SubPc}$	TQY^a
1	n. r.[b]	-	-	-	3.40 ns	48.22 µs	-
24	n. r.[b]	-	-	-	3.07 ns	60.01 µs	-
25	n. r.[b]	-	-	-	2.37 ns	50.01 µs	-
26	4.28 ps	16.62 ps	108.25 ns	2.57 ns	n. r.[b]	-	157%
27	4.08 ps	16.84 ps	108.37 ns	2.89 ns	n. r.[b]	-	162%
28	3.80 ps	17.54 ps	108.09 ns	2.65 ns	n. r.[b]	-	167%

[a] Determined by following the intensification of the transient bleaching of the Pnc$_2$ moiety and comparing the relative intensities of the evolution associated spectra for the Pnc$_2$ $^1(S_1S_0)$ and the $^1(T_1T_1)$ state, respectively. [b] n. r. = not resolvable. Lifetimes are either too long to be resolved with fsTA or too short to be resolved with nsTA.

Table 15. Summary of kinetic data of SubPc-Cl derivatives **1**, **24** and **25** and SubPc-Pnc_2 conjugates **26**-**28** and TQYs of **26**-**28** obtained from fsTA and nsTA in benzonitrile.

	fsTA				nsTA		
	$^1(S_1)_{SubPc}$	$^1(S_1S_0)_{Pnc2}$	$^{CT}(S_1S_0)_{Pnc2}$	$^1(T_1T_1)_{Pnc2}$	$^1(S_1)_{SubPc}$	$^3(T_1)_{SubPc}$	TQY^a
1	n. r.[b]	-	-	-	3.09 ns	64.69 µs	-
24	n. r.[b]	-	-	-	2.86 ns	83.88 µs	-
25	n. r.[b]	-	-	-	2.19 ns	103.41 µs	-
26	3.34 ps	11.17 ps	61.22 ns	2.36 ns	n. r.[b]	-	206%
27	2.81 ps	13.22 ps	80.84 ns	2.50 ns	n. r.[b]	-	168%
28	3.24 ps	21.83 ps	96.81 ns	2.53 ns	n. r.[b]	-	169%

[a] Determined by following the intensification of the transient bleaching of the Pnc_2 moiety and comparing the relative intensities of the evolution associated spectra for the Pnc_2 $^1(S_1S_0)$ and the $^1(T_1T_1)$ state, respectively. [b] n. r. = not resolvable. Lifetimes are either too long to be resolved with fsTA or too short to be resolved with nsTA. [c] An error margin in the range of ±10% may be considered when determining the TQYs.

Regarding FRET rate constants, only minor differences were found between the three SubPc-Pnc_2 conjugates. As a matter of fact, FRET rate constant of $2.33 \cdot 10^{11}$ s^{-1}, $2.45 \cdot 10^{11}$ s^{-1}, and $2.63 \cdot 10^{11}$ s^{-1} were determined for **26**, **27** and **28** in toluene, respectively.

In light of these experimental findings, we looked into effects stemming from the spectral overlap between the SubPc fluorescence and the Pnc_2 absorption as well as their relative distance. To this end, theoretical FRET rate constants were calculated by means of Equations 19-24.[277,426]

The FRET distance *R* for SubPc-Pnc_2 **26**, that is, the distance between the SubPc unit and the Pnc_2 unit, was calculated by means of Equation 19:

$$R = R_0 \left(\frac{1-E}{E}\right)^{\frac{1}{6}} \quad \text{(Eq. 19)}$$

where R_0 is the critical energy donor-acceptor distance at which the FRET efficiency *E* is 50%.

E was determined from the experimental lifetimes obtained from fsTA and TCSPC measurements by Equation 20:

[426] M. A. Hink, N. V. Visser, J. W. Borst, A. van Hoek, A. J. Visser, *J. Fluoresc.* **2003**, *13*, 185-188.

$$E = 1 - \frac{\tau_{DA}}{\tau_D} \quad \text{(Eq. 20)}$$

in which τ_{DA} is the experimental fluorescence lifetime of the energy donor-acceptor conjugate (*i.e.*, SubPc-Pnc$_2$ **26**) and τ_D is the experimental fluorescence lifetime of the energy donor (*i.e.*, SubPc-Cl **1**). In particular, we employed τ_{DA} and τ_D as determined by transient absorption studies (Tables 14 and 15) and TCSPC experiments (Tables 12 and 13), respectively.

On the other hand, R_0 was calculated *via* Equation 21:

$$R_0 = 0.2108(\kappa^2 \varphi_F n^{-4} J)^{\frac{1}{6}} \quad \text{(Eq. 21)}$$

where κ^2 is the orientation factor, ϕ_F is the fluorescence quantum yield of the energy donor, n is the refractive index of the solvent and J is the spectral overlap between the SubPc fluorescence and the Pnc$_2$ absorption. For κ^2, a value of 2/3 (~0.67) was employed (which corresponds to a random orientation of the dipoles of the donor and acceptor), as often used for non-rigid systems.[427] This description is not expected to be fully appropriate to describe the real situation in the investigated SubPc-Pnc$_2$ conjugates. Nevertheless, since the value of κ^2 for the SubPc-Pnc$_2$ derivatives is unknown and the use of other values would just influence the magnitude of R_0 but not the overall picture, the calculations were based on a κ^2 value of 2/3. The refractive indices n were taken as 1.496 and 1.528 for toluene and benzonitrile, respectively.[428] The degree of spectral overlap was calculated as:

$$J = \int_0^\infty F_D(\lambda)\varepsilon_A(\lambda)\lambda^4 d\lambda \quad \text{(Eq. 22)}$$

being F_D the fluorescence intensity of the donor at wavelength λ and ε_A the extinction coefficient of the acceptor at wavelength λ. In particular, the fluorescence spectra of the donor must be normalized to fulfil Equation 23:

$$\int_0^\infty F_D(\lambda) d\lambda = 1 \quad \text{(Eq. 23)}$$

In this way, for **26** in toluene, a FRET distance R of 15.20 Å was calculated. This value is in reasonable agreement with what is expected for a typical SubPc-to-Pnc$_2$ distance. Next, for **27** and **28**, taking the same FRET distance R of 15.20 Å, theoretical FRET rate constants of 3.07 × 10^{11} and 2.73 × 10^{11} s^{-1} were derived, respectively, by means of Equation 24.

[427] L. Loura, *Int. J. Mol. Sci.* **2012**, *13*, 15252-15270.
[428] M. Lechner, *Refractive indices of pure liquids and binary liquid mixtures (supplement to III/38),* Springer-Verlag, Heidelberg, Berlin, **2008**.

$$k_{FRET} = \left(\frac{1}{\tau_D}\right)\left(\frac{R_0}{R}\right)^6 \quad \text{(Eq. 24)}$$

The calculated values are in very good agreement with those found experimentally (*vide supra*). A summary of the parameters used for the FRET rate constants calculation as well as the resulting values in toluene and benzonitrile are reported in Tables 16 and 17, respectively.

Table 16. Summary of the parameters used for the FRET rate constant calculations and resulting values in toluene.

	τ_{DA} / ps (TA)	τ_D / ns (TCSPC)	ϕ_F	J / $M^{-1}cm^{-1}nm^4$	R_0 / Å	R / Å	k_{FRET} / 10^{11} s^{-1}
26	4.28	3.30	0.30	$2.71 \cdot 10^{15}$	46.01	15.20	2.33
27	4.08	3.01	0.31	$3.15 \cdot 10^{15}$	47.45	15.20	3.07
28	3.80	2.47	0.16	$4.45 \cdot 10^{15}$	45.00	15.20	2.73

Table 17. Summary of the parameters used for the FRET rate constant calculations and resulting values in benzonitrile.

	τ_{DA} / ps (TA)	τ_D / ns (TCSPC)	ϕ_F	J / $M^{-1}cm^{-1}nm^4$	R_0 / Å	R / Å	k_{FRET} / 10^{11} s^{-1}
26	3.34	3.04	0.27	$2.68 \cdot 10^{15}$	44.49	14.29	2.99
27	2.81	2.83	0.25	$3.14 \cdot 10^{15}$	45.11	14.29	3.50
28	3.24	2.31	0.17	$4.41 \cdot 10^{15}$	44.76	14.29	4.09

It is interesting to observe that a better spectral overlap between energy donor and acceptor in, for example, hexathiooctyl-substituted SubPc-Pnc_2 **28** does not lead to a larger FRET rate constant when compared to **26** and **27**. This can be rationalized on the basis of the fact that the fluorescence quantum yields of the SubPc energy donors, which are lowest for $(SC_8H_{17})_6$SubPc-Cl precursor **25**, overcompensate those benefits stemming from a larger spectral overlap integral. In other words, the bathochromic shift in SubPc fluorescence when going from **26** to **27** and **28** as it stems from the SubPc peripheral substitution pattern (*i.e.*, from the π-donating ability and the number of π-donor ring substituents) is balanced by lower fluorescence quantum yields, thus resulting in subtle differences in terms of FRET rate constants.

2.3.2 Synthesis and study of SubPc-Pnc$_2$ conjugates featuring different spacers

2.3.2.1 Design, synthesis and characterization of SubPc-Pnc$_2$ conjugates featuring different spacers

In order to get further insights into the combination of i-FRET and i-SF, a different design strategy was employed to tune the interchromophoric interactions within the successive series of SubPc-Pnc$_2$ conjugates. In contrast with the set of multicomponent derivatives investigated in the previous section, in which the D-A separation was kept constant and the energy donating characteristics of the SubPc were modulated by proper functionalization of the macrocycle, in this case we aimed to reach control over i-FRET by tailoring the structural characteristics of the molecular spacer (and, in turn, the spatial arrangement between the SubPc and Pnc$_2$ units) rather than the energy-donor SubPc.

As already mentioned, distance and relative orientation between chromophores contribute to regulate the efficiency of the FRET process, along with the spectral overlap between donor emission and acceptor absorption. In light of this, the molecular bridge was tailored in terms of both length and flexibility by varying the number of constituting aryl units and/or methylene groups. In particular, four SubPc-Pnc$_2$ conjugates were synthesized by axial substitution reaction from H$_{12}$SubPc-Cl **1**, employing different 6,6'-linked, *meta*-arranged Pnc$_2$s bearing a hydroxy, methoxy, phenoxy or benzyloxy group linked to the bridging phenylene unit (**29**-**32**, Figure 118).

As for Pnc$_2$ **17**, Pnc$_2$s **29**-**32** were provided by the research group of Prof. Rik Tykwinski at the University of Alberta in Edmonton, Canada.

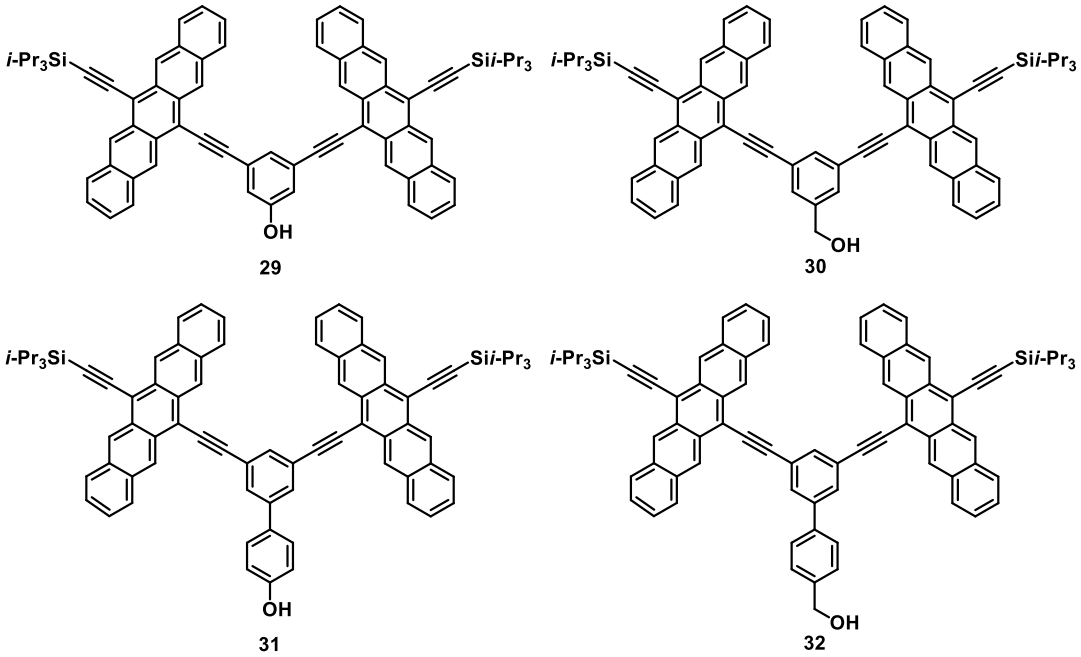

Figure 118. Chemical structure of Pnc_2 derivatives **29**-**32**.

Reaction with alcohols (and, in particular, aryl alcohols) represents by far the most commonly employed method for the axial functionalization of SubPcs due to its simple and relatively high-yielding procedure.[8] In particular, reaction with phenols is typically carried out by heating a mixture of the SubPc and an excess of the corresponding alcohol in high-boiling aromatic solvents. Nevertheless, as for the preparation of SubPc-Pnc_2 conjugates **26**-**28**, also in this case we opted for replacing the axial halogen ligand *via* generation of an activated SubPc intermediate by treatment of the starting SubPc-Cl with AgOTf (Scheme 9).[48] This approach allows to reduce the equivalents of nucleophile employed in the reaction and permits to replace the axial halogen ligand in milder reaction conditions. Moreover, this strategy is preferable in the presence of sterically congested nucleophile, which is the case of the employed Pnc_2 species. Finally, the activation of the axial position by means of a triflate derivative allows for the easier introduction of alkyl alcohol functionalities. In this way, SubPc-Pnc_2 conjugates **33**-**36** were obtained in 16-26% yields. As observed in the synthesis of SubPc-Pnc_2 derivatives **26**-**28**, also in this case considerable amounts of by-products coming from the decomposition of the Pnc_2 precursors were found in the reaction mixtures. In this connection, it is worth to mention that upon reducing the reaction temperature from 50 °C to room temperature even lower yields were obtained, which can be rationalized in light of the steric hindrance of the Pnc_2 derivatives

and the progressive hydrolysis of the SubPc-OTf intermediate over time. As a matter of fact, higher amounts of by-products from the hydrolysis of the activated SubPc-OTf species were found in reactions carried out at lower temperatures.

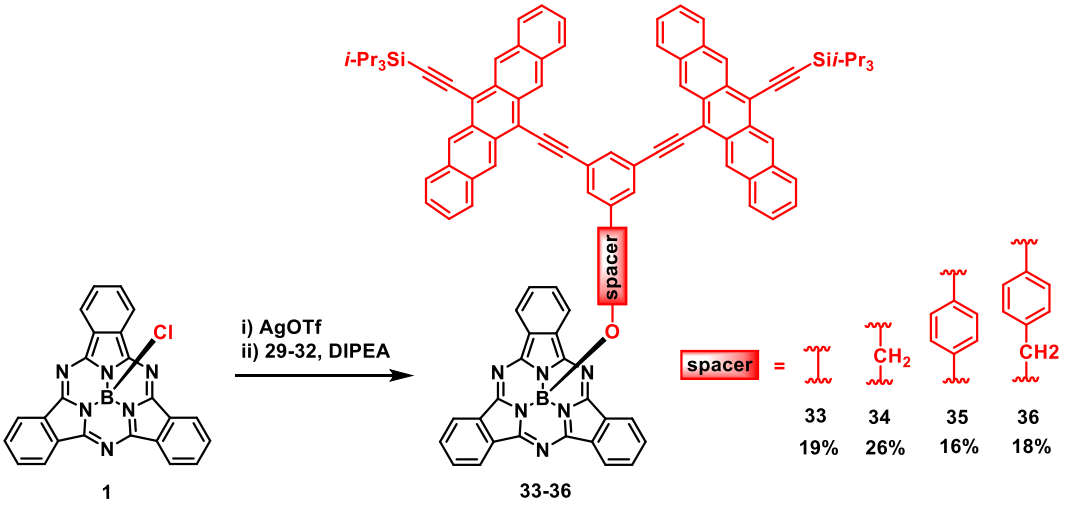

Scheme 9. Synthesis of SubPc-Pnc$_2$ conjugates **33**-**36** from SubPc-Cl precursor **1**.

The novel SubPc-Pnc$_2$ derivatives were fully characterized by means of ^{1}H-NMR, ^{13}C-NMR, ^{11}B-NMR, UV-vis and IR spectroscopy and HRMS. Unfortunately, single crystals suitable for X-ray diffraction analysis could not be obtained despite testing several crystallization conditions. As observed for SubPc-Pnc$_2$ conjugates **26**-**28**, signals corresponding to the dimeric structures of the investigated conjugates were observed in MALDI mass spectra of **33**-**36**, probably due to π-π stacking interactions between the pentacene units.

The proton signals of **33**-**36** in the corresponding ^{1}H-NMR spectra were assigned with the help of COSY and NOESY experiments. As an example, the ^{1}H-NMR spectra of SubPc-Pnc$_2$ **33** and **34** are shown in Figures 119 and 120. The effect of the diatropic ring current of the SubPc macrocycle is evident on the signals of the protons of the axial ligand nearest to the SubPc core (*e.g.*, 3 in Figures 119 and 120) which are shifted upfield. The H-H COSY spectrum of **33**, showing the correlations between the protons of the pentacene moieties along with that between the protons of the *meta*-phenylene spacer and that between the peripheral proton of the SubPc macrocycle is reported in Figure 121. In particular, the multiplets at 8.00-7.98 and 8.27-8.25 can be assigned to proton 6 and 9 (Figure 119) as they correlate with both the signals of 5/10 and that of 7/8. Finally, "inner" Pnc$_2$ protons (*i.e.*, 5 and 6 in Figure 119) were distinguished from "outer" protons (*i.e.*, 9 and 10 in Figure 119), by taking advantage of the NOESY correlation of

the signal corresponding to 5 with the signals of the phenylene bridge as well as of the aforementioned correlations in the COSY spectrum.

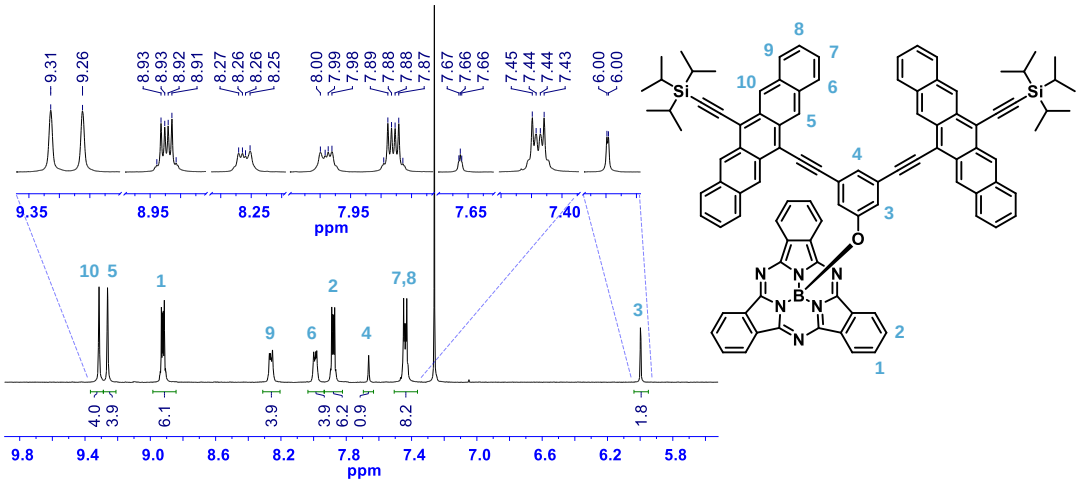

Figure 119. ^{1}H-NMR spectrum (500 MHz, $CDCl_3$) of SubPc-Pnc$_2$ **33**. Inset: zoom of the aromatic protons' peaks.

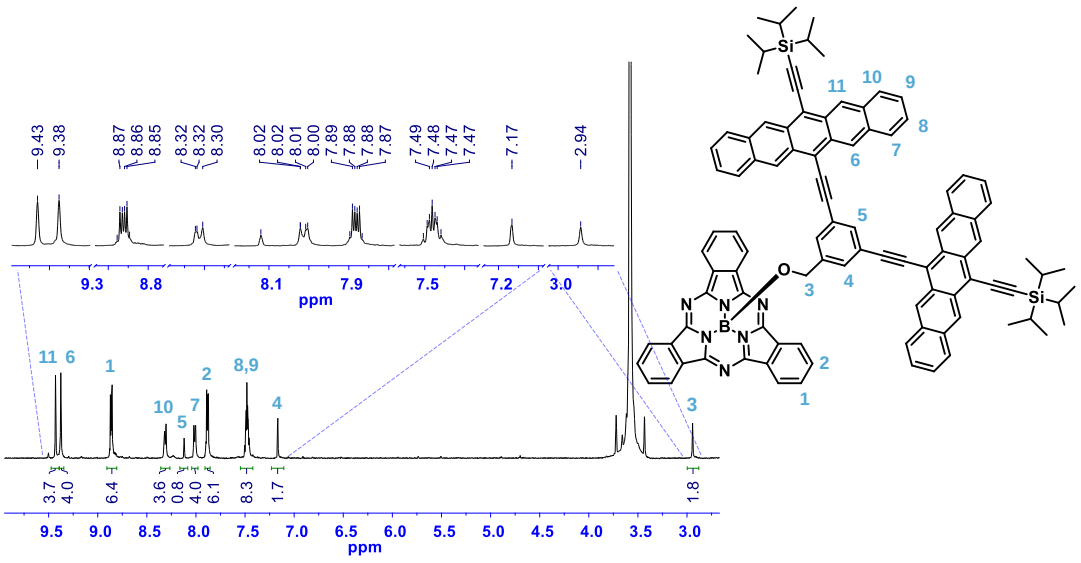

Figure 120. Partial ^{1}H-NMR spectrum (500 MHz, THF-d_8) of SubPc-Pnc$_2$ **34**. Inset: zoom of some of the protons' peaks.

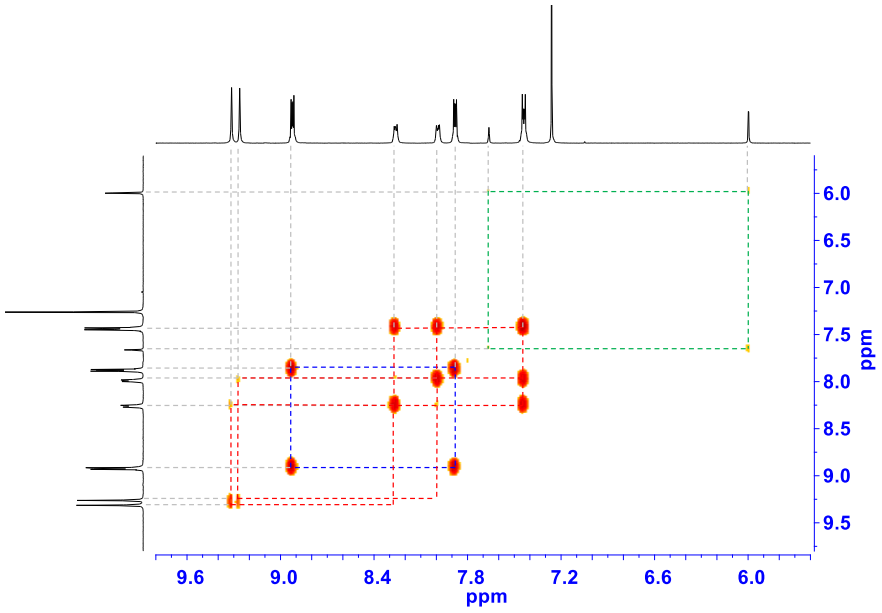

Figure 121. Zoom of the region between 9.8 ppm and 5.6 ppm of the H-H COSY NMR spectrum (500 MHz, $CDCl_3$) of **33** showing the correlations between the peripheral proton of the SubPc macrocycle (blue dashed lines), the protons of the pentacene moieties (red dashed lines) and the protons of the *meta*-phenylene spacer (green dashed lines).

2.3.2.2 Photophysical properties of SubPc-Pnc$_2$ conjugates featuring different spacers

The impact of the structural characteristics of the molecular spacer on the interchromophoric interactions within the four SubPc-Pnc$_2$ conjugates **33**-**36** was investigated through comprehensive photophysical assays. The photophysical studies discussed in this section were performed in collaboration with the research group of Prof. Dirk Guldi at Friederich-Alexander University in Erlangen, Germany.

Steady-state absorption studies

First of all, the absorption features in toluene of SubPc-Pnc$_2$ conjugates **33**-**36**, SubPc-Cl reference **1** and Pnc$_2$ precursors **29**-**32** were probed. The absorption characteristics of **1** have already been discussed in section 2.3.1.2. Regarding the starting Pnc$_2$ derivatives **29**-**32**, similarly to what observed for Pnc$_2$ **17**, their absorption spectra are dominated by short-wavelength absorptions in the 300-450 nm region as well as by long-wavelength absorptions in the 500-700 nm region, with long-wavelengths maxima at 659/600 nm (Figure 122).

In line with what observed for SubPc-Pnc_2 conjugates **26**-**28** in section 2.3.1.2, the absorption spectra of **33**-**36** are the linear superimposition of the spectra of the individual chromophores, namely SubPc and Pnc_2 (Figure 122). In other words, none of the investigated SubPc-Pnc_2 conjugates reveals any sizeable ground-state electronic communication between the SubPc and the Pnc_2. Remarkably, the absorption features of the two chromophores are complementary and cover nearly the whole visible region of the spectrum, that is, the conjugates are almost panchromatic. It is worth to note that the absorption spectra of **33**-**36** are virtually identical in terms of both absorption maxima and extinction coefficients. As a matter of fact, SubPc Q-band absorption maxima at 565, 564, 563 and 562 nm are observed for **33**, **34**, **35** and **36**, respectively, whereas the long-wavelength absorption maxima of the Pnc_2 unit are centered at 662/660 nm.

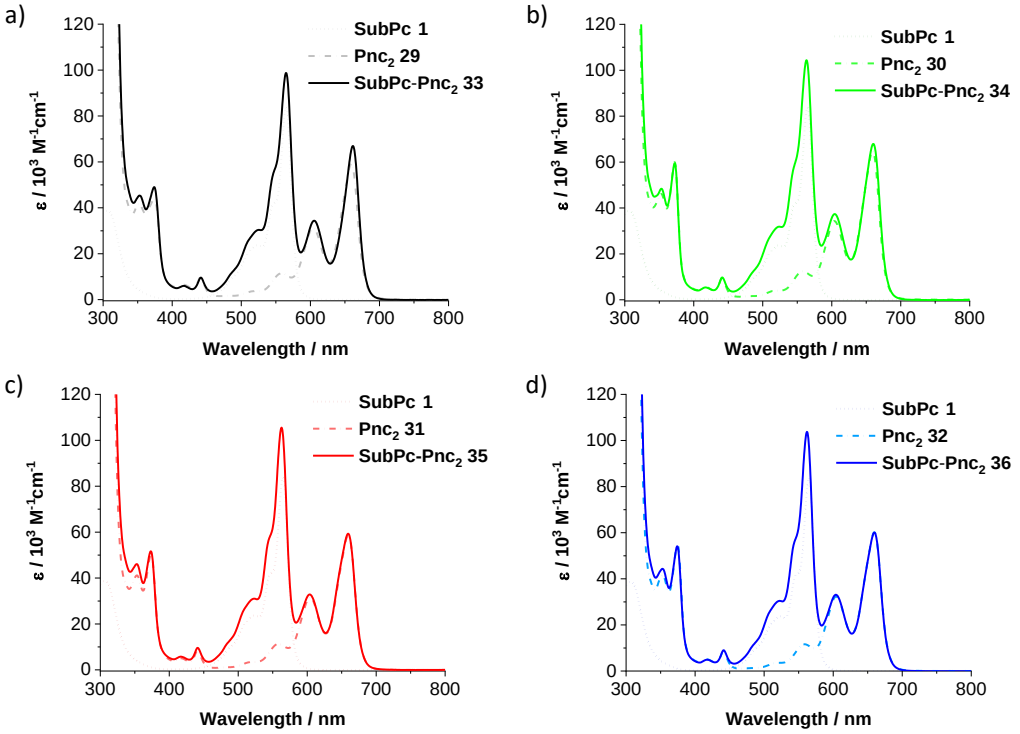

Figure 122. Steady-state absorption spectra of a) SubPc-Cl **1**, Pnc_2 **29** and SubPc-Pnc_2 **33**, b) SubPc-Cl **1**, Pnc_2 **30** and SubPc-Pnc_2 **34**, c) SubPc-Cl **1**, Pnc_2 **31** and SubPc-Pnc_2 **35**, d) SubPc-Cl **1**, Pnc_2 **32** and SubPc-Pnc_2 **36** in toluene.

Steady-state fluorescence studies

Different conclusions can be drawn from fluorescence experiments. Fluorescence quantum yields were determined using 1) for the SubPc fluorescence, Rhodamine 6G in ethanol (ϕ_F = 0.95[423]) and 2) for the Pnc$_2$ fluorescence, ZnPc in toluene (ϕ_F = 0.30[424]) as reference compounds. The experimental data obtained from UV-vis emission spectroscopy and TCSPC measurements in toluene with SubPc-Pnc$_2$ conjugates **33**-**36**, Pnc$_2$ references **29**-**32** and SubPc-Cl **1** are summarized in Table 18.

Table 18. Fluorescence emission maxima, fluorescence quantum yields and fluorescence lifetimes of Pnc$_2$ **29**-**32**, SubPc-Pnc$_2$ **33**-**36** and SubPc-Cl **1** in toluene.

	λ_{max} / nm		ϕ_F / %		τ_F	
Compound	**SubPc[a]**	**Pnc$_2$[b]**	**SubPc[a]**	**Pnc$_2$[b]**	**SubPc[a]**	**Pnc$_2$[b]**
29	-	664	-	1.47	-	<100 ps[c]
30	-	664	-	0.75	-	<100 ps[c]
31	-	664	-	1.03	-	<100 ps[c]
32	-	665	-	0.80	-	<100 ps[c]
33	571	665	0.05	1.06	<50 ps[c]	-
34	571	665	0.03	0.90	<50 ps[c]	-
35	570	664	0.12	1.19	<50 ps[c]	-
36	569	665	0.09	0.66	<50 ps[c]	-
1	570	-	28.81	-	3.35 ns	-

[a] Values refer to the SubPc-centered fluorescence. [b] Values refer to the Pnc$_2$-centered fluorescence. [c] Lifetime is below the resolution limit of the TCSPC setup.

In contrast to SubPc-Cl reference **1**, which exhibits a ϕ_F as high as 28.8% in toluene, upon photoexcitation of **33**-**36** into the SubPc Q-band region (*i.e.*, at 500 nm) a strongly quenched SubPc-centered fluorescence is observed, with fluorescence quantum yields on the order of 0.1% or lower (Figure 123 and Table 18). Similarly to what observed for SubPc-Pnc$_2$ derivatives **26**-**28** in section 2.3.1.2, emission from the SubPc in **33**-**36** is replaced by a weak Pnc$_2$ emission. As a matter of fact, fluorescence quantum yields on the order of 1% can be determined for the Pnc$_2$ emission in SubPc-Pnc$_2$ conjugates **33**-**36**. These experimental findings, along with fluorescence lifetimes relative to the SubPc-centered emission shorter than 50 ps as determined

from TCSPS experiments, infer that photoexcitation of the SubPc is followed by efficient i-FRET, which populates the Pnc_2 singlet excited state.

A closer look at the fluorescence data reveals some differences between the fluorescence quantum yields relative to the SubPc-centered emission in SubPc-Pnc_2 conjugates **33**-**36**. In particular, the fluorescence quantum yield for the SubPc emission is higher for **35** (*i.e.,* 0.12%) than for **33** (*i.e.*, 0.05%), which differs from the former for the lack of an aryl unit within the bridging unit (Table 18). The same trend is observed when shifting from **36** to **34** (*i.e.*, 0.09% *versus* 0.03%), which also differ to each other for the presence or absence of an additional aryl moiety within the molecular spacer, respectively. This suggests that the quenching of the SubPc-centered emission is dependent on the length of the spacer. Moreover, the flexibility of the linker in **34** and **36** enables a closer through-space approach than the rigidity of the spacer in **33** and **35**, yielding lower values of ϕ_F for the SubPc-centered emission.

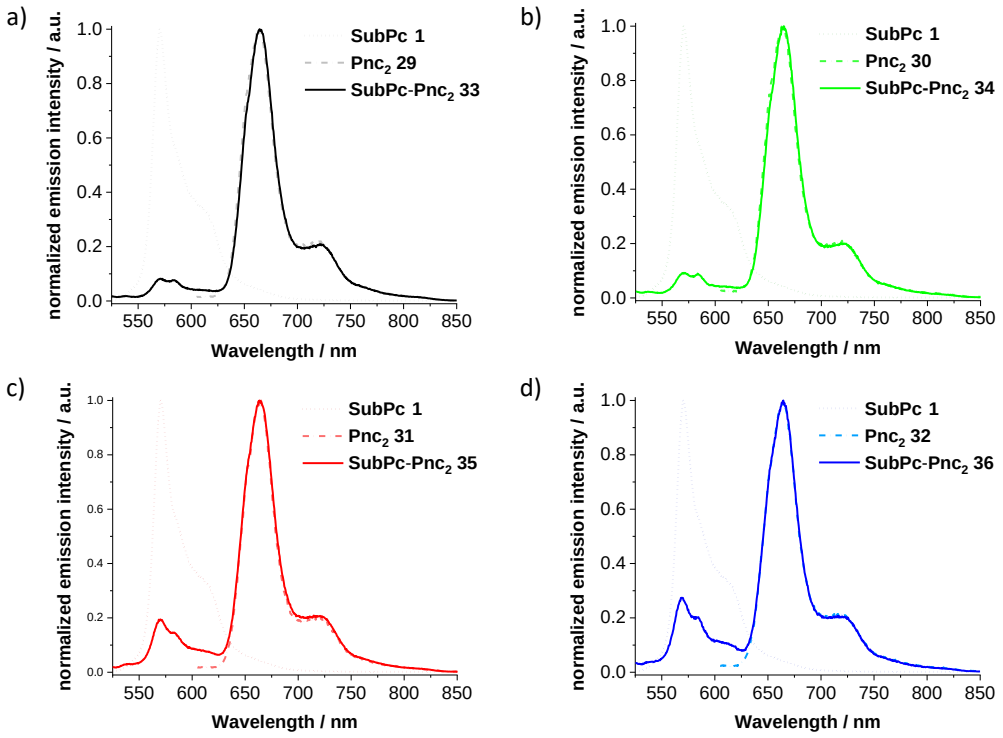

Figure 123. Steady-state fluorescence spectra (λ_{ex} = 500 nm) of a) SubPc-Cl **1**, Pnc_2 **29** and SubPc-Pnc_2 **33**, b) SubPc-Cl **1**, Pnc_2 **30** and SubPc-Pnc_2 **34**, c) SubPc-Cl **1**, Pnc_2 **31** and SubPc-Pnc_2 **36**, d) SubPc-Cl **1**, Pnc_2 **32** and SubPc-Pnc_2 **36** in toluene.

Transient absorption studies

Pump-probe experiments were performed in order to further elucidate the influence of the structural characteristics of the molecular spacer on the excited-state interactions within SubPc-Pnc$_2$ conjugates **33**-**36**.

First of all, the transient absorption features of Pnc$_2$s **29**-**33** were examined. The differential absorption spectra of **29**-**33** are very similar to each other. For all the investigated derivatives, photoexcitation at 632 nm in toluene leads to the instantaneous formation of the Pnc$_2$ singlet excited state. Exemplary fsTA spectra relative to Pnc$_2$s **29** and **31** are given in Figures 124 and 125. For these derivatives, the characteristics features of the Pnc$_2$ $^1(S_1S_0)$ state include minima at 600 and 660 nm as well as maxima at 450 and 510 nm. As the Pnc$_2$ singlet excited state decays, new transient features at *ca.* 448, 473, and 505 nm are observed, which are in excellent agreement with the triplet excited state fingerprints of dimeric pentacenes.[402] On the basis of these results and considering that the Pnc$_2$ $^1(S_1S_0)$ state decays on a timescale of several hundred picoseconds, we postulate that SF is operative *en route* towards the Pnc$_2$ triplet excited state, given the fact that spin-allowed i-SF is two orders of magnitude faster than spin-forbidden ISC. Finally, the ground state of the Pnc$_2$ moiety is recovered nearly quantitatively.

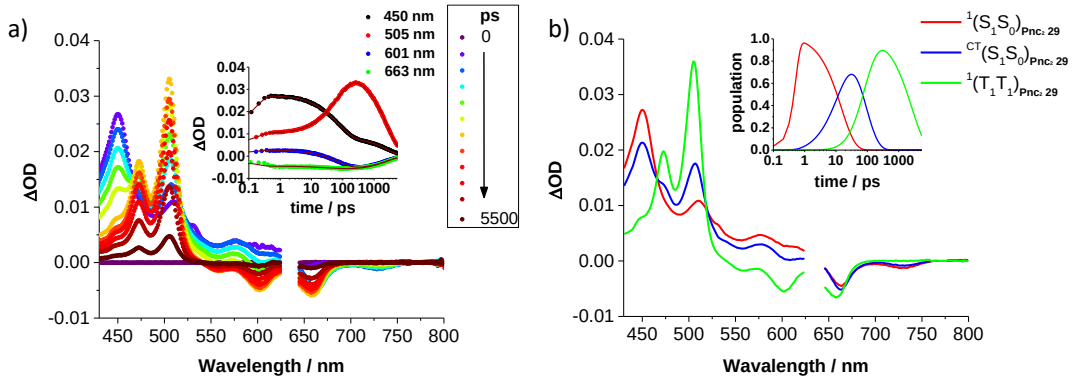

Figure 124. a) Differential absorption spectra (visible) obtained upon fsTA experiments (632 nm) of Pnc$_2$ **29** in toluene with time delays between 0 and 5500 ps at room temperature. Single wavelength kinetics at 450 (black), 505 (red), 601 (blue), and 663 nm (green) monitoring the dynamics of the singlet excited state ($^1(S_1S_0)$: 14.87 ps), intermediate state ($^{CT}(S_1S_0)$: 79.92 ps), and triplet excited state ($^1(T_1T_1)$: 2.63 ns), as well as fits to the data (red lines) are shown in the inset. b) Evolution associated spectra of the transient absorption data of **29** shown in (a). The red spectrum illustrates the initially formed Pnc$_2$ $^1(S_1S_0)$ state, while the blue and green spectra are those of the intermediate $^{CT}(S_1S_0)$ state and the multiexcitonic $^1(T_1T_1)$ state of Pnc$_2$, respectively. The inset depicts the relative populations of $^1(S_1S_0)$, $^{CT}(S_1S_0)$, and $^1(T_1T_1)$.

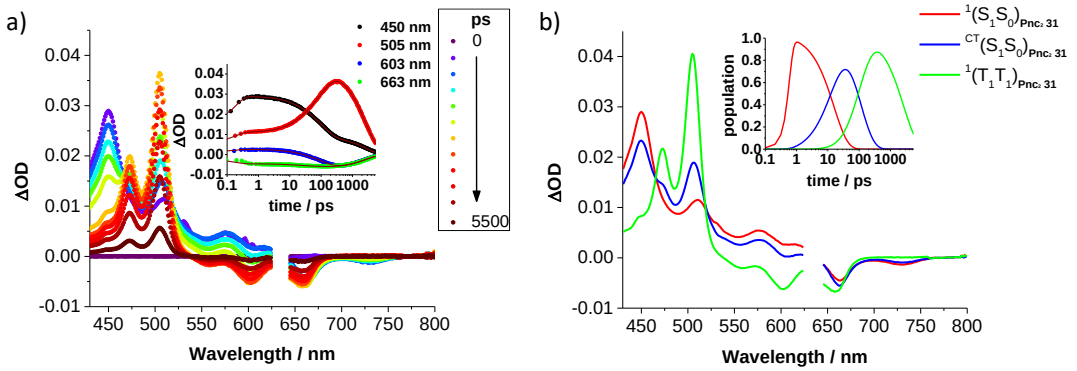

Figure 125. a) Differential absorption spectra (visible) obtained upon fsTA experiments (632 nm) of Pnc_2 **31** in toluene with time delays between 0 and 5500 ps at room temperature. Single wavelength kinetics at 450 (black), 505 (red), 603 (blue), and 663 nm (green) monitoring the dynamics of the singlet excited state ($^1(S_1S_0)$: 15.83 ps), intermediate state ($^{CT}(S_1S_0)$: 106.78 ps), and triplet excited state ($^1(T_1T_1)$: 2.66 ns) dynamics, as well as fits to the data (red lines) are shown in the inset. b) Evolution associated spectra of the transient absorption data of **31** shown in (a). The red spectrum illustrates the initially formed Pnc_2 $^1(S_1S_0)$ state, while the blue and green spectra are those of the intermediate Pnc_2 $^{CT}(S_1S_0)$ state and the multiexcitonic Pnc_2 $^1(T_1T_1)$ state, respectively. The inset depicts the relative populations of $^1(S_1S_0)$, $^{CT}(S_1S_0)$, and $^1(T_1T_1)$.

Global analyses of the raw data required the use of a three-species kinetic model. The first and third species are the Pnc_2 singlet and triplet excited states, which lifetimes in **29**-**33** are in the range of 16 ± 2 ps and 2.5 ± 0.2 ns, respectively (Table 19). On the other hand, the nature of the second species can be related to that of a singlet excited state mixed with a CT character, $^{CT}(S_1S_0)$, which mediates i-SF. This is in line with what observed for Pnc_2 **17** in section 2.3.1.2.

Surprisingly, the structural characteristics of the spacer have an influence on the rate of i-SF. In this connection, it is interesting to note the differences in lifetimes of the Pnc_2 $^{CT}(S_1S_0)$ state when comparing **29**/**30** (*i.e.*, 84 ± 5 ps) with **31**/**32** (*i.e.*, 105 ± 2 ps), that is, when adding an aryl unit in the molecular structure of the *meta*-phenylene linker tethering the two pentacene moieties. In other words, the additional aryl group in **31**/**32** slows down the formation of the Pnc_2 triplet excited state with respect to what observed in **29**/**30**. The impact of the spacer on the rate of i-SF is rather curious considering that in all the investigated derivatives the spatial orientation of the two pentacene moieties is identical, as dictated by the *meta*-phenylene bridge. A possible rationale for this finding is based on electronic considerations, and will be discussed in section 2.3.2.3. Regarding TQYs, values around 162-169% were determined for **29**-**32**, which are similar to that previously observed for Pnc_2 **17**.

Table 19. Summary of kinetic data of Pnc$_2$s **29**-**32**, SubPc-Pnc$_2$ conjugates **33**-**36**, and SubPc-Cl **1** obtained from fsTA and nsTA as well as TQYs in toluene.

	fsTA				nsTA		
	$^1(S_1)_{SubPc}$	$^1(S_1S_0)_{Pnc2}$	$^{CT}(S_1S_0)_{Pnc2}$	$^1(T_1T_1)_{Pnc2}$	$^1(S_1)_{SubPc}$	$^3(T_1)_{SubPc}$	$TQY^{a,b}$
29	-	14.87 ps	79.92 ps	2.63 ns	-	-	169%
30	-	17.13 ps	88.83 ps	2.50 ns	-	-	167%
31	-	15.83 ps	106.78 ps	2.66 ns	-	-	162%
32	-	16.62 ps	104.92 ps	2.68 ns	-	-	165%
33	0.90 ps	19.04 ps	72.64 ps	2.28 ns	n. r.[c]	-	173%
34	0.70 ps	7.28 ps	77.38 ps	2.51 ns	n. r.[c]	-	165%
35	3.46 ps	17.38 ps	118.26 ns	2.91 ns	n. r.[c]	-	156%
36	1.28 ps	14.74 ps	104.09 ns	2.89 ns	n. r.[c]	-	161%
1	n. r.[c]	-	-	-	3.55 ns	51.64 µs	-

[a] Determined following the intensification of the transient bleaching of the Pnc$_2$ moiety and comparing the relative intensities of the evolution associated spectra for the Pnc$_2$ $^1(S_1S_0)$ and the $^1(T_1T_1)$ state, respectively. [b] An error margin in the range of ±20% may be considered when determining the TQYs due to residual contributions from SubPc centered bleaching/stimulated emission. [c] n. r. = not resolvable. Lifetimes are either too long to be resolved with fsTA or too short to be resolved with nsTA.

Then, SubPc-Cl reference **1** was probed. In line with what observed for SubPc-Cl derivatives in section 2.3.1.2 (Figures 113 and 114), ISC from the SubPc singlet excited state to populate the SubPc triplet excited state follows photoexcitation at 530 nm, with lifetimes of the $^1(S_1)$ state and $^3(T_1)$ state of 3.6 ns and 51.6 µs, respectively.

The same SubPc-based singlet excited state fingerprints were also detected in pump-probe experiments with SubPc-Pnc$_2$ conjugates **33**-**36** upon 530 nm photoexcitation. Nevertheless, instead of affording the corresponding SubPc $^3(T_1)$ state as observed for SubPc-Cl **1**, these transform *via* i-FRET in less than 10 ps into a transient intermediate, which resembles the Pnc$_2$ singlet excited state. Subsequently, the formation of minima at, for example, 560, 600, and 658 nm as well as maxima at 448, 473, and 505 nm for **33** and **35**, assists in corroborating the formation of the Pnc$_2$ triplet excited state *via* i-SF (Figures 126 and 127). In other words, in derivatives **33**-**36** i-FRET funnels excited-state energy from the SubPc singlet excited state (which is populated by photoexcitation) to the Pnc$_2$ ground state, populating the Pnc$_2$ singlet excited state. The latter is subsequently converted into a pair of correlated triplet excited states through

i-SF. The deactivation cascade of SubPc-Pnc$_2$ conjugates **33**-**36** upon excitation of the SubPc unit resembles that observed for derivatives **26**-**28** in section 2.3.1.2, for which the *modus operandi* was a quantitative, unidirectional and ultrafast i-FRET from the SubPc to the Pnc$_2$, followed by almost quantitative i-SF (Figure 117).

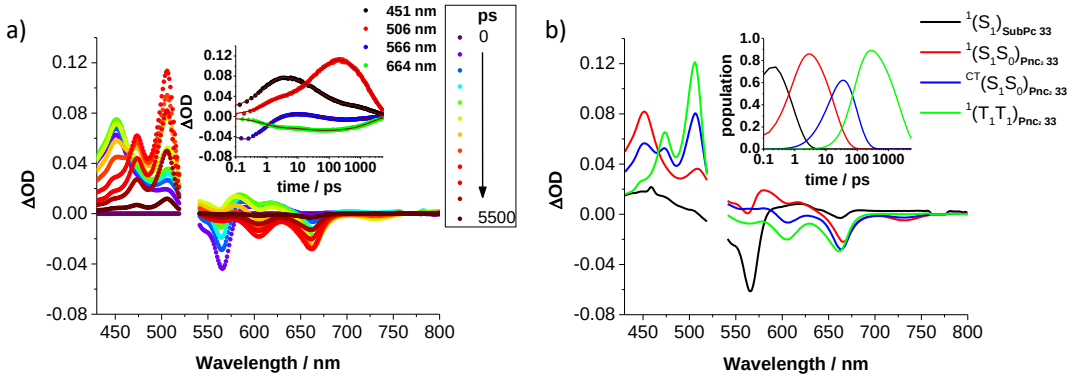

Figure 126. a) Differential absorption spectra (visible) obtained upon fsTA experiments (530 nm) of SubPc-Pnc$_2$ **33** in toluene with several time delays between 0 and 5500 ps at room temperature. Single wavelength kinetics at 451 (black), 506 (red), 566 (blue), and 664 nm (green) monitoring the singlet excited state ($^1(S_1)$: 0.90 ps), singlet excited state ($^1(S_1S_0)$: 19.04 ps), intermediate state ($^{CT}(S_1S_0)$: 72.64 ps), and triplet excited state ($^1(T_1T_1)$: 2.28 ns) dynamics, as well as fits to the data (red lines) are shown in the inset. b) Evolution associated spectra of the transient absorption data of **33** shown in (a). The black spectrum illustrates the initially formed SubPc $^1(S_1)$ state, while the red, blue, and green spectra are those of the Pnc$_2$ $^1(S_1S_0)$ state, the intermediate Pnc$_2$ $^{CT}(S_1S_0)$ state, and the multiexcitonic Pnc$_2$ $^1(T_1T_1)$ state, respectively. The inset depicts the relative populations of $^1(S_1)$, $^1(S_1S_0)$, $^{CT}(S_1S_0)$, and $^1(T_1T_1)$.

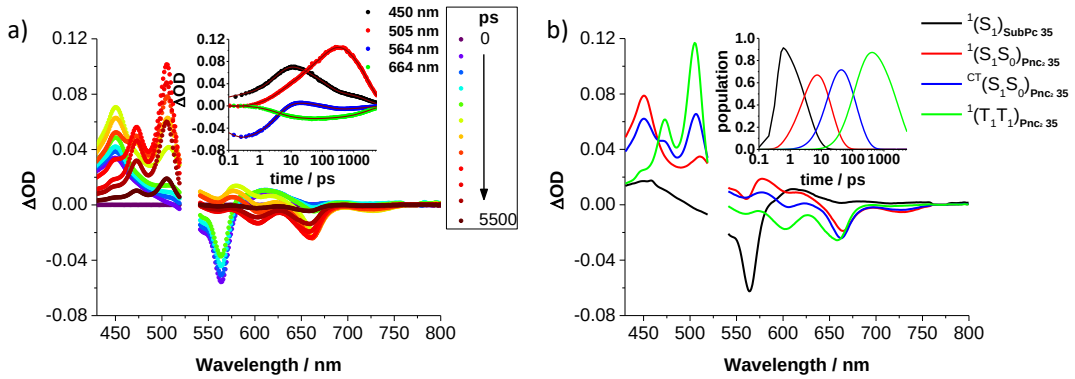

Figure 127. a) Differential absorption spectra (visible) obtained upon fsTA experiments (530 nm) of SubPc-Pnc$_2$ **35** in toluene with several time delays between 0 and 5500 ps at room temperature. Single wavelength kinetics at 450 (black), 505 (red), 564 (blue), and 664 nm (green) monitoring the dynamics of the singlet excited state ($^1(S_1)$: 3.46 ps), singlet excited state ($^1(S_1S_0)$: 17.38 ps), intermediate state ($^{CT}(S_1S_0)$: 118.26 ps), and triplet excited state ($^1(T_1T_1)$: 2.91 ns) dynamics, as well as fits to the data (red lines) are shown in the inset. b) Evolution associated spectra of the transient absorption data of **35** shown in (a). The black spectrum illustrates the initially formed SubPc $^1(S_1)$ state, while the red, blue, and green spectra are those of the Pnc$_2$ $^1(S_1S_0)$ state, the intermediate Pnc$_2$ $^{CT}(S_1S_0)$ state, and the multiexcitonic Pnc$_2$ $^1(T_1T_1)$ state, respectively. The inset depicts the relative populations of $^1(S_1)$, $^1(S_1S_0)$, $^{CT}(S_1S_0)$, and $^1(T_1T_1)$.

A kinetic model based on four species was employed for global analyses. The first species is the SubPc $^1(S_1)$ state. In line with the conclusions on **29**-**32**, the second and fourth species are the singlet and triplet excited states of Pnc$_2$, respectively, whereas the third species is the i-SF mediating state.

The lifetime of the first species, namely the SubPc singlet excited state, varies from 0.70 ps for **34** to 0.90 ps for **33**, 1.28 ps for **36** and 3.46 ps for **35** (Table 19). This trend compares well with that observed for the fluorescence quantum yields of the SubPc-centered emission in **33**-**36** (Table 18), and allows to outline the impact of the structural characteristics of the spacer on the dynamics of i-FRET. On one hand, the reduced spacer length in **33** compared to **35** and in **34** compared to **36** affords higher rate constants for i-FRET. On the other hand, the increased flexibility of the linkage in **34** compared to **33** and in **36** compared to **35** enables faster i-FRET.

FRET distances *R* for SubPc-Pnc$_2$ derivatives **33**-**36**, that is, the distances between the SubPc and the Pnc$_2$ units within the conjugates, were calculated from the experimental data by means of Equations 19-23 (please refer to section 2.3.1.2 for further details).[277,426] A summary of the parameters used for FRET distance calculations as well as the resulting *R* values are reported in Table 20. As in section 2.3.1.2, experimental lifetimes of the energy D-A conjugates **33**-**36**

obtained from fsTA experiments and experimental lifetime of the energy donor **1** obtained from TCSPS measurements were employed for the determination of the FRET distances. In this case, for κ^2 we used the values obtained from computational studies (section 2.3.2.3), whereas the refractive index n was taken as 1.496 for toluene.[428] The calculated FRET distances follow essentially the same trend observed for the ϕ_Fs relative to the SubPc-centered emission and the fluorescence lifetimes of the SubPc singlet excited state in the SubPc-Pnc_2 conjugates **33**-**36**, and are in line with what expected on the basis of the structural characteristics (namely, length and flexibility) of the molecular spacers.

Table 20. Summary of the parameters used for the FRET rate constants calculation and resulting values in toluene.

	τ_{DA} / ps (fsTA)	τ_D / ns (TCSPC)	ϕ_F	J / $M^{-1}cm^{-1}nm^4$	R_0 / Å	R / Å	k_{FRET} / 10^{11} s^{-1}
33	0.90	3.35	0.29	$2.31 \cdot 10^{15}$	43.54	11.06	11.11
34	0.70	3.35	0.29	$2.52 \cdot 10^{15}$	46.68	11.37	14.29
35	3.46	3.35	0.29	$2.32 \cdot 10^{15}$	46.05	14.64	2.89
36	1.28	3.35	0.29	$2.38 \cdot 10^{15}$	47.59	13.13	6.75

On the other hand, the dynamics following FRET are essentially unaffected by the presence of the SubPc. As a matter of fact, singlet and triplet excited state lifetimes of Pnc_2 in the range of 15 ps and 2.5 ns, respectively, are determined **33**-**36**, which are similar to those observed for Pnc_2 **29**-**32** (Table 19).

2.3.2.3 Theoretical calculations on SubPc-Pnc_2 conjugates featuring different spacers

To rationalize the impact of the structural characteristics of the molecular spacer on i-FRET and i-SF dynamics, theoretical calculations were carried out in collaboration with Prof. Timothy Clark at Friedrich-Alexander University Erlangen-Nürnberg in Erlangen, Germany.

Geometries of SubPc-Pnc_2 **33**-**36** were optimized at the B3LYP[429]-D3[385]/6-31G(d)[429] level of DFT. Additional geometry optimizations using a polarizable continuum model for solvation in toluene gave little changes compared to gas-phase calculations.[430] The gas-phase structures of SubPc-Pnc_2 **33**-**36** are shown in Figure 128. The most important interactions between the chromophore units are C-H···aromatic hydrogen bonds. In the most stable structure of **33**, one pentacene acts

[429] W. J. Hehre, R. Ditchfield, J. A. Pople, *J. Chem. Phys.* **1971**, *54*, 724-728.
[430] J. Tomasi, B. Mennucci, R. Cammi, *Chem. Rev.* **2005**, *105*, 2999-3094.

as H-bond donor towards the SubPc, whereas in **34** the roles are reversed. Inter-pentacene H-bonds dominate in **35**, while the most stable conformation of **36** features the SubPc as H-bond donor towards one of the pentacenes. Notably, in the latter derivative, interchromophoric interactions cause the linker to fold and, in turn, bring the SubPc and Pnc$_2$ chromophores closer together. Thus, for this conjugate, an alternative extended conformation was investigated (Figure 128), which was found to be approximately 10 kcal mol^{-1} less stable than the folded one both in the gas phase and in toluene. However, it should be considered that an aromatic solvent like toluene is likely to replace the intramolecular C-H···aromatic hydrogen bonds responsible for the folding of the spacer and, thereby, to stabilize the stretched conformation. In this connection, it is worth to mention that we do not expect the continuum solvent model to be able to reproduce this effect.

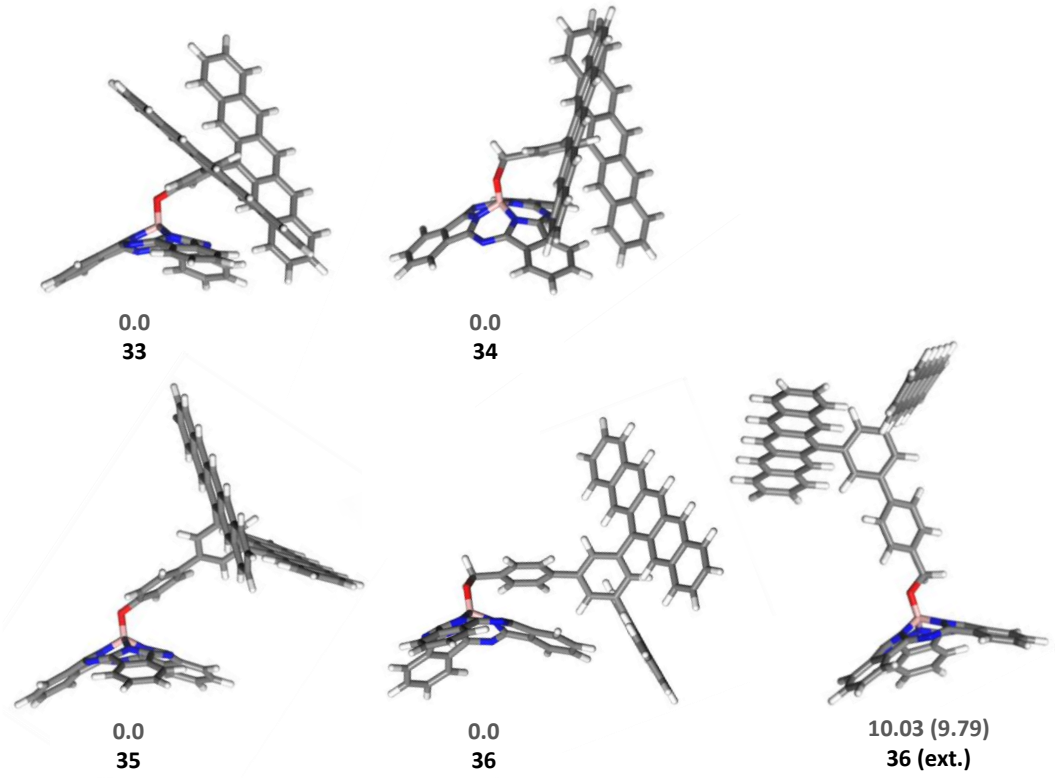

Figure 128. Most stable optimized geometries of **33**-**36** and optimized geometry of **36** in the extended conformation. Relative gas phase energies in kcal mol^{-1} are given below the structures. For the optimized geometry of **36** in the stretched conformation, the corresponding energy with a polarizable continuum model solvent simulation in toluene is given in parentheses.

In order to examine the excited states, AM1 configuration-interaction calculations with an implicit solvent treatment were performed on the optimized geometries of **33**-**36**.[431,432] For **36**, the stretched conformation was also considered. The results are summarized in Table 21. In line with what observed in the experimental measurements discussed in section 2.3.2.2, the state energies are essentially the same for **33**-**36** in all the investigated conformations. The two lowest singlet states are local pentacene excitations, one for each pentacene, and are generally localized on one unit. The third lowest singlet state is, in contrast, a local SubPc excitation, and is approximately 0.29 eV higher in energy than the pentacene singlet excited states. The calculated gap between the two types of local excitation, on the order of a few tenths of an electron volt, indicates that i-FRET is energetically feasible in the investigated systems.

Table 21. Calculated vertical absorption energies, interchromophore distances and angles between transition dipoles for compound **33**-**36**. The results are shown for the most stable conformation in every case except **36**, for which the extended conformation is also shown.

	Excitation Energy (eV)			R (Å)	Angle (°)	κ^2/R^6
	Pentacene	SubPc	Δ			
33	2.080 2.093	2.378	0.285	2.776	35	0.001268
34	2.087 2.102	2.369	0.267	2.661	62	0.002277
35	2.099 2.102	2.393	0.291	6.492	62	$1.08\cdot10^{-5}$
36 ext.	2.108 2.109	2.395	0.286	12.635	8	$2.36\cdot10^{-7}$
36	2.091 2.107	2.393	0.286	2.725	82	0.002937

[431] M. J. Dewar, E. G. Zoebisch, E. F. Healy, J. J. Stewart, *J. Am. Chem. Soc.* **1985**, *107*, 3902-3909.
[432] G. Rauhut, T. Clark, T. Steinke, *J. Am. Chem. Soc.* **1993**, *115*, 9174-9181.

However, i-FRET not only depends on the energy difference, which is essentially constant in **33**-**36** and is neglected in the analysis, but also on the distance between the chromophores and the angle between the transition dipoles. For SubPc-Pnc$_2$ conjugates **33**-**36**, orientation factors κ^2 were calculated from the angles given in Table 21.[427] As can be deducted from Equations 21 and 24 (section 2.3.1.2), κ^2/R^6 should correlate with the i-FRET rate. Figure 129 shows the correlation if we assume as representative the stretched conformation of **36**. The calculated results are consistent with the experiments except for **36**, for which we infer that specific solvation effects stabilize the more extended conformations in toluene.

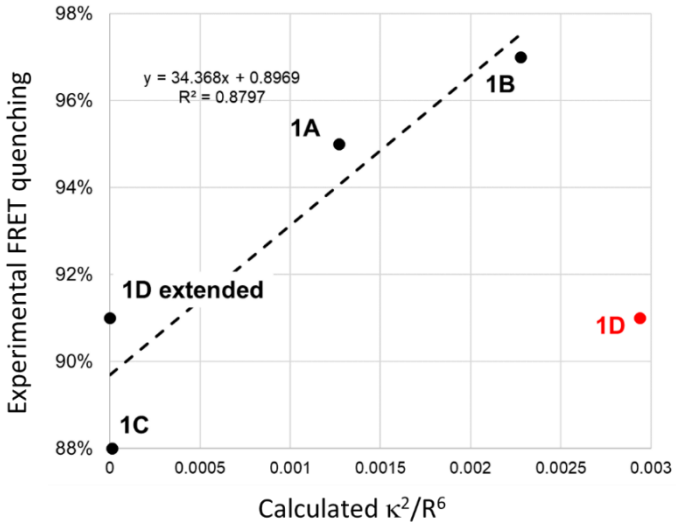

Figure 129. Correlation between the experimental FRET quenching and calculated κ^2/R^6 for **33**-**36** assuming the extended conformation for **36**.

Besides the effect on i-FRET rates, the molecular structure of the spacer has an influence also on i-SF dynamics, as suggested by transient absorption measurements (section 2.3.2.2). This experimental finding may be rationalized in terms of electronic considerations. In other words, slight differences in the electronic distribution of the spacer are possible as a result of the different substitution. Orbital delocalization calculations provided decisive support to this hypothesis. The first pentacene-based acceptor orbital for **33** and **35** are shown in Figure 130 as representative examples. In particular, **33** shows only very limited electronic delocalization, while **35** exhibits a pentacene acceptor orbital that is fairly delocalized over both pentacenes and the bridging phenyl. This is a consequence of a quinone-like conjugation pattern in **35** that allows the pentacenes to interact and is demonstrated most clearly by the optimized bond lengths corresponding to the bonds between the pentacenes and the bridging phenyl group.

Whereas in **33** these are typical C–C single bonds, with bond lengths of 1.540 and 1.542 Å, they shortened remarkably to 1.491 and 1.495 Å in **35**, indicating strong conjugation between the bridging phenyl and the pentacenes. As a matter of fact, conjugation in **35** is so strong that it partially suppresses SF.

Although it should be mentioned that the interpretation is difficult because of the complex nature of the excitations, in terms of individual single excitations, both low-lying singlet and triplet excited states of **29** have higher dipole moments than the ground state by 0.7-1.0 Debye, compared with a difference of 27-31 Debye for the CT states. The energy difference between the lowest excited singlet and the lowest singlet CT state is 0.5 eV lower in **29** than in **31**.

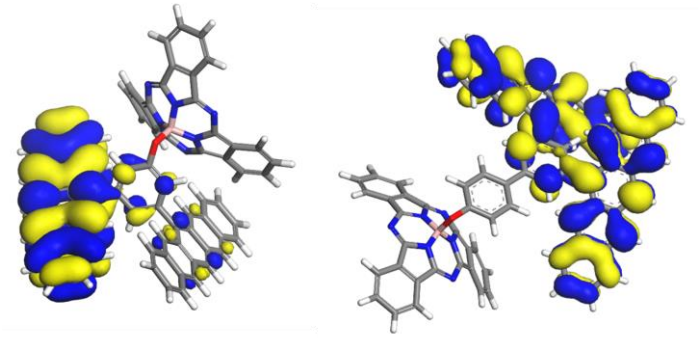

33 **36**

Figure 130. First pentacene-based acceptor orbitals (LUMO+2) for **33** and **35**, respectively.

2.4 Summary and conclusions

In this Chapter, we presented the design, synthesis and study of a series of novel multicomponent systems in which a synergy between nearly panchromatic absorption throughout most of the visible region of the solar spectrum and SF has been realized through integration of a light harvesting moiety, namely a SubPc, and a SF chromophore, namely a Pnc_2.

The design of the investigated derivatives was aimed to ensure: 1) the complementarity between the absorption of the antenna unit and the absorption of the SF-performing unit, in order to optimize the efficiency of light harvesting; 2) a good overlap between the fluorescence emission of the light-harvesting unit and the absorption of the SF moiety, and, in turn, a fast i-FRET towards the latter upon excitation of the antenna; 3) the absence of any electron transfer interaction between the chromophores, in order to guarantee high i-SF quantum yields; 4) the efficiency of i-SF within the energy acceptor moiety.

To this end, properly functionalized SubPcs and 6,6'-linked, *meta*-phenylene tethered Pnc_2 units were chosen for the preparation of the target conjugates. The starting Pnc_2s were linked to the axial position of the macrocycle by substitution reaction of the apical halogen in SubPc-Cl precursors *via* generation of an activated SubPc-OTf intermediate.

Steady-state absorption and fluorescence studies along with transient absorption measurements were carried out to shed light on the interchromophoric interactions within the SubPc-Pnc_2 conjugates. Notably, all the investigated derivatives feature a nearly panchromatic absorption across the visible region of the solar spectrum, and no, or only marginal, ground-state interactions between the SubPc and the Pnc_2 units. Remarkably, photoexcitation of the SubPc moiety activates a sequence of i-FRET and i-SF within the SubPc-Pnc_2 systems. As a matter of fact, the SubPc unit acts as energy-donor antenna by means of singlet-singlet i-FRET, which funnels energy unidirectionally to the Pnc_2 where efficient i-SF takes place (Figure 131).

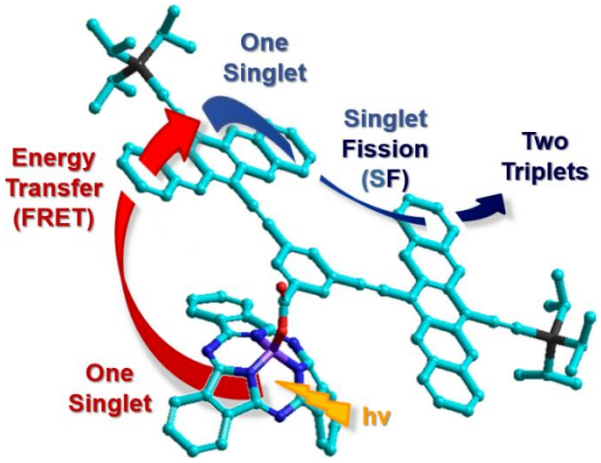

Figure 131. Cartoon depicting the activation of a sequence of i-FRET and i-FS upon photoexcitation of the SubPc unit in SubPc-Pnc_2 conjugates.

Control over FRET dynamics was reached by tailoring the chemical structure the SubPc-Pnc_2 conjugates and, in particular, by means of either a modular SubPc approach or rational spacer design.

In the first series of SubPc-Pnc_2 conjugates (*i.e.*, **26**-**28**), the energy-donor characteristics of the SubPc were modulated in order to tune i-FRET. To this end, the SubPc periphery was decorated with different substituents to fine-tune the optical properties of the macrocycle and, in turn, the overlap between SubPc emission and Pnc_2 absorption, which contributes to determine the rate of FRET. Three different SubPcs (namely, perhydrogenated, triphenoxy-substituted and hexathiooctyl-substituted) were integrated as light harvester energy donors, whereas the energy acceptor Pnc_2 was anchored to the central boron atom of the macrocycle through a carboxylate group. Photophysical measurements revealed only subtle differences between the i-FRET rate constants for the three SubPc-Pnc_2 conjugates. This is due to the fact that the bathochromic shift of the SubPc fluorescence observed when moving from the hydrogenated species to the thioether-substituted derivative *via* the phenoxy-functionalized conjugate is compensated by lower fluorescence quantum yields, thus resulting in minor changes in terms of i-FRET dynamics.

In the second sequence of SubPc-Pnc_2 conjugates (*i.e.*, **33**-**36**), the molecular spacer rather than the energy-donor SubPc was tailored in order to provide control over the interchromophoric interactions. In particular, the distance and orientation between the two chromophores were modulated by tailoring the length and flexibility of the bridging unit. Four different SubPc-Pnc_2

conjugates were prepared and investigated, in which a perhydrogenated SubPc was linked *via* different molecular spacers to the Pnc_2 moiety. Comprehensive photophysical assays indicated that the structural features of the spacer have an appreciable impact on i-FRET. As a matter of fact, the quenching of the SubPc-centered emission was found to be dependent on the length of the spacer, being higher for derivatives lacking an additional aryl moiety within the bridging unit (namely, **33** and **34**). Moreover, the flexibility of the linker in **34** and **36** enables a closer through-space approach in comparison with **33** and **35**, respectively, which results in lower fluorescence quantum yields of the SubPc-centered emission. The experimental trend for the lifetimes of the SubPc singlet excited state in SubPc-Pnc_2 conjugates **33**-**36** (*i.e.*, **34** < **33** < **36** < **35**) compares well with that observed for ϕ_F values, indicating that both a reduced length of the spacer and an increased flexibility of the linkage enable faster i-FRET. The results of theoretical calculations are consistent with the experiments, corroborating the importance of the molecular spacer on the regulation of i-FRET dynamics.

Surprisingly, the structural characteristics of the spacer were found to have a profound impact not only on i-FRET, but also on i-SF dynamics. As a matter of fact, the presence of an additional aryl groups slows down SF by a factor of ca. 1.6. This experimental finding may be rationalized taking into account the existence of slight differences in the electronic make-up of the spacer as a consequence of the different substitution. In particular, theoretical calculations indicated that whereas **33** exhibits only very limited delocalization of the first pentacene-based acceptor orbital, a quinone-like conjugation pattern in **35** affords a pentacene-based acceptor orbital that is fairly delocalized over both pentacenes and the bridging phenyl. In other words, conjugation in **35** is so strong that it partially suppresses SF.

Overall, the results presented in this Chapter constitute a step forward towards the optimization of the molecular design for the panchromatic activation of molecular SF, as they show the possibility to initiate i-SF in a spectral range that varies from 300 to 700 nm. The study of FRET-activated i-SF in model molecular systems such the ones investigated in this Chapter is of crucial importance in view of the potential exploitation of SF in photovoltaics, as it constitutes a promising strategy to enhance photon management and, in turn, improve the performances of solar energy conversion devices.

2.5 Experimental section

2.5.1 Materials and methods

Chemicals (reagent grade) and solvents (synthetic grade, anhydrous, HPLC grade, spectroscopy grade and deuterated) were purchased from Aldrich Chemical, Alfa Aesar, Acros Organics, TCI and Scharlau. Chemical reagents were used without further purification. Synthetic grade solvents were used for chemical reactions and column chromatography purifications and anhydrous solvents were used for reactions under dry conditions. Additionally, some solvents were further dried with previously activated molecular sieves (3 or 4 Å), or with a solvent purifying system by Innovative Technology Inc. MD-4-PS. Oxygen- and moisture-sensitive reactions were carried out using standard Schlenk line techniques.

Chromatography: the monitoring of the reactions has been carried out by thin layer chromatography (TLC), employing aluminum sheets coated with silica gel type 60 F254 (0.2 mm thick, Merck). The analysis of the TLCs was carried out with a UV lamp of 254 and 365 nm. Column chromatography was performed using silica gel (230-400 mesh, 0.040-0.063 mm, Merck). Preparative liquid chromatography was carried out on 20 × 20 cm glass plates precoated with silica gel 60 F254 0.5 mm (Merck). Size exclusion chromatography was performed on Bio-Beads^{TM} S-X1 Support (200-400 mesh). Eluents are indicated for each particular case.

Nuclear Magnetic Resonance (NMR): NMR spectra were recorded with a Bruker AVANCE 300 (300 MHz), a Bruker AVANCE-II 300 (300 MHz), and a Bruker DRX-500 (500 MHz) instruments in the Organic Chemistry Department of UAM or in the Interdepartmental Investigation Service of UAM. The deuterated solvent employed is indicated for each case. Chemical shifts (δ) are reported in ppm, and coupling constants (J) are reported in hertz (Hz). For ^{1}H-NMR and ^{13}C-NMR spectra, δ are measured relative to residual solvent signals using literature reference values.[379] The following abbreviations are used to indicate the multiplicity in ^{1}H-NMR spectra: s, singlet; d, doublet; t, triplet; q, quartet; quint, quintet; m, multiplet.

Mass Spectrometry (MS) and High-Resolution Mass Spectrometry (HRMS): Matrix Assisted Laser Desorption/Ionization-Time of Flight (MALDI-TOF) mass spectra were recorded in the Interdepartmental Investigation Service of UAM, using a Bruker ULTRAFLEX III spectrometer equipped with a Nd:YAG laser operating at 355 nm. The different matrixes employed are indicated for each spectrum. Mass spectrometry data are expressed in *m/z* units.

Steady State Absorption and Fluorescence Spectroscopy: steady-state absorption spectra were recorded in the Organic Chemistry Department of UAM and at Friederich-Alexander University in Erlangen, employing a V660 spectrophotometer from Jasco and a Lambda 2

spectrophotometer from Perkin Elmer. Steady-state fluorescence measurements were carried out with a FluoroMax®-3 fluorometer from Horiba Jobin Yvon. Fluorescence quantum yields were determined by means of gradient analyses. Spectroscopic grade solvents were used for spectroscopic measurements.

Transient absorption Spectroscopy: Femtosecond and nanosecond transient absorption spectra were recorded at Friederich-Alexander University in Erlangen using transient pump-probe spectroscopy. Transient absorption spectra were recorded using transient absorption pump-probe detection systems (HELIOS and EOS, Ultrafast Systems). The probe beam consisted of white light (~420-800/1500 nm), generated by focusing a fraction of the 1000 (1050) Hz Ti:Sapphire output (Clark-MXR, CPA-2110 (CPA-2101), 775-nm fundamental, ~150 fs pulse width) onto a sapphire disk (fsTA, 2 mm and 10 mm). Unconverted 775-nm intensity was minimized by using a 750-nm low pass filter or an 850-nm long pass filter for the visible and the near-infrared region, respectively. For nsTA, the white light (~370-900/1600 nm) was generated by a photonic crystal fiber supercontinuum laser source (1064 nm fundamental, 2 kHz, ~1 ns pulse width). The pump pulses at 530 (532) and 632 (633) nm were generated with a non-collinear optical parametric amplifier (NOPA; Clark-MXR).

Time-correlated single photon counting (TCSPC). Fluorescence lifetimes were determined at Friederich-Alexander University in Erlangen by time-correlated single photon counting (TCSPC) technique using a FluoroLog3 emission spectrometer (Horiba) equipped with an R3809U-58 MCP (Hamamatsu) and a SuperK Extreme high-power supercontinuum fiber laser EXB-6 (NKT) exciting at 530, 532 and 632 nm (~150 ps pulse width).

Infrared Spectroscopy (FT-IR): infrared spectra were recorded in the Interdepartmental Investigation Service of UAM with a Bruker IFS66v FTIR spectrometer.

Melting point (MP): melting points were measured in open-end capillary tubes by using a Büchi 504392-S apparatus, and are uncorrected.

Theoretical calculations: geometries were optimized at the B3LYP[383]/6-31G(d)[429] level of DFT with Grimme's D3 dispersion correction.[385] Absorption spectra were calculated using the AM1 semiempirical Hamiltonian[431] using a singles-only configuration interaction (CIS) with 32 occupied and 32 virtual orbitals in the active space. FRET orientation factors κ^2 were calculated according to Loura[427] using the AM1-CIS transition dipoles for the relevant excited singlets from the ground state.

2.5.2 Synthetic procedures

2.5.2.1 Synthetic procedures for the preparation of the SubPc-Pnc$_2$ conjugates featuring different peripheral substituents

4-Phenoxyphthalonitrile **18**[433]

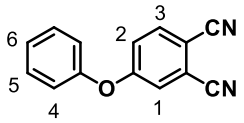

Phenol (1.10 g, 12 mmol) was added to a suspension of 4-nitrophthalonitrile (2.10 g, 12 mmol) and dry K_2CO_3 (2.50 g, 18 mmol) in dry dimethylacetamide (DMAC) (20 mL) under argon atmosphere. The resulting mixture was stirred at 90 °C for 24 h and subsequently poured onto 100 of cold water. The precipitate was collected by filtration and subjected to column chromatography on silica gel using DCM/hexane 2:3 (v/v) as eluent. In this way, 4-phenoxyphthalonitrile **18** was obtained as a white solid in 92% yield (2.46 g).

^{1}H-NMR (300 MHz, $CDCl_3$): δ (ppm) = 7.72 (d, $^3J_{H\text{-}H}$ = 8.2 Hz, 1H; H-3), 7.48 (dd, $^3J_{H\text{-}H}$ = $^3J_{H\text{-}H}$' = 7.6 Hz, 2H; H-5), 7.35-7.20 (m, 3H, H-1; H-2, H-6), 7.08 (d, $^3J_{H\text{-}H}$ = 7.6 Hz, 2H; H-4).

4,5-Dichlorophthalic anhydride **19**[434]

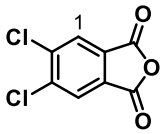

A solution of 4,5-dichlorophthalic acid (15.00 g, 64 mmol) in acetic anhydride (25 mL) was heated to reflux while distilling the acetic acid formed in the reaction. After 5 h, the remaining acetic acid was removed by vacuum distillation. The solid obtained was stirred over 12 h in petroleum ether, and subsequently filtered and thoroughly washed with the same solvent (3 x 20 mL). In this way, 4,5-dichlorophthalic anhydride was obtained in 98% yield (13.60 g).

^{1}H-NMR (300 MHz, DMSO-d_3): δ (ppm) = 8.12 (s, 2H; H-1).

[433] H. Uchida, H. Tanaka, H. Yoshiyama, P. Y. Reddy, S. Nakamura, T. Toru, *Synlett* **2002**, *2002*, 1649-1652.
[434] D. Wöhrle, M. Eskes, K. Shigehara, A. Yamada, *Synthesis* **1993**, *1993*, 194-196.

4,5-Dichlorophthalimide **20**[434]

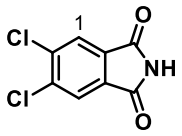

A mixture of 4,5-dichlorophthalic anhydride **19** (13.50 g, 62 mmol) and formamide (20 mL) was stirred at 200 °C during 3 h. Then, the reaction mixture was allowed to cool down to room temperature, and the precipitate was filtered, washed with water (1 x 20 mL) and vacuum-dried. In this way, 4,5-dichlorophthalimide **20** was obtained as a white solid in 92% yield (12.40 g).

^{1}H-NMR (300 MHz, DMSO-d_3): δ (ppm) = 8.10 (s, 2H; H-1).

4,5-Dichlorophthalamide **21**[434]

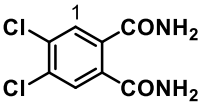

A suspension of 4,5-dichlorophthalimide **20** (12.40 g, 57 mmol) in 33% aqueous ammonia (225 mL) was stirred for 36 h at room temperature. The white solid obtained was filtered, washed with water (3 x 15 mL) and vacuum-dried. In this way, 4,5-dichlorophthalamide **21** was obtained as a white solid in 89% yield (11.90 g).

^{1}H-NMR (300 MHz, DMSO-d_3): δ (ppm) = 7.95 (s (broad), 2H; NH_2), 7.72 (s, 2H; H-1), 7.45 (s (broad), 2H; NH_2).

4,5-Dichlorophthalonitrile **22**[434]

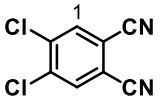

Freshly distilled thionyl chloride (42 mL) was cautiously poured over dry DMF (60 mL) at 0 °C under argon atmosphere. The mixture was vigorously stirred at 0 °C during 2 h and then 4,5-dichlorophthalamide **21** (11.90 g, 51 mmol) was added. The reaction mixture was stirred for 12 h at room temperature and subsequently poured onto crushed ice (100 mL). The slightly grey precipitate was filtered and washed with water (1 x 20 mL). Upon recrystallization from MeOH, 4,5-dichlorophthalonitrile was obtained as a white solid in 88% yield (8.90 g).

^{1}H-NMR (300 MHz, $CDCl_3$): δ (ppm) = 7.94 (s, 2H; H-1).

4,5-Dioctylthiophthalonitrile **23**[434]

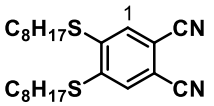

1-Octanethiol (4.6 mL, 26.8 mmol) was added to a suspension of 4,5-dichlorophthalonitrile **22** (2.40 g, 12 mmol) and dry K_2CO_3 (5.00 g, 36 mmol) in dry DMAC (30 mL) under argon atmosphere. The resulting mixture was stirred at 90 °C during 8 h and subsequently poured onto 100 of cold water. The precipitate was collected by filtration and dissolved in DCM. Then, this solution was washed with bleach (3 x 50 mL), water (3 x 50 mL) and brine (50 mL) and dried over $MgSO_4$. After filtration of the drying agent, the solvent was evaporated under reduced pressure and the yellow solid obtained was recrystallized from EtOH. In this way, 4,5-dioctylthiophthalonitrile **23** was obtained as white needles in 79% yield (4.00 g).

^{1}H-NMR (300 MHz, $CDCl_3$): δ (ppm) = 7.40 (s, 2H; H-1), 3.0 (m, 4H; $SC\underline{H}_2$), 1.85-1.60 (m, 4H; $SCH_2C\underline{H}_2$), 1.60-1.35 (m, 4H; $S(CH_2)_2C\underline{H}_2$), 1.35-1.15 (m, 16H; $S(CH_2)_3(C\underline{H}_2)_4$), 0.88 (m, 6H; CH_3).

Subphthalocyanine **24**[435]

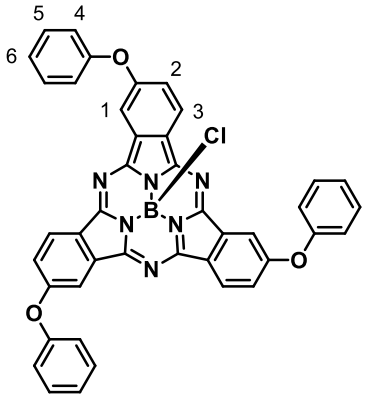

***C*$_3$-(OPh)$_3$SubPc-Cl**

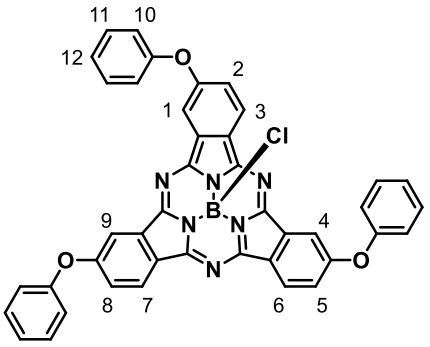

***C*$_1$-(OPh)$_3$SubPc-Cl 24**

4-phenoxyphthalonitrile **18** (1.00 g, 4.5 mmol) was dissolved in 3 mL of 1,2-dichlorobenzene under argon atmosphere. Then, a 1.0 M solution of BCl_3 in *p*-xylene (4.5 mL, 4.50 mmol) was added and the mixture was refluxed for 15 min under vigorous stirring. The reaction mixture was then allowed to cool down to room temperature and flushed with argon. After evaporating the solvent under reduced pressure, the crude was purified by column chromatography on silica

[435] D. González-Rodríguez, T. Torres, E. L. Denardin, D. Samios, V. Stefani, D. S. Corrêa, *J. Organomet. Chem.* **2009**, *694*, 1617-1622.

gel using hexane/AcOEt 4:1 (v/v) as eluent. During the process, the C_3 and C_1 regioisomers of $(OPh)_3$SubPc-Cl were separated. Recrystallization from DCM/MeOH/water afforded C_1-$(OPh)_3$SubPc-Cl **24** as a purple solid in 25% yield.

***C*$_3$-(OPh)$_3$SubPc-Cl:**

^{1}H-NMR (300 MHz, $CDCl_3$): δ (ppm) = 8.76 (d, $^3J_{H\text{-}H}$ = 8.8 Hz, 3H; H-3), 8.32 (d, $^4J_{H\text{-}H}$ = 2.3 Hz, 3H; H-1), 7.59 (dd, $^3J_{H\text{-}H}$ = 8.8 Hz, $^4J_{H\text{-}H}$ = 2.3 Hz, 3H; H-2), 7.42 (dd, $^3J_{H\text{-}H}$ = $^3J_{H\text{-}H}$' = 7.6 Hz, 6H; H-5), 7.21 (d, $^3J_{H\text{-}H}$ = 7.6 Hz, 3H; H-6), 7.15 (d, $^3J_{H\text{-}H}$ = 7.6 Hz, 6H; H-4).

UV-vis ($CHCl_3$): λ_{max} (nm) (log ε (dm^3 mol^{-1} cm^{-1})) = 572 (4.83), 526 (sh), 3.12 (4.49), 281 (5.58).

MP > 250 °C.

***C*$_1$-(OPh)$_3$SubPc-Cl (24):**

^{1}H-NMR (300 MHz, $CDCl_3$): δ (ppm) = 8.83 (d, $^3J_{H\text{-}H}$ = 8.8 Hz, 1H; H-3/H-6/H-7), 8.82 (d, $^3J_{H\text{-}H}$ = 8.8 Hz, 1H; H-3/H-6/H-7), 8.76 (d, $^3J_{H\text{-}H}$ = 8.8 Hz, 1H; H-3/H-6/H-7), 8.36 (d, $^4J_{H\text{-}H}$ = 2.3 Hz, 1H; H-1/H-4/H-9), 8.30 (d, $^4J_{H\text{-}H}$ = 2.3 Hz, 1H; H-1/H-4/H-9), 8.29 (d, $^4J_{H\text{-}H}$ = 2.3 Hz, 1H; H-1/H-4/H-9), 7.63 (dd, $^3J_{H\text{-}H}$ = 8.8 Hz, $^4J_{H\text{-}H}$ = 2.3 Hz, 1H; H-2/H-5/H-8), 7.61 (dd, $^3J_{H\text{-}H}$ = 8.8 Hz, $^4J_{H\text{-}H}$ = 2.3 Hz, 1H; H-2/H-5/H-8), 7.58 (dd, $^3J_{H\text{-}H}$ = 8.8 Hz, $^4J_{H\text{-}H}$ = 2.3 Hz, 1H; H-2/H-5/H-8), 7.5-7.0 (m, 15H; H-10, H-11, H-12).

UV-vis (toluene): λ_{max} (nm) (log ε (dm^3 mol^{-1} cm^{-1})) = 572 (4.83), 526 (sh), 3.12 (4.49), 281 (5.58).

MP > 250 °C.

Subphthalocyanine **25**[22]

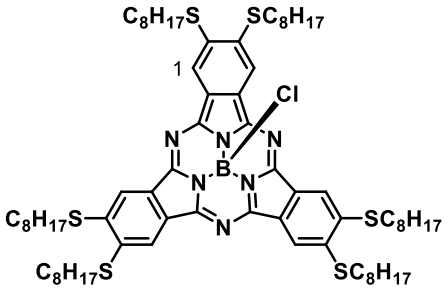

A 1.0 M solution of BCl_3 in *p*-xylene (2.4 mL, 2.4 mmol) was added to 4,5-dioctylthiophthalonitrile **23** (1.00 g, 2.4 mmol) under argon atmosphere and the mixture was heated at 120 °C for 10 min under vigorous stirring. The reaction mixture was then allowed to cool down to room temperature and flushed with argon. After evaporating the solvent under reduced pressure, the crude was dissolved in a toluene/THF 10:1 (v/v) mixture and passed through a short silica plug. The solvent was evaporated under reduced pressure, and the product was purified by column chromatography on silica gel using hexane/AcOEt 15:1 (v/v) as eluent. In this way, $(SC_8H_{17})_6$SubPc-Cl **25** was obtained as a viscous blue solid in 40% yield.

^{1}H-NMR (300 MHz, $CDCl_3$): δ (ppm) = 8.57 (s, 6H; H-1), 3.34-3.17 (m, 12H; $SC\underline{H}_2$), 1.92-1.80 (m, 12H; $SCH_2C\underline{H}_2$), 1.67-1.53 (m, 12H; $S(CH_2)_2C\underline{H}_2$), 1.44-1.22 (m, 48H; $S(CH_2)_3(C\underline{H}_2)_4$), 0.93-0.82 (m, 18H; $C\underline{H}_3$).

UV-vis (toluene): λ_{max} (nm) (log ε ($dm^3\ mol^{-1}\ cm^{-1}$)) = 599 (4.93), 551 (sh), 411 (4.38), 387 (4.38), 307 (4.73), 291 (4.74).

SubPc-Pnc_2 conjugate **26**

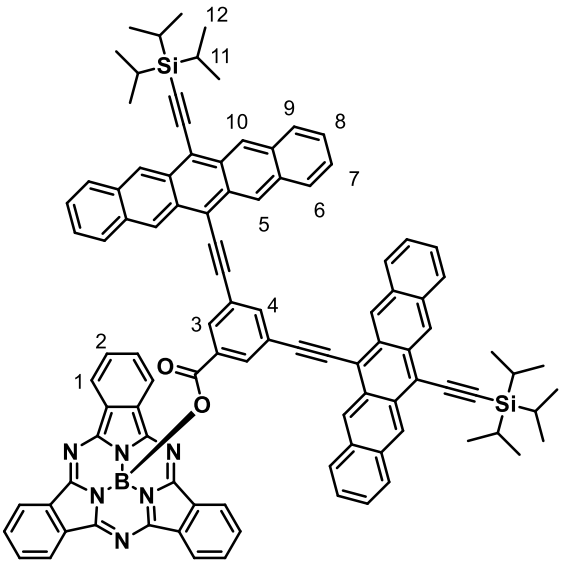

H_{12}SubPc-Cl **1** (10.8 mg, 0.025 mmol) and AgOTf (8.0 mg, 0.031 mmol) were dissolved in anhydrous chlorobenzene (3 mL) under argon atmosphere and the reaction mixture was stirred at 40 °C until the disappearance of the starting SubPc-Cl, which was monitored by TLC (30 minutes). At this point, Pnc_2 **17** (34.0 mg, 0.031 mmol) and DIPEA (5.46 µL, 0.031 mmol) were added and the reaction mixture was stirred at 50 °C during 6 h. To limit light exposure, the reaction flask was covered in aluminum foil. The solvent was evaporated under reduced pressure and the solid residue was subjected to column chromatography on silica gel using toluene/EtOAc 25:1 (v/v) as eluent. The product was then recrystallized from a DCM/MeOH mixture to afford **26** as a purple solid in 12% yield (4.4 mg).

^{1}H-NMR (300 MHz, $CDCl_3$): δ (ppm) = 9.26 (s, 4H; H-10), 9.10 (s, 4H; H-5), 8.98-8.95 (AA'XX' system, 6H; H-1), 8.21 (s, 1H; H-4), 7.99-7.92 (m, 14H; H-2, H-6, H-9), 7.74 (d, $^{4}J_{H\text{-}H}$ = 1.4 Hz, 2H; H-3), 7.43-7.35 (m, 8H; H-7, H-8), 1.39-1.36 (m, 42H; H-11, H-12).

^{13}C-NMR (125.7 MHz, $CDCl_3$): δ (ppm) = 165.04, 151.91, 132.47, 132.43, 131.28, 130.66, 130.43, 130.16, 128.84, 128.76, 126.64, 126.33, 126.24, 125.87, 124.18, 122.58, 117.20, 116.48, 107.75, 104.77, 89.30, 19.15, 11.83.

^{11}B-NMR (160.4 MHz, $CDCl_3$): δ (ppm) = -14.35.

MS (MALDI-TOF, DCTB): *m/z* = 1477.6 $[M]^+$, 2955.4 $[2M]^+$.

HRMS: *m/z* Calculated for $[C_{101}H_{81}BN_6O_2Si_2]$: 1477.6085; Found: 1477.6090.

UV-vis (toluene): λ_{max} (nm) (log ε ($dm^3\ mol^{-1}\ cm^{-1}$)) = 661 (4.77), 605 (4.50), 565 (5.00), 548 (sh), 522 (sh), 441 (4.00), 373 (4.64), 351 (4.64), 312 (5.65).

FT-IR (ATR): *v* (cm^{-1}) = 3052, 2926, 2860, 2121, 1701 (C=O), 1586, 1452, 1387, 1332, 1246 (C-O), 1197, 1170, 1132, 1023, 998, 874, 768, 739, 697, 678, 572.

SubPc-Pnc_2 conjugate **27**

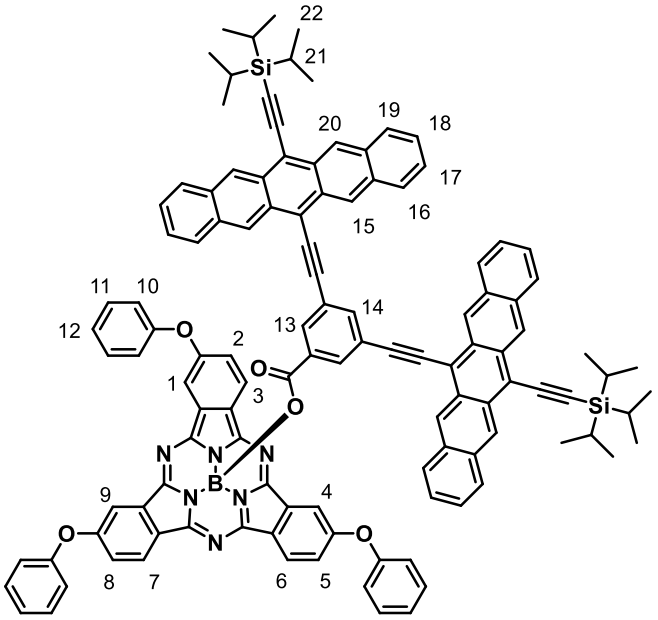

$(OPh)_3$SubPc-Cl **24** (17.7 mg, 0.025 mmol) and AgOTf (8.0 mg, 0.031 mmol) were dissolved in anhydrous chlorobenzene (3 mL) under argon atmosphere and the reaction mixture was stirred at room temperature until the disappearance of the starting SubPc-Cl, which was monitored by TLC (40 minutes). At this point, Pnc_2 **17** (34.0 mg, 0.031 mmol) and DIPEA (5.46 µL, 0.031 mmol) were added and the reaction mixture was stirred at 50 °C during 4 h. To limit light exposure, the reaction flask was covered in aluminum foil. The solvent was evaporated under reduced pressure and the solid residue was subjected to column chromatography on silica gel using heptane/EtOAc 5:1 (v/v) as eluent. Recrystallization from a DCM/MeOH mixture afforded **27** as a purple solid in 11% yield (4.8 mg).

^{1}H-NMR (300 MHz, $CDCl_3$): δ (ppm) = 9.30 (s, 4H; H-20), 9.14 (s, 4H; H-15), 8.90 (d, $^3J_{H\text{-}H}$ = 8.7 Hz, 1H; H-3/H-6/H-7), 8.88 (d, $^3J_{H\text{-}H}$ = 8.4 Hz, 1H; H-3/H-6/H-7), 8.83 (d, $^3J_{H\text{-}H}$ = 8.7 Hz, 1H; H-3/H-6/H-

7), 8.41 (d, $^4J_{H-H}$ = 2.1 Hz, 1H; H-1/H-4/H-9), 8.37 (d, $^4J_{H-H}$ = 2.1 Hz, 1H; H-1/H-4/H-9), 8.35 (d, $^4J_{H-H}$ = 2.1 Hz, 1H; H-1/H-4/H-9), 8.24 (t, $^4J_{H-H}$ = 1.5 Hz, 1H; H-14), 8.03-7.95 (m, 8H; H-16, H-19), 7.75 (d, $^4J_{H-H}$ = 1.5 Hz, 2H; H-13), 7.67-7.58 (m, 3H; H-2, H-5, H-8), 7.45-7.40 (m, 14H; H-11, H-17, H-18), 7.23-7.14 (m, 9H; H-10, H-12), 1.40-1.37 (m, 42H; H-21, H-22).

^{13}C-NMR (125.7 MHz, $CDCl_3$): δ (ppm) = 164.17, 159.97, 156.64, 148.33, 140.042, 133.59, 132.51, 132.48, 130.67, 130.45, 130.34, 130.32, 128.84, 126.68, 126.37, 126.26, 125.44, 124.60, 124.21, 124.10, 123.67, 121.98, 121.83, 120.10, 120.00, 119.94, 116.94, 110.51, 107.57, 104.28, 102.12, 19.16, 11.85.

^{11}B-NMR (160.4 MHz, $CDCl_3$): δ (ppm) = -14.42.

MS (MALDI-TOF, DCTB): *m/z* = 1753.6 $[M]^+$, 3507.3 $[2M]^+$.

HRMS: *m/z* Calculated for $[C_{119}H_{93}BN_6O_5Si_2]$: 1753.6873; Found: 1753.6875.

UV-vis (toluene): λ_{max} (nm) (log ε ($dm^3\ mol^{-1}\ cm^{-1}$)) = 661 (4.93), 604 (4.68), 571 (5.17), 523 (sh), 441 (4.24), 371 (4.90), 347 (sh), 313 (5.88).

FT-IR (ATR): ν (cm^{-1}) = 3054, 2924, 2857, 2114, 1697 (C=O), 1589, 1455, 1399, 1332, 1242 (C-O), 1197, 1154, 1124, 1072, 1015, 952, 876, 740, 691, 676, 585.

SubPc-Pnc$_2$ conjugate **28**

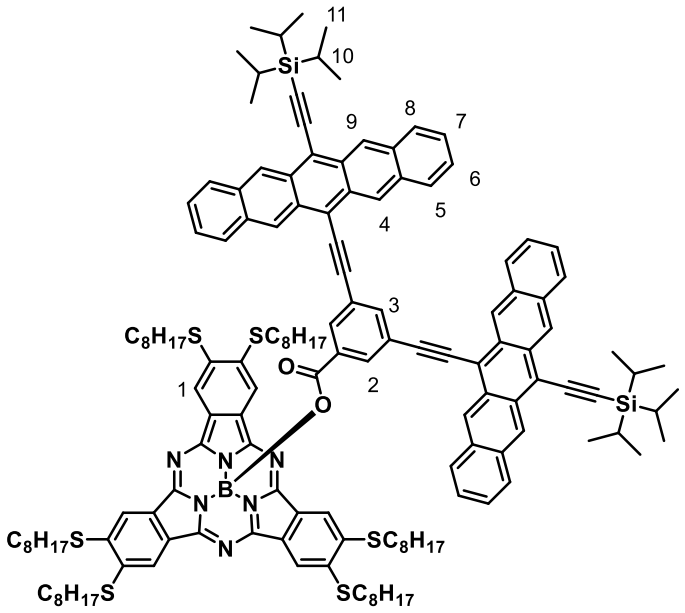

$(SC_8H_{17})_6$SubPc-Cl **25** (32.4 mg, 0.025 mmol) and AgOTf (8.0 mg, 0.031 mmol) were dissolved in anhydrous chlorobenzene (3 mL) under argon atmosphere and the reaction mixture was stirred at room temperature until the disappearance of the starting SubPc-Cl, which was monitored by

TLC (10 minutes). At this point, Pnc_2 **17** (34.0 mg, 0.031 mmol) and DIPEA (5.46 µL, 0.031 mmol) were added and the reaction mixture was stirred at 50 °C during 3 h. To limit light exposure, the reaction flask was covered in aluminum foil. The solvent was evaporated under reduced pressure and the dark blue residue was dissolved in heptane/EtOAc 15:1 (v/v) and passed through a short silica plug. The solvent was evaporated and the solid residue was subjected to size exclusion chromatography using $CHCl_3$ as eluent to remove the hydrolyzed SubPc subproduct. After evaporation of the solvent, preparative liquid chromatography was carried out using heptane/EtOAc 15:1 (v/v) as eluent to purify the target compound from the corresponding µ-oxo dimer. The product was then recrystallized from a DCM/MeOH mixture to afford **28** as a blue solid in 9% yield (5.3 mg).

^{1}H-NMR (300 MHz, $CDCl_3$): δ (ppm) = 9.29 (s, 4H; H-9), 9.13 (s, 4H; H-4), 8.71 (s, 6H; H-1), 8.23 (t, $^4J_{H\text{-}H}$ = 1.5 Hz, 1H; H-3), 8.00-7.94 (m, 8H; H-8, H-5), 7.76 (d, $^4J_{H\text{-}H}$ = 1.5 Hz, 2H; H-2), 7.44-7.36 (m, 8H; H-7, H-6), 3.33-3.18 (m, 12H; $SC\underline{H}_2$) 1.91-1.81 (m, 12H; $SCH_2C\underline{H}_2$); 1.62-1.52 (m, 12H; $S(CH_2)_2C\underline{H}_2$), 1.44-1.26 (m, 90H; $S(CH_2)_3(C\underline{H}_2)_4$, H-10, H-11), 0.87-0.83 (m, 18H; $S(CH_2)_7C\underline{H}_3$).

^{13}C-NMR (125.7 MHz, $CDCl_3$): δ (ppm) = 164.06, 151.18, 140.87, 137.85, 132.47, 132.42, 131.94, 130.63, 130.40, 128.79, 128.70, 126.66, 126.34, 126.24, 125.82, 124.22, 120.03, 119.20, 113.13, 107.76, 104.78, 102.47, 89.38, 33.92, 31.96, 29.38, 29.34, 29.29, 28.67, 22.80, 19.15, 14.23, 11.85.

^{11}B-NMR (160.4 MHz, $CDCl_3$): δ (ppm) = -14.22.

MS (MALDI-TOF, DCTB): *m/z* = 2342.3 $[M]^+$, 4688.9 $[2M]^+$.

HRMS: *m/z* Calculated for $[C_{149}H_{177}BN_6O_2S_6Si_2]$: 2342.1889; Found: 2342.1924.

UV-vis (toluene): λ_{max} (nm) (log ε ($dm^3\ mol^{-1}\ cm^{-1}$)) = 662 (4.56), 602 (5.03), 581 (sh), 559 (sh), 438 (sh), 415 (4.52), 373 (4.71), 354 (4.66), 312 (5.52).

FT-IR (ATR): ν (cm^{-1}) = 3049, 2922, 2856, 2126, 1703 (C=O), 1592, 1453, 1374, 1257 (C-O), 1179, 1112, 1015, 875, 802, 739, 725, 705, 676, 585.

2.5.2.2 Synthetic procedures for the preparation of the SubPc-Pnc$_2$ conjugates featuring different spacers

SubPc-Pnc$_2$ conjugate **33**

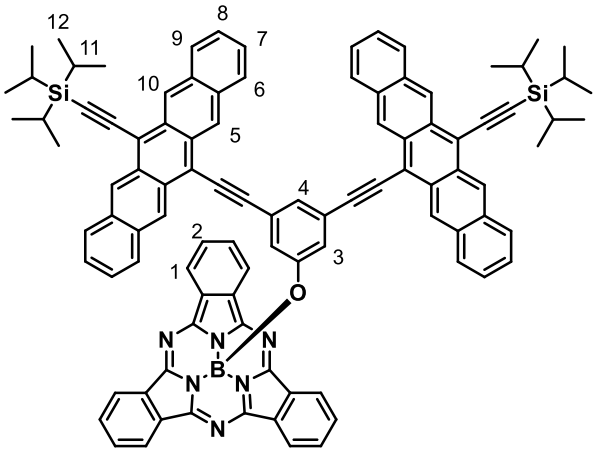

H_{12}SubPc-Cl **1** (10.8 mg, 0.025 mmol) and AgOTf (34.0 mg, 0.031 mmol) were dissolved in anhydrous toluene (1 mL) under argon atmosphere and the reaction mixture was stirred at 40 °C until the disappearance of the starting SubPc-Cl, which was monitored by TLC (30 minutes). At this point, Pnc$_2$ **29** (33.1 mg, 0.031 mmol) and DIPEA (5.46 µL, 0.031 mmol) were added and the reaction mixture was stirred at 50 °C during 5 h. To limit light exposure, the reaction flask was covered in aluminum foil. The reaction mixture was then passed through a short Celite plug. The solvent was evaporated under reduced pressure and the product was purified by size exclusion chromatography using $CHCl_3$ as eluent. Recrystallization from a DCM/hexane mixture afforded **33** as a purple solid in 19% yield (6.8 mg).

^{1}H-NMR (500 MHz, $CDCl_3$): δ (ppm) = 9.31 (s, 4H; H-10), 9.26 (s, 4H; H-5), 8.94-8.91 (AA'XX' system, 6H; H-1), 8.27-8.25 (m, 4H; H-9), 8.00–7.98 (m, 4H; H-6), 7.90-7.86 (AA'XX' system, 6H; H-2), 7.76 (t, $^4J_{H\text{-}H}$ = 1.5 Hz, 1H; H-4), 7.45-7.43 (m, 8H; H-7, H-8), 6.00 (d, $^4J_{H\text{-}H}$ = 1.5 Hz, 2H; H-3), 1.40-1.39 (m, 42H; H-11, H-12).

^{13}C-NMR (125.7 MHz, $CDCl_3$): δ (ppm) = 151.92, 132.53, 132.49, 131.28, 131.27, 130.77, 130.42, 130.24, 129.11, 128.83, 127.85, 126.60, 126.24, 126.12, 124.73, 122.54, 122.16, 118.75, 117.85, 107.50, 104.93, 103.60, 88.49, 19.18, 11.88.

^{11}B-NMR (160.4 MHz, $CDCl_3$): δ (ppm) = -14.51.

MS (MALDI-TOF, DCTB): *m/z* = 1449.6 $[M]^+$, 2898.3 $[2M]^+$.

HRMS: *m/z* Calculated for $[C_{100}H_{81}BN_6OSi_2]$: 1449.6136; Found: 1449.6167.

UV-vis (toluene): λ_{max} (nm) (log ε ($dm^3\ mol^{-1}\ cm^{-1}$)) = 661 (4.83), 606 (4.54), 565 (4.99), 549 (sh), 525 (4.48), 442 (3.98), 417 (3.78), 374 (4.69), 353 (4.66).

FT-IR (KBr): *v* (cm^{-1}) = 3047, 2938, 2861, 2124 (C≡C), 1629, 1578, 1458, 1381, 1325, 1288, 1198, 1168, 1131, 1052 (B-O), 877, 738, 677, 592.

SubPc-Pnc_2 conjugate **34**

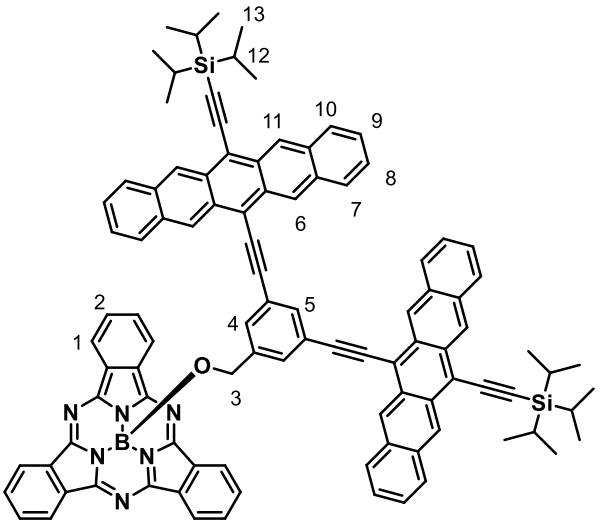

H_{12}SubPc-Cl **1** (10.8 mg, 0.025 mmol) and AgOTf (34.0 mg, 0.031 mmol) were dissolved in anhydrous toluene (1 mL) under argon atmosphere and the reaction mixture was stirred at 40 °C until the disappearance of the starting SubPc-Cl, which was monitored by TLC (30 minutes). At this point, Pnc_2 **30** (33.5 mg, 0.031 mmol) and DIPEA (5.46 µL, 0.031 mmol) were added and the reaction mixture was stirred at 50 °C during 13 h. To limit light exposure, the reaction flask was covered in aluminum foil. The reaction mixture was then passed through a short Celite plug. The solvent was evaporated under reduced pressure and the product was purified by size exclusion chromatography using $CHCl_3$ as eluent. Recrystallization from a DCM/hexane mixture afforded **34** as a purple solid in 26% yield (9.5 mg).

^{1}H-NMR (500 MHz, THF-d_8): δ (ppm) = 9.43 (s, 4H; H-11), 9.38 (s, 4H; H-6), 8.88–8.85 (AA'XX' system, 6H; H-1), 8.32-8.30 (m, 4H; H-10), 8.12 (s, 1H; H-5), 8.02-8.00 (m, 4H; H-7), 7.90-7.87 (AA'XX' system, 6H; H-2), 7.50-7.46 (m, 8H; H-8, H-9), 7.17 (s, 2H; H-4), 2.94 (s, 2H; H-3), 1.44-1.43 (m, 42H, H12; H-13).

^{13}C-NMR (125.7 MHz, THF-d_8): δ (ppm) = The rather low solubility of this product prevented the registration of a clear ^{13}C-NMR spectrum.

^{11}B-NMR (160.4 MHz, THF-d_8): δ (ppm) = -14.22.

MS (MALDI-TOF, DCTB): *m/z* = 1463.7 $[M]^+$, 29275 $[2M]^+$.

HRMS: *m/z* Calculated for [$C_{101}H_{83}BN_6OSi_2$]: 1463.6292; Found: 1463.6302.

UV-vis (toluene): λ_{max} (nm) (log ε (dm^3 mol^{-1} cm^{-1})) = 660 (4.83), 605 (4.57), 564 (5.02), 547 (sh), 524 (4.50), 441 (3.99), 417 (3.73), 373 (4.77), 353 (4.68).

FT-IR (KBr): ν (cm^{-1}) = 3048, 2940, 2862, 2127 (C≡C), 1619, 1585, 1458, 1381, 1288, 1233, 1176, 1132, 1113 (B-O), 878, 739, 676, 591.

SubPc-Pnc_2 conjugate **35**

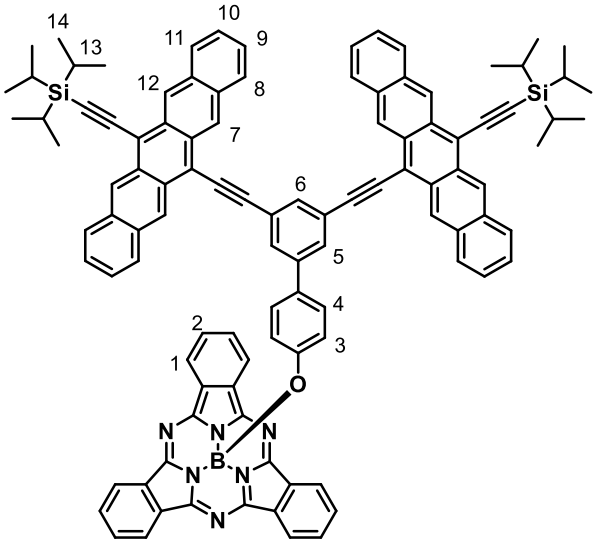

H_{12}SubPc-Cl **1** (10.8 mg, 0.025 mmol) and AgOTf (8.0 mg, 0.031 mmol) were dissolved in anhydrous toluene (1 mL) under argon atmosphere and the reaction mixture was stirred at 40 °C until the disappearance of the starting SubPc-Cl material, which was monitored by TLC (30 minutes). At this point, Pnc_2 **31** (35.5 mg, 0.031 mmol) and DIPEA (5.46 µL, 0.031 mmol) were added and the reaction mixture was stirred at 50 °C during 5 h. To limit light exposure, the reaction flask was covered in aluminum foil. The reaction mixture was then passed through a short Celite plug. The solvent was evaporated under reduced pressure and the product was purified by size exclusion chromatography using $CHCl_3$ as eluent. Recrystallization from a DCM/hexane mixture afforded **35** as a purple solid in 16% yield (6.2 mg).

^{1}H-NMR (500 MHz, THF-d_8): δ (ppm) = 9.47 (s, 4H; H-12), 9.37 (s, 4H; H-7), 8.89-8.86 (AA'XX' system, 6H; H-1), 8.45 (s, 1H; H-6), 8.22-8.20 (m, 4H; H-11), 8.15 (d, $^4J_{H-H}$ = 1.5 Hz, 2H; H-5), 8.01-7.99 (m, 4H; H-8), 7.97-7.94 (AA'XX' system, 6H; H-2), 7.47-7.43 (m, 8H; H-9, H-10), 7.41 (d, $^3J_{H-H}$ = 8.5 Hz, 2H; H-4), 5.61 (d, $^3J_{H-H}$ = 8.5 Hz, 2H; H-3), 1.43-1.42 (m, 42H; H-13, H-14).

^{13}C-NMR (125.7 MHz, THF-d_8): δ (ppm) = The rather low solubility of this product prevented the registration of a clear ^{13}C-NMR spectrum.

^{11}B-NMR (160.4 MHz, THF-d_8): δ (ppm) = -14.49.

MS (MALDI-TOF, DCTB): *m/z* = 1525.6 $[M]^+$, 3051.4 $[2M]^+$.

HRMS: *m/z* Calculated for $[C_{106}H_{85}BN_6OSi_2]$: 1525.6449; Found: 1525.6489.

UV-vis (toluene): λ_{max} (nm) (log ε ($dm^3\ mol^{-1}\ cm^{-1}$)) = 660 (4.77), 604 (4.52), 563 (5.02), 548 (sh), 524 (4.49), 441 (3.98), 417 (3.76), 373 (4.71), 353 (4.66).

FT-IR (KBr): *v* (cm^{-1}) = 3046, 2940, 2862, 2123 (C≡C), 1609, 1583, 1511, 1461, 1375, 1328, 1287, 1248, 1198, 1172, 1133, 1049 (B-O), 877, 738, 675, 584.

SubPc-Pnc_2 conjugate **36**

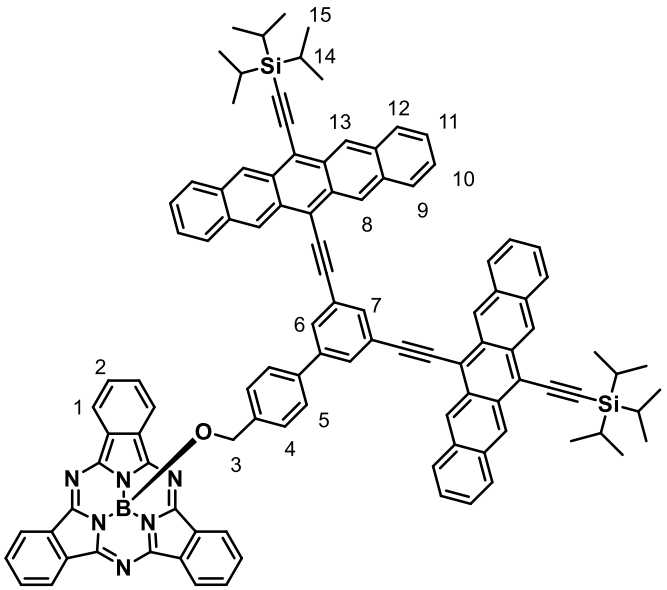

H_{12}SubPc-Cl **1** (10.8 mg, 0.025 mmol) and AgOTf (8.0 mg, 0.031 mmol) were dissolved in anhydrous toluene (1 mL) under argon atmosphere and the reaction mixture was stirred at 40 °C until the disappearance of the starting SubPc-Cl, which was monitored by TLC (30 minutes). At this point, Pnc_2 **32** (35.9 mg, 0.031 mmol) and DIPEA (5.46 µL, 0.031 mmol) were added and the reaction mixture was stirred at 50 °C during 13 h. To limit light exposure, the reaction flask was covered in aluminum foil. The reaction mixture was then passed through a short Celite plug. The solvent was removed by evaporation under reduced pressure and the product was purified by size exclusion chromatography using $CHCl_3$ as eluent. Recrystallized from a DCM/hexane mixture afforded **36** as a purple solid in 18% yield (7.0 mg).

^{1}H-NMR (300 MHz, $CDCl_3$): δ (ppm) = 9.17 (s, 8H; H-8, H-13), 8.89-8.84 (AA'XX' system, 6H; H-1), 8.27 (s, 1H; H-7), 7.96-7.88 (m, 14H; H-2, H-9, H-12), 7.84 (d, $^4J_{H\text{-}H}$ = 1.5 Hz, 2H; H-6), 7.42-7.30 (m, 10H; H-5, H-10, H-11), 6.67 (d, $^3J_{H\text{-}H}$ = 8.1 Hz, 2H; H-4), 2.83 (s, 1H; H-3), 1.39-1.38 (m, 42H; H-14, H-15).

^{13}C-NMR (125.7 MHz, $CDCl_3$): δ (ppm) = 151.54, 142.28, 139.60, 138.19, 133.18, 132.37, 131.17, 130.61, 130.55, 130.33, 129.91, 128.82, 128.78, 126.91, 126.87, 126.60, 126.25, 126.15, 125.90, 124.72, 122.27, 118.80 117.59, 108.11, 107.40, 104.86, 103.78, 89.06, 61.70, 19.19, 11.88.

^{11}B-NMR (160.4 MHz, $CDCl_3$): δ (ppm) = -14.51.

MS (MALDI-TOF, DCTB): *m/z* = 1539.7 $[M]^+$, 3078.6 $[2M]^+$.

HRMS: *m/z* Calculated for $[C_{107}H_{87}BN_6O_2Si_2]$: 1539.6606; Found: 1539.6541.

UV-vis (toluene): λ_{max} (nm) (log ε ($dm^3\ mol^{-1}\ cm^{-1}$)) = 660 (4.78), 604 (4.52), 562 (5.02), 546 (sh), 523 (4.48), 441 (3.95), 417 (3.71), 374 (4.73), 353 (4.65).

FT-IR (KBr): ν (cm^{-1}) = 3043, 2938, 2861, 2122 (C≡C), 1616, 1582, 1459, 1377, 1288, 1232, 1176, 1130, 1107 (B-O), 876, 739, 676, 590.

Chapter 3

Optical Resolution and Insights into the Organization of Inherently Chiral Subphthalocyanines

3.1 Introduction and background

Chirality is a fundamental symmetry property which has long fascinated chemists. Owing to the inherent chirality of nature, the importance of this property in a biological context is well-recognized. Indeed, chirality has been extensively considered in biomedically focused application areas, such as drug design and development.[436]

Despite the undiscussed value of chiral species and interactions in biomedicine, the exploitation of chirality has not constituted until now a common approach for the design of novel functional materials for technological applications. However, in light of the added value of chiral molecules, chirality is gaining nowadays growing interest in the frame of technologically related fields, and new design strategies that take chirality into account are emerging.[437] As such, chirality provides molecular systems with additional intriguing properties (*e.g.* chiroptical responses,[438] chiral-induced spin selectivity (CISS)[439] or chirality-dependent organization[440-442]) ultimately leading to new functionalities.[437] Thus, the potential impact of chirality on advances in technology is extremely high.

With a view to the preparation of high-performance organic devices, the understanding of the collective behavior of multiple units in the bulk (that is, their supramolecular organization as well as material properties such as charge transport) is of utmost importance along with the comprehension of the structure and properties of the isolated molecules.[443] Nevertheless, differences in the solid-state organization of molecular systems with different chiral compositions (*e.g.*, racemic *versus* enantiopure) are often overlooked when considering the technological potential of chiral organic materials.[437] This is rather surprising if we consider that changes in the chiral composition may lead, in principle, to different material properties, while maintaining the same molecular properties of the system. In other words, chiral organic materials offer the intriguing possibility to tailor the performances of (opto)electronic devices by tuning their chiral composition without modifying their molecular structure.[437]

---

[436] W. H. Brooks, W. C. Guida, K. G. Daniel, *Curr. Top. Med. Chem.* **2011**, *11*, 760-770.
[437] J. R. Brandt, F. Salerno, M. J. Fuchter, *Nat. Rev. Chem.* **2017**, *1*, 1-12.
[438] D.-W. Zhang, M. Li, C.-F. Chen, *Chem. Soc. Rev.* **2020**, *49*, 1331-1343.
[439] R. Naaman, Y. Paltiel, D. H. Waldeck, *Nat. Rev. Chem.* **2019**, *3*, 250-260.
[440] Y. Zhu, N. Gergel, N. Majumdar, L. R. Harriott, J. C. Bean, L. Pu, *Org. Lett.* **2006**, *8*, 355-358.
[441] T. Hatakeyama, S. Hashimoto, T. Oba, M. Nakamura, *J. Am. Chem. Soc.* **2012**, *134*, 19600-19603.
[442] F. Pop, P. Auban-Senzier, A. Frackowiak, K. Ptaszynski, I. Olejniczak, J. D. Wallis, E. Canadell, N. Avarvari, *J. Am. Chem. Soc.* **2013**, *135*, 17176-17186.
[443] Z. B. Henson, K. Müllen, G. C. Bazan, *Nat. Chem.* **2012**, *4*, 699-704.

In this connection, some preliminary studies have been presented in which the bulk properties of organic materials with different chiral composition have been compared.[440-442] Interestingly, these studies demonstrated the potential of chirality as a means to control charge transport in the bulk. As an example, photoinduced charge transport in films of azaboradibenzo[6]helicene was found to be highly dependent on the chiral composition of the material (Figure 132a). Whereas films obtained from the racemate exhibited only hole mobility, enantiopure films exhibited both hole and electron mobility, being the latter even higher than the former.[441] As another example, considerably different conductivities have been reported for enantiopure and racemic crystalline radical cation TTF salts (Figure 132b).[442] In both these cases, the observed differences in terms of bulk properties were attributed to the different crystalline packing of racemic and enantiopure species.

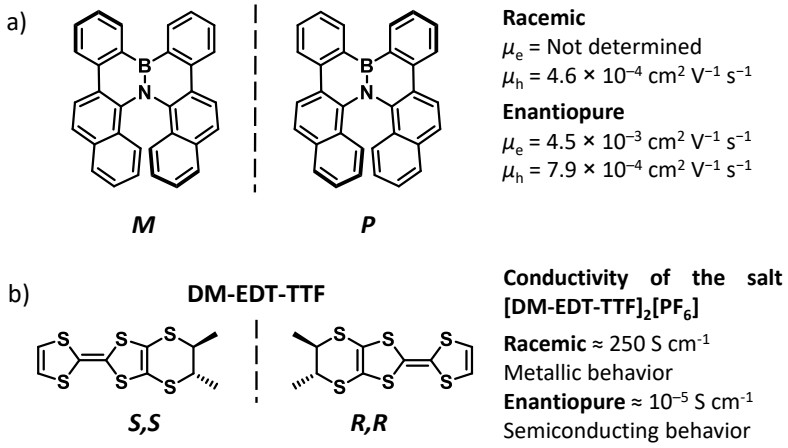

Figure 132. Examples of materials exhibiting chiral composition-dependent bulk properties.[441,442]

As described in the Introduction of this Thesis, SubPcs have shown to hold great promises as candidates for (opto)electronic applications by virtue of their outstanding optical and electronic properties (*e.g.* intense light absorption, strong fluorescence emission, rich redox chemistry, strong dipole moment, and excellent charge transport capabilities, among others).[8] Besides these characteristics, SubPcs also feature intriguing structural properties. In particular, due to their cone-shaped geometry, these macrocycles are intrinsically non-centrosymmetric. Thus, each of the C_1-and C_3-symmetric SubPc regioisomers obtained from cyclotrimerization reaction of a non C_{2v}-symmetric phthalonitrile precursor *(e.g.*, a *meta*- or *ortho*-monosubstituted phthalonitrile) is inherently chiral and is obtained as a racemic mixture of enantiomers (*i.e.*, *P* and *M* for the C_3 regioisomer, and *MPP* and *MMP* for the C_1 regioisomer). The possible isomers for a trisubstituted SubPc featuring a *meta* functionalization pattern are shown in Figure 133.

The steps for the assignment of the absolute configuration of C_3-symmetric SubPcs, which are based on the use of the *P*/*M* stereodescriptor system commonly employed to designate the chirality of chiral buckybowl molecules and exploit the CIP sequence rules, have been described in the first Chapter of this Thesis (section 1.3.2.2).[375,376] For C_1-symmetric SubPcs, the same rules can be followed.

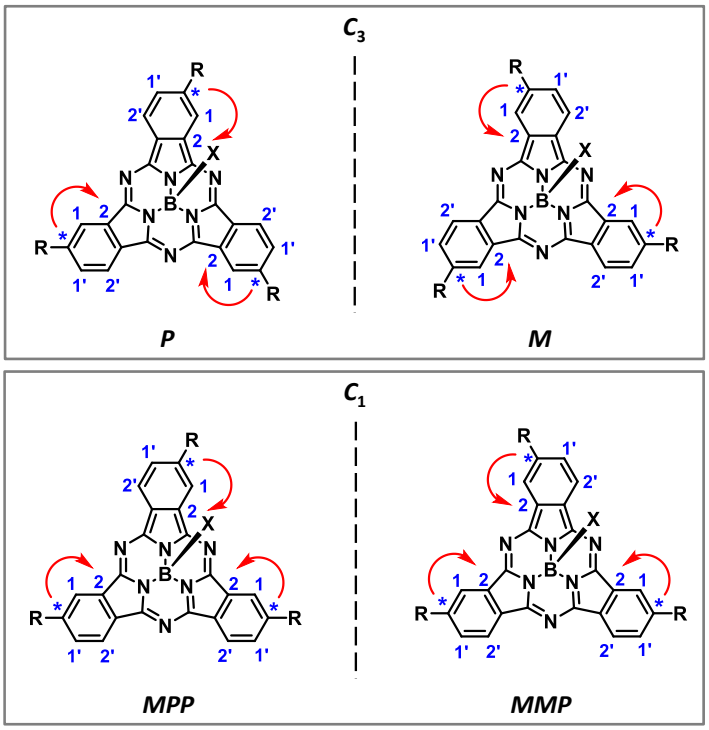

Figure 133. Molecular structure of the enantiomers of C_3- and C_1-symmetric *meta*-trisubstituted SubPcs.

In this connection, it is worth to mention that other π-conjugated bowl-shaped molecules, such as corannulenes, sumanenes or hemifullerenes, have been investigated as chiral molecular materials for optoelectronics, showing intriguing electronic properties.[376,444] Nevertheless, these systems present major drawbacks (such as poor light absorption features or a low energy barrier for bowl-to-bowl racemization) which limit their practical application.

[444] A. Szumna, *Chem. Soc. Rev.* **2010**, *39*, 4274-4285.

To sum up, in light of the unique structural, optical and electronic properties of SubPcs, and taking into account the high potential of chiral molecules in technologically relevant fields, optically pure SubPc derivatives constitute extremely promising candidates as advanced functional materials for application in (opto)electronic devices. Thus, it is not surprising that the preparation of enantiopure SubPcs has always constituted a key goal in SubPc chemistry. However, despite the enormous potential of optically pure SubPc species, just a few reports have been published dealing with the optical resolution of inherently chiral SubPcs.

In 2000, Claessens and Torres reported the first analytical resolution of racemic SubPcs. In this work, the enantiomers of both the C_3 and C_1 regioisomers of *meta*-substituted I_3SubPc-Cl were isolated by chiral HPLC.[37] Two years later, Kobayashi *et al.* published the semi-preparative resolution of a C_3-symmetric SubPc prepared from cyclotrimerization reaction of 3-nitro-5-*t*-butylphthalonitrile, which enabled to measure the first CD spectra of enantiopure SubPc species.[33] Almost a decade after this report, the optical resolution of C_3- and C_1-symmetric 1,2-SubNc derivatives by chiral HPLC was presented by Shimizu and co-workers.[445] In this case, the crystal structure of the isolated enantiomers was successfully resolved by means of X-ray diffraction analysis, which allowed to establish for the first time a correlation between CD spectra and absolute configuration of optically pure SubPc species. The enantiomers of a C_3-symmetric SubPc-F bearing three peripheral amide groups in the *meta* positions were also separated by analytical chiral HPLC, allowing for the study of their self-assembly properties in solution (*vide infra*).[105,174]

An alternative approach towards the optical resolution of inherently chiral SubPcs consists in the derivatization of the racemic SubPc species with an enantiopure chiral auxiliary, followed by separation of the resulting diastereomers and subsequent removal of the resolving agent from the isolated diastereomeric derivatives. Curiously, this strategy has never been exploited yet for the preparation of enantiopure SubPcs. Nevertheless, in this context, it is worth to mention a few significative publications dealing with the introduction of chiral elements through derivatization of either the axial or the peripheral positions of the SubPc macrocycle.

Interestingly, in the oxidation of an asymmetric SubPc bearing an *ortho* thioether substituent to the corresponding sulfoxide derivative, a high degree of diastereoselectivity induced by the intrinsically chiral SubPc core was observed (Scheme 10).[112] As a matter of fact, a 95:5 diastereomeric mixture was obtained in the investigated conditions, and the two diastereomers could be separated by column chromatography. Remarkably, the oxidation of the *meta*-

[445] S. Shimizu, A. Miura, S. Khene, T. Nyokong, N. Kobayashi, *J. Am. Chem. Soc.* **2011**, *133*, 17322-17328.

substituted analogue did not show any selectivity as it led to the formation of a 1:1 mixture of diastereomers, which could only be separated by HPLC.

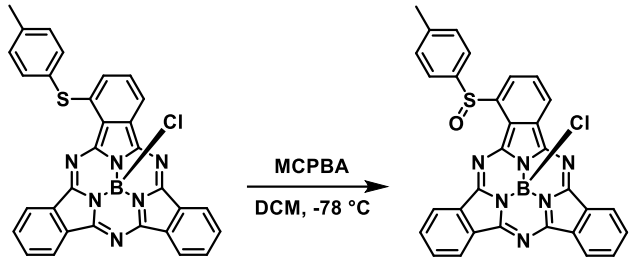

Scheme 10. Diastereoselective oxidation reaction of an *ortho-*, thioether-substituted SubPc described by González-Rodríguez and Torres.[112]

In 2003, a couple of SubPc dimers linked by either racemic 1,1'-bi(2-naphthol) (BINOL) or enantiopure (*R*)-(+)-BINOL was reported by Kobayashi, Durfee and co-workers (Figure 134).[446]

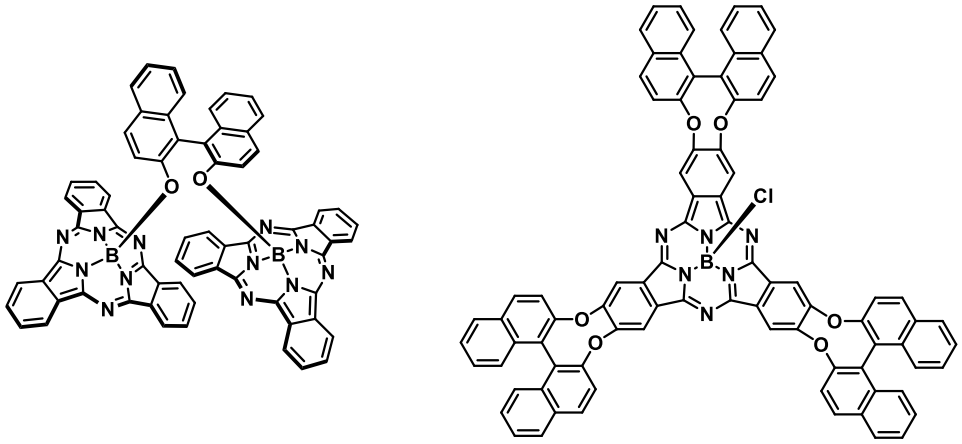

Figure 134. Left: Structure of the optically active BINOL-bridged SubPc dimer investigated by Kobayashi, Durfee and co-workers.[446] Right: Structure of the chiral binaphthoxy-functionalized SubPc reported by Kobayashi, Jiang and co-workers.[29]

Interestingly, CD measurements with the optically active dimer evidenced an induced CD on the SubPc generated by the chiral binaphthyl unit. More recently, (*R*)- and (*S*)-1,1'-bi(2-naphthoxy) substituents were introduced at the periphery of the SubPc macrocycle (Figure 134).[29] Also in

[446] T. Fukuda, M. M. Olmstead, W. S. Durfee, N. Kobayashi, *Chem. Commun.* **2003**, 1256-1257.

this case, an induced CD in the SubPc absorption region was observed. A similar substituent-induced CD signal had already been reported for binaphthyl-substituted Pcs.[447]

These publications demonstrate the interest of the scientific community towards the preparation of enantiopure SubPcs. Nevertheless, none of these reports presented a feasible methodology for the efficient optical resolution of inherently chiral SubPc species, which is of crucial importance in view of the potential exploitation of optically pure SubPc derivatives for technological applications.

Moreover, the study of the organization of enantiopure SubPcs has been rarely addressed, and the contributions in this area are only recent.

The solution self-assembly of a chiral SubPc bearing three peripheral arylamide groups and an axial fluorine substituent has been thoroughly investigated by González-Rodríguez, Torres, Ortí and co-workers (Figure 135).[105,174] Remarkably, this C_3-symmetric SubPc can undergo self-assembly either as a dimer or as a polymeric columnar stack, depending solely on the solvent nature (namely, aromatic *versus* aliphatic).[174] Moreover, each of these aggregation modes exhibits prominent and exclusive chiral self-sorting behavior, as emerged from the study of the assembly of racemic and enantiopure samples. Whereas the *M* and *P* SubPc enantiomers tend to narcissistically self-sort in the dimer regime, they socially self-sort in the polymer regime, showing an alternate columnar stacking order.

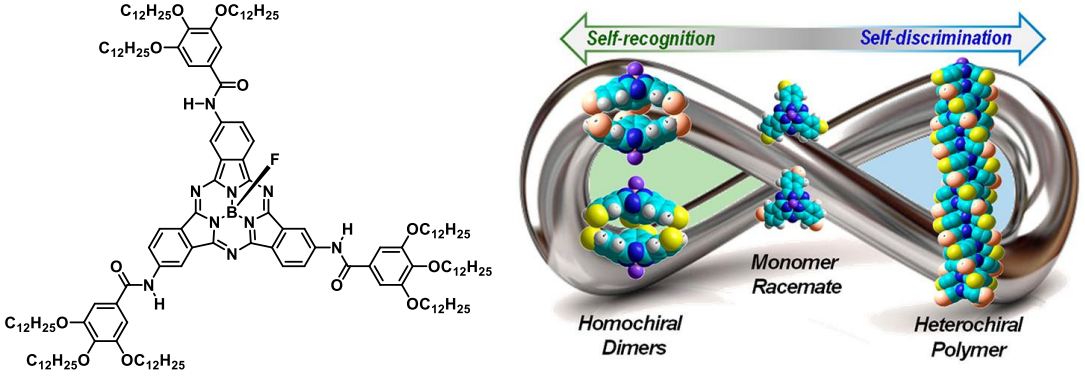

Figure 135. Structure of the C_3-symmetric SubPc investigated by González-Rodríguez, Torres, Ortí and co-workers and cartoon depicting the dual-mode chiral self-assembly. Adapted from ref. 174.

[447] N. Kobayashi, R. Higashi, B. C. Titeca, F. Lamote, A. Ceulemans, *J. Am. Chem. Soc.* **1999**, *121*, 12018-12028.

Very recently, and concomitantly with the development of this Thesis, the solid-state organization of several SubPcs bearing fluorine as substituent at both the axial and peripheral positions of the macrocycle and differing from each other for the peripheral substitution pattern (including chiral C_3- and C_1-symmetric trisubstituted derivatives) was systematically investigated by Miyajima and co-workers (Figure 136).[448]

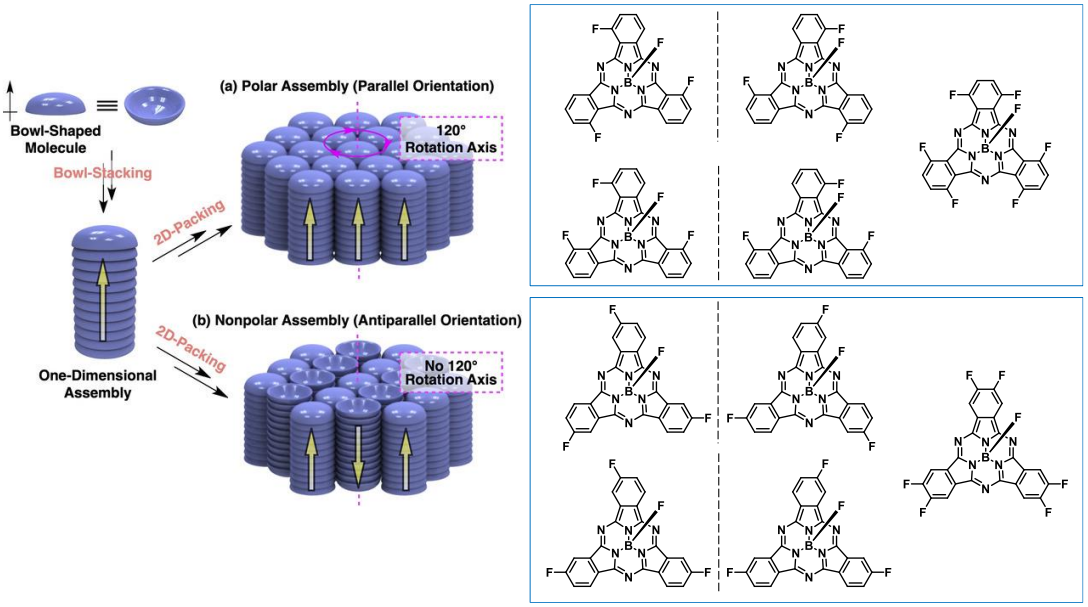

Figure 136. Cartoon depicting polar and non-polar assemblies with bowl-shaped molecules and structure of the SubPc derivatives investigated by Miyajima and co-workers. Adapted from ref. 448.

All the investigated derivatives arrange in the solid state in one-dimensional columnar stacks. Interestingly, the orientation of the columns within the crystal was found to depend on the position (namely, *ortho versus meta*) of the peripheral substituents. As a matter of fact, for hexa-substituted and tri-substituted SubPcs (either C_3-symmetric or C_1-symmetric, racemic or enantiopure) featuring an *ortho* functionalization pattern, the columnar stacks were found to organize in a parallel orientation, thus forming polar assemblies. In other words, all the investigated *ortho*-substituted SubPcs form polar crystals regardless of the number of fluorine atoms (3 or 6), molecular symmetry (C_3 or C_1) and optical purity (racemic or enantiopure). On the other hand, SubPcs bearing fluorine atoms at the *meta* positions of the macrocycle

[448] C. Zhang, Y. Guo, D. He, J. Komiya, G. Watanabe, T. Ogaki, C. Wang, A. Nihonyanagi, H. Inuzuka, H. Gong, Y. Yi, K. Takimiya, D. Hashizume, D. Miyajima, *Angew. Chem. Int. Ed.* **2021**, *60*, 3261-3267.

(including C_3 and C_1 tri-substituted derivatives, both racemic and enantiopure, as well as the hexa-substituted species), were found to form non-polar assemblies with an antiparallel orientation of the SubPc columns.

In summary, the scarceness of reports on the preparation and study of enantiopure SubPcs, along with the outstanding features of these chromophores and the intriguing properties provided by chirality, render the development of feasible and efficient methods for the optical resolution of inherently chiral SubPcs as well as the investigation of their organization features highly desirable to enable advances in SubPc-based (opto)electronic applications.

In addition to their potential as functional materials for molecular optoelectronics, enantiopure SubPcs also constitute a useful tool for the study of SubPc reactivity. To the date, only one report on the mechanism of axial substitution in SubPcs has been presented.[68] In this work, a bimolecular σ-bond metathesis mechanism was postulated for the axial ligand exchange reaction between SubPc-Cl and phenols. Remarkably, no mechanistic studies have been conducted on the reactivity of activated SubPc precursors nor on axial ligand exchange reactions in the presence of boron trihalides. The study of axial reactivity in optically pure SubPc derivatives (*e.g.* by monitoring the optical purity of the resulting substituted species) would enable to investigate the mechanistic aspects of axial substitution reactions, exploring the possibility of a bowl-to-bowl inversion of the SubPc cone-shaped macrocycle or probing the configurational stability of enantiopure SubPc species.

3.2 Specific objectives of Chapter 3

The main goal of this Chapter is the efficient optical resolution of an inherently chiral, C_3-symmetric SubPc and the study of the solid-state and on-surface organization of the racemic and enantiopure species, in view of the potential implementation of optically pure SubPcs in technological applications.

This Chapter is divided into two different sections.

The first part of this Chapter is centered on the optical resolution of a racemic SubPc derivative through different approaches, that is, by semipreparative chiral HPLC or *via* derivatization with a chiral auxiliary. The final aim is the presentation of feasible procedures for the efficient preparation of enantiopure SubPcs in such amounts as to allow for further investigations on their chirality-related properties and functionalities.

The second part of the Chapter is aimed to the study of the organization of inherently chiral SubPcs, either racemic or enantiopure. In particular, we will investigate the crystalline solid-state arrangement of a C_3-symmetric SubPc as a function of the chiral composition. Moreover, we aim to get further insights into the organization of enantiopure SubPc derivatives by exploring their on-surface arrangement.

3.3 Results and discussion

3.3.1 Efficient optical resolution of an inherently chiral SubPc

3.3.1.1 Optical resolution of C_3-symmetric I_3SubPc-Cl by chiral HPLC

As mentioned in the Introduction and background of this Chapter, in light of the intriguing properties related to chirality (such as emission of circularly polarized light, control of spin and tunable organization), chiral molecules constitute valuable building blocks with considerable added value in terms of potential applications as molecular materials in technologically relevant fields.[437] Taking into account the outstanding optical and electronic properties of SubPcs, as well as the inherent chirality of SubPcs obtained from cyclotrimerization of non-C_{2V} phthalonitrile precursors,[8] the efficient preparation of enantiopure SubPcs in highly desirable in view of their potential applications in optoelectronics.

To this end, the availability of feasible procedures for the effective optical resolution of racemic SubPcs is of crucial importance. Surprisingly, only a few reports have been published dealing with the optical resolution of inherently chiral SubPc derivatives.[33,37,105,448] In all of these work, chiral resolution of racemic SubPcs was accomplished by means of chiral HPLC. Most remarkably, no particular attention has been apparently focused on the optimization of the separation conditions in order to scale-up the preparation of enantiopure SubPc species, and an efficient method to obtain isolated SubPc enantiomers remains unreported so far.

In this connection, *meta*-substituted, C_3-symmetric I_3SubPc-Cl constitutes an extremely versatile, inherently chiral SubPc species, which efficient optical resolution would be of strategic importance for several applications. On one hand, the presence of a halogen atom at the axial position should improve the crystallinity and the solid-state packing, which is key in view of potential applications in devices. On the other hand, I_3SubPc-Cl constitutes a valuable synthon for the preparation of a large variety of SubPc derivatives which chirality-related properties could be exploited in numerous application fields, as both the axial and peripheral substituents can be easily replaced through well-known synthetic methodologies.[8] As described in the Introduction of this Thesis, efficient axial substitution in mild conditions can be carried out by generation on an activated SubPc species upon treatment of the starting SubPc-Cl with a triflate reagent or $AlCl_3$, allowing for the introduction of O-, N- and S-based nucleophiles.[48,51] Moreover, C-based nucleophiles can be introduced at the apical position of the macrocycle either by reaction of the SubPc-Cl precursor with Grignard reagents, or by activation of the axial position with $AlCl_3$ and subsequent reaction with alkynyl-TMS derivatives.[52,86] On the other hand, the peripheral iodine atoms of the macrocycle can be easily substituted by means of metal-catalyzed

cross-coupling reactions.[8,96] Finally, the preparation of enantiopure I_3SubPc-Cl would enable to investigate the mechanistic aspects of SubPc reactivity, allowing, for example, to explore the possibility of a bowl-to-bowl inversion of the macrocycle or to corroborate the configurational stability of optically pure SubPcs.

Meta-subtituted, C_3-symmetric I_3SubPc-Cl **9** was prepared as a racemic mixture of enantiomers by cyclotrimerization of 4-iodophthalonitrile. Purification from the C_1 regioisomer was carried out by column chromatography on silica gel.[37] The HPLC resolution of racemic I_3SubPc-Cl **9** was performed using a semipreparative chiral column. Several elution conditions differing in the composition of the eluent mixture, flux, and temperature, were scanned to accomplish the resolution of the chromatographic peaks corresponding to the two enantiomers, and finely tuned with the aim to maximize their separation, in view of the following scale-up. The HPLC chromatogram of racemic I_3SubPc-Cl **9** in the optimized elution conditions, showing two well-resolved peaks with a 1:1 area ratio, as well as the chromatograms of the isolated enantiomers, are reported in Figure 137.

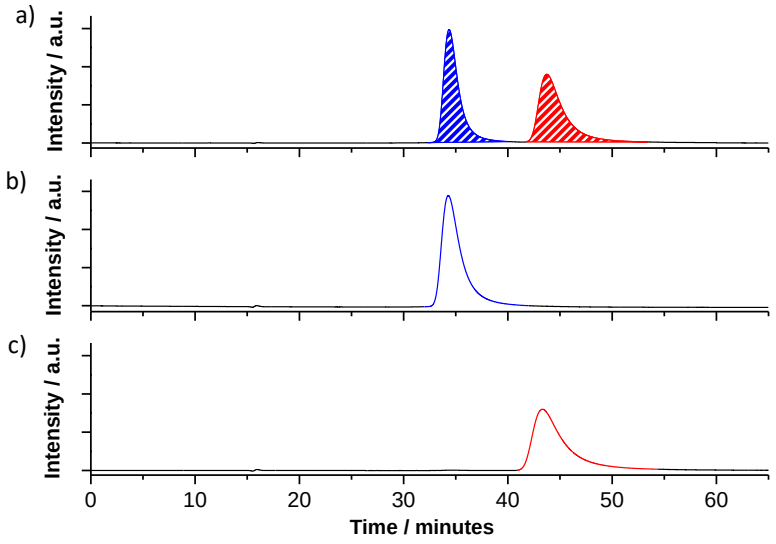

Figure 137. a) HPLC chromatogram of racemic I_3SubPc-Cl **9**. The percentage areas of the first and second peaks are 50.0% and 50.0%, respectively. b,c) HPLC chromatograms of the isolated enantiomers. HPLC conditions: eluting solvent mixture = toluene/*n*-hexane 50:50 (v/v); flow rate = 1.2 mL min^{-1}; temperature = 10 °C; detection wavelength = 570 nm).

Subsequently, sample concentration and injection volume were optimized by monitoring the absorbance at the SubPc absorption maximum, in order to maximize the amount of enantiopure

SubPc obtained from a single run (Figure 138). In this way, a separation rate of nearly 9 mg per day of racemic SubPc **9** could be reached. It is worth to mention that, as expected, the enantiopure species are configurationally stable in the investigated conditions, which constitutes a fundamental requirement for their use as chiral molecular materials in organic devices.

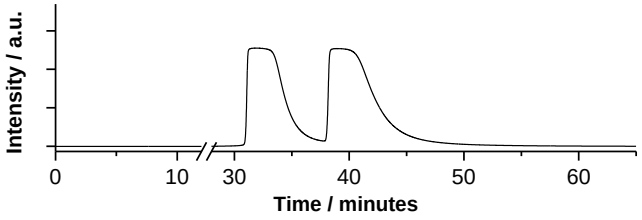

Figure 138. HPLC chromatogram of racemic I_3SubPc-Cl SubPc **9** with peaks corresponding to the two enantiomers in the experimental condition employed for the optical resolution on a semi-preparative scale (concentration of the injected solution: 1.8 mg/mL; injected volume: 200 µL; eluting solvent mixture = toluene/*n*-hexane 50:50; flow rate = 1.2 mL min^{-1}; temperature = 10 °C, detection wavelength = 570 nm). Performing runs of 60 minutes, a separation rate of nearly 9 mg per day of racemic SubPc **9** can be calculated.

The isolated species were characterized by means of CD spectroscopy to corroborate their enantiomeric relationship. As expected, the CD spectra of the first and second eluted fractions are mirror images of each other (Figure 139).

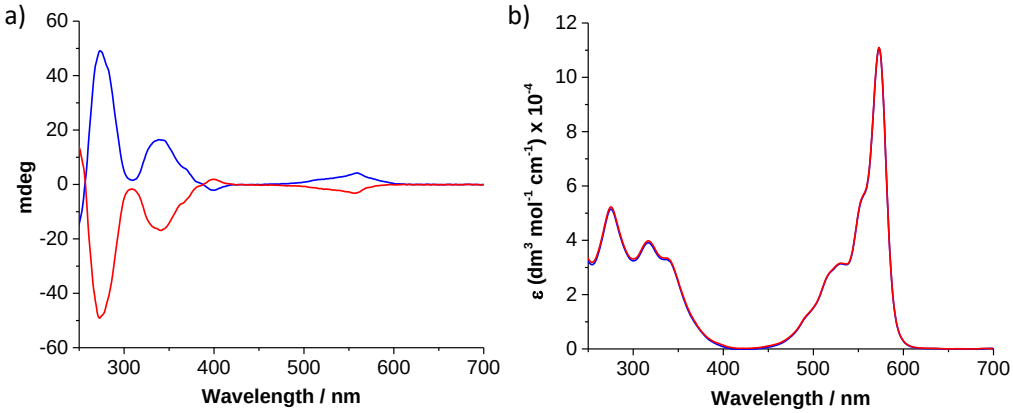

Figure 139. a) CD spectra of the first (blue spectrum) and second eluted (red spectrum) enantiomers of I_3SubPc-Cl **9** in $CHCl_3$ ($c = 2.0 \times 10^{-5}$ M). b) UV-vis absorption spectra of the first (blue spectrum) and second eluted (red spectrum) enantiomers of I_3SubPc-Cl **9** in $CHCl_3$ ($c = 7.0 \times 10^{-6}$ M).

Remarkably, single crystals of the isolated enantiomers suitable for X-ray diffraction analysis were obtained by slow diffusion of methanol in chloroform. The resolution of the crystal structure of the enantiopure species allowed to unequivocally assign their absolute configuration. In particular, the first eluted species was shown to corresponds to the *M* enantiomer, whereas the second eluted species was observed to corresponds to the *P* enantiomer (Figure 140). The unambiguous assignment of the absolute configuration to isolated enantiomers of inherently chiral SubPcs had no precedent in SubPc chemistry until the very recent report of Miyajima and co-workers.[448]

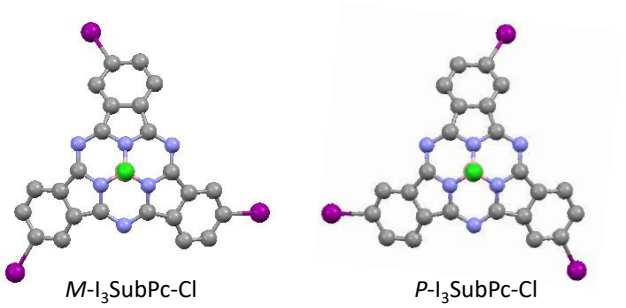

M-I_3SubPc-Cl (first eluted enantiomer)

P-I_3SubPc-Cl (second eluted enantiomer)

Figure 140. Crystal structure of the (left) first and (right) second eluted enantiomers of I_3SubPc-Cl **9**. In the figures, the B atom is eclipsed by the apical Cl atom.

3.3.1.2 Optical resolution of C_3-symmetric I_3SubPc-Cl *via* derivatization with a chiral auxiliary

In the previous section, diastereomeric interactions with a chiral stationary phase have been exploited for the optical resolution of inherently chiral I_3SubPc-Cl **9** by HPLC. An alternative strategy for the preparation of enantiopure SubPc species consists in the derivatization of a racemic SubPc with a chiral, optically pure reagent. Upon separation of the resulting diastereomers and subsequent removal of the chiral auxiliary from the isolated diastereomeric species, it would be possible to obtain the pure enantiomers of the starting SubPc. In comparison with optical resolution by chiral HPLC, this method presents the advantage to allow for the obtention of enantiomerically pure SubPcs by common laboratory techniques. Remarkably, this approach has never been employed yet for the optical resolution of inherently chiral *meta*-substituted SubPc derivatives. As a matter of fact, in all the published papers dealing with the separation of racemic SubPcs into their component enantiomers, chiral HPLC technique has been exploited.[33,37,105,448]

To this end, we aimed to probe BINOL and its derivatives as resolving agents for inherently chiral SubPcs. BINOL and functionalized BINOL species constitute extremely versatile compounds,

which chirality stems from the hindered rotation around the single C-C bond that results in the formation of two enantiomeric atropisomers (Figure 141).[449,450] The high rotation barrier and the consequent high thermal stability of the enantiomeric species enable their use in a large variety of organic reactions.[449] As a matter of fact, BINOL-based derivatives have been extensively employed as both chiral reagents and chiral ligands in stoichiometric and catalytic asymmetric synthesis, respectively. In the frame of SubPc chemistry, enantiopure BINOL has been employed as axial bridging unit or ring substituent for the preparation of optically active SubPc dimer or peripherally-substituted SubPcs (Figure 134).[29,446]

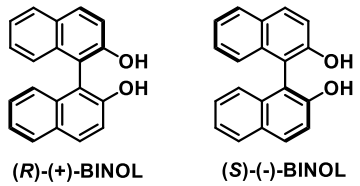

Figure 141. Chemical structure of (*R*)-(+)-BINOL and (*S*)-(-)-BINOL.

In this case, derivatization of racemic I_3SubPc-Cl **9** with BINOL was performed through axial substitution of the chlorine ligand. The axial approach is preferable than functionalization of the peripheral positions of the macrocycle, as both the replacement of the apical halogen substituent and the subsequent removal of the resolving agent can be carried out by straightforward procedures. In particular, the replacement of axial aryloxy moieties with chlorine can be easily performed by treatment of the substituted SubPc with boron trichloride.[8]

First of all, we attempted the chiral resolution of racemic I_3SubPc-Cl **9** using (*R*)-BINOL as chiral auxiliary. Replacement of the axial chlorine ligand was carried out upon prior activation of the SubPc axial position in order to prevent racemization of the resolving agent, as this strategy allows for the use of milder reaction conditions with respect to that employed in one-step axial substitution reactions.[48,51] In particular, axial substitution was performed by treatment of the SubPc precursor with $AlCl_3$, following a procedure reported by the group of Bender (Scheme 11).[51] In these conditions, a complex is formed in which the aluminum interact with the apical chlorine ligand and one of the outer nitrogen atoms of the macrocycle. Subsequent addition of (*R*)-BINOL and quenching of the resulting complex with pyridine afforded I_3SubPc-BINOL **37** in 46% yield. A similar reaction yield (namely, 44%) was obtained by performing the axial ligand

[449] J. M. Brunel, *Chem. Rev.* **2005**, *105*, 857-898.
[450] J. M. Brunel, *Chem. Rev.* **2007**, *107*, PR1-PR45.

exchange reaction *via* generation of a SubPc-OTf intermediate through reaction of I_3SubPc-Cl **9** with AgOTf, following the methodology reported by Guilleme *et al.*[48]

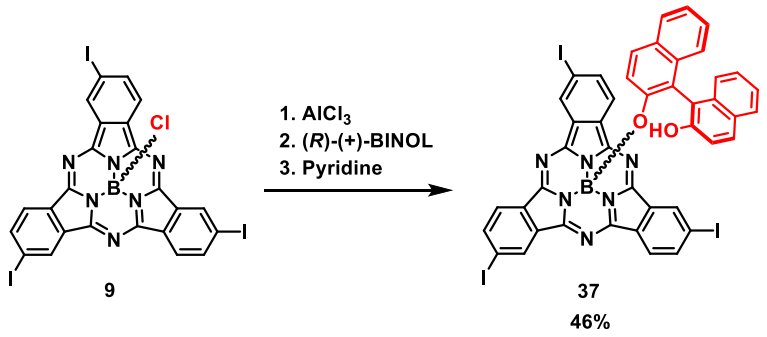

Scheme 11. Synthesis of I_3SubPc-BINOL **37** from I_3SubPc-Cl **9**.

This reaction results in the formation of a mixture of two diastereomers, as evidenced by the presence of two set of signals in the ^{1}H-NMR spectrum of the product (Figure 142). From the 1:1 ratio between the integrals of the signals corresponding to the protons of the SubPc macrocycle in the two species, it can be inferred that axial derivatization of I_3SubPc-Cl **9** with (*R*)-BINOL is not diastereoselective.

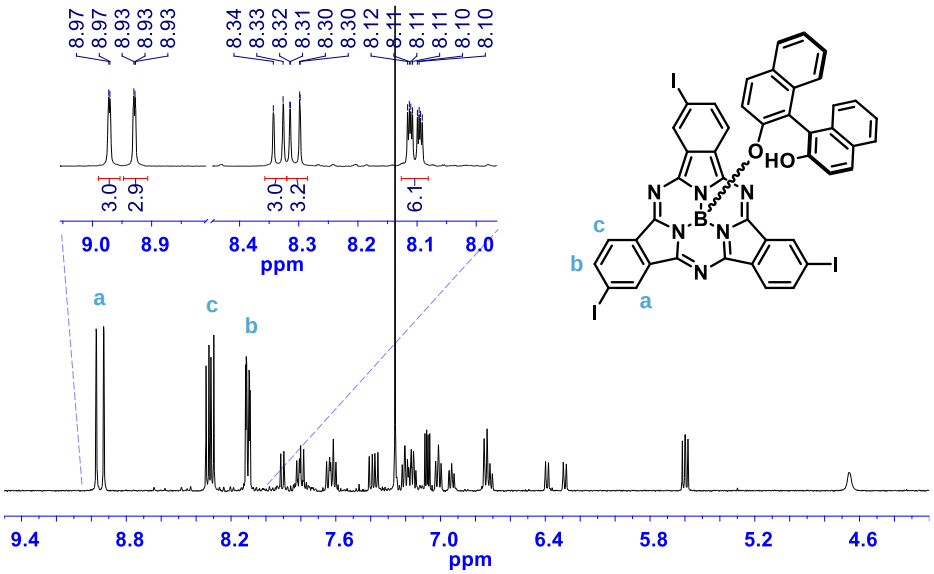

Figure 142. ^{1}H-NMR spectrum (500 MHz, $CDCl_3$) of I_3SubPc-BINOL **37**. Inset: zoom of the signals of the isoindolic protons of the SubPc macrocycle.

Unfortunately, separation of the diastereomers by column chromatography on silica gel turned out to be not feasible. As a matter of fact, despite testing numerous eluent conditions in TLC, in no case two resolved spot were observed, and a column chromatography attempt carried out by using the most promising eluent mixture on TLC among the ones tested (namely, $CHCl_3$/toluene 2:3) did not afford any pure diastereomeric fraction.

Thus, other BINOL derivatives were tested as resolving agents. In particular, derivatization with (*R*)-(+)-3,3'-dibromo-1,1'-bi-2-naphthol (hereafter referred to as (*R*)-dibromo-BINOL) afforded two distinct spots in TLC (R_f = 0.36 and 0.31 in DCM/heptane 3:1), rendering this derivative a good candidate for the optical resolution of *meta*-I_3SubPc-Cl **9**. Axial substitution of I_3SubPc-Cl **9** with (*R*)-dibromo-BINOL *via* activation of the axial position with $AlCl_3$ afforded I_3SubPc-dibromoBINOL **38** in 62% overall yield (Figure 143).

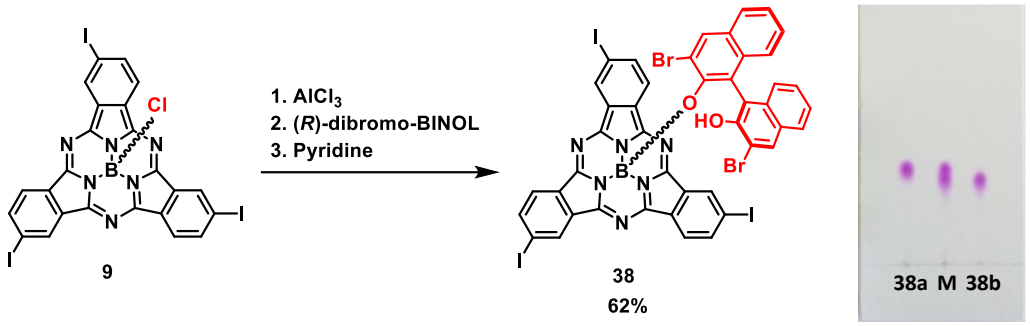

Figure 143. (Left) Synthesis of I_3SubPc-dibromo-BINOL **38** from I_3SubPc-Cl **9**. (Right) TLC of the two diastereomers separated by column chromatography (eluent: DCM/heptane 3:1).

As observed for derivatization with (*R*)-BINOL, the ^{1}H-NMR spectrum of the product showed the formation of a 1:1 mixture of diastereomers, indicating that the replacement of the axial chlorine ligand in I_3SubPc-Cl **9** with (*R*)-dibromo-BINOL is not diastereoselective (Figure 144).

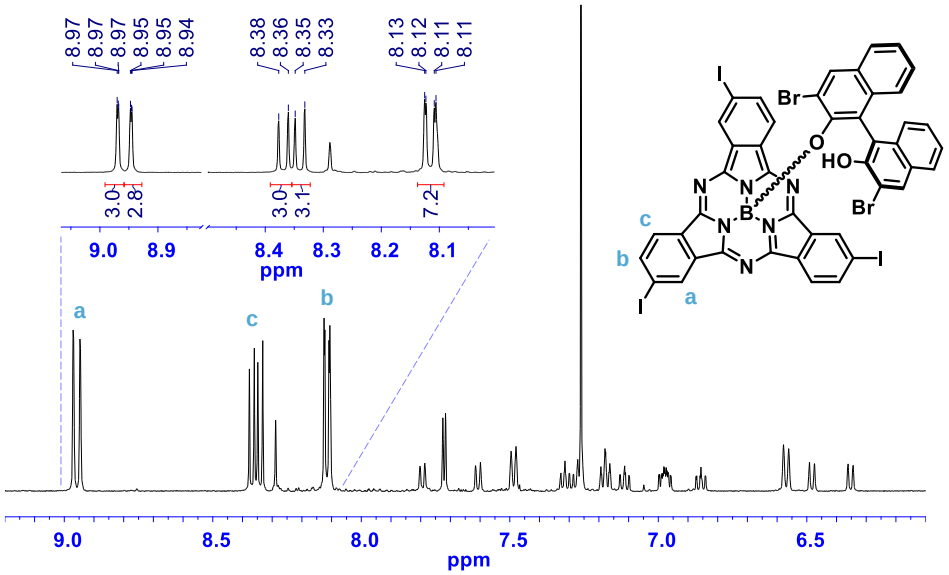

Figure 144. Partial ^{1}H-NMR spectrum (500 MHz, $CDCl_3$) of I_3SubPc-dibromo-BINOL **38**. Inset: zoom of the signals of the benzene protons of the SubPc macrocycle. The integral of the signals of the benzene protons marked with "b" is due to the overlap with the signal of an aromatic proton of the axial ligand (see Figure 148).

In order to further confirm this evidence, and to be able to check the purity of the separated diastereomeric fractions after column chromatography, HPLC eluting conditions were optimized in order to resolve the peaks corresponding to the two diastereomers. In line with what indicated by NMR analysis, the HPLC chromatogram of the diastereomeric mixture showed the presence of two peaks with similar relative areas (Figure 145).

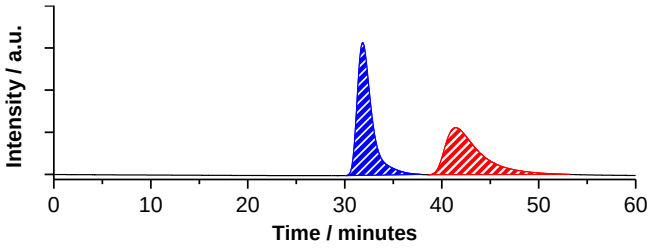

Figure 145. HPLC chromatogram of I_3SubPc-dibromo-BINOL **38** (diastereomeric mixture). The percentage areas of the first and second peaks are 52.7% and 47.3%, respectively. HPLC conditions: eluting solvent mixture = toluene/*n*-hexane 70:30 (v/v); flow rate = 1.0 mL min^{-1}; temperature = 10 °C; detection wavelength = 570 nm).

The separation of the two diastereomers was successfully achieved by column chromatography on silica gel using a mixture of DCM/heptane 3:1 (v/v) as eluent. Hereafter, the first and second eluted I_3SubPc-dibromo-BINOL diastereomers will be referred to as **38a** and **38b**, respectively. Please note that the elution order is referred to column chromatography on silica gel in the elution conditions employed to separate the two diastereomers. Elution order in HPLC is inverted, that is, the retention time of **38b** in HPLC is lower than the retention time of **38a**.

In particular, column chromatography of the crude allowed to isolate 100% pure **38a** (Figure 146a), whereas the second eluted collected fraction, which was enriched in **38b,** was shown to contain a 10.4% of **38a**, as evidenced by HPLC analysis (Figure 146b). Upon further purification of the second eluted fraction by a second chromatographic column, the purity of **38b** was increased up to 94.2 % (Figure 146c).

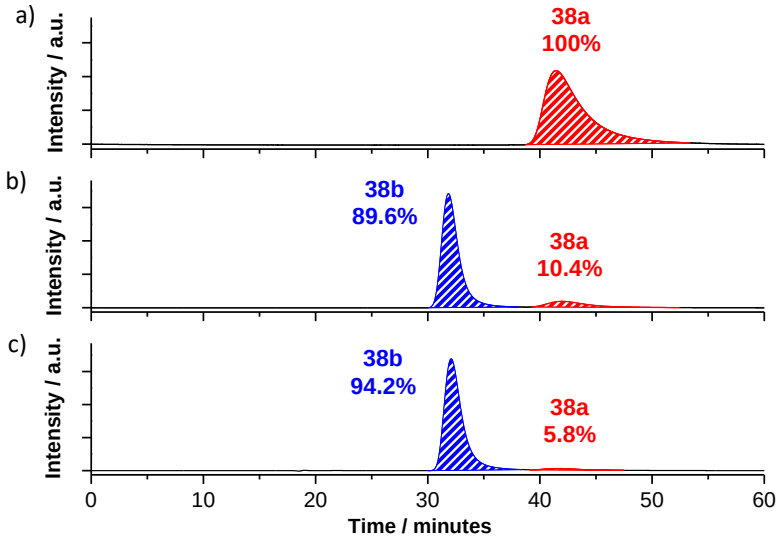

Figure 146. HPLC chromatogram of a) the first eluted fraction of I_3SubPc-dibromo-BINOL **38** after the first column chromatography, b) the second eluted fraction of I_3SubPc-dibromo-BINOL **38** after the first column chromatography, and c) the second eluted fraction of I_3SubPc-dibromo-BINOL **38** after the second column chromatography. The percentage areas of the first and second peaks are indicated for each chromatogram. HPLC conditions: eluting solvent mixture = toluene/*n*-hexane 70:30 (v/v); flow rate = 1.0 mL min^{-1}; temperature = 10 °C; detection wavelength = 570 nm).

The CD spectra of the isolated diastereomers show positive and negative bands in the 240-700 nm region, which resemble the absorption bands in the corresponding UV-vis spectra (Figure 147).

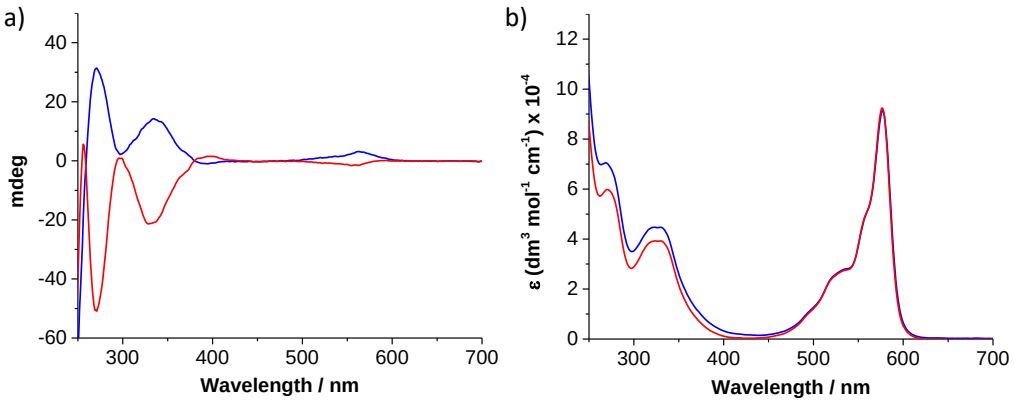

Figure 147. a) CD spectra of **38a** (red spectrum) and **38b** (blue spectrum) in $CHCl_3$ ($c = 2.0 \times 10^{-5}$ M). b) UV-vis absorption spectra of **38a** (red spectrum) and **38b** (blue spectrum) in $CHCl_3$ ($c = 7.0 \times 10^{-6}$ M).

The ^{1}H-NMR spectra of the isolated diastereomers **38a** and **38b** are shown in Figure 148. Signals were assigned with the help of H-H COSY and H-H NOESY experiments. As an example, the H-H COSY and H-H NOESY spectra of **38a**, showing the correlations between the protons of the naphthyl unit linked to the B atom and between the protons of the naphthyl unit bearing the free hydroxyl group, are shown in Figures 149 and 150. The effect of the diatropic ring current of the aromatic SubPc macrocycle is particularly visible on the signals of protons 8 and 8' of the axial ligand, which appear between 6.35 and 6.57 ppm.

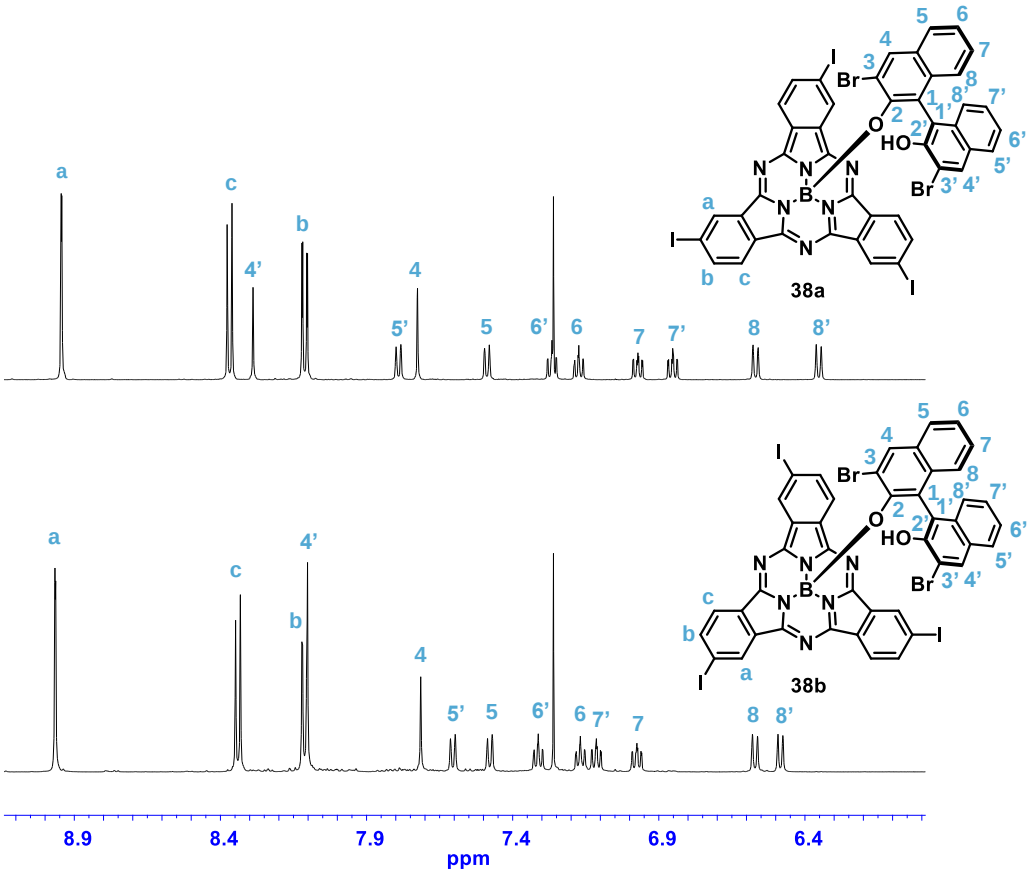

Figure 148. Partial ^{1}H-NMR spectra (500 MHz, $CDCl_3$) of I_3SubPc-dibromo-BINOL **38a** and **38b**.

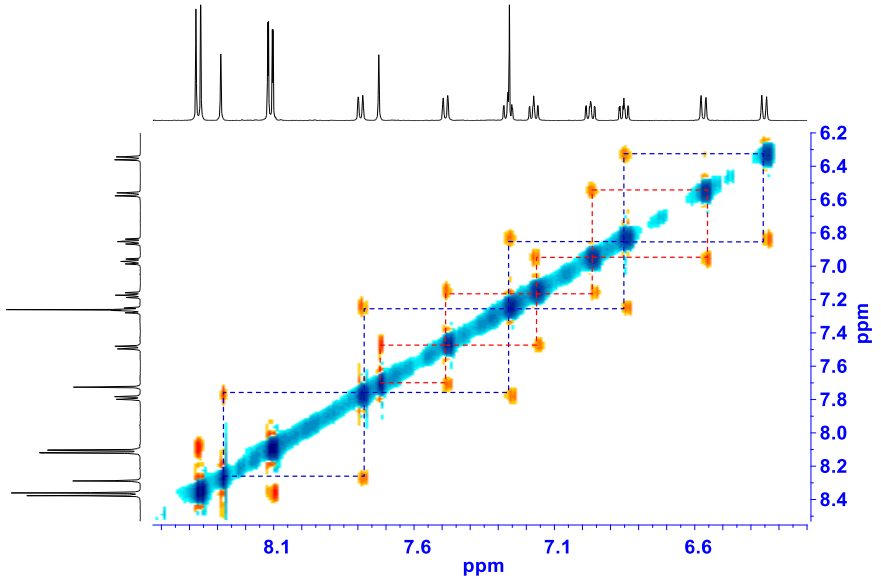

Figure 149. Zoom of the region between 8.5 ppm and 6.2 ppm of the H-H COSY NMR spectrum (500 MHz, $CDCl_3$) of **38a**. Red lines and blue lines indicate the correlation between the protons of the naphthyl unit linked to the B atom and between the protons of the naphthyl unit bearing the free hydroxyl group, respectively.

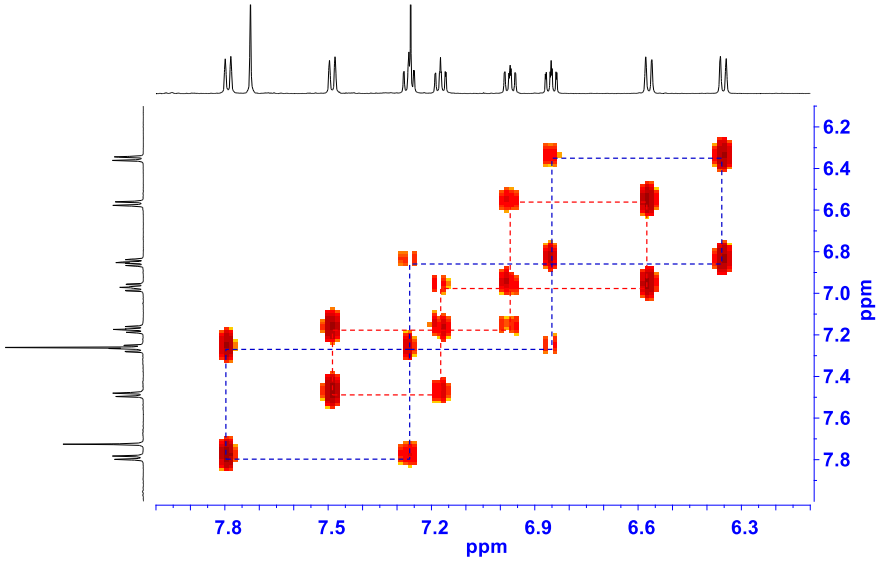

Figure 150. Zoom of the region between 8.0 ppm and 6.1 ppm of the H-H NOESY NMR spectrum (500 MHz, $CDCl_3$) of **38a.** Red lines and blue lines indicate the correlation between the protons of the naphthyl unit linked to the B atom and between the proton of the binaphthyl unit bearing the free hydroxyl group, respectively.

The removal of the resolving agent from the separated I_3SubPc-dibromo-BINOL diastereomers **38a** and **38b** was carried out by reaction with an excess of BCl_3 (*i.e.*, 10 equiv.) at 50 °C in toluene (Scheme 12). In these conditions, the *P*-**9** and *M*-**9** enantiomeric species were obtained in excellent yield (*i.e.* 96%) and high enantiomeric excesses from reaction of **38a** and **38b**, respectively. As a matter of fact, the product obtained from the removal of the chiral auxiliary from **38a** (namely, *P*-**9**) contains only a 2.3% of *M*-**9** enantiomer, as revealed by HPLC analysis (Figure 151a). On the other hand, the product obtained from reaction of **38b**, that is, *M*-**9**, contains a slightly higher amount of *P*-**9** (namely, 8.8%). This is in line with the lower purity of the corresponding preursor diastereomer (Figure 146), which was obtained as second eluted fraction from column chromatography.

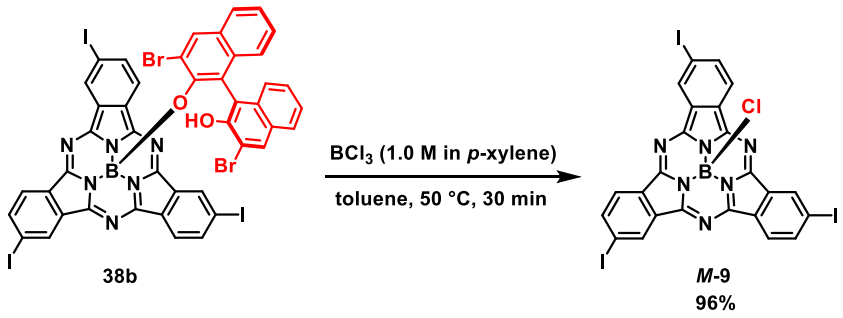

Scheme 12. Replacement of the chiral auxiliary in **38b** with a chlorine atom to afford *M*-**9**.

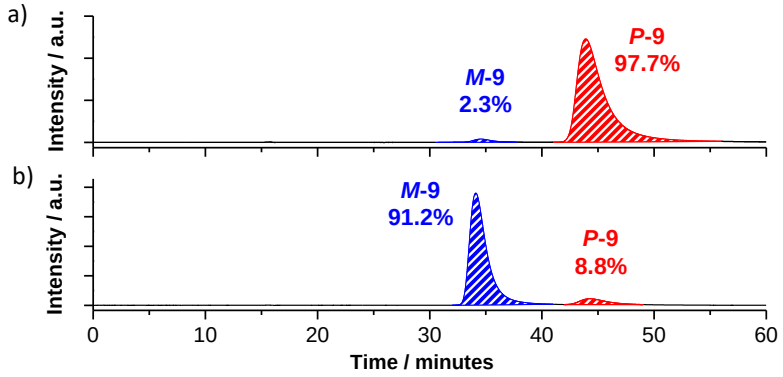

Figure 151. HPLC chromatogram of a) the product obtained from the removal of the chiral auxiliary from I_3SubPc-dibromo-BINOL **38a**, and b) the product obtained from the removal of the chiral auxiliary from I_3SubPc-dibromo-BINOL **38b**. The percentage areas of the first and second peaks are indicated for each chromatogram. HPLC conditions: eluting solvent mixture = toluene/*n*-hexane 50:50 (v/v); flow rate = 1.2 mL min^{-1}; temperature = 10 °C; detection wavelength = 570 nm).

From a comparison between the signs of the CD signals of the isolated diastereomers and that of the resulting enantiomeric species (Figures 139 and 147), and taking into account the similarity between the purity of the diastereomeric precursors and that of the enantiomeric products, we infer that configuration is retained upon removal of the chiral auxiliary in the investigated conditions. In light of the aforementioned, the replacement of the axial naphthoxy ligand is likely to take place by interaction of the boron halide with the central boron atom from the convex face of the SubPc cone-shaped macrocycle. This is in agreement with the bimolecular σ-bond metathesis mechanism postulated for the axial ligand exchange reaction between SubPc-Cl derivatives and phenols.[68]

Notably, these experimental findings are in contrast with what was observed for an *ortho*-substituted, C_3-symmetric I_3SubPc analogue in our research group.[451] In that case, a remarkably lower enantiomeric excess (namely, 68.4%) was detected upon removal of the apical BINOL ligand from an isolated diastereomer in the presence of BCl_3 in slightly harder conditions, which was ascribed to a partial bowl-to-bowl inversion of the macrocycle. This difference may be attributed, in principle, to steric and/or electronic effects arising from the different peripheral substitution pattern of the SubPc (*i.e.*, *meta versus ortho*).

With the aim to investigate the possibility of a bowl inversion in the *meta*-substituted I_3SubPc-Cl derivative, we realized a qualitative test on enantiopure *M*-**9** employing experimental conditions similar to that in which the inversion of the *ortho*-substituted species takes place (*i.e.*, 20 equiv. of BCl_3, 70 °C), monitoring the optical purity of the reaction mixture by chiral HPLC. In these conditions, no racemization was observed for *M*-**9** even after 24 hours. On the other hand, treatment of enantiopure *M*-**9** with a large excess of BCl_3 (namely, 60 equiv.) at 70 °C led to a significant racemization of the starting material. This finding, along with what was observed in our research group with *ortho*-substituted I_3SubPc-Cl,[451] point out the possibility for SubPc derivatives to undergo bowl-to-bowl inversion. In this connection, it is worth to mention that evidence of bowl inversion in contracted porphyrinoids has been reported by Osuka and Yoshida for B-methoxy subporphyrins.[452] In this work, interconversion between β-(4-methoxyphenylsulfinyl)SubP diastereomers was observed to take place in protic solvents such as methanol or ethanol. In particular, a dramatic acceleration of the process was observed upon addition of trifluoroacetic acid. In light of these findings, a mechanism involving the protonation-induced generation of SubP borenium cations followed by nucleophilic attack by alcohols was proposed.

[451] L. Tejerina González, Ph.D. Thesis, Universidad Autónoma de Madrid, Madrid, Spain, 2017.
[452] K. Yoshida, A. Osuka, *Chem. Eur. J.* **2015**, *21*, 11727-11734.

3.3.2 Insights into the organization of racemic and enantiopure SubPc species

3.3.2.1 Solid-state organization of *C*$_3$-symmetric I$_3$SubPc-Cl

As mentioned in the Introduction and background of this Chapter, the study of the organization of multiple molecular units in the bulk if of key importance for the design of high-performance devices, along with the understanding of single-molecule characteristics.[443] As an example, it is well-known that the charge transport properties of bulk materials, which greatly influence the performances of (opto)electronic devices, strongly depend on molecular packing.[453] In the frame of chiral organic materials, different solid-state arrangements may be expected when considering different chiral compositions.[437] Thus, the realization of comparative studies of the organization of racemic and enantiopure SubPc derivatives in the solid state is of great interest in view of their potential implementation as molecular materials in technological applications.

In order to evaluate the differences between *C*$_3$-symmetric I$_3$SubPc-Cl species in terms of solid-state organization as a function of the chiral composition, X-ray diffraction analysis of single crystals of racemic and optically pure samples was performed. As for the isolated *P*-**9** and *M*-**9** enantiomers, single crystals of racemic I$_3$SubPc-Cl **9** were obtained by slow diffusion of methanol in chloroform.

Within the crystal structure of racemic I$_3$SubPc-Cl **9**, molecules are organized in concave-convex, tail-to-tail homochiral dimers linked together through π-π interactions between the isoindolic benzene rings (Figures 152 and 153).[34] In turn, the dimers are arranged in homochiral columnar stacks. Within the columns, stabilizing Cl···π interactions between the axial halogen atoms and the isoindolic benzene rings of molecules belonging to adjacent stacked dimers can be observed (Figure 153).

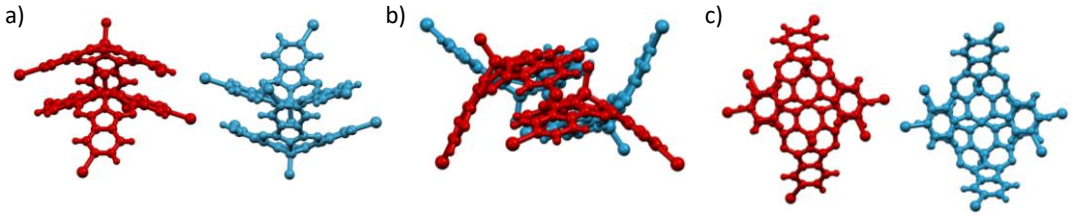

Figure 152. a) Front, b) lateral and c) top view of a portion of the X-ray crystal structure of racemic I$_3$SubPc-Cl **9** showing the formation of homochiral dimers. The *P* enantiomer has been colored in red and the *M* enantiomer has been colored in blue for the sake of clarity.

[453] Z.-F. Yao, J.-Y. Wang, J. Pei, *Cryst. Growth Des.* **2018**, *18*, 7-15.

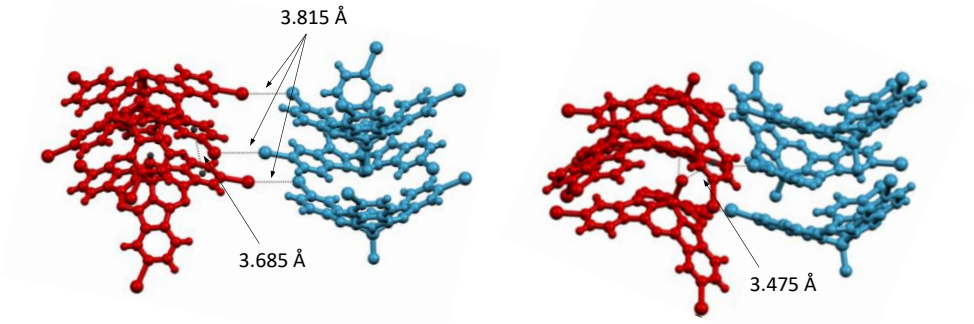

Figure 153. Two different views of a portion of the X-ray crystal structure of racemic I_3SubPc-Cl **9** evidencing the interactions within homochiral columns and between adjacent homochiral columns composed of SubPcs of opposite chirality. The *P* enantiomer has been colored in red and the *M* enantiomer has been colored in blue for the sake of clarity.

Interestingly, the arrangement of the homochiral columns within the crystal varies depending on the direction considered. While along one direction alternating homochiral columns formed by molecules of opposite chirality are organized in an antiparallel arrangement (Figure 154), in another direction columnar stacks composed of molecules of the same chirality run parallel between them (Figure 155). As a result, a laminar organization is obtained (Figures 154d and 155d). Halogen-halogen interactions between the peripheral iodine atoms of molecules of the same or opposite chirality belonging to adjacent columns can be observed (Figure 153).

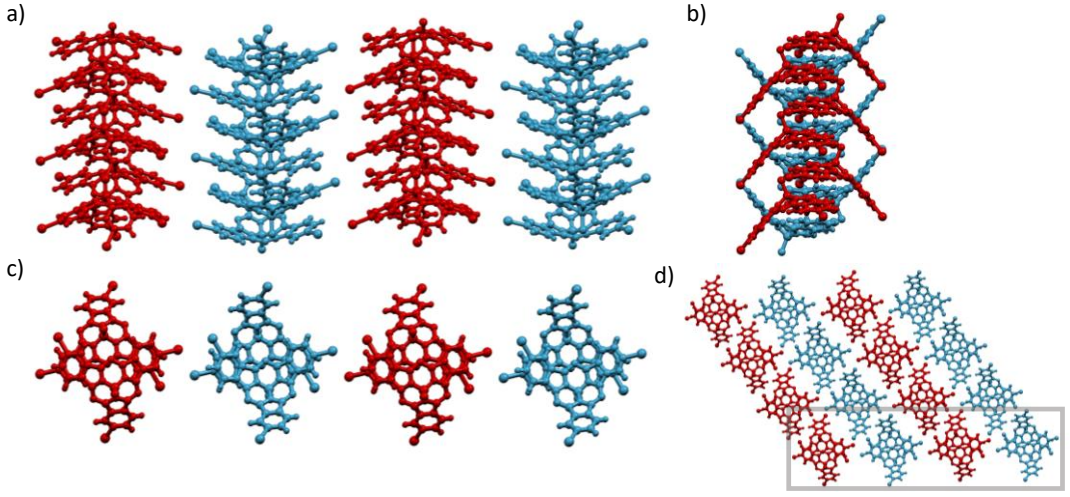

Figure 154. a) Front, b) lateral and c) top view of the portion of the X-ray crystal structure of racemic I_3SubPc-Cl **9** framed in d) showing the antiparallel arrangement adopted by adjacent homochiral columns composed of molecules of opposite chirality. The *P* enantiomer has been colored in red and the *M* enantiomer has been colored in blue for the sake of clarity.

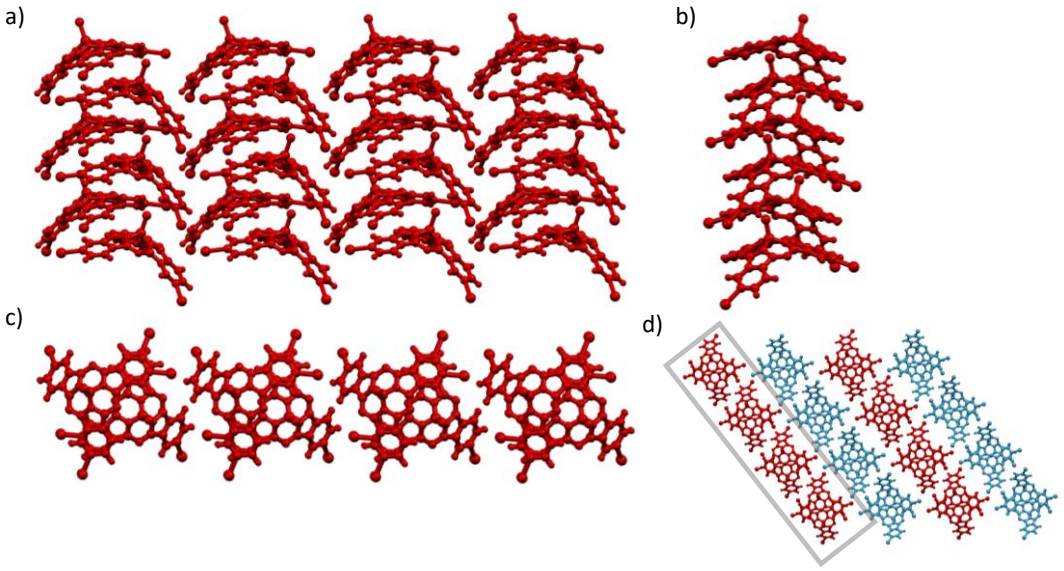

Figure 155. a) Front, b) lateral and c) top view of the portion of the X-ray crystal structure of racemic I_3SubPc-Cl **9** framed in d) showing the parallel arrangement adopted by adjacent homochiral columns composed of molecules of the same chirality. The *P* enantiomer has been colored in red and the *M* enantiomer has been colored in blue for the sake of clarity.

The *M*-**9** and *P*-**9** enantiopure species show an appreciably different crystal packing with respect to racemic I_3SubPc-Cl **9**, that is to say, assembly in the solid state is sensitive to chiral composition. As observed for racemic I_3SubPc-Cl **9**, in the crystal structure of the optically pure derivatives molecules are arranged in concave-convex, tail-to-tail homochiral dimers through π-π interactions between the isoindolic benzene rings (Figures 156 and 157). The dimers are stacked into homochiral columns, which are further stabilized by Cl···π interactions involving the axial chlorine atoms and the isoindolic benzene rings of stacked molecules belonging to adjacent dimers (Figure 157).

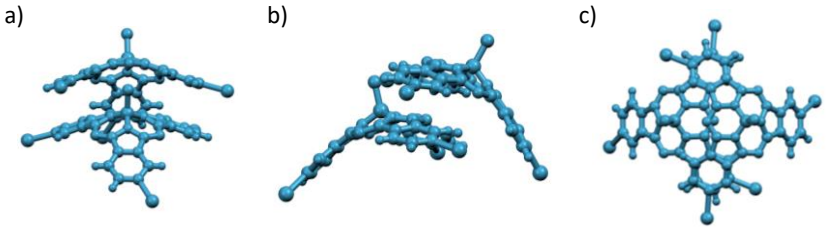

Figure 156. a) Front, b) lateral and c) top view of a portion of the X-ray crystal structure of enantiopure I_3SubPc-Cl *M*-**9** showing the formation of homochiral dimers.

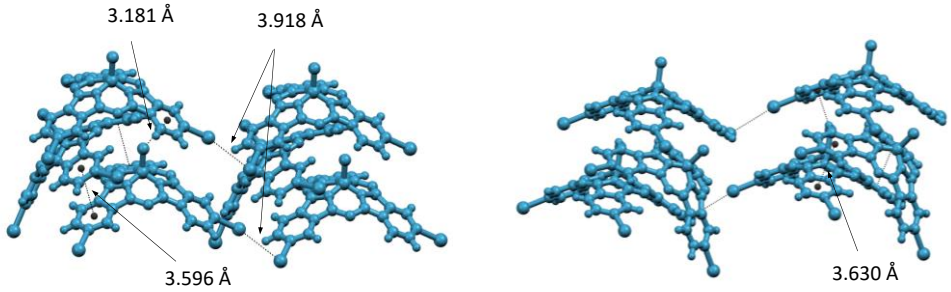

Figure 157. Two different views of a portion of the X-ray crystal structure of enantiopure I_3SubPc-Cl *M*-**9** evidencing the interactions within and between adjacent columns.

Remarkably, all the columnar stacks are organized in a parallel arrangement regardless the considered direction within the crystal, in contrast to what observed for racemic SubPc **9** (Figure 158). Molecules belonging to adjacent columns interact by means of halogen-halogen interactions between the iodine atoms decorating the periphery of the SubPc macrocycle (Figure 157).

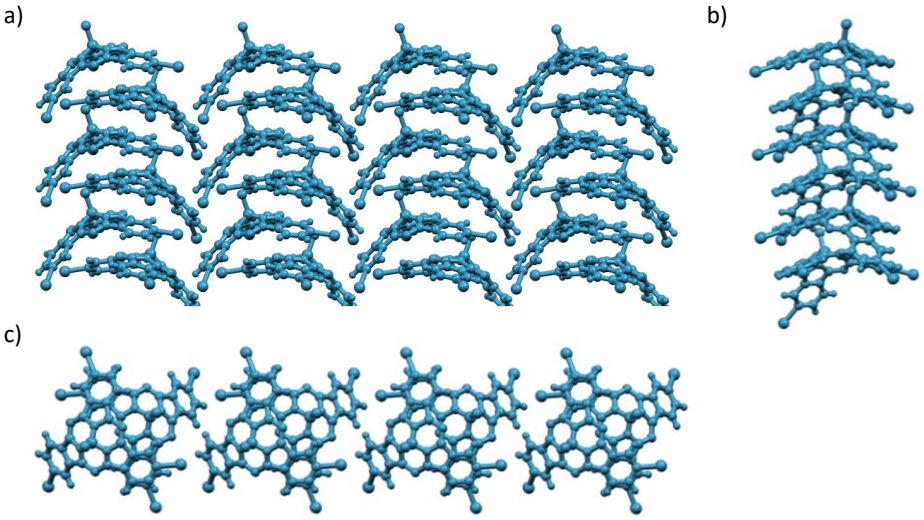

Figure 158. a) Front, b) lateral and c) top view of a portion of the X-ray crystal structure of enantiopure I_3SubPc-Cl *M*-**9** showing the parallel arrangement adopted by adjacent columns.

Curiously, these experimental findings are in contrast with what observed by Miyajima and co-workers for peripherally and axially fluorinated SubPcs.[448] In that case, the parallel *versus* antiparallel arrangement of the columnar stacks was found to depend solely on the *meta* or

ortho position of the peripheral substituents, whereas it was unaffected by the number of ring substituents (*i.e.*, 3 *versus* 6), the regioisomery (*i.e.*, C_3 *versus* C_1) and the chiral composition (*i.e.*, racemic *versus* enantiopure) of the sample (Figure 136). In this connection, it is worth to mention that, in order to realize a comparative study, the efficient optical resolution of C_1-symmetric I_3SubPc-Cl was also attempted and successfully accomplished. Nevertheless, any effort to grow single crystals of the racemic and enantiopure C_1 derivatives suitable for X-ray diffraction analysis was unsuccessful. A possible rationale for the different tendency towards crystallization of the C_1-symmetric and the C_3-symmetric isomers could be constituted by the higher solubility of former with respect to the latter.

The observed differences in the organization of the columnar stacks within the crystal structures of racemic and enantiopure species of the same SubPc derivative is of great interest in view of the potential application of inherently chiral SubPcs in technological devices, as it would allow to tune the bulk properties of the materials simply by tailoring its chiral composition. In particular, the parallel arrangement found in the crystal structures of enantiopure *M*-**9** and *P*-**9**, with all the SubPc units pointing towards the same direction, is quite unusual for columnar SubPc packings, which usually exhibit an antiparallel organization.[62,146] This highly directional, polar columnar assembly renders the investigated enantiopure SubPcs intriguing candidates as semiconductor and ferroelectric materials.[24,156] As such, the different arrangement of the columnar stacks within the crystal structures of racemic and enantiopure samples of SubPc **9** is expected to have an impact on the charge carrier transporting ability of the materials. In this connection, charge carrier mobility measurements are currently being conducted in collaboration with the research group of Prof. Shu Seki at Kyoto University, Japan.

3.3.2.2 On-surface organization of C_3-symmetric I_3SubPc-Cl

In order to get further insights into the self-assembly behavior of chiral SubPc species, we decided to investigate their organization on metal surfaces (namely, Au(111), Ag(111) and Cu(111)) by means of STM technique. These studies were performed in collaboration with the research group of Dr. Jorge Lobo Checa at the University of Zaragoza, Spain.

Unfortunately, room temperature deposition of enantiopure *M*-**9** on Ag(111) and Cu(111) substrates yielded highly irregular polymeric structures (Figure 159). This is likely due to the high reactivity of the C-I bonds, which undergo cleavage upon reaching the metal surface.

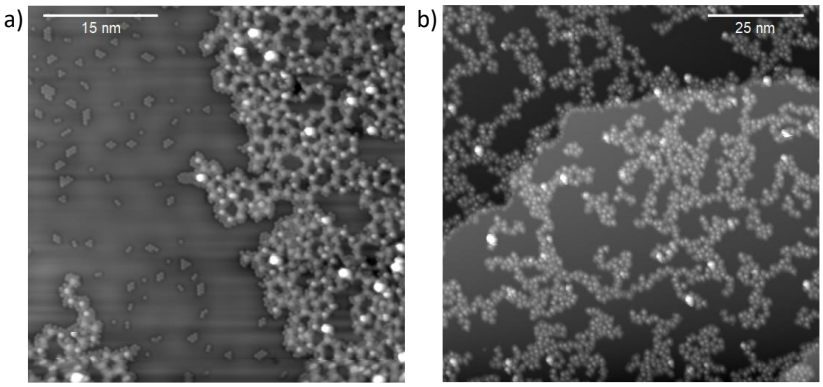

Figure 159. STM images obtained after deposition of *M*-**9** on a) Ag(111) and b) Cu(111) at room temperature. Imaging conditions: a) V_S = -100 mV; I_t = 100 pA, b) V_S = 1000 mV; I_t = 100.

On the other hand, upon deposition of enantiopure *M*-**9** on Au(111) at room temperature, SubPc molecules mostly preserve their peripheral iodine substituents, leading to the generation of more ordered structures. Nevertheless, it should me stated that also in this case order is quite poor. Moreover, the right-handed or left-handed propeller shape of the adsorbed species cannot be unambiguously distinguished. Different kinds of assemblies can be observed, as shown in Figure 160. The formation of these arrangement can in principle be rationalized on the basis of dipole-dipole $N_{im}\cdots I$ interactions (where N_{im} refers to the iminic nitrogen atoms) and C-H$\cdot\cdot$I interactions between adjacent molecules. As a matter of fact, in the observed assemblies, and in particular in the hexagonal arrays shown in Figures 160b-c, the peripheral iodine atoms point toward the outer nitrogen atoms of the SubPc macrocycle. Electrostatic potential map simulations by means of DFT calculations could be performed to confirm this hypothesis.

As it can be observed in close-up STM images, whereas some molecules show a central bright point, which can be attributed to a Cl-up adsorption configuration (that is, with the B-Cl moiety pointing toward the vacuum side of the interface),[163,169,173] others do not. This could be related, in principle, to either a Cl-down configuration (that is, with the B-Cl moiety pointing toward the Cu surface) or to the presence of dechlorinated molecules which interact with the surface through the concave aromatic face (the so-called DeCl-up configuration). In particular, the brightness of the contrast points to the presence of DeCl-up molecules. This is in line with what proposed in a recent report of Monti, Zojer and co-workers, who investigated the self-assembly of H_{12}SubPc-Cl on Cu(111) my means of STM and DFT studies.[169] In this work, different adsorption configurations where observed, corresponding to Cl-up molecules and DeCl-up molecules resulting from surface-catalyzed dichlorination, whereas no evidence was found for

Cl-down molecules. As a matter of fact, the latter was shown to be an unstable configuration for unsubstituted SubPc-Cl deposited on Cu(111).

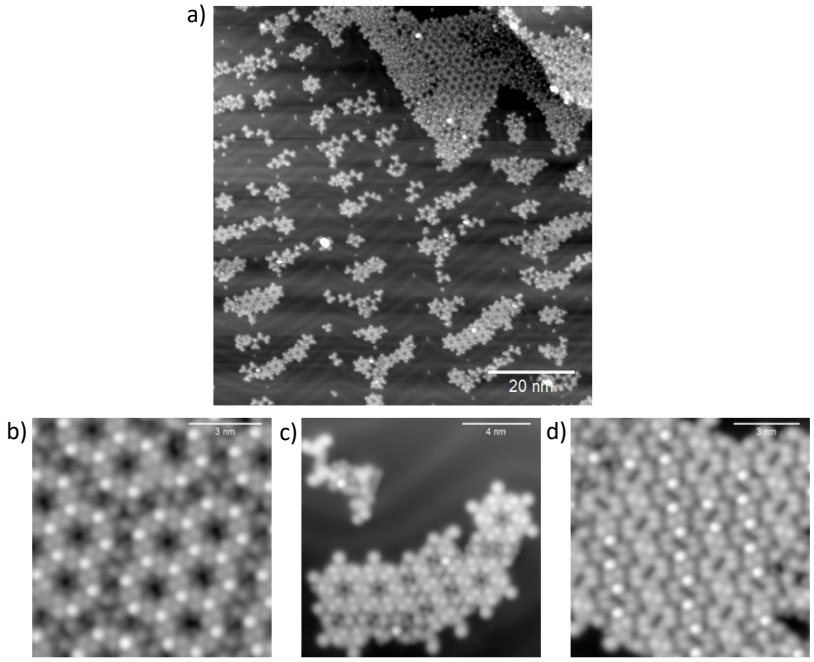

Figure 160. STM images after deposition of *M*-**9** on Au(111) surface held at room temperature. Imaging conditions: a) V_S = 100 mV; I_t = 100 pA, b) V_S = -100 mV; I_t = 100 pA, c) V_S = 100 mV; I_t = 100 pA, d) V_S = 100 mV; I_t = 100 pA.

Subsequent annealing at 94 °C and 195 °C led to the formation of polymerized yet irregular structures (Figure 161). Iodine atoms lay on the substrate around the polymeric structures, forming assemblies.

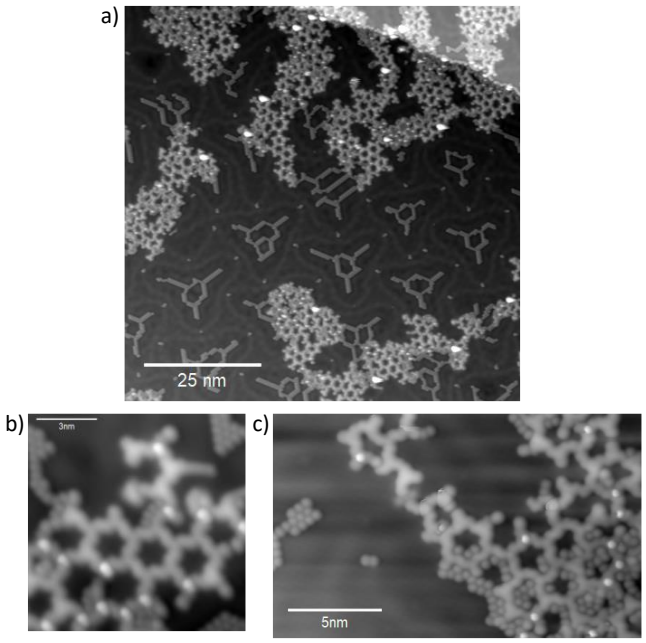

Figure 161. STM images after annealing at 195 °C of *M*-**9** deposited on Au(111) surface held at room temperature. Imaging conditions: a) V_S = -100 mV; I_t = 100 pA, b) V_S = -100 mV; I_t = 100 pA, c) V_S = 100 mV; I_t = 100 pA, d) V_S = -100 mV; I_t = 100 pA.

In summary, in light of the lack of highly ordered structures upon deposition on Au(111) and the formation of irregular polymeric structures upon deposition on Ag(111) and Cu(111) substrates even at room temperature due to C-I bonds cleavage, any conclusive result could be obtained from STM measurements with enantiopure I_3SucPc-Cl derivatives. Optimization of the molecular design in terms of axial and peripheral substituents is needed in order to improve the on-surface organization of inherently chiral, C_3-symmetric SubPc species. In this regard, further investigations are being carried out in our research group.[454]

[454] J. Labella Santodomingo, Ph.D. Thesis, Universidad Autónoma de Madrid, Madrid, Spain, in progress.

3.4 Summary and conclusions

In this Chapter, we presented the feasible and efficient optical resolution of C_3-symmetric I_3SubPc-Cl **9** through semi-preparative chiral HPLC or by derivatization with a chiral auxiliary, and we investigated the solid-state and on-surface organization of the enantiopure species (Figure 162).

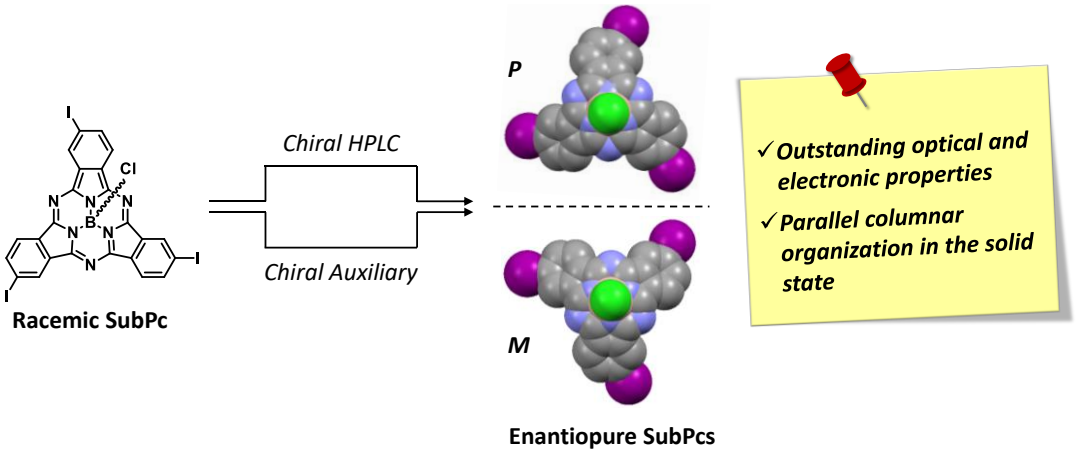

Figure 162. Graphical abstract summarizing the results of Chapter 3.

Optimized HPLC elution conditions allowed for the preparation of enantiopure *M*-**9** and *P*-**9** at a rate of tens of milligrams per week. The enantiomeric relationship between the isolated species was corroborated by means of CD spectroscopy and X-ray diffraction analysis, which also allowed to unambiguously assign the absolute configuration of each enantiomer. On the other hand, derivatization with a chiral auxiliary allowed to carry out the efficient optical resolution of racemic I_3SubPc-Cl **9** by common laboratory techniques. In particular, axial substitution of **9** with an enantiopure dibromo-BINOL derivative enabled the separation of the resulting diastereomers by column chromatography, and subsequent replacement of the resolving agent with a chlorine atom afforded the isolated enantiomers of the starting SubPc in excellent yield with satisfactory enantiomeric excesses. To the best of our knowledge, the optical resolution of inherently chiral, *meta*-substituted SubPcs based on the use of chiral auxiliaries has no precedent in literature.

The organization of the enantiomerically pure derivatives at both crystalline solid-state and on-surface levels was evaluated by means of X-ray diffraction analysis and STM measurements, respectively.

The comparison between the crystal structures of racemic and enantiopure samples of C_3-I_3SubPc-Cl revealed remarkable differences in terms of crystal packing. As a matter of fact, both species organize in concave-convex, tail-to-tail dimers that, in turns, arrange to form homochiral columns. Nevertheless, whereas racemic I_3SubPc-Cl **9** exhibits an antiparallel columnar organization, within the crystal structure of the pure enantiomers columnar stacks organize in an unusual parallel arrangement (Figure 163). The sensitiveness of crystalline solid-state packing on chiral composition is of great interest in view of the potential implementation of inherently chiral molecules in technological applications, as it offers the exciting possibility to tune the material properties (and, in turn, the device performances) by simply tailoring its optical purity.

Unfortunately, any conclusive result could be obtained from STM measurements, as deposition of the enantiopure species on Au(111), Ag(111) and Cu(111) surfaces did not lead to the formation of an ordered lattice. In particular, extensive spontaneous cleavage of the C-I bonds was observed on Ag(111) and Cu(111) substrates even at room temperature.

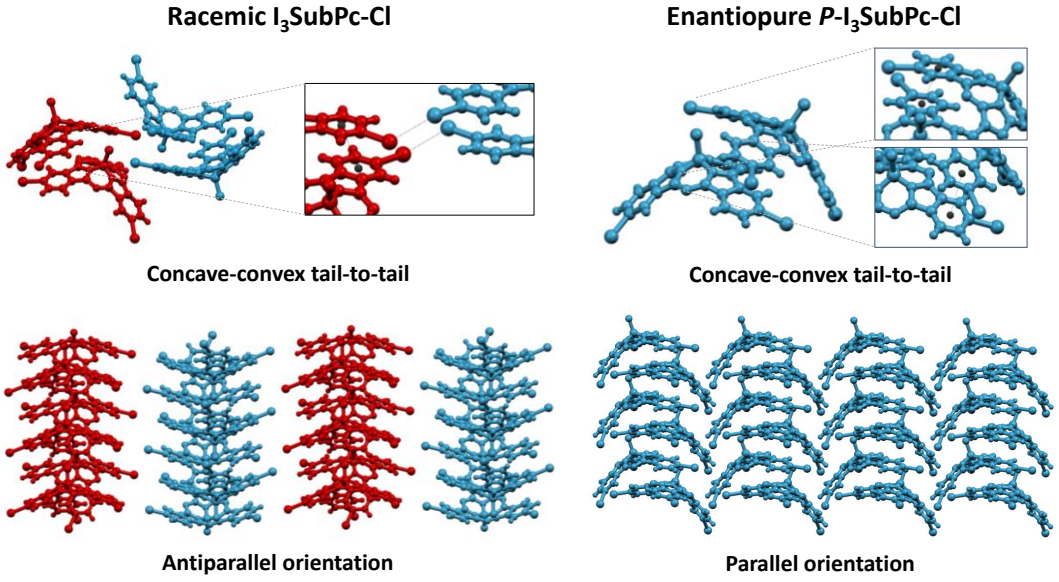

Figure 163. X-ray structure of racemic and enantiopure C_3-symmetric I_3SubPc-Cl.

The availability of feasible procedures for the efficient preparation of enantiopure SubPc derivatives, as well as the investigation of their bulk organization, is of key importance in view of the potential applications of optically pure SubPcs as molecular materials in technological devices. In particular, the highly directional columnar arrangement within the crystal structure of the *M*-**9** and *P*-**9** enantiopure species, along with the excellent structural, optical and

electronic properties of SubPcs, render these derivatives highly appealing candidate as, for example, semiconductor or ferroelectric materials. In this connection, charge carriers mobility measurements are being carried out in order to explore the potential of the investigated derivatives in electronic and optoelectronic technologies. Moreover, optically pure I_3SubPc-Cl species constitute extremely versatile synthons for the preparation of a large variety of SubPc-based derivatives through functionalization of either the axial or the peripheral positions, opening the door to the study of the chirality-induced properties of these chromophores. Finally, enantiopure I_3SubPc-Cl derivatives constitute a powerful means to explore the mechanistic aspects of SubPc reactivity, such as the possibility of a bowl-to-bowl inversion of the macrocycle.

3.5 Experimental section

3.5.1 Materials and methods

Chemicals (reagent grade) and solvents (synthetic grade, anhydrous, HPLC grade, spectroscopy grade and deuterated) were purchased from Aldrich Chemical, Alfa Aesar, Acros Organics, TCI and Scharlau. Chemical reagents were used without further purification. Synthetic grade solvents were used for chemical reactions and column chromatography purifications and anhydrous solvents were used for reactions under dry conditions. Additionally, some solvents were dried with a solvent purifying system by Innovative Technology Inc. MD-4-PS. Oxygen- and moisture-sensitive reactions were carried out using standard Schlenk line techniques.

Chromatography: the monitoring of the reactions has been carried out by thin layer chromatography (TLC), employing aluminum sheets coated with silica gel type 60 F254 (0.2 mm thick, Merck). The analysis of the TLCs was carried out with a UV lamp of 254 and 365 nm. Column chromatography was performed using silica gel (230-400 mesh, 0.040-0.063 mm, Merck). Eluents are indicated for each particular case. High-performance liquid chromatography (HPLC) was performed using an Agilent 1200 equipment with a Daicel CHIRALPAK IC semi-preparative chiral column (particle size 5 µm, dimensions 10 mm ø x 250 mm). HPLC grade solvents were used. HPLC conditions for the optical resolution of I_3SubPc-Cl **9**: eluting solvent mixture = toluene/*n*-hexane 50:50 (v/v); flow rate = 1.2 mL min^{-1}; temperature = 10 °C; detection wavelength = 570 nm. HPLC conditions for the optical resolution of I_3SubPc-dibromo-BINOL **38**: eluting solvent = toluene/*n*-hexane 70:30 (v/v); flow rate = 1.0 mL min^{-1}; temperature = 10 °C; detection wavelength = 570 nm.

Nuclear Magnetic Resonance (NMR): NMR spectra were recorded with a Bruker AVANCE 300 (300 MHz), a Bruker AVANCE-II 300 (300 MHz), and a Bruker DRX-500 (500 MHz) instruments in the Organic Chemistry Department or in the Interdepartmental Investigation Service of UAM. The deuterated solvent employed is indicated for each case. Chemical shifts (δ) are reported in ppm, and coupling constants (J) are reported in hertz (Hz). For ^{1}H-NMR and ^{13}C-NMR spectra, δ are measured relative to residual solvent signals using literature reference values.[379] The following abbreviations are used to indicate the multiplicity in ^{1}H-NMR spectra: s, singlet; d, doublet; t, triplet; q, quartet; quint, quintet; m, multiplet.

Mass Spectrometry (MS) and High-Resolution Mass Spectrometry (HRMS): Matrix Assisted Laser Desorption/Ionization-Time of Flight (MALDI-TOF) mass spectra were recorded in the Interdepartmental Investigation Service of UAM, using a Bruker ULTRAFLEX III spectrometer

equipped with a Nd:YAG laser operating at 355 nm. The different matrixes employed are indicated for each spectrum. Mass spectrometry data are expressed in *m/z* units.

Steady State Absorption Spectroscopy: steady-state absorption spectra were recorded in the Organic Chemistry Department of UAM employing a JASCO-V660 spectrophotometer. Spectroscopic grade solvents were used for spectroscopic measurements.

Circular dichroism (CD) Spectroscopy: CD spectra were recorded in IMDEA Nanociencia using a JASCO V-815 spectrometer equipped with a JASCO Peltier ETCT-762 temperature controller.

Infrared Spectroscopy (FT-IR): infrared spectra were recorded in the Interdepartmental Investigation Service of UAM with a Bruker IFS66v FTIR spectrometer.

X-Ray Spectroscopy: X-Ray diffraction analysis was performed in the Interdepartmental Investigation Service of UAM with a Bruker KAPPA APEX II (X8 APEX) single-crystal diffractometer with Mo source (λ = 0.71073 Å). Data are corrected with the SADABS program. Intensities are calculated with the SAINT software. The structures are resolved and refined using the Bruker SHELXTL Software Package.

Melting point (MP): melting points were measured in open-end capillary tubes by using a Büchi 504392-S apparatus, and are uncorrected.

3.5.2 Synthetic procedures

Subphthalocyanine **9**

The synthetic procedure for the preparation of racemic I_3SubPc-Cl **9** has been described in Chapter 1 (section 1.5.2.2).

XRD: Single crystals of racemate **9** and enantiopure *M*-**9** and *P*-**9** were obtained by slow diffusion of methanol in chloroform. Selected crystallographic data are summarized in Tables 22-24.

Table 22. Selected crystallographic data for racemate **9**.

Chemical formula	$C_{24}H_9BClI_3N_6O$
Formula weight	824.33 g/mol
Crystalline system	Monoclinic
Space group	P 1 21/n 1
Volume	2562.3(2) $Å^3$
Density	2.137 g cm^{-3}
Z	4
a	13.6481(5) Å
b	7.2351(4) Å
c	26.4186(13) Å
α	90°
β	100.829(2)°
γ	90°
R	3338 data; I>2σ(I) R1 = 0.0424, wR2 = 0.1046
	all data R1 = 0.0740, wR2 = 0.1341

Table 23. Selected crystallographic data for *M*-**9**.

Chemical formula	$C_{24}H_9BClI_3N_6O$
Formula weight	824.33 g/mol
Crystalline system	Monoclinic
Space group	P 1 21 1
Volume	1288.9(3) $Å^3$
Density	2.124 g cm^{-3}
Z	2
a	13.576(2) Å
b	7.2064(11) Å
c	13.839(2) Å
α	90°
β	107.831(7)°
γ	90°
R	3254 data; I>2σ(I) R1 = 0.0437, wR2 = 0.0910
	all data R1 = 0.0800, wR2 = 0.1295

Table 24. Selected crystallographic data for *P*-**9**.

Chemical formula	$C_{24}H_9BClI_3N_6O$
Formula weight	824.33 g/mol
Crystalline system	Monoclinic
Space group	P 1 21 1
Volume	1287.35(8) $Å^3$
Density	2.127 g cm^{-3}
Z	2
a	13.6218(4) Å
b	7.1896(3) Å
c	13.8017(5) Å
α	90°
β	107.747(2)°
γ	90°
R	4517 data; I>2σ(I) R1 = 0.0253, wR2 = 0.0725
	all data R1 = 0.0287, wR2 = 0.2878

Subphthalocyanine **37** (mixture of diastereomers)

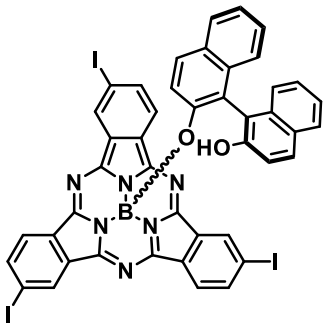

I_3SubPc-Cl **9** (50 mg, 0.06 mmol) and $AlCl_3$ (12.4 mg, 0.09 mmol) were dissolved in anhydrous chlorobenzene (2 mL) under argon atmosphere and the reaction mixture was stirred at 60 °C for 30 minutes. Then, a solution of (*R*)-BINOL (35.4 mg, 0.12 mmol) in anhydrous chlorobenzene (1 mL) was added, and the mixture was stirred at 60 °C for 14 hours. At this point, 0.5 mL of pyridine were added, and the reaction mixture was stirred for 5 additional minutes. The reaction mixture was then allowed to cool down to room temperature and the solvent was evaporated under reduced pressure. The crude product was purified as a mixture of diastereomers by column chromatography on silica gel using DCM/toluene 4:1 (v/v) as eluent. Recrystallization from a DCM/MeOH/water mixture afforded I_3SubPc-BINOL **37** as a purple solid in 46% yield (30 mg).

^{1}H-NMR (500 MHz, $CDCl_3$): δ (ppm) = 8.97 (d, $^4J_{H\text{-}H}$ = 1.5 Hz, 3H), 8.93 (s, $^4J_{H\text{-}H}$ = 1.5 Hz, $^5J_{H\text{-}H}$ = 0.5 Hz, 3H), 8.34 (dd, $^3J_{H\text{-}H}$ = 8.0 Hz, $^5J_{H\text{-}H}$ = 0.5 Hz, 3H), 8.31 (dd, $^3J_{H\text{-}H}$ = 8.0 Hz, $^5J_{H\text{-}H}$ = 0.5 Hz, 3H), 8.12-8.09 (m, 6H), 7.91 (d, $^3J_{H\text{-}H}$ = 8.5 Hz, 1H), 7.82 (d, $^3J_{H\text{-}H}$ = 8.0 Hz, 1H), 7.79 (d, $^3J_{H\text{-}H}$ = 8.5 Hz, 1H), 7.65-7.60 (m, 6H), 7.40 (d, $^3J_{H\text{-}H}$ = 8.5 Hz, 1H), 7.37 (d, $^3J_{H\text{-}H}$ = 8.5 Hz, 1H), 7.22-7.19 (m, 2H), 7.18-7.14 (m, 2H), 7.03-7.00 (m, 2H), 6.95-6.92 (m, 2H), 6.75-6.70 (m, 3H), 6.39 (d, $^3J_{H\text{-}H}$ = 8 Hz, 1H), 6.29 (d, $^3J_{H\text{-}H}$ = 8.5 Hz, 1H), 6.51-5.58 (m, 2H), 4.66 (s (broad), 2H).

^{13}C-NMR (125.7 MHz, $CDCl_3$): δ (ppm) = 151.09, 151.01, 150.97, 150.89, 149.91, 149.79, 147.98, 147.97, 138.60, 133.53, 133.52, 133.06, 133.04, 132.10, 132.03, 131.46, 131.40, 130.23, 130.21, 130.17, 129.97, 129.81, 129.73, 129.63, 128.87, 128.86, 127.90, 127.87, 127.84, 127.74, 127.74, 126.47, 126.36, 126.31, 126.29, 126.04, 125.26, 125.11, 124.59, 123.44, 13.41, 123.29, 120.75, 120.06, 118.54, 118.54, 114.79, 114.77, 96.12, 96.10.

^{11}B-NMR (160.4 MHz, $CDCl_3$): δ (ppm) = -15.07.

MS (MALDI-TOF, DCTB): *m/z* = 772.9 [M-axial ligand]$^+$, 1057.9 [M]$^+$.

HRMS: *m/z* Calculated for [$C_{44}H_{22}BI_3N_6O_2$]: 1057.9033; Found: 1057.9030.

UV-vis (toluene): λ_{max} (nm) (log ε (dm^3 mol^{-1} cm^{-1})) = 574 (4.87), 556 (sh), 534 (sh), 326 (4.48), 272 (4.70).

FT-IR (ATR): ν (cm^{-1}) = 3521, 3056, 2919, 2853, 1694, 1598, 1551, 1503, 1439, 1385, 1261, 1233, 1169, 1141, 1077, 1056, 1042, 815, 765, 744, 703, 656, 598, 528.

Subphthalocyanine **38**

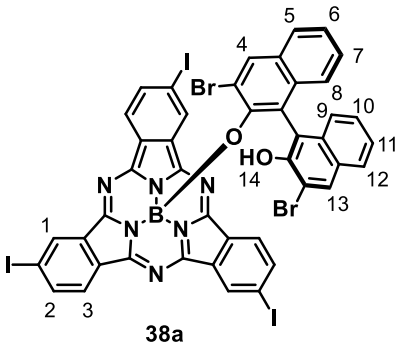

38a

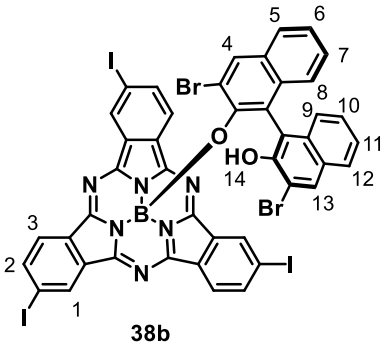

38b

I_3SubPc-Cl **9** (50 mg, 0.06 mmol) and $AlCl_3$ (12.4 mg, 0.09 mmol) were dissolved in anhydrous chlorobenzene (2 mL) under argon atmosphere and the reaction mixture was stirred at 60 °C for 30 minutes. Then, a solution of (*R*)-dibromo-BINOL (27.5 mg, 0.06 mmol) in anhydrous chlorobenzene (2 mL) was added, and the mixture was stirred at 60 °C for 14 hours. At this point, 0.5 mL of pyridine were added, and the reaction mixture was stirred for 5 additional minutes. The work-up procedures followed for the purification of I_3SubPc-dibromo-BINOL **38** as a mixture of diastereomers and for the separation of I_3SubPc-dibromo-BINOL diastereomers **38a** and **38b**, as well as the corresponding yields, are indicated below.

*Purification of I_3SubPc-dibromo-BINOL **38** as a mixture of diastereomers.* The reaction mixture was allowed to cool down to room temperature and the solvent was evaporated under reduced pressure. The crude product was purified as a mixture of diastereomers by column chromatography on silica gel using DCM/heptane 3:1 (v/v) as eluent. Recrystallization from a DCM/MeOH/water mixture afforded I_3SubPc-dibromo-BINOL **38** as a purple solid in 62% overall yield (47 mg).

*Purification of isolated I_3SubPc-dibromo-BINOL diastereomers **38a** and **38b**.* The reaction mixture was allowed to cool down to room temperature and the solvent was evaporated under reduced pressure. The crude product was purified by column chromatography on silica gel (6 cm ø x 23 cm) using DCM/heptane 3:1 (v/v) as eluent (Rf **38a** = 0.36; Rf **38b** = 0.31). **38a** (first eluted diastereomer) and **38b** (second eluted diastereomer) were collected separately with a purity of 100% and 89.6%, respectively. The second eluted fraction was subjected to a second column chromatography on silica gel (6 cm ø x 23 cm, eluent: DCM/eptane 3:1), which afforded **38b** with a purity of 94.2%. Recrystallization from a DCM/MeOH/water mixture afforded the isolated I_3SubPc-dibromo-BINOL diastereomers **38a** and **38b** as purple solids in 28% and 27% yield, respectively.

Diastereomer 38a

^{1}H-NMR (500 MHz, $CDCl_3$): δ (ppm) = 8.74 (dd, $^{4}J_{H\text{-}H}$ = 1.5 Hz, $^{5}J_{H\text{-}H}$ = 0.5 Hz, 3H; H-1), 8.37 (dd, $^{3}J_{H\text{-}H}$ = 8.0 Hz, $^{5}J_{H\text{-}H}$ = 0.5 Hz, 3H; H-3), 8.29 (s, 1H; H-13), 8.11 (dd, $^{3}J_{H\text{-}H}$ = 8.0 Hz, $^{4}J_{H\text{-}H}$ = 1.5 Hz, 3H; H-2), 7.79 (d, $^{3}J_{H\text{-}H}$ = 8.0 Hz, 1H; H-12), 7.73 (s, 1H; H-4), 7.49 (d, $^{3}J_{H\text{-}H}$ = 8.0 Hz, 1H; H-5), 7.28-7.25 (ddd, $^{3}J_{H\text{-}H}$ = 7.9 Hz, $^{3}J_{H\text{-}H}$' = 6.8 Hz, $^{4}J_{H\text{-}H}$ = 1.0 Hz, 1H; H-11), 7.19-7.16 (ddd, $^{3}J_{H\text{-}H}$ = 7.9 Hz, $^{3}J_{H\text{-}H}$' = 6.8 Hz, $^{4}J_{H\text{-}H}$ = 1.0 Hz, 1H; H-6), 6.99-6.96 (ddd, $^{3}J_{H\text{-}H}$ = 8.5 Hz, $^{3}J_{H\text{-}H}$' = 6.8 Hz, $^{4}J_{H\text{-}H}$ = 1.0 Hz, 1H; H-7), 6.87-6.84 (ddd, $^{3}J_{H\text{-}H}$ = 8.5 Hz, $^{3}J_{H\text{-}H}$' = 6.8 Hz, $^{4}J_{H\text{-}H}$ = 1.0 Hz, 1H; H-10), 6.57 (d, $^{3}J_{H\text{-}H}$ = 8.5 Hz, 1H; H-8), 6.35 (d, $^{3}J_{H\text{-}H}$ = 8.5 Hz, 1H; H-9), 5.17 (s, 1H; H-14).

^{13}C-NMR (125.7 MHz, $CDCl_3$): δ (ppm) = 151.18, 150.01, 147.38, 145.26, 138.61, 133.22, 132.94, 132.50, 132.09, 132.02, 131.40, 130.70, 129.69, 127.13, 126.99, 126.61, 126.59, 126.40, 125.76, 125.47, 124.90, 123.46, 122.84, 116.55, 116.41, 114.06, 96.12.

^{11}B-NMR (160.4 MHz, $CDCl_3$): δ (ppm) = -14.92.

MS (MALDI-TOF, DCTB): *m/z* = 772.9 [M-axial ligand]$^{+}$, 1215.7 [M]$^{+}$.

HRMS: *m/z* Calculated for [$C_{44}H_{20}BBr_2I_3N_6O_2$]: 1215.7227; Found: 1215.7243.

UV-vis ($CHCl_3$): λ_{max} (nm) (log ε ($dm^3\ mol^{-1}\ cm^{-1}$)) = 577 (4.96), 559 (sh), 536 (sh), 324 (4.59), 270 (4.78).

FT-IR (ATR): ν (cm^{-1}) = 3497, 3061, 1738, 1601, 1548, 1494, 1436, 1263, 1240, 1177, 1141, 1087, 1042, 1023, 1001, 880, 818, 770, 744, 705, 600, 590, 518.

MP > 250 °C.

Diastereomer 38b

^{1}H-NMR (500 MHz, $CDCl_3$): δ (ppm) = 8.97 (d, $^{4}J_{H\text{-}H}$ = 1.0 Hz, 3H; H-1), 8.34 (d, $^{3}J_{H\text{-}H}$ = 8.0 Hz, 3H; H-3), 8.12-8.10 (m, 4H; H-2, H-13), 7.71 (s, 1H; H-4), 7.61 (d, $^{3}J_{H\text{-}H}$ = 8.0 Hz, 1H; H-12), 7.48 (d, $^{3}J_{H\text{-}H}$ = 8.0 Hz, 1H; H-5), 7.33-7.30 (ddd, $^{3}J_{H\text{-}H}$ = 8.0 Hz, $^{3}J_{H\text{-}H}$' = 6.8 Hz, $^{4}J_{H\text{-}H}$ = 1.0 Hz, 1H; H-11), 7.18-7.15 (ddd, $^{3}J_{H\text{-}H}$ = 8.0 Hz, $^{3}J_{H\text{-}H}$' = 6.8 Hz, $^{4}J_{H\text{-}H}$ = 1.0 Hz, 1H; H-6), 7.13-7.10 (ddd, $^{3}J_{H\text{-}H}$ = 8.5 Hz, $^{3}J_{H\text{-}H}$' = 6.8 Hz, $^{4}J_{H\text{-}H}$ = 1.0 Hz, 1H; H-10), 6.99-6.96 (ddd, $^{3}J_{H\text{-}H}$ = 8.5 Hz, $^{3}J_{H\text{-}H}$' = 6.8 Hz, $^{4}J_{H\text{-}H}$ = 1.0 Hz, 1H; H-7), 6.57 (d, $^{3}J_{H\text{-}H}$ = 8.5 Hz, 1H; H-8), 6.48 (d, $^{3}J_{H\text{-}H}$ = 8.5 Hz, 1H; H-9), 5.18 (s, 1H; H-14).

^{13}C-NMR (125.7 MHz, $CDCl_3$): δ (ppm) = 151.14, 150.33, 147.33, 145.31, 138.60, 133.14, 132.67, 132.42, 132.12, 132.03, 132.02, 131.44, 130.68, 129.65, 127.28, 126.97, 126.94, 126.58, 126.38, 125.99, 125.45, 124.66, 123.40, 122.74, 116.94, 116.46, 113.84, 96.12.

^{11}B-NMR (160.4 MHz, $CDCl_3$): δ (ppm) = -14.88.

MS (MALDI-TOF, DCTB): *m/z* = 772.9 [M-axial ligand]$^{+}$, 1215.7 [M]$^{+}$.

HRMS: *m/z* Calculated for [$C_{44}H_{20}BBr_2I_3N_6O_2$]: 1215.7227; Found: 1215.7239.

UV-vis ($CHCl_3$): λ_{max} (nm) (log ε ($dm^3\ mol^{-1}\ cm^{-1}$)) = 577 (4.96), 559 (sh), 536 (sh), 323 (4.65), 268 (4.85).

FT-IR (ATR): ν (cm^{-1}) = 3492, 3060, 1731, 1600, 1550, 1497, 1436, 1262, 1239, 1177, 1141, 1087, 1042, 1023, 1001, 880, 818, 770, 744, 705, 600, 590, 518.

MP > 250 °C.

Subphthalocyanines *M*-**9** and *P*-**9**

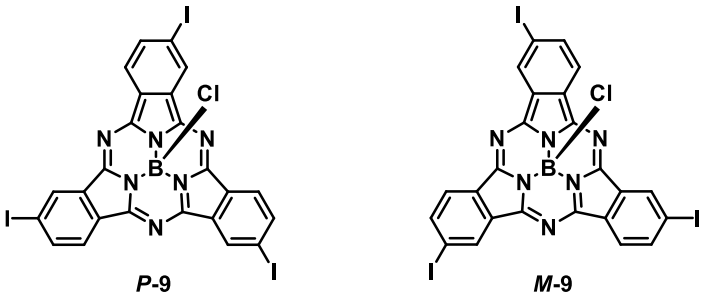

A 1.0 M solution of BCl_3 in *p*-xylene (206 µl, 206 µmol) was added to a solution of either **38a** or **38b** (25 mg, 20.6 µmol) in anhydrous toluene (2.0 mL) under argon atmosphere and the mixture was stirred at 50 °C for 30 min. The reaction mixture was then allowed to cool down to room temperature and flushed with argon. After evaporating the solvent under reduced pressure, the crude was purified by a short silica plug in toluene. Recrystallization from DCM/MeOH afforded *P*-**9** and *M*-**9** as purple solids in 96% yield (16 mg).

The characterization of the pure enantiomers of SubPc **9** corresponds with that reported for the racemic derivative in section 1.5.2.2.

Resumen y Conclusiones

Introducción y objetivo general de la Tesis

Las subftalocianinas como materiales moleculares

Las subftalocianinas (SubPcs) son macrociclos aromáticos formados por tres unidades de 1,3-diiminoisoindol fusionadas a través de los átomos de nitrógeno y organizadas alrededor de un átomo de boro, que a su vez está unido a un sustituyente axial (Figura 1). A pesar de comprender un núcleo aromático de 14 electrones π, las SubPcs exhiben una geometría cónica debido a la coordinación tetraédrica del átomo de boro central, representando así uno de los pocos ejemplos conocidos de moléculas aromáticas no planas.

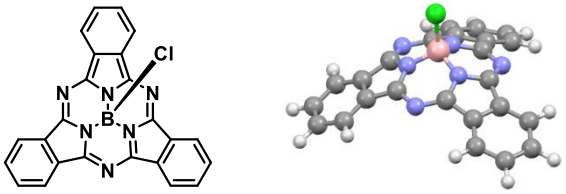

Figura 1. Estructura química y modelo de barras y esferas de H_{12}SubPc-Cl.

Las SubPcs se sintetizan generalmente mediante reacción de ciclotrimerización de un ftalonitrilo precursor en presencia de un trihaluro boro (BCl_3 o BBr_3) en cantidades estequiométricas, en disolventes aromáticos de alto punto de ebullición. Cuando el ftalonitrilo de partida no posee simetría C_{2v}, la reacción de ciclotrimerización produce una mezcla de regioisómeros con simétria C_3 y C_1, cada cual es a su vez intrínsecamente quiral y se obtiene como mezcla racémica de dos enantiómeros (*P* y *M* para el regioisómero C_3, y *MPP* y *MMP* para el regioisómero C_1).

Como consecuencia de las restricciones en términos de variedad de grupos funcionales impuestas por las condiciones de reacción empleadas en la síntesis de SubPcs, se han desarrollado varias estrategias sintéticas para la funcionalización de las posiciones axial y periféricas del macrociclo. La introducción de funcionalidades adecuadas en dichas posiciones permite modular las propiedades físico-químicas de estos derivados, controlar su organización supramolecular, así como incorporar estos macrociclos en sistemas multicomponente.

Además de por sus características estructurales y su versatilidad sintética, las SubPc destacan por sus propiedades fotofísicas y electroquímicas. En concreto, estos derivados se caracterizan por una intensa absorción en la región UV-vis del espectro electromagnético, con coeficientes de extinción molar del orden de $5\text{-}6\cdot10^4$ M^{-1} cm^{-1} y energías de excitación superiores a 2.0 eV, una fuerte emisión de fluorescencia e interesantes propiedades redox.

Las características estructurales, ópticas y electrónicas de las SubPcs, junto con una creciente comprensión de la morfología de los materiales moleculares basados en estos derivados, han dado lugar a aplicaciones en varios campos tecnológicos. En particular, durante las últimas décadas, las SubPcs han sido ampliamente estudiadas en el marco de la fotovoltaica molecular, consolidándose como candidatos prometedores no solo como materiales aceptores sino también como materiales dadores.

Sistemas dador-aceptor para conversión de energía solar

El creciente consumo mundial de energía, el agotamiento progresivo de los combustibles fósiles y el cambio climático asociado a su uso intensivo son algunos de los principales problemas del mundo moderno. Una de las estrategias más prometedoras y sostenibles para cubrir la demanda mundial de energía a largo plazo es el uso de la energía solar. Durante las últimas décadas, se han dedicado muchos esfuerzos al desarrollo de sistemas fotosintéticos artificiales para comprender y controlar los eventos primarios que tienen lugar en el proceso fotosintético a nivel molecular. Dicha comprensión es de fundamental importancia para el desarrollo de dispositivos capaces de convertir de manera eficiente la luz solar en otras formas de energía, como la energía eléctrica o la energía química almacenada en forma de combustibles químicos.

Debido a la complejidad intrínseca de los sistemas fotosintéticos naturales, normalmente se adopta un enfoque modular, que consiste en el diseño, la preparación y el estudio de modelos sintéticos estructuralmente más simples con el objetivo de reproducir solo uno o algunos de los procesos fundamentales que ocurren en la fotosíntesis natural, como la transferencia de energía o la transferencia de electrones fotoinducida. En su versión más sencilla, estos sistemas multicomponente consisten en una unidad dadora (D) y una unidad aceptora de electrones (A) enlazadas mediante interacciones covalentes o supramoleculares. En estos sistemas D-A, la fotoexcitación de una de las unidades constituyentes puede dar lugar a transferencia de energía o electrones entre los dos componentes.

Las propiedades estructurales, fotofísicas y electroquímicas de las SubPcs, junto con su versatilidad sintética, las convierten en candidatos ideales para la preparación de dichos sistemas D-A. De hecho, las SubPcs han sido ampliamente utilizadas para este propósito en combinación con una variedad de derivados tales como fullerenos y porfirinoides, entre otros.

El objetivo general de la presente Tesis Doctoral es la preparación de nuevos sistemas basados en subftalocianinas y el estudio de sus propiedades para su potencial aplicación en tecnologías solares.

Capítulo 1. Subftalocianinas funcionalizadas con unidades TCBD-anilina: estereoisomería y propiedades fotofísicas

El primer Capítulo de esta Tesis doctoral se centra en la síntesis y en el estudio de diferentes sistemas D-A constituidos por subftalocianinas funcionalizadas en las posiciones axial y/o periféricas del macrociclo con unidades tetracianobuta-1,3-dieno(TCBD)-anilina, en vista de su potencial aplicación como materiales fotoactivos en áreas tecnológicas relacionadas con la conversión de energía solar.

El TCBD es una unidad electron-actractora que ha sido ampliamente utilizada para la construcción de sistemas D-A no planos. Los sistemas basados en TCBD exhiben características fisicoquímicas interesantes, como unas fuertes interacciones intramoleculares de transferencia de carga y un comportamiento redox muy activo, que los convierten en candidatos prometedores para aplicaciones (opto)electrónicas. Además, la rotación restringida alrededor del enlace sencillo C-C central de la unidad de TCBD y la organización casi ortogonal de las dos unidades de dicianovinilo resulta en la formación de atropisómeros.

El diseño de los derivados de SubPc investigados en este Capítulo tiene como objetivo el estudio del impacto de la introducción de unidades de TCBD-anilina y del patrón de sustitución de la subftalocianina sobre las características estructurales y optoelectrónicas de los conjugados. En el caso de SubPcs sustituidas en la posición axial, también se ha estudiado el efecto de la naturaleza de los sustituientes periféricos sobre las propriedades electroquímicas y fotofísicas de los derivados.

Este Capítulo se compone de tres secciones.

En la ***primera sección*** se ha descrito la síntesis de cuatro derivados basados en una unidad de SubPc funcionalizada en las posiciones axial, periféricas, o axial y periféricas con una, tres o cuatro unidades TCBD-anilina (Figura 2). La introducción de los grupos TCBD se ha llevado a cabo mediante reacción de cicloadición-retroelectrociclación a partir de las correspondientes SubPcs sustituidas con alquinilos en presencia de tetracianoetileno. Por su parte, los derivados de SubPc funcionalizados en la posición axial con etinil-anilina se han preparado a través de una reacción de sustitución axial de lo correspondientes precursores clorados con un reactivo de Grignard, mientras que la funcionalización de las posiciones periféricas del macrociclo con grupos alquinilos se ha realizado por medio de una reacción de acoplamiento cruzado de Sonogashira catalizada por paladio a partir de los correspondientes derivados iodados en la periferia.

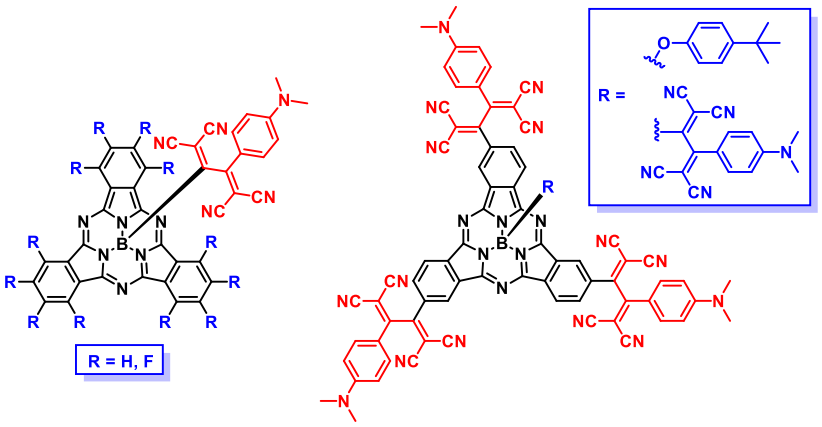

Figura 2. Estructura molecular de los derivados de SubPc funcionalizados con unidades TCBD-anilina investigados en el Capítulo 1.

En la ***segunda sección*** del Capítulo 1 se han investigado las características estructurales de los derivados de SubPc sintetizados. Estudios de diffracción de rayos X de las SubPcs funcionalizadas en la posición axial han evidenciado la geometría casi ortogonal de la unidad de TCBD axial y han revelado un distinto empaquetamiento en el estado solido (*i.e.*, en forma de dímeros o de agregados columnares) para el derivado hidrogenado y el derivado fluorado. La resolución óptica de dichos derivados, que se obtienen como mezclas racémicas de dos atropisómeros, se ha realizado mediante cromatografía líquida de alta eficacia empleando una columna quiral (Figura 3). El análisis de difracción de rayos X de las especies aisladas ha permitido asignar inequivocablemente la configuración absoluta de cada atropisomero, algo sin precedentes en la química de los sistemas basados en TCBD.

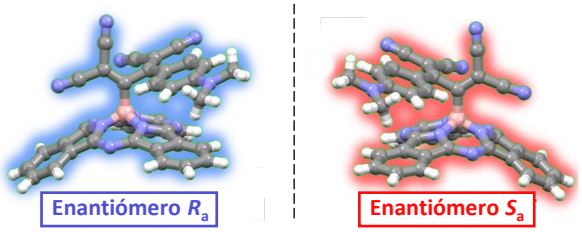

Figura 3. Enantiómeros del derivado quiral H_{12}SubPc-TCBD-anilina.

Asimismo, se ha investigado el proceso de racemización de las especies enantiopuras mediante medidas de dicroísmo circular y cálculos teóricos. Dichos estudios han revelado un mecanismo de interconversión entre enantiómeros activado por la luz y desencadenado por la

fotogeneración del estado excitado de triplete, que hace posible la rotación alrededor del eje quiral estéricamente congestionado de la unidad de butadieno. Ese comportamiento se distingue de lo descrito en literatura por un derivado de fullereno-TCBD-anilina y de lo observado para un derivado análogo de subporfirina funcionalizado en la posición axial con TCBD-anilina, que se caracterizan por un proceso de racemización térmicamente inducido.

Por otro lado, en los derivados de SubPc sustituidos en las posiciones periféricas, la combinación entre la quiralidad axial de las unidades de TCBD, la quiralidad inherente de la unidad de SubPc y la formación de distintos confórmeros tras la rotación de las unidades de TCBD-anilina perifericas alrededor de los enlaces C-C que las connectan al macrociclo, da lugar a varios posibles estereoisómeros. Aunque a temperatura ambiente estas especies se interconvierten rápidamente en la escala de tiempos de la resonancia magnética nuclear, dichos procesos de interconversión se ralentizan significativamente al bajar la temperatura, tal y como se deduce de los experimentos de resonancia magnética nuclear de protón a temperatura variable.

En la ***tercera sección*** de este Capítulo se han estudiado las propiedades electroquímicas y fotofísicas de los nuevos derivados con el objetivo de investigar las interacciones en el estado fundamental y en el estado excitado. El estudio de dichas interacciones en sistemas D-A es crucial para su potencial implementación en áreas tecnológicas enfocadas a la conversión de energía solar. En concreto, la caracterización de los nuevos derivados ha evidenciado que la introducción de unidades TCBD-anilina tiene un impacto profundo sobre las características ópticas y electrónicas de los sistemas basados en SubPcs.

En los derivados funcionalizados en la posición axial, las interacciones están determinadas por las características electrónicas del macrociclo, que dependen en última instancia de la naturaleza de lo sustituyentes periféricos. En concreto, el derivado hidrogenado presenta interacciones de transferencia de carga en el estado fundamental. Por otro lado, en el caso del derivado fluorado, las evidencias experimentales apuntan a formación de un exciplejo debido a la instauración de interacciones intramoleculares entre la unidad de anilina rica en electrones y la superficie π del macrociclo fluorado. Además, la fotoexcitación de ambos derivados resulta en procesos de separación de carga (Figura 4).

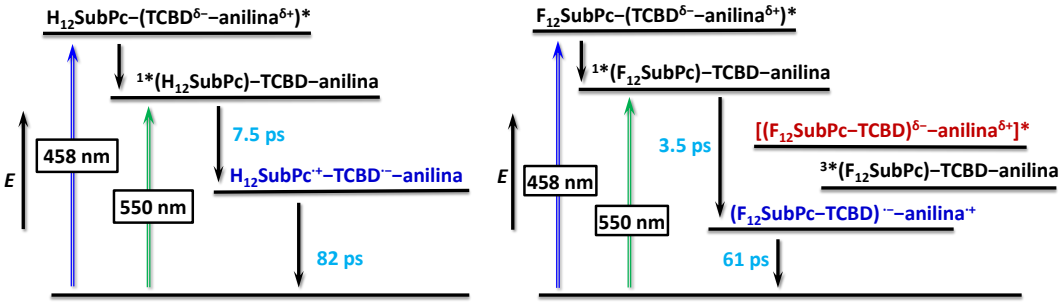

Figura 4. Diagramas energéticos que representan la desactivación del conjugado H_{12}SubPc-TCBD-anilina en tolueno y del conjugado F_{12}SubPc-TCBD-anilina en benzonitrilo después de la excitación de la unidad de SubPc y del estado de trasferencia de carga de la unidad de TCBD-anilina.

Con respecto a los derivados sustituidos en la periferia, se han detectado intensas interacciones de transferencia de carga en el estado fundamental entre la SubPc y las unidades electrón atrayentes de TCBD. Dichas interacciones son particularmente intensas en el caso del derivado funcionalizado con una unidad de TCBD adicional en la posición apical. Además, la fotoexitación da lugar a procesos de transferencia de carga y/o transferencia electrónica de la SubPc electron-dadora a las unidades de TCBD electrón deficientes, que están determinados por el patrón de sustitución de la SubPc. En concreto, la presencia de una unidad de TCBD axial permite la formación de un estado de separación de carga.

En resumen, la caracterización estructural, electroquímica y fotofísica de los derivados sintetizados ha proporcionado información interesante sobre sus características estereoquímicas y las interacciones en el estado fundamental y excitado, revelando que la posición de anclaje de las unidades de TCBD-anilina tiene un efecto destacable sobre las características estructurales y optoelectrónicas de los conjugados investigados. El peculiar mecanismo de racemización de los derivados de SubPc-TCBD-anilina sustituidos en la posición axial los convierte en sistemas interesantes para potenciales aplicaciones en el área de los interruptores moleculares controlados por la luz. Por otro lado, vistas las propiedades electroquímicas y fotofísicas de los sistemas investigados, dichos derivados constituyen candidatos prometedores para aplicaciones en fotovoltaica molecular.

Capítulo 2. Modulación de transferencia de energía y activación de fisión de singlete en conjugados subftalocianina-pentaceno

El segundo Capítulo de esta Tesis doctoral se centra en el diseño, la síntesis y el estudio de nuevos sistemas multicomponente en los que se ha integrado una unidad antena - concretamente, una SubPc - y un material capaz de producir fisión de singlete (SF) - concretamente, un dímero de pentaceno - con el objetivo de realizar una sinergia entre absorción pancromática y SF. En estos derivados, el proceso de SF a cargo de la unidad de dímero de pentaceno es activado por medio de una transferencia de energía desde la unidad de SubPc.

La fisión de singlete es un proceso en el que una molécula orgánica en el estado excitado de singlete ($^1(S_1)$) comparte su energía de excitación con una molécula adyacente en el estado fundamental ($^1(S_0)$) para formar un par de tripletes correlacionados con carácter general de singlete ($^1(T_1T_1)$). Posteriormente, el par de tripletes correlacionados se separa en dos estados excitados de triplete independientes 2 x $^3(T_1)$. Como tal, la fisión de singlete permite la generación de dos estados excitados a partir de un solo fotón, y constituye por lo tanto un medio prometedor para mejorar la eficiencia de conversión de luz solar en energía eléctrica en dispositivos fotovoltaicos. En particular, la combinación entre absorción pancromática y fisión de singlete tiene un gran potencial para mejorar la gestión de fotones y, en consecuencia, optimizar los rendimientos de las celdas solares.

El diseño de los derivados investigados en este Capítulo tiene como objetivo garantizar 1) la complementariedad entre la absorción de la unidad fotorreceptora y de la unidad interesada por el proceso de SF, con el fin de optimizar la absorción de luz en el rango visible del espectro solar; 2) un buen solapamiento entre la emisión de fluorescencia de la unidad antena y la absorción de la unidad de SF y, por lo tanto, la rapidez del proceso de transferencia de energía intramolecular hacia esta última tras la excitación de la unidad fotorreceptora; 3) la ausencia de cualquier interacción de transferencia de electrones entre los dos cromóforos, a fin de garantizar altos rendimientos cuánticos de SF intramolecular; 4) la eficiencia del proceso de SF intramolecular a cargo de la unidad aceptora de energía.

Los derivados investigados están formados por una SubPc funcionalizada en la posición axial con una unidad de dímero de pentaceno (Pnc_2), y se han preparado mediante reacción de sustitución del ligando halógeno apical en las correspondientes especies SubPc-Cl de partida a través de la generación de un intermedio activado SubPc-OTf. En concreto, se han preparado e investigado dos series distintas de derivados SubPc-Pnc_2, cuyos constituyentes difieren respectivamente en el patrón de sustitución periférica del macrociclo de SubPc y en el

espaciador molecular que conecta los dos cromóforos, con el objetivo de modular las interacciones intercromofóricas (Figura 5).

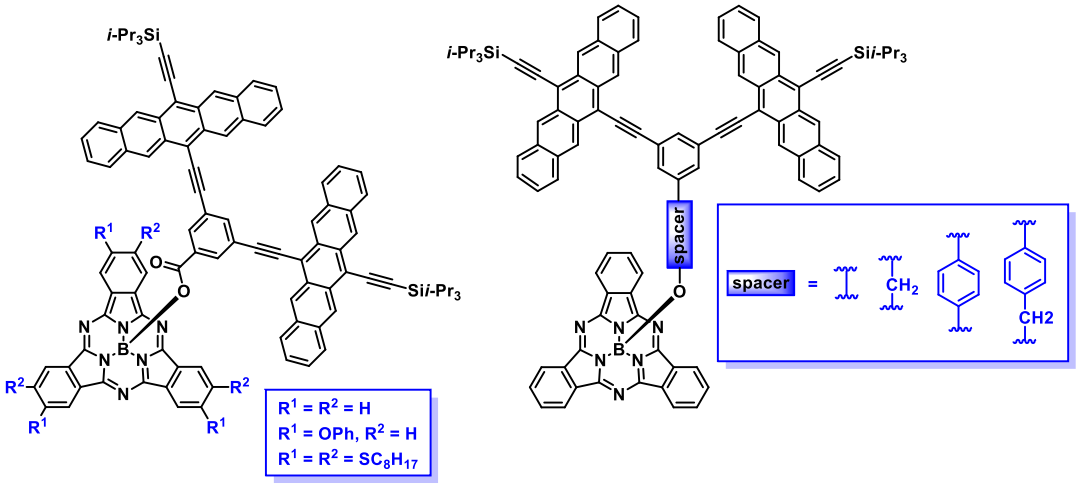

Figura 5. Estructura molecular de los derivados de SubPc-Pnc_2 investigados en el Capítulo 2.

Se han llevado a cabo estudios de absorción y fluorescencia junto con medidas de absorción transitoria para investigar las interacciones intercromofóricas en el estado fundamental y en el estado excitado. Todos los derivados investigados exhiben una absorción casi pancromática en la región visible del espectro solar, y no presentan interacciones en el estado fundamental entre las unidades de SubPc y Pnc_2. Es interesante hacer constar que la fotoexcitación de la unidad de SubPc activa una secuencia de transferencia de energía de resonancia de Förster (FRET) y SF en todos los sistemas multicomponente investigados (Figura 6). En concreto, la unidad de SubPc actúa como antena y dador de energía por medio de una transferencia de energía intramolecular singlete-singlete, que canaliza la energía unidireccionalmente al Pnc_2 donde tiene lugar un eficiente proceso de fisión de singlete intramolecular.

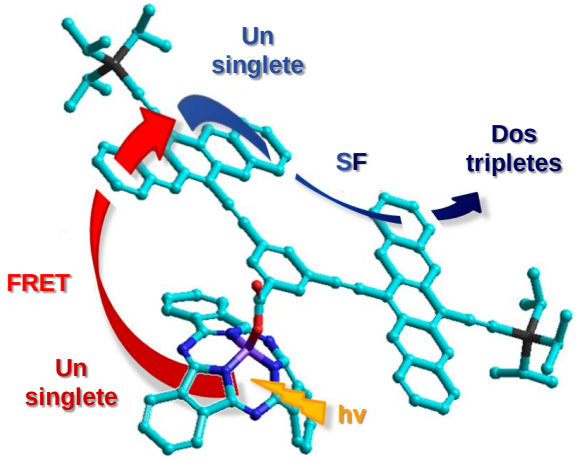

Figura 6. Representación de la secuencia de procesos de FRET y SF activada mediante fotoexcitación de la unidad de SubPc en los derivados SubPc-Pnc_2.

Mediante el diseño racional de los derivados SubPc-Pnc_2 se ha logrado cierto control sobre las dinámicas del proceso de FRET intramolecular.

En la ***primera sección*** del Capítulo, las interacciones intercromofóricas se han regulado modulando las características de la unidad de SubPc dadora de energía. Para ello, se ha decorado la periferia de la SubPc con diferentes sustituyentes (concretamente, átomos de hidrogeno, grupos fenoxi y grupos tiooctilo) con el fin de modular las propiedades ópticas del macrociclo y, a su vez, la entidad del solapamiento entre la emisión de la SubPc y la absorción del Pnc_2, lo que contribuye a la determinación de la constante de velocidad del proceso de FRET. Las medidas fotofísicas han revelado diferencias mínimas entre las constantes de velocidad de transferencia de energía para los tres conjugados investigados. Esto es debido a que el desplazamiento batocrómico de la fluorescencia de la SubPc al aumentar del cáracter π-dador de los sustituyentes está compensado por un menor rendimiento cuánticos de fluorescencia.

En la ***segunda sección*** del Capítulo, las dinámicas del proceso de FRET intramolecular se han regulado mediante la variación de las características estructurales de la unidad espaciadora, y a su vez, de la distancia y orientación entre los dos cromóforos. En concreto, la unidad espaciadora se ha modulado en términos de longitud y flexibilidad variando el número de unidades arilo y grupos metileno. El efecto de las características estructurales del espaciador sobre las dinámicas de FRET se ha investigado y racionalizado mediante medidas experimentales y cálculos teóricos. Los ensayos fotofísicos realizados han indicado que el espaciador tienen un impacto apreciable sobre el proceso de FRET intramolecular. En concreto, las medidas de fluorescencia han indicado

que la extinción de la emisión centrada en la SubPc depende de la longitud del espaciador, siendo los correspondientes rendimientos cuánticos de fluorescencia más altos para los derivados que presentan una unidad de arilo adicional en el espaciador. Además, se ha observado que una mayor flexibilidad del espaciador resulta en menores rendimientos cuánticos de fluorescencia de la emisión centrada en SubPc. Los tiempos de vida del estado excitado de singlete de la SubPc en los derivados SubPc-Pnc_2 siguen la misma tendencia observada para los rendimientos cuánticos de fluorescencia, lo que indica que tanto la menor longitud como la flexibilidad creciente del espaciador aceleran el proceso de transferencia de energía. Los resultados de los cálculos teóricos son consistentes con los datos experimentales, y corroboran por lo tanto la importancia del espaciador en la regulación de las dinámicas de FRET en los derivados investigados.

Sorprendentemente, se ha observado que las características estructurales del espaciador tienen un impacto profundo también en las dinámicas de SF intramolecular. De hecho, la presencia de un grupo arilo adicional ralentiza la SF en un factor de aproximadamente 1.6. La influencia del espaciador en la velocidad del proceso de SF se puede racionalizar teniendo en cuenta la existencia de ligeras diferencias en la distribución electrónica de la unidad puente como consecuencia de la diferente sustitución. En particular, los cálculos teóricos han indicado que mientras en ausencia de la unidad adicional de arilo la deslocalización del primer orbital aceptor basado en pentaceno es muy limitada, en presencia de dicha unidad este orbital está deslocalizado tanto sobre los pentacenos como sobre la unidad de fenilo puente. Dicha conjugación es tan fuerte que suprime parcialmente la SF.

En general, los resultados presentados en este Capítulo constituyen un paso adelante hacia la optimización del diseño molecular para la activación pancromática de la SF, ya que ofrecen la posibilidad de iniciar este proceso en un rango espectral que varía de 300 a 700 nm. El estudio de la combinación de i-FRET e i-SF en modelos moleculares como los que se han investigado en este Capítulo es de crucial importancia en el marco de la conversión de energía solar, ya que constituye una estrategia prometedora para mejorar los rendimientos de los dispositivos fotovoltaicos.

Capítulo 3. Resolución óptica y estudios sobre la organización de subftalocianinas inherentemente quirales

El tercer Capítulo de esta Tesis doctoral tiene como objetivo la resolución óptica eficiente de una SubPc inherentemente quiral con simetría C_3 y el estudio de la organización de las especies enantiopuras en el estado sólido y en superficies, en vista de la potencial implementación de derivados de SubPc ópticamente puros como materiales moleculares en aplicaciones tecnológicas.

Este Capítulo se organiza en dos secciones distintas.

En la ***primera sección***, se ha presentado la resolución óptica de un derivado racémico de SubPc (concretamente, C_3-I_3SubPc-Cl) a través de cromatografía líquida de alta eficacia empleando una columna semipreparativa quiral o mediante derivatización con un auxiliar quiral. Con respecto a la separación mediante cromatografía quiral, la optimización de las condiciones de elución ha permitido la preparación de especies de SubPc enantiopuras a una escala de decenas de miligramos. La relación enantiomérica entre los derivados aislados se ha corroborado mediante espectroscopía de dicroísmo circular y análisis de difracción de rayos X, que también ha permitido asignar de forma inequívoca la configuración absoluta de las especies enantiopuras. Por otro lado, la derivatización con un auxiliar quiral ha permitido llevar a cabo la resolución óptica del derivado de C_3-I_3SubPc-Cl racémico mediante técnicas comunes de laboratorio. En particular, la funcionalización de la posición axial del macrociclo con un derivado enantiopuro de dibromo-BINOL ha permitido la separación de los diastereoisómeros resultantes mediante cromatografía en columna, y la posterior reacción con tricloruro de boro ha proporcionado los enantiómeros aislados de la SubPc de partida con excesos enantioméricos satisfactorios y en excelente rendimiento. Notablemente, la resolución óptica de SubPcs racémicas inherentemente quirales basada en el uso de auxiliares quirales no tiene precedentes en la literatura.

En la ***segunda sección***, se ha investigado la organización de SubPcs inherentemente quirales racémicas y enantiopuras tanto a nivel de estado sólido cristalino como en superficie mediante análisis de difracción de rayos X y medidas de microscopía de efecto túnel, respectivamente. En particular, se ha investigado la organización en el estado sólido de C_3-I_3SubPc-Cl en función de su composición quiral. La comparación entre el empaquetamiento en estado sólido de muestras racémicas y enantiopuras ha revelado diferencias notables. Ambas especies se organizan en dímeros cóncavo-convexos cola-cola que, a su vez, forman columnas homoquirales. Sin embargo, mientras que el material racémico exhibe una organización antiparalela de los agregados columnares, dichos agregados se organizan antiparalelamente dentro de la

estructura cristalina de los enantiómeros puros (Figura 7). La sensibilidad del empaquetamiento cristalino a la composición quiral es de gran interés en vista de la posible implementación de moléculas inherentemente quirales en aplicaciones tecnológicas, ya que ofrece la posibilidad de modular las propiedades del material (y, a su vez, el rendimiento del dispositivo) simplemente adaptando su pureza óptica.

Desafortunadamente, no se han obtenido resultados concluyentes de los experimentos de microscopia de efecto túnel. En concreto, la deposición un derivado C_3-I_3SubPc-Cl enantiopuro en superficies de Au(111), Ag(111) y Cu(111) no ha conducido en las condiciones experimentales investigadas a la formación de una red ordenada. En particular, se ha observado una escisión espontánea extensa de los enlaces C-I en sustratos de Ag(111) y Cu(111) incluso a temperatura ambiente.

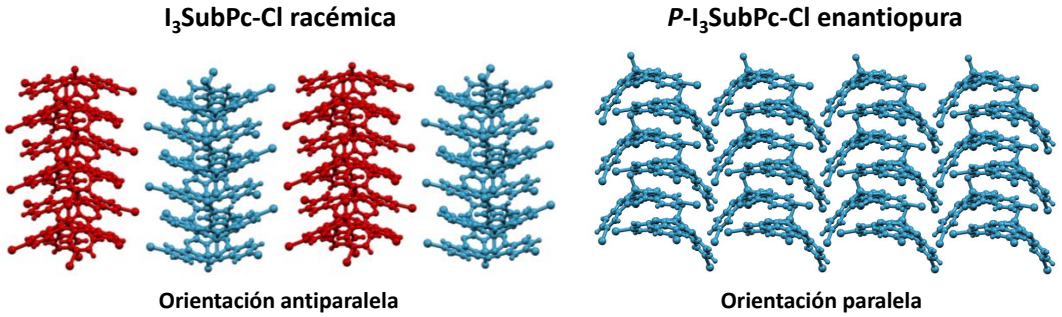

Figura 7. Empaquetamiento cristalino de especies racémicas y enantiopuras de C_3-I_3SubPc-Cl.

La organización altamente direccional de los agregados columnares en la estructura cristalina de las especies enantiopuras, junto con las excelentes propiedades estructurales, ópticas y electrónicas de las SubPcs, convierten estos derivados en candidatos muy interesantes para aplicaciones tecnológicas. Además, las especies de I_3SubPc-Cl ópticamente puras constituyen precursores extremadamente versátiles para la preparación de una extensa variedad de sistemas basados en SubPcs mediante la funcionalización de las posiciones axiales y periféricas, lo que abre paso a la investigación de sus propiedades relacionadas con la quiralidad. Finalmente, los derivados enantiopuros de I_3SubPc-Cl constituyen especies estratégicas para investigar los aspectos mecanísticos de la reactividad de SubPcs, como la posibilidad de una inversión del macrociclo en dichos derivados.